

4000

NRL Report 7964

12 MAY REC'D

AD

Electroacoustic Modeling of Magnetostrictive Shells and Rings

Part 2 - EIGSHIP Predicted Performance; Experimental Measurements; and Computer Listing of EIGSHIP

S. HANISH

Acoustics Division

and

B. J. KING, R. BAIER, AND P. H. ROGERS

*Transducer Branch
Acoustics Division*

April 19, 1976



NAVAL RESEARCH LABORATORY
Washington, D.C.

Approved for public release: distribution unlimited.

UNCLASSIFIED

SECURITY CLASSIFICATION OF THIS PAGE (When Data Entered)

| REPORT DOCUMENTATION PAGE | | READ INSTRUCTIONS BEFORE COMPLETING FORM |
|--|--|---|
| 1. REPORT NUMBER NRL Report 7964 | 2. GOVT ACCESSION NO. | 3. RECIPIENT'S CATALOG NUMBER |
| 4. TITLE (and Subtitle) ELECTROACOUSTIC MODELING OF MAGNETOSTRICTIVE SHELLS AND RINGS, Part 2 - EIGSHIP PREDICTED PERFORMANCE, EXPERIMENTAL MEASUREMENTS, AND COMPUTER LISTING OF EIGSHIP | 5. TYPE OF REPORT & PERIOD COVERED Interim report on a continuing NRL Problem | |
| | 6. PERFORMING ORG. REPORT NUMBER | |
| 7. AUTHOR(s) S. Hanish, B.J. King, R.V. Baier, and P.H. Rogers | 8. CONTRACT OR GRANT NUMBER(s) | |
| 9. PERFORMING ORGANIZATION NAME AND ADDRESS Naval Research Laboratory Washington, D.C. 20375 | 10. PROGRAM ELEMENT, PROJECT, TASK AREA & WORK UNIT NUMBERS NRL Problem S01-29 Project RR 131-03-41, Task 5227 | |
| 11. CONTROLLING OFFICE NAME AND ADDRESS Department of the Navy Office of Naval Research Arlington, Va. 22217 | 12. REPORT DATE April 19, 1976 | |
| | 13. NUMBER OF PAGES 185 | |
| 14. MONITORING AGENCY NAME & ADDRESS (if different from Controlling Office) | 15. SECURITY CLASS. (of this report) Unclassified | |
| | 15a. DECLASSIFICATION/DOWNGRADING SCHEDULE | |
| 16. DISTRIBUTION STATEMENT (of this Report) Approved for public release; distribution unlimited | | |
| 17. DISTRIBUTION STATEMENT (of the abstract entered in Block 20, if different from Report) | | |
| 18. SUPPLEMENTARY NOTES | | |
| 19. KEY WORDS (Continue on reverse side if necessary and identify by block number) Acoustic loading on shells Ring transducers, free-flooded Magnetostriction Ring transducers, magnetostrictive Magnetostrictive shells Fortran computer program Mathematical modeling Piezoactive modal coupling | | |
| 20. ABSTRACT (Continue on reverse side if necessary and identify by block number) The mathematical model of the electroacoustic performance of a force-driven free-flooding magnetostrictive cylinder shell used as an underwater sound transducer, originally developed in NRL Report 7767, Dec. 1974, has been coded into a computer program called EIGSHIP. This program is designed to predict electrical and mechanical impedances of the loaded shell, transmitting responses, electroacoustic efficiency, surface velocities, far-field beam patterns, and other relevant performance parameters. An experimental check on the prediction capabilities of EIGSHIP was undertaken on three specially constructed magnetostrictive shells which were tested under water (Continued) | | |

DD FORM 1473
1 JAN 73EDITION OF 1 NOV 65 IS OBSOLETE
S/N 0102-014-6601

UNCLASSIFIED

SECURITY CLASSIFICATION OF THIS PAGE (When Data Entered)

20. Abstract (Continued)

load conditions in an indoor test facility. A full discussion of the comparison of predicted and measured performance is presented. The coded listing of EIGSHIP and instructions on its input requirements and output format are furnished in detail. Samples of typical computer runs are displayed and commented on.

CONTENTS

| | | |
|-------|--|----|
| 1. | INTRODUCTION | 1 |
| 2. | PHYSICAL MODELS AND TEST PROCEDURE | 1 |
| 3. | INPUT FACTORS IN THE IMPLEMENTATION OF EIGSHIP | 4 |
| 4. | GRAPHICAL RECORD OF EIGSHIP PREDICTIONS AND EXPERIMENTAL MEASUREMENTS | 8 |
| 5. | METHODS USED IN INTERPRETING EIGSHIP PREDICTIONS AND EXPERIMENTAL MEASUREMENTS | 22 |
| 5.1 | Interpretation of Electrical-Impedance X -vs- R Plots | 23 |
| 5.1.1 | Blocked Impedance | 24 |
| 5.1.2 | Motional Impedance | 25 |
| 5.1.3 | Electrical-Impedance Plots | 25 |
| 5.1.4 | Nonresonant Water Modes | 27 |
| 5.2 | Motional-Impedance Analysis and X_m -plus- X_L Plots | 27 |
| 5.2.1 | Motional-Impedance Phases | 27 |
| 5.2.2 | X_m -plus- X_L Plots | 28 |
| 5.3 | Strain and Kinetic Energy Formulas | 30 |
| 6. | AN ELECTRIC-IMPEDANCE ANALYSIS OF THE ACOUSTIC PERFORMANCE OF RING C | 31 |
| 6.1 | EIGSHIP Prediction of Surface Velocity | 33 |
| 6.2 | Computer Determination of Resonant Frequencies in Air and Calculation of EIGSHIP Input Data | 33 |
| 6.3 | Predicted Total Electrical Impedance and Its Theoretical Significance | 36 |
| 6.3.1 | Electrical Impedance Disturbance in the Vicinity of 4 kHz | 36 |
| 6.3.2 | Electrical Impedance Disturbance in the Vicinity of 8 kHz | 37 |
| 6.3.3 | Electrical Impedance Disturbance Above 14 kHz | 38 |
| 6.4 | Far-Field Radiation Predictions in Simple-Model Cases | 39 |
| 6.4.1 | Zeros of Far-Field Radiation in the Radial Direction | 39 |
| 6.4.2 | Confined-Fluid-Cylinder Modes | 41 |

CONTENTS (Continued)

| | | |
|------|---|-----|
| 6.5 | Measurement of Experimental Curves of Total Impedance in Water | 42 |
| 6.6 | Transmitting Responses Predicted by EIGSHIP | 42 |
| | 6.6.1 Dependence on Mechanical Resistance | 43 |
| | 6.6.2 Dependence on the Product K^2h^2 | 43 |
| | 6.6.3 Effect of Cavity-Mode Radiation | 44 |
| | 6.6.4 Effect of Interior Support Structure | 45 |
| 6.7 | Axial Constant-Current Transmitting-Response Curves | 46 |
| | 6.7.1 Comparison of Theoretical and Measured Responses | 46 |
| | 6.7.2 Effects of Alterations in the Internal Support Structure and Coil Windings | 46 |
| 7. | THE COMPUTER PROGRAM EIGSHIP | 48 |
| 7.1 | Input and Introductory Calculations | 49 |
| | 7.1.1 Data Cards | 49 |
| | 7.1.2 Modal Calculations | 55 |
| | 7.1.3 Thickness Correction Factors | 58 |
| 7.2 | Basic Performance Characteristics Calculation and Output | 59 |
| | 7.2.1 First Page of Output: Radial Velocity and B and S Model | 59 |
| | 7.2.2 Second Page of Output: EIGSHIP Model | 63 |
| 8. | CONCLUSION TO PART 2 | 66 |
| 9. | ACKNOWLEDGMENTS | 67 |
| 10. | REFERENCES AND BIBLIOGRAPHY | 67 |
| 10.1 | References | 67 |
| 10.2 | Bibliography | 68 |
| | APPENDIX A -- Computer Listing of EIGSHIP | 70 |
| | APPENDIX B -- Computer Listing of DTRMNT and a Sample Input and Output | 134 |
| | APPENDIX C -- Computer Listing of EIGFNS and a Sample Input and Output | 142 |
| | APPENDIX D -- Sample Input and Resultant Output of Program EIGSHIP | 155 |

CONTENTS (Continued)

APPENDIX E — Definition of Material Parameters 171
APPENDIX F — Numerical Investigation of the Axial Transmitting Response 177
APPENDIX G — Specific Acoustic Impedance of the Shell and Shell Motion 180

ELECTROACOUSTIC MODELING OF MAGNETOSTRICTIVE SHELLS AND RINGS

Part 2 -- EIGSHIP PREDICTED PERFORMANCE, EXPERIMENTAL MEASUREMENTS, AND COMPUTER LISTING OF EIGSHIP

1. INTRODUCTION

In Part 1, a previous NRL Report [1], the authors undertook the task of mathematical modeling of the electroacoustic performance of magnetostrictive shells and rings. The most fully developed model presented was that of a magnetostrictive shell, wound toroidally with copper wire, submerged free flooded in an infinite unbounded homogeneous medium, and driven in forced vibration by an applied electric field. The theoretical analysis of this model was aimed at the prediction of absolute (rather than relative) values of electroacoustic performance parameters, such as electrical impedance, mechanical radiation impedance, far field acoustic pressure patterns, transmitting response, electroacoustic conversion efficiency, surface (mechanical) velocity, and "resonant" frequencies. For literature citations the reader is referred to Ref. 1 and this report's bibliography.

In this report the theoretical model that was developed in Part 1 has been coded into a digital computer program called EIGSHIP, capable of delivering predictions on these seven electroacoustic performance factors of a free-flooded magnetostrictive shell when the geometric construction and piezomagnetic properties of the shell material are furnished as input. Since the original purpose of the modeling was to enable designers of magnetostrictive shells to optimize design parameters by rapid calculation of alternative construction and materials, it was deemed desirable in the course of the modeling to construct physical models of several cylindrical shell transducers and compare measurements of their performance in an underwater acoustic facility with the predicted performance. A study of both the experimental measurements and the corresponding predicted performance is reviewed in detail herein.

2. PHYSICAL MODELS AND TEST PROCEDURE

The ring transducers (labeled A, B, and C) used in the experiments were three "cube-textured" nickel (CTN) rings fabricated by the International Nickel Company. The principal differences among the three rings are in their height dimensions (also called lengths, Table 1). The ring cores were scroll wound, which means that they were made by winding the CTN metal strips of thickness 0.2032 mm about a mandrel and using a bonding agent to consolidate the ring.

Each of the cores (consolidated rings) was separately mounted as shown in Fig. 1. The mounting structure was designed to hold the core in a fixed position in the windings

Table 1 — Dimensional and Elastic Parameters of Rings A, B, and C

| Ring | Length, l (mm) | Outside Radius (mm) | Inside Radius (mm) | Mean Radius, a (mm) | Thickness, b (mm) | Young's Modulus Y at Constant Magnetic Induction (N/m^2) | Poisson Ratio, ν | Density, ρ (kg/m^3) |
|------|------------------------|---------------------------|--------------------------|--------------------------------|---------------------------|---|----------------------------|------------------------------------|
| A | 20.29 | 69.105 | 62.455 | 65.78 | 6.65 | 1.28×10^{11} | 0.38 | 8234 |
| B | 49.30 | 69.145 | 62.295 | 65.72 | 6.85 | 1.28×10^{11} | 0.38 | 8400 |
| C | 90.55 | 69.30 | 62.45 | 65.87 | 6.85 | 1.26×10^{11} | 0.38 | 8400 |

without appreciably clamping it. The mounting structure was designed to be acoustically transparent in the excitation frequency range of interest. The core was wound with 144 turns of No. 18 Teflon-insulated copper wire supported by four copper hoops above and below the ring core. The hoops, in turn, were supported by two sets of three spokes emanating from the hubs at the geometric center of the ring transducer. The hubs were held apart and the entire structure was kept rigid by a threaded 6.35-mm (1/4-inch) steel bolt. The motion of the core was isolated from the supporting structure by pads of rho-C rubber.

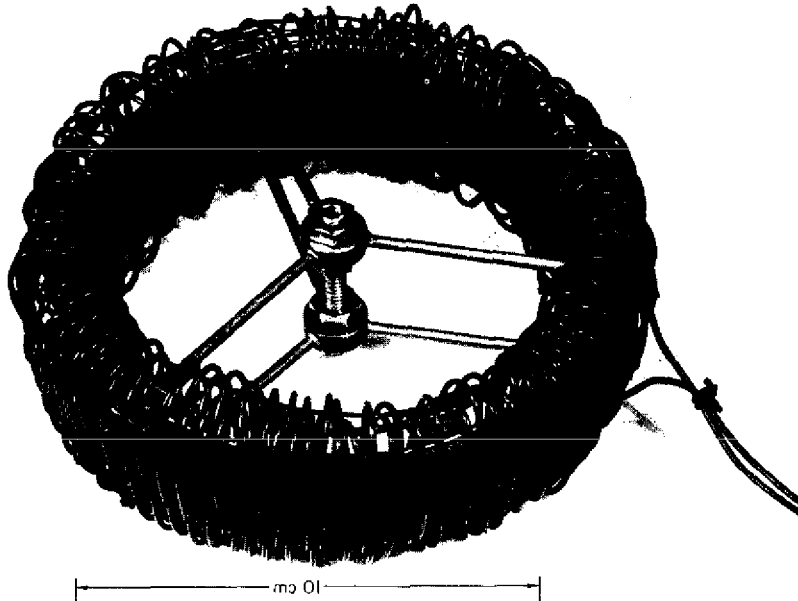


Fig. 1 — Model transducer

Each ring was driven by an ac current while simultaneously polarized by a dc current, and a suitable blocking circuit was used to keep the direct current from circulating in the ac source and to keep the dc source itself from shorting out the ac source.

The test procedures adopted were designed to check the validity of the EIGSHIP prediction model by electric impedance analysis (of current and voltage at the electrical terminals) of the force-driven transducer, and comparison of these predictions with underwater sound measurements in a calibration tank. Two types of calibration signal were used: CW signals at the electrical terminals, with the transducer under no load (in air), and square-wave-modulated carrier signals for underwater measurements. In both cases the dc polarizing current I_0 was 4 amperes, which corresponded to a magnetizing field of $H_0 = NI_0/(2\pi a) = 0.14$ ampere per meter, for a mean radius a of the ring and for N turns of exciting coil. The ac excitation current was held constant for all frequencies at 15 milliamperes (rms) when measuring electrical impedances and at 100 milliamperes

when measuring underwater transmitting current responses and directivity patterns. This change in amplitude was one of convenience. Because both levels were low it did not affect the validity of the experiments.

In air the transducer was suspended freely under effectively zero mechanical constraint and driven by a CW signal. Sixty values of input electrical impedance were directly measured at the electrical terminals over the frequency range of the lowest radial resonance. The measured data were corrected for the contribution to the total electrical impedance from the blocking circuit.

In water the transducer was subjected to a standard underwater calibration in the NRL Acoustic Research Test Tank [2] which is provided with pulse-modulation and gating circuits and with geometric positioning devices to allow a free-field steady-state calibration in the frequency ranges of interest. An NRL model F36 standard hydrophone was used as a receiver, occasionally replaced by an F50. The total electrical impedance was measured by a Scientific Atlanta Pulse Vector Immittance Meter and corrected for the presence of a blocking circuit. Sixty values of electrical impedance were measured over the frequency range of test.

3. INPUT FACTORS IN THE IMPLEMENTATION OF EIGSHIP

The computer program EIGSHIP was used to predict the electroacoustic performance of rings A, B, and C. A detailed description of EIGSHIP is given in Section 7, where fundamental parameters of computer program input are listed and defined. Since the desired input quantities are not always available in the literature or easily accessible to experimental determination, it was often necessary to make some compromises with the precise definitions. We indicate here how we obtained the input parameters from our air measurements. However, if in a particular case better values of input quantities or better methods for obtaining them are available to the prospective users of EIGSHIP, they should be used. (Many of the parameters*, such as a , b , ρ , N , ν , and t are easily and directly obtainable and will not be discussed.) We begin with Young's modulus.

The real part Y_R of the complex Young's modulus, taken at constant magnetic induction, was obtained by the following procedure. The ring was electrically driven in air at constant current over the range of frequencies covering the lowest radial mode, and the total electrical reactive impedance (X_{tot}) was plotted versus frequency. The (interpolated) crossover frequency ($= \omega_1$) where $X_{tot} \rightarrow +\infty$ jumps to $X_{tot} \rightarrow -\infty$ is taken to be the resonant frequency. Knowing the effective mass (M_1) of the ring, we then calculated the effective stiffness $K_1 = M_1 \omega_1^2$ in the lowest radial mode [1, Eq. 6.10]. The real number K_1 so determined is the magnitude of the stiffness under conditions of constant magnetic intensity (constant H). In theory K_1 is a complex number given by the formula

$$K_1 = \frac{2\pi A \theta}{a} Y \left(1 - \frac{\mu^S \chi_{\theta\theta}}{Y} \right)$$

*See Glossary, Part I, and discussion below.

(as discussed further in Appendix C of Part 1 [1], where $A_\theta = b\ell$, μ^S is the reversible permeability at constant strain, X is the eddy-current and hysteresis factor, and $h_{\theta\theta}$ is an effective piezomagnetic constant.

Both Young's modulus Y and the eddy-current and hysteresis factor χ_1 are complex numbers with small imaginary parts. Neglecting small quantities, we write K_1 as the real number

$$K_1 \approx \frac{2\pi A_\theta}{a} Y_R (1 - k_1^2 \chi_R).$$

The quantity $k_1^2 \chi_R$, where k is the coefficient of electromechanical coupling, is obtainable by other measurements. Thus the real part of Young's modulus is calculated from the relation

$$Y_R = \frac{(K_1)_{\text{meas}} a}{2\pi A_\theta (1 - k_1^2 \chi_R)},$$

where $(k_1)_{\text{meas}} = M_1 (\omega_1^2)_{\text{meas}}$. Computed in this way the magnitude of Y_R is equivalent to the Young's modulus taken at constant-voltage drive. The resonant frequency associated with Y_R by the formula

$$\Omega_1 = \sqrt{\frac{2\pi A_\theta Y_R}{aM_1}}$$

is the mechanical resonant frequency in the first radial mode at constant-voltage drive. This calculated Ω_1 compares favorably in magnitude with the resonant frequency obtained by driving the core of a specific ring (ring C) mechanically and observing with an accelerometer the frequency of the maximum radial velocity in the first radial mode.

The effective Poisson ratio ν and the resistivity ρ_e of the core material was furnished to us by the International Nickel Co., who fabricated the three INCO rings, A, B, and C.

The relative reversible permeability at constant strain (μ_{rel}^S) proved difficult to measure directly, since this required a satisfactory method of mechanically clamping the magnetostriuctive ring. Instead we measured the permeability at constant (zero) stress, namely μ^T and then calculated μ^S from a knowledge of k^2 by the formula

$$\mu^S = \mu^T (1 - k^2 Y_R).$$

The measurement of μ^T is made by determining the total electrical reactance X_{tot} at very low frequency under zero stress (no external load). Since

$$X_{tot} = \frac{\omega N^2}{2\pi a} [\mu^T \chi_R b\ell + \mu_0 (b'\ell' - b\ell)],$$

where $b'\ell'$ is the area enclosed by the coil surrounding the ring and $b\ell$ is the cross-sectional area of the ring, we find

$$\mu^T \chi_R = \frac{(X_{tot})2\pi a}{\omega N^2 b\ell} - \mu_0 \frac{(b'\ell' - b\ell)}{b\ell}$$

and

$$\mu^S = \mu_{rel} \mu_0$$

Thus, by measuring the slope of $X_{tot} = \text{Im } Z_{tot}$ over the low-frequency range and using this formula, one obtains $\mu^T \chi_R$, which immediately yields $\mu^S \chi_R$, provided that the coefficient of electromechanical coupling k is known.

The effective coefficient of electromechanical coupling k can be measured by electrical impedance analysis. It is known [3] that

$$\frac{D_Z}{Q_Z X_C} = \frac{k^2}{1 - k^2 \chi_R} \left(\frac{\chi_0^2}{\chi_R} \right), \quad \chi_0 = |\chi|,$$

in which D_Z and X_C are the diameter and clamped reactance respectively of the electrical motional impedance loop and Q_Z is the mechanical Q determined by

$$Q_Z^I = \frac{\omega M}{R_m' + R_m''} = \frac{\omega_R}{\omega_3 - \omega_2},$$

in which R_m' , R_m'' , ω_R , ω_3 , ω_2 are defined in Part 1 (Section 6 and Appendix A). ($Q_Z^I = Q_1^I$ as defined by Eq. 6.23 of Part 1.) When a leakage magnetic flux is present and is included in the clamped impedance, we set

$$\frac{D_Z}{Q_Z X_b} = \frac{k^2 \chi_R^2 \kappa}{(1 - k^2 \chi_R) \chi_R}$$

where

$$X_b = X_c + X_{e\ell},$$

in which X_b is the imaginary part of the blocked impedance, X_c is the imaginary part of the core impedance, and $X_{e\ell}$ is the imaginary part of the copper-loss leakage impedance. For small copper and core loss we assume $\kappa \equiv X_c/X_b$, so that

$$\frac{D_Z}{Q_Z X_b} = \frac{D_Z \kappa}{Q_Z X_c} = \frac{k^2 \chi_R^2 \kappa}{(1 - k^2 \chi_R) \chi_R} \equiv \alpha$$

Thus

$$k^2 \chi_R \approx \frac{\alpha}{\alpha + \kappa}.$$

When so calculated, k^2 is approximately the dynamic material coupling factor.

The value of k^2 obtained enables us to determine an *effective* piezomagnetic constant $h_{\theta\theta}$ by use of the formula

$$h_{\theta\theta} = \sqrt{\frac{k^2 Y_R}{\mu_{\text{rel}}^S \mu_0}}$$

An equivalent formula for $h_{\theta\theta}$ [1, p. 78] includes all parameters noted here but in somewhat different form.

The constant-current mechanical Q_1^I is determined from motional impedance analysis by use of

$$Q_1^I = \frac{\omega_r}{\omega_3 - \omega_2}$$

[1, pp. 77 and 78]. Here $\omega_r = \omega_1^I$ is the resonant frequency of the ring in the lowest radial mode when driven in air at constant current, and ω_2 and ω_3 are the quadrantal

frequencies. When $Q_1^f > 10$, one can determine these frequencies from a plot of magnitude of radial velocity (air) versus frequency in the vicinity of the first radial resonance. We have used the motional diagram technique for measuring Q_1^f .

The direct measurement of Q_n^f for $n > 1$ by impedance analysis is not practical, because the higher numbered motional impedance loops generally have small sizes which cannot be accurately measured and because the higher order modes tend to nest within each other, exhibiting such close coupling as to make separation of modes questionable. Since Q_n^f is needed in the analysis, we assumed that it can be estimated by allowing the purely mechanical resistance (R_m'' as defined in Part 1) to be a constant for each mode. The modal mass is presently defined as the static mass in EIGSHIP.

The basic limitations and assumptions contained in this section provide an adequate input statement for the parameters of EIGSHIP when the amplitude of forced electrical drive is low enough to assure quasi-linear operation. At high-power drive they must be modified. High-power drive is not discussed in this report.

4. GRAPHICAL RECORD OF EIGSHIP PREDICTIONS AND EXPERIMENTAL MEASUREMENTS

When an acceptable set of input parameters of the three transducers A, B, and C was supplied the computer program EIGSHIP delivered all the predicted performance data over the frequency ranges of interest. At the same time experiments were run on physical models as noted in Section 2.

We present EIGSHIP predictions and experimental measurements in the following series of graphs and associated texts. The notation of Butterworth and Smith appearing in the text and on the graphs signifies a comparison of the data with a theoretical analysis modeled after the classic Butterworth and Smith analysis [4], which describes the limiting case of a one-dimensional model of a magnetostrictive ring wherein the ring velocity is radial only and is a constant over the length of the ring. In each figure, part (a) is the experimental graph, part (b) is the EIGSHIP theoretical graph, and part (c) is the Butterworth and Smith model graph.

Figures 2, 3, and 4 are graphs of the electrical driving point impedance in air, displayed separately as resistive and reactive components, for ring A (small ring), ring B (middle ring) and ring C (long ring), plotted as a function of the driving frequency.

Figure 2a illustrates how ring A behaves in air as a function of frequency when observed at the electrical terminals over the frequency range $0 < f < 20$ kHz. The frequency of maximum (motional) electrical resistance (to close approximation the air resonant frequency) is 9.2 kHz. It is from this graph that the physical parameters of reversible magnetic permeability (μ), Young's elastic modulus (Y^B), the electromechanical coupling coefficient (k), and the piezomagnetic stress constant (h) are evaluated by the methods noted. These parameter values were then used in the computer program EIGSHIP to produce the graphs in Fig. 2b. As is to be expected for ring A these graphs duplicate Fig. 2a very well. For illustrating the results of using a simpler mathematical model, we present graphs in Fig. 2c using the Butterworth and Smith theoretical model. For ring A the Butterworth model agrees well with the EIGSHIP model.

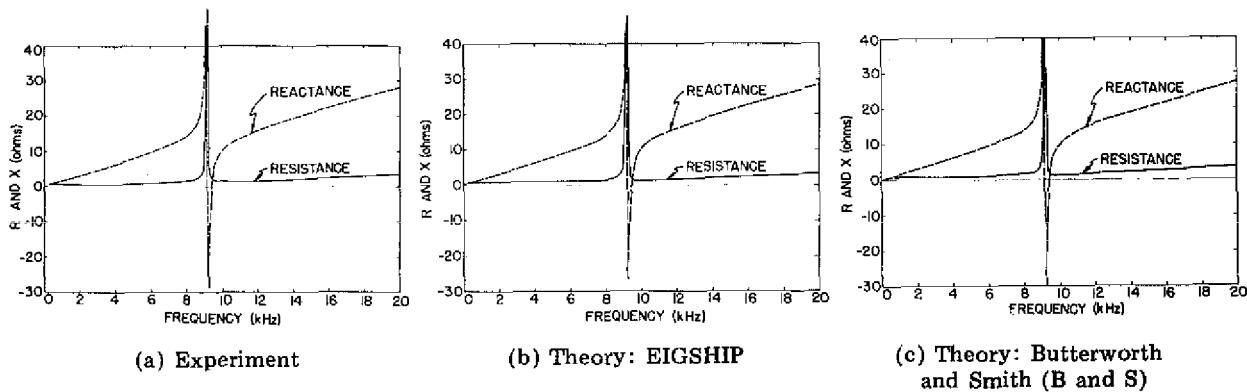


Fig. 2 — Electrical driving-point impedance in air of ring A

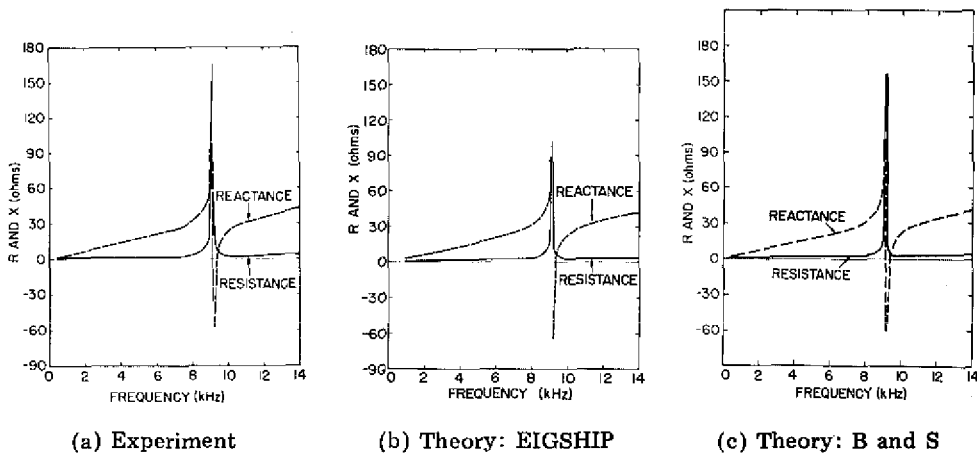


Fig. 3 — Electrical driving-point impedance in air of ring B

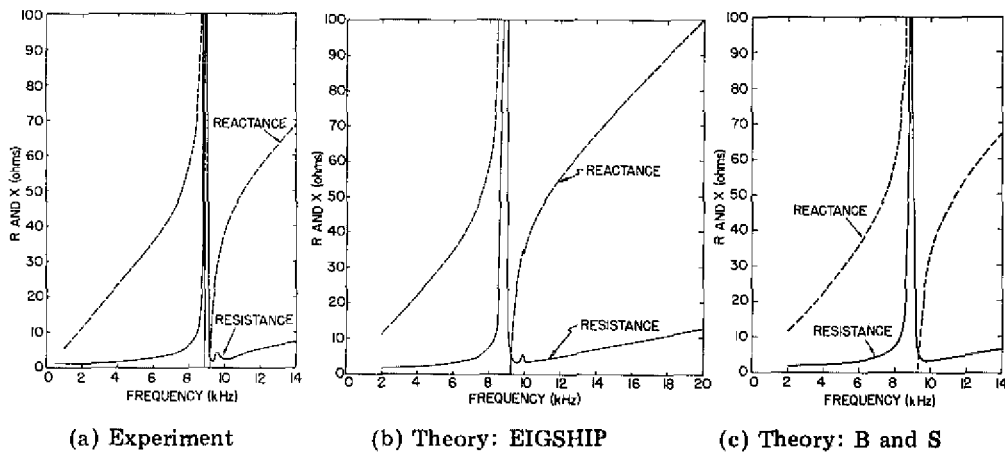


Fig. 4 — Electrical driving-point impedance in air of ring C

Figures 3a, 3b, and 3c are graphs of the electrical driving point impedance [1, Eq. 5.24] in air for ring B. Again these graphs are similar to each other and to those in Fig. 2. The values of the electrical impedance components of ring B are larger than the impedance components of ring A by roughly the ratio of its length to the length of ring A. The radial resonant frequency is nearly the same as ring A at 9.15 kHz. The Butterworth and Smith model for ring B agrees with the EIGSHIP model.

Figures 4a, 4b, and 4c are graphs of the electrical driving-point impedance in air for ring C. A comparison of the three graphs in Fig. 4 shows that in general there is good agreement in shape and magnitude except that the "barrel mode" (a radial-motion mode with two nodes along the length of the ring) is predicted by EIGSHIP to be 9.9 kHz whereas the experiment indicates that it is at 9.6 kHz and it does not appear in the Butterworth and Smith model. It is difficult to specify the accuracy of the experimental measurements near this frequency because of the low values of the motional impedance components.

Figures 5, 6, and 7 are graphs of the electrical driving-point impedance (resistive and reactive) components in water as a function of frequency for rings A, B, and C. Comparison of Figs. 5a and Fig. 5b shows that the resonant frequency is approximately 7.6 kHz and that the values of the EIGSHIP impedance components at resonance are larger than the experiment by about 5 percent. Again the Butterworth and Smith model is in good agreement with the EIGSHIP model. Comparisons of the graphs in Figs. 6a and 6b for ring B shows a resonant frequency of 5.8 kHz and shows EIGSHIP reactance 10 percent larger than the experiment and EIGSHIP resistance 30 percent larger than the experiment near the resonant frequency. The graph for the Butterworth and Smith model (Fig. 6c) is in good agreement with EIGSHIP, and all three graphs are in excellent agreement with each other off resonance. The magnitude of the motional impedance predicted by EIGSHIP near 14 kHz is too small to be observed by the experiment. Comparison of Figs. 7a and 7b for ring C shows that the frequencies at which the lower frequency peaks occur (near 4 kHz) disagree by about 100 Hz, whereas the frequencies at which the next higher frequency peaks occur (near 8 kHz) agree. EIGSHIP (Fig. 7b) shows a definite peak at a frequency of 9.3 kHz, at which a response in the experimental data is barely perceptible. Comparison of the impedance components shows that EIGSHIP predicted values near resonance are from 20 to 60 percent larger than the experimental values. The Butterworth and Smith model in Fig. 7c agrees well with EIGSHIP except that peaks at 8 kHz and 9.3 kHz the Butterworth and Smith model appears to integrate through and thereby smooth these peaks. Examination of Figs. 4 and 7 shows that the peak in the impedance at 4 kHz is a lowest cavity type mode, the peak at 8 kHz is the first radial ring mode loaded by the water reactance, and the peak at 9.3 kHz is the second radial mode loaded by the water load.

Figures 8, 9, and 10 present graphs of the computed reactive component of the mechanical impedance and the computed reactive component of the radiation load versus the frequency for ring A, ring B and ring C respectively. (Electrical reactance is discussed in Section 5.1). The reactive component of the mechanical impedance is computed from the theoretical strain energy (appropriate formulas in Section 5.6) of the elastic system. For quick interpretation in visual inspection the negative of the mechanical reactance is plotted in these figures. Consequently, where these graphs either touch or cross each

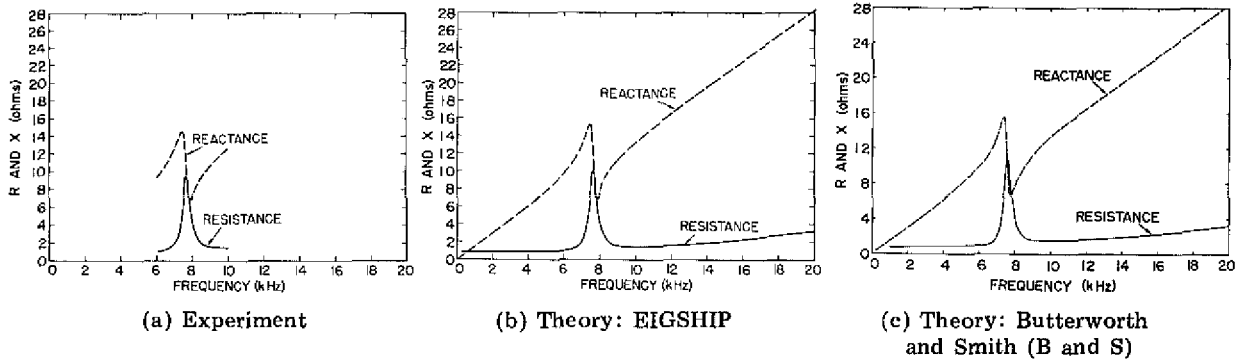


Fig. 5 -- Electrical driving-point impedance in water of ring A

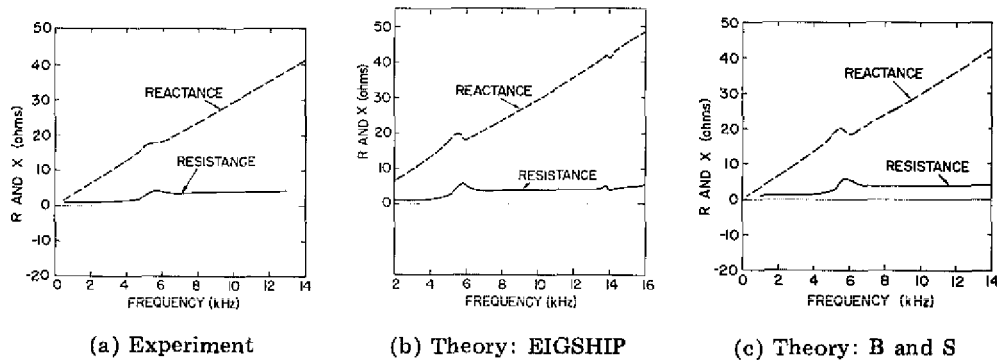


Fig. 6 -- Electrical driving-point impedance in water of ring B

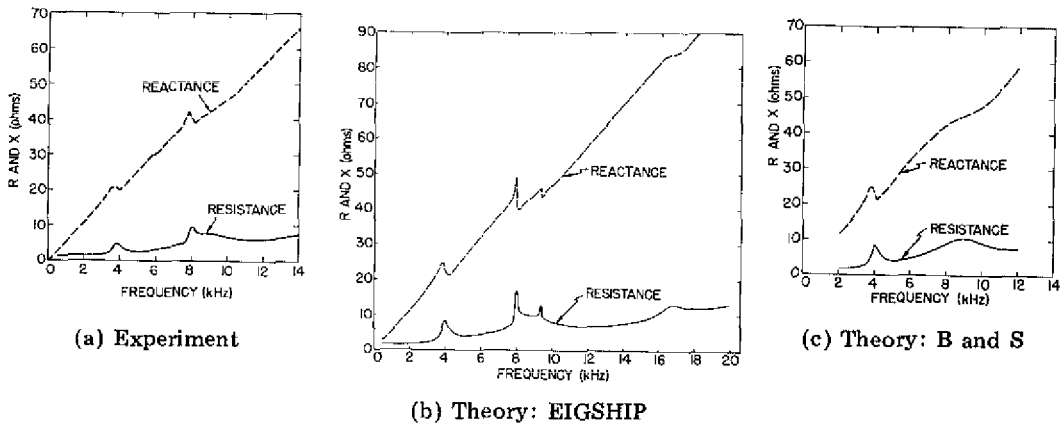


Fig. 7 -- Electrical driving-point impedance in water of ring C

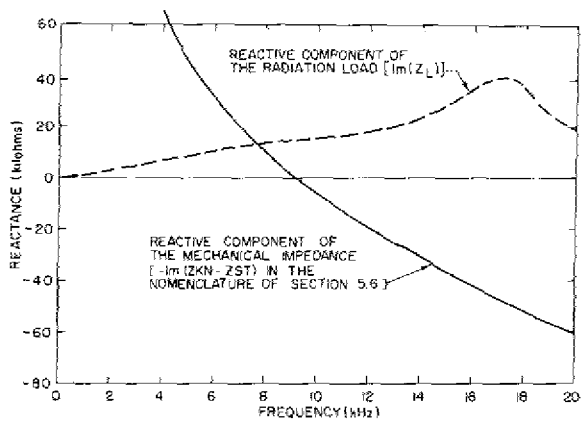


Fig. 8 — Computed reactive component of the mechanical impedance and the computed reactive component of the radiation load for ring A in water (EIGSHIP)

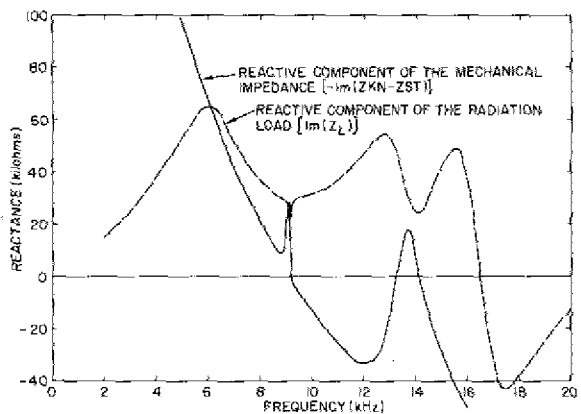


Fig. 9 — Computed reactive component of the mechanical impedance and the computed reactive component of the radiation load for ring B in water (EIGSHIP)

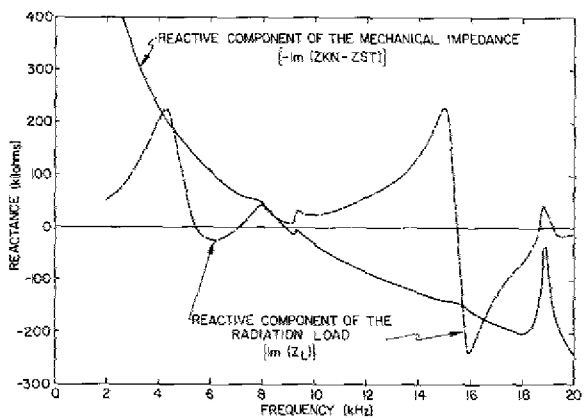


Fig. 10 — Computed reactive component of the mechanical impedance and the computed reactive component of the radiation load for ring C in water (EIGSHIP)

other the net mechanical reactance of the transducer plus the water load is 0. In Fig. 8 for ring A, the mechanical reactance curve of the elastic shell crosses the water reactance curve at about 7.6 kHz, and the electrical driving-point reactance in water (Fig. 5b) is a minimum at about 7.9 kHz. The mechanical reactance curve passes through 0 at 9.2 kHz, whereas the electrical driving-point reactance (Fig. 2b) in air is a minimum at 9.25 kHz.

In Fig. 9 for ring B, the mechanical reactance of the elastic shell either touches or crosses the reactive water load at 6.1, 9.1, and 9.2 kHz and goes through 0 at 9.2, 13.2, and 14.2 kHz. The electrical driving-point reactance in water (Fig. 6b) has minima at 6 and 14 kHz and in air (Fig. 3b) has a minimum at 9.2 kHz. In Fig. 10 for ring C, the mechanical reactance of the elastic shell either touches or crosses the reactive water load at 4.1, 4.6, 8.5, 15.7, and 16.5 kHz and goes through 0 at 8.9 kHz. The electrical driving-point reactance in water (Fig. 7b) has minima at 4.2, 8.1, 9.3, and 17 kHz and in air (Fig. 4b) has minima at 9.1 and 9.9 kHz.

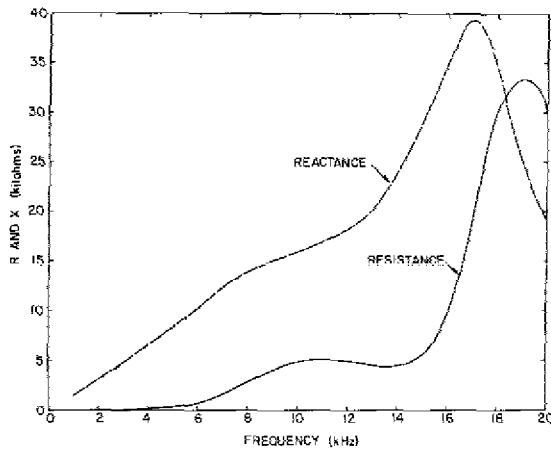
Figures 11, 12, and 13 present for rings A, B, and C respectively comparisons between the computed resistive and reactive components of the radiation load as a function of frequency for the EIGSHIP model and the Butterworth and Smith model. The radiation load in EIGSHIP is calculated by dividing the acoustic power by an average of the magnitude squared of the surface band velocities and multiplying the result by the total surface area of the ring. In the Butterworth and Smith model of the radiation load the same formalism is employed with a single reference surface velocity.*

In Figs. 11a and 11b the shapes of the radiation load for ring A are quite similar, differing only by a scale factor in the value of the load. The radiation loads for ring B in Figs. 12a and 12b are in reasonable agreement except near 9 and 14 kHz. At these frequencies EIGSHIP reflects the influence of the first radial elastic mode (9 kHz) and the second radial elastic mode (14 kHz) on the velocity distribution.

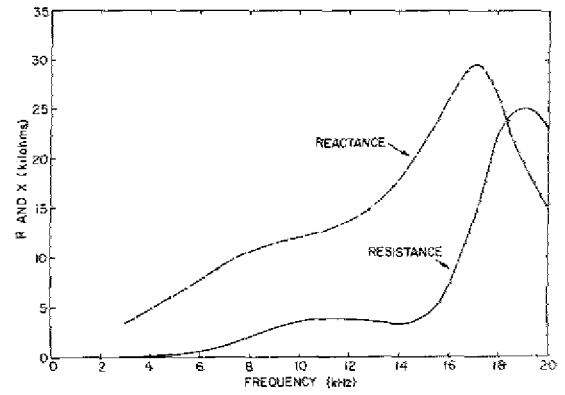
For ring C in Figs. 13a and 13b the Butterworth and Smith model radiation-load components provide an envelope within which the EIGSHIP radiation-load components oscillate. The frequencies of the acoustic cavity type mode (defined and discussed in Section 5.1.3) at 5 and 15.5 kHz as well the values of the radiation load components are well represented by the Butterworth and Smith model. In Fig. 13a the erratic behavior of the EIGSHIP-model radiation load is due to the first and second radial elastic modes. At these frequencies, 8 and 9.3 kHz, the real part of the radiation load is small.

Figures 14, 15, and 16 present graphs of the real acoustic power delivered to the water medium as a function of frequency for the EIGSHIP model and the Butterworth and Smith model for ring A, ring B, and ring C. For ring A (Fig. 14) both models yield identical results; therefore only one curve is drawn. In Figs. 15 and 16 the curve for the Butterworth and Smith model essentially follows that of the EIGSHIP model except near 14 and 8 kHz respectively.

*See Section 7 and Fig. 39 for definition and numbering of bands.

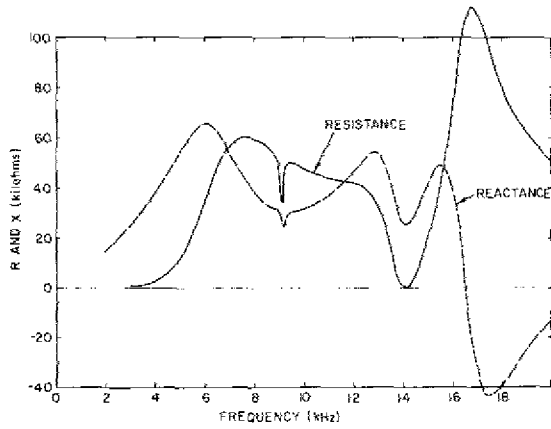


(a) Theory: EIGSHIP

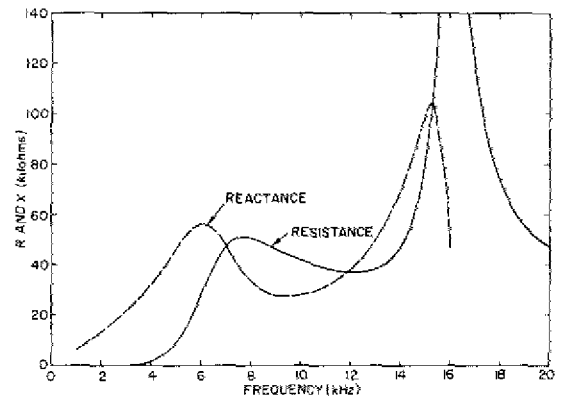


(b) Theory: B and S

Fig. 11 — Resistive and reactive components of the radiation load for ring A

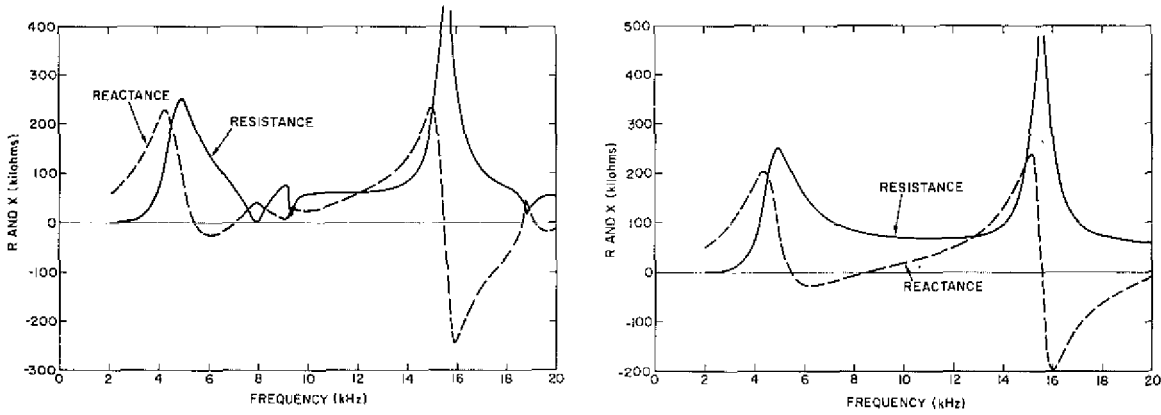


(a) Theory: EIGSHIP



(b) Theory: B and S

Fig. 12 — Resistive and reactive components of the radiation load for ring B



(a) Theory: EIGSHIP (b) Theory: B and S
 Fig. 13 — Resistive and reactive components of the radiation load for ring C

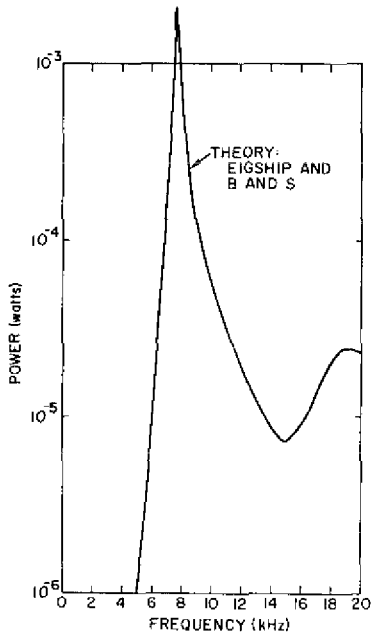


Fig. 14 — Acoustic power into water medium for ring A

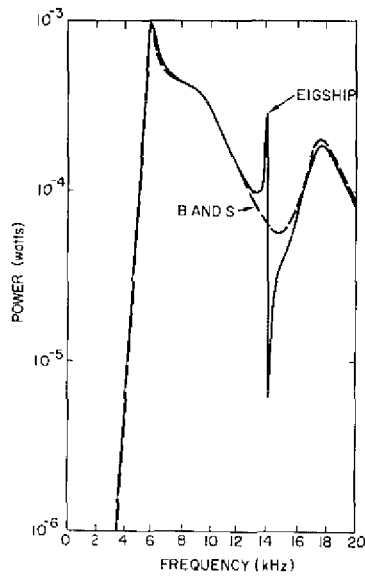


Fig. 15 — Acoustic power into water medium for ring B

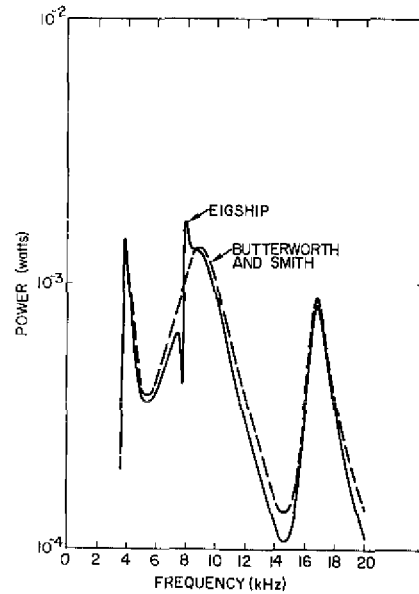


Fig. 16 — Acoustic power into water medium for ring C

Figures 17, 18, and 19 present graphs for rings A, B, and C respectively that compare the power-conversion efficiency of the EIGSHIP model and the Butterworth and Smith model. In Fig. 17 for ring A the efficiency predicted by the Butterworth and Smith model essentially duplicates the efficiency predicted by the EIGSHIP model. In Fig. 18 for ring B again the Butterworth and Smith model follows the EIGSHIP model except at the second-radial-mode resonant frequency of 14 kHz. In Fig. 19 for ring C (the long ring) the graph from the Butterworth and Smith model again follows the graph from the EIGSHIP model except at the 8-kHz and 9.3-kHz resonances, and it peaks at its own radial resonant frequency of 9 kHz. In each of these three figures the efficiency curves reflect the same behavior as the acoustic power curves in Figs. 14, 15, and 16.

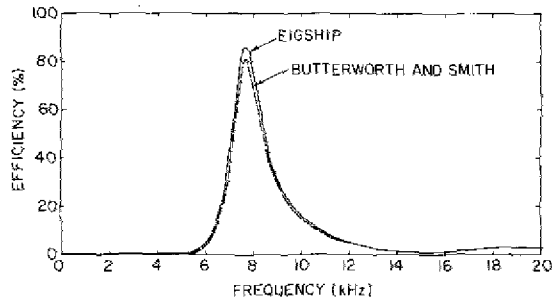


Fig. 17 — Computed power-conversion efficiency for ring A

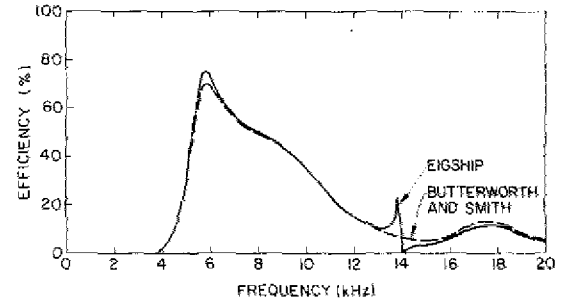


Fig. 18 — Computed power-conversion efficiency for ring B

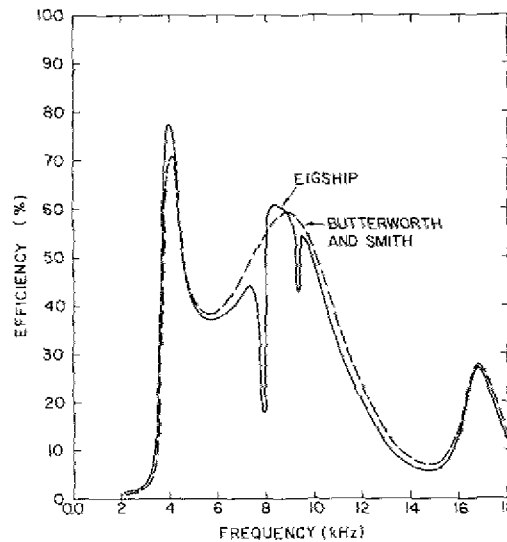


Fig. 19 — Computed power-conversion efficiency for ring C

Figures 20, 21, and 22 present graphs for rings A, B, and C respectively, comparing the experiment with the theoretical predictions of EIGSHIP of the constant-current transmitting response for ring A, ring B and ring C. The constant-current transmitting response is taken in two directions: in the plane of the ring on an extended radius and on the geometric axis (z) of the ring. The constant-current transmitting response is 20 log of the calculated value of the acoustic pressure in the far field of the source, referred back to 1 meter, when the source is driven at 1 ampere over the frequency range of interest.

Figure 20, which displays the transmitting current response for ring A, shows that for the in-plane response the EIGSHIP prediction is in good agreement with experiment, with a 2-dB discrepancy at the radial resonance of the ring at a frequency of 7.6 kHz and with greater discrepancies in the region of frequencies greater than 12 kHz, possibly due to the effect of the coil winding (Section 6). The comparison of the axial response of ring A between theory and experiment is not as good, possibly due to low level of signal (in noise) and the presence of the ring holder.

In Fig. 21 for ring B the radial (in-plane) response comparison is good, with EIGSHIP being about 2.5 dB larger than the experimental value at the cavity resonance frequency of 5.8 kHz. EIGSHIP correctly predicts the peaks and holes in the in-plane (radial) and on-axis responses except for an additional dip in the experimental curve at 6.4 kHz.

In Fig. 22 for ring C, the EIGSHIP prediction for the radial (in-plane) response is again within about 2 dB of the experimental data over the frequency range shown. The EIGSHIP-predicted axial response agrees in frequency with the experimental data for the resonant peaks at 4 and 8 kHz but disagrees in predicting the frequency at the minimum response occurring at 14.8 and 16.8 kHz. In addition the agreement in the magnitude of the axial constant-current transmitting response between theory and experiment is the poorest of any of the rings.

Figures 23 through 25 are selected far-field directivity patterns, some of which correspond to notable features of the transmitting current responses. The in-plane pressure level at 0 degrees was arbitrarily adjusted for each plot.

Figure 26 shows theoretical and experimental values for the magnitude of surface acoustic pressure along the length of the ring at several frequencies. At 7800 Hz (theoretical) and 7825 Hz (experimental) the surface pressure distribution is primarily due to the presence of the first radial mode. At higher frequencies both theory and experiment show that the center of the ring no longer has the highest magnitude of pressure. This is a result of surface pressure cancellation due to the presence of the barrel mode. A one-degree-of-freedom model such as that of Butterworth and Smith would not predict this behavior. The experimental evidence thus demonstrates the presence of a barrel mode.

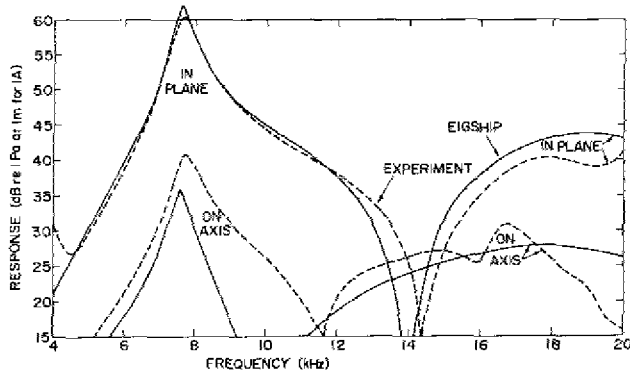


Fig. 20 — Constant-current transmitting response for ring A at 1 meter in the plane of the ring and on the axis of the ring when driven at 1 ampere

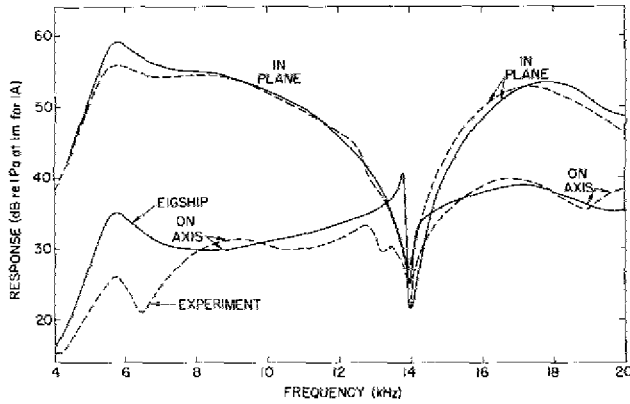


Fig. 21 — Constant-current transmitting response for ring B at 1 meter in the plane of the ring and on the axis of the ring when driven at 1 ampere

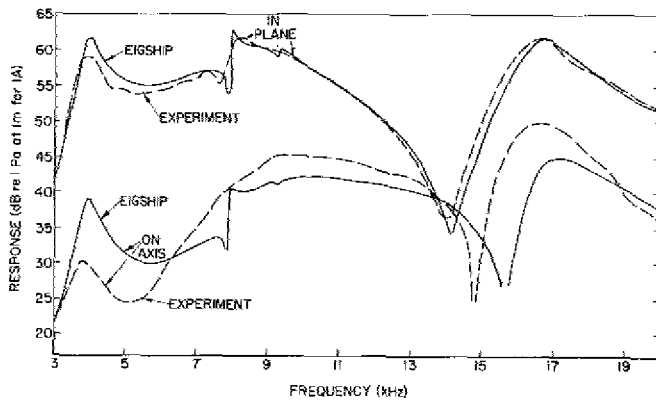
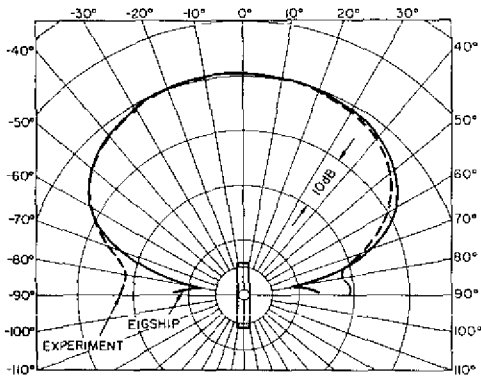
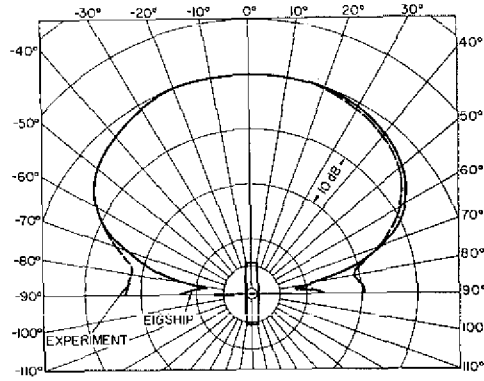


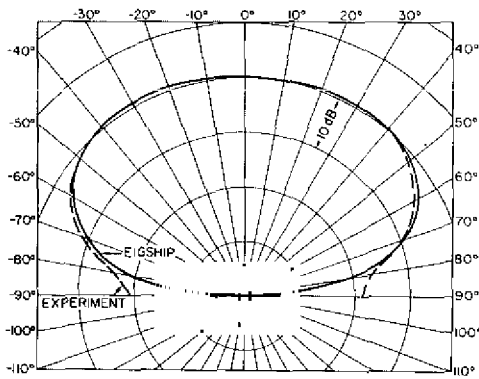
Fig. 22 — Constant-current transmitting response for ring C at 1 meter in the plane of the ring and on the axis of the ring when driven at 1 ampere



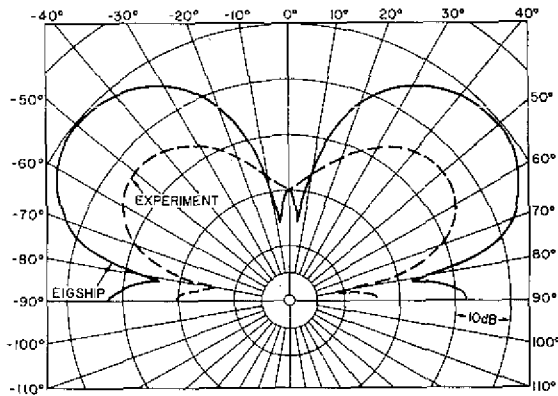
(a) At 7.6 kHz



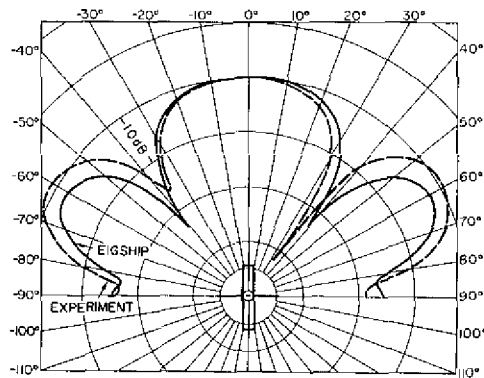
(b) At 8.0 kHz



(c) At 10 kHz



(d) At 14 kHz



(e) At 18 kHz

Fig. 23 — Far-field directivity patterns at selected frequencies for ring A

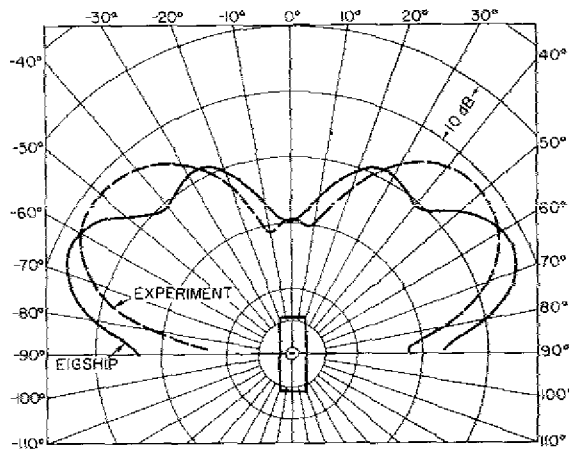
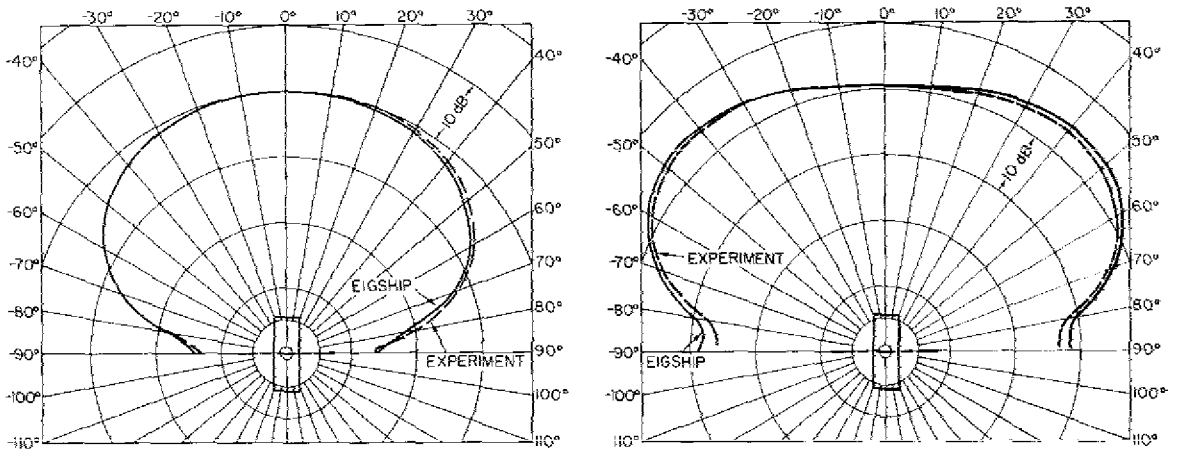
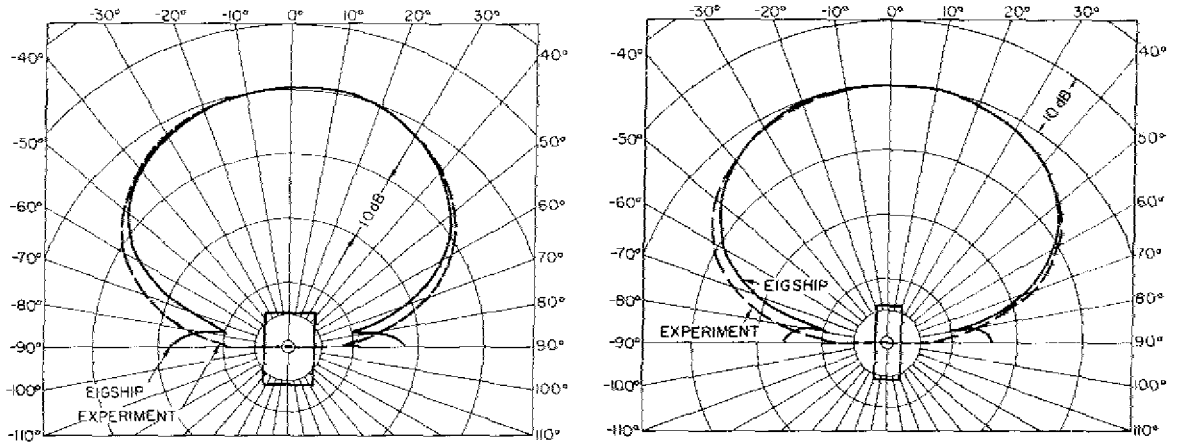


Fig. 24 — Far-field directivity patterns at selected frequencies for ring B

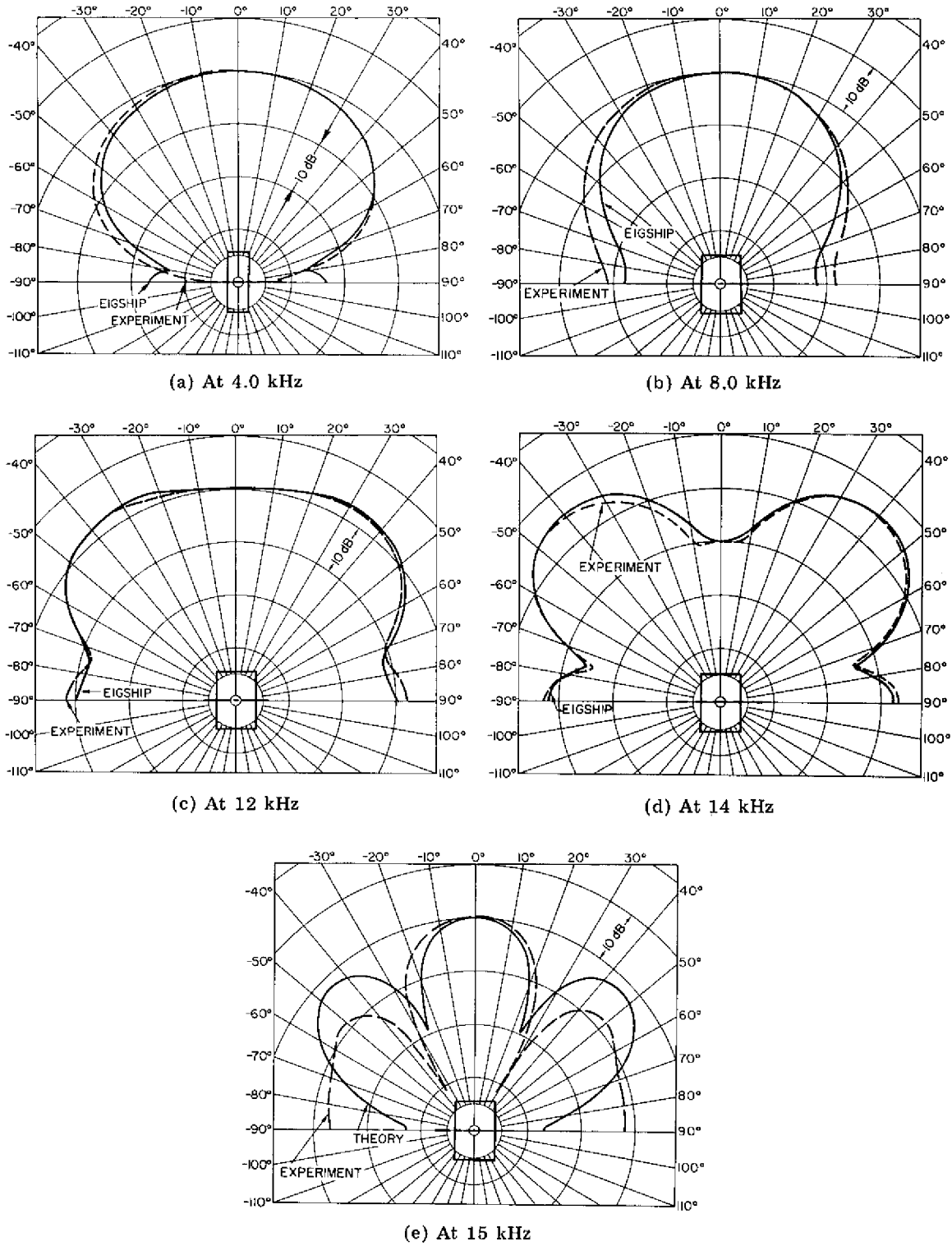


Fig. 25 — Far-field directivity patterns at selected frequencies for ring C

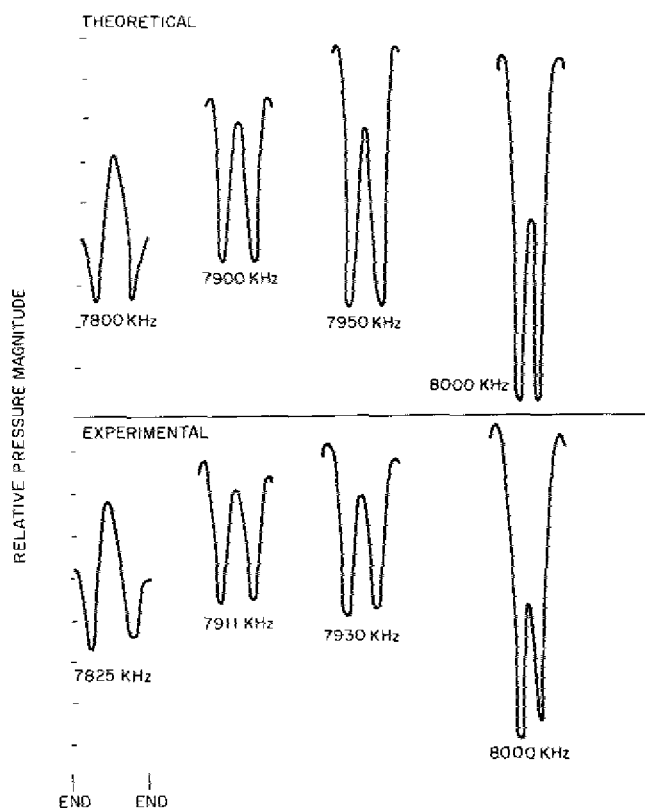


Fig. 26 -- Outer-surface acoustic pressure distribution along the height of ring C

Figures 27 through 29 are graphs of calculated quantities based on EIGSHIP and Butterworth and Smith models. Figure 27 is a graph of the magnitude of the radial velocity in air of band 9 (second band from the top among eight outer-surface bands) on ring C plotted as a function of frequency for the EIGSHIP model and the Butterworth and Smith model and of the axial velocity on band 10 of ring C for the EIGSHIP model (the axial velocity not being available in the Butterworth and Smith model). Figure 28 is a graph of these velocity magnitudes on ring C in water.

5. METHODS USED IN INTERPRETING EIGSHIP PREDICTIONS AND EXPERIMENTAL MEASUREMENTS

The graphical displays of EIGSHIP predictions and experimental measurements given in Figs. 2 through 28 show complicated behavior of the force-driven magnetostrictive shell. We believe they require special tools for their interpretation. To interpret the significance of these graphs in connection with parameters of voltage and current at the electrical terminals, we have used the method of X-vs-R electrical-impedance plots. Similarly to interpret the significance of these graphs in connection with the mechanical terminals of the model we have used the method of X_m -plus- X_L mechanical-reactance plots. A

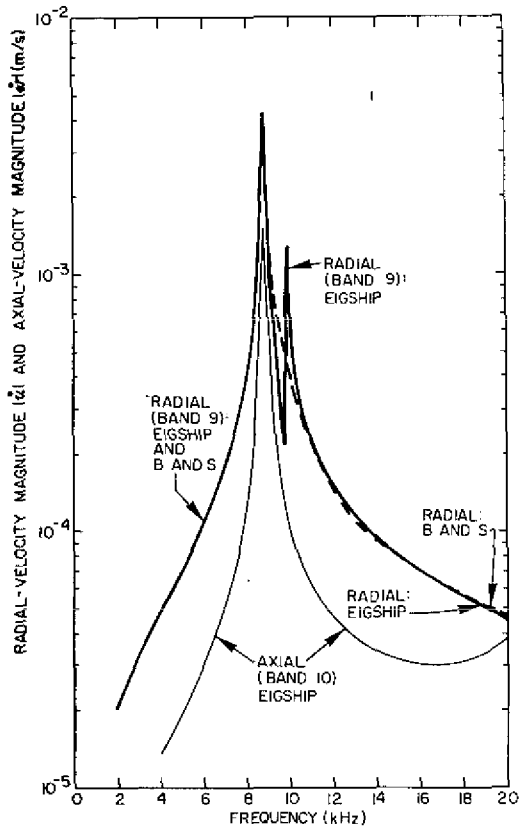


Fig. 27 — Velocity magnitudes for ring C in air. Bands are numbered according to Fig. 2 in Ref. 1 and Fig. 39 in the present report.

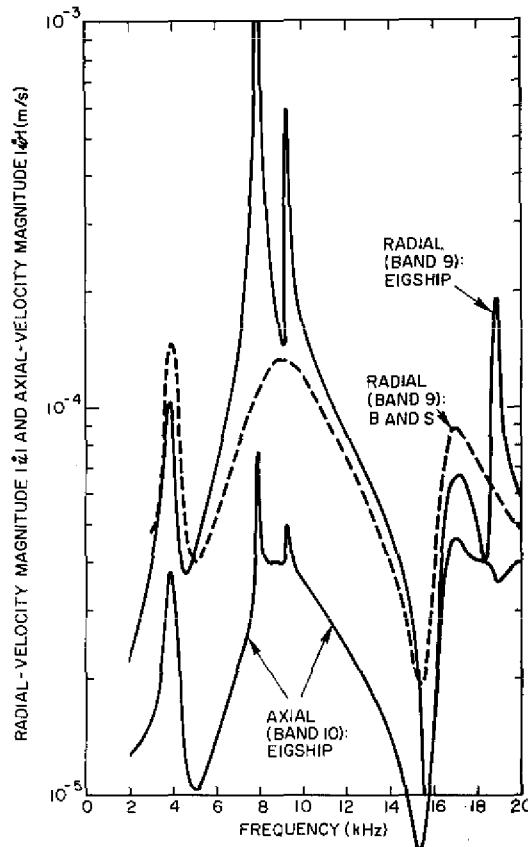


Fig. 28 — Velocity magnitudes for ring C in water

combination of parameters from both types of plots then enables us to interpret the results generated by the mathematical model, as well as to interpret measurements performed by experiments on physical models. The basic features of these plot types will be discussed in the next sections, with explanations of their use in interpretation of transducer performance. In discussing X_m -plus- X_L plots we will briefly review the concepts of *cylinder modes* to aid in understanding the important parameters of radial stiffness and longitudinal (fluid) inertia of the water-loaded shell. In addition we will review the method of obtaining the mechanical reactance X_m of the shell through use of strain energy methods.

5.1 Interpretation of Electrical-Impedance X -vs- R Plots

The electrical input impedance of an electromechanical transducer is the sum of the blocked impedance and the motional impedance. We discuss these two impedances for the case of a toroidally wound magnetostrictive ring.

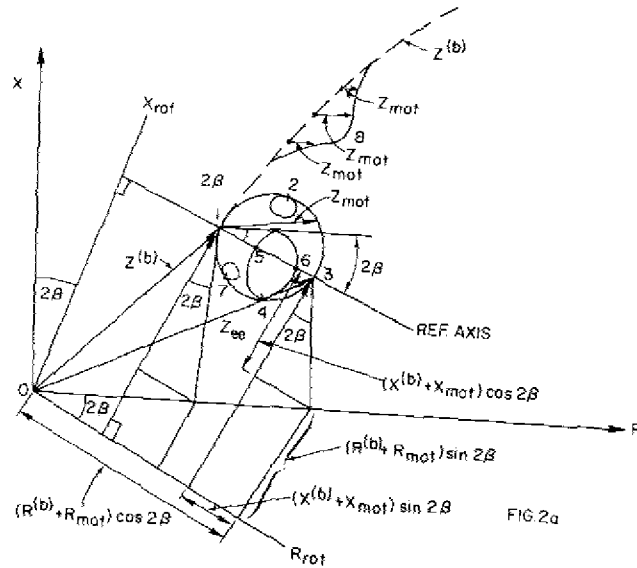


Fig. 29 — Blocked and motional electrical impedance referenced to the rotated coordinate system (R_{rot} , X_{rot}), drawn to illustrate several operating conditions.

5.1.1 Blocked Impedance

The blocked impedance is that of a nickel-core toroidal coil for which

$$Z^{(b)} = R^{(b)}(\omega) + j \omega L^{(b)}(\omega) = R + j X. \quad (5.1)$$

When both R and L are weak functions of ω (are nearly constant), the blocked impedance is an essentially vertical line on an X -vs- R plot. For high enough frequency however both R and L are (gently increasing) functions of frequency due to electrical properties of coil and core, excluding hysteresis and eddy currents. Hence an X -vs- R plot of blocked impedance is a smooth curve with positive slope extending upward from $\omega = 0$. The electrical phase associated with $Z^{(b)}$ is

$$\phi^{(b)} = \tan^{-1} \frac{X^{(b)}}{R^{(b)}}. \quad (5.2)$$

For small resistance losses this angle tends to $+90^\circ$.

5.1.2 Motional Impedance

When the nickel core is driven by external forces distributed over its surface, it vibrates in several (possible infinite) modes of a thin elastic shell. This motion is reflected at the electrical terminals as an added impedance, namely, the motional impedance Z_{mot} , whose mathematical form is given by Eq. (5.24) of Part 1 [1]. This equation shows that Z_{mot} is proportional to the ratio of shell velocity to driving current or, equivalently, inversely proportional to the mechanical impedance of the shell. When the shell is loaded by an unbounded fluid, its mechanical impedance exhibits an indefinite number of maxima and minima (mechanical resonances) as a function of frequency of forced drive. Thus an X -vs- R plot of total impedance consists of a series of (connected) loops of varying size, indefinite in number, tending to become merged into an irregular curve as $\omega \rightarrow \infty$.

5.1.3 Electrical-Impedance Plots

A sketch of idealized blocked and motional electrical impedance is shown in Fig. 29, drawn for the condition of high mechanical Q (>10). When referred to the X -vs- R axes the maximum Z_{mot} vector is inclined at an angle 2β to the horizontal (R axis) due to hysteresis and eddy currents. Since in the following discussion the angle 2β is extraneous, it is convenient to refer all vectors to axes X_{rot} and R_{rot} obtained by rotating the original X and R axes clockwise by the angle 2β . Thus

$$\begin{aligned} (Z_{ee})_{rot} &= (R_{ee})_{rot} + j(X_{ee})_{rot}, \\ (R_{ee})_{rot} &= [R^{(b)} + R_{mot}] \cos 2\beta - [X^{(b)} + X_{mot}] \sin 2\beta, \\ (X_{ee})_{rot} &= [X^{(b)} + X_{mot}] \cos 2\beta + [R^{(b)} + R_{mot}] \sin 2\beta. \end{aligned}$$

In the rotated system (abscissa R_{rot} and ordinate X_{rot}) we define a frequency of *mechanical resonance* ω_f to be that frequency satisfying two requirements:

- ω_f is approached from a positive phase of Z_{mot} , and
- ω_f satisfies the relation

$$(X_{ee})_{rot} = X_{rot}^{(b)} = X^{(b)} \cos 2\beta + R^{(b)} \sin 2\beta. \quad (5.3)$$

These conditions imply that at mechanical resonance

$$(X_{mot})_{rot} = 0$$

or

$$X_{mot} = - \frac{R_{mot} \sin 2\beta}{\cos 2\beta}. \quad (5.4)$$

The electrical phase associated with the motional impedance is defined as

$$\begin{aligned} (\phi_{mot})_{rot} &= \tan^{-1} \left(\frac{X_{mot}}{R_{mot}} \right)_{rot} \\ &= \tan^{-1} \left(\frac{X_{mot} \cos 2\beta + R_{mot} \sin 2\beta}{R_{mot} \cos 2\beta - X_{mot} \sin 2\beta} \right). \end{aligned} \quad (5.5)$$

The various vectors and angles associated with electrical impedance are shown in the idealized sketch of Fig. 29, where both conventional X , and R axes and rotated X_{rot} , and R_{rot} axes are shown. We will use this figure to explain significant features of electrical impedance plots.

To simplify the explanation we also show (Fig. 30) a phase diagram of $(\phi_{mot})_{rot}$ vs frequency. In the following discussion we will use the word *point* to indicate frequency as a parameter and we will assume the blocked impedance $Z^{(b)}$ to (loosely) represent the average blocked impedance over the entire frequency range covered by the major loop 1-2-3-4-7-1:

- At point 1 the electrical impedance is purely blocked ($Z_{ee} = Z^{(b)}$). The motional phase is (asymptotically) $+90^\circ$.
- Between points 1 and 3 the phase $(\phi_{mot})_{rot}$ is positive and diminishing. At point 3 the phase is zero. By definition point 3 is a frequency of mechanical resonance.
- The negative phase $(\phi_{mot})_{rot}$ at point 4 abruptly decreases and becomes 0 at point 5; the phase is positive between points 5 and 6, decreasing to 0 again at point 6; then the phase becomes negative, returning to point 4. By definition the interior loop 4-5-6 has a frequency of mechanical resonance at 6.
- At point 7 the negative phase undergoes a rapid change of a few degrees with increase in frequency, always remaining negative. (A similar event occurs at point 2 where the positive phase undergoes a rapid change of a few degrees but always remains positive.) Points 7 and 2 are frequencies at which a nonresonant change in transducer motion occurs due to "sudden" local changes in (net) stiffness or inertia of the water-loaded transducer under forced drive.

- From the completed loop at 7 to point 1 the phase remains negative and approaches -90° as point 1 is reached.
- At point 1 the idealized phase changes abruptly from -90° to $+90^\circ$.

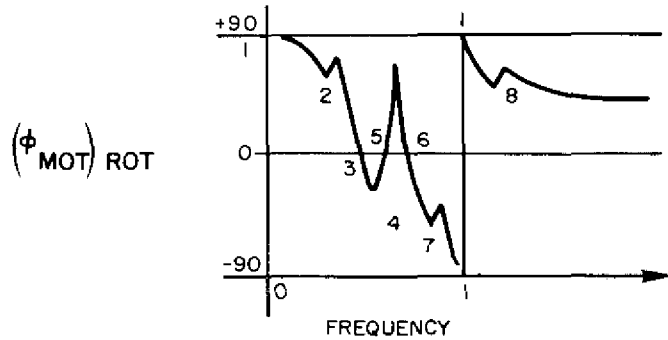


Fig. 30 — Phase diagram that pertains to Fig. 29

5.1.4 Nonresonant Water Modes

In the vicinity of point 8, where the mechanical stiffness of the system changes markedly, the mechanical phase (Eq. 5.9) executes a sharp change of a few degrees but always remains of one sign. This change in stiffness originates in the water (inertial) load, which being a function of frequency may become relatively large at some given point but not large enough to cancel the shell (loaded) stiffness completely. The total impedance curve rapidly changes in curvature but does not form a resonant loop. The condition at point 8 is called here a *nonresonant water mode*.

5.2 Motional Impedance Analysis and $X_m + X_L$ Plots

5.2.1 Motional-Impedance Phase

Under an external mechanical load of mechanical impedance $Z_L (=R_L + j X_L)$ the electrical motional impedance of an electromechanical transducer in forced drive is given [5] by

$$Z_{mot} = A^2 e^{-j2\beta} |Y_m| e^{-j\phi_m} , \quad (5.6)$$

where A is the absolute value of the vector force factor $Z_{em} (=R_{em} + jX_{em})$ and β is the force-factor angle. The symbol $|Y_m|$ is the absolute value of the total mechanical admittance of the transducer, and ϕ_m is the total mechanical admittance angle. Thus, in accordance with these definitions,

$$A^2 = R_{em}^2 + X_{em}^2 \text{ and } \tan 2\beta = \frac{-2R_{em} X_{em}}{R_{em}^2 - X_{em}^2}, \quad (5.7)$$

$$|Y_m| = \left| \frac{1}{Z_m + Z_L} \right| = \frac{R_m + R_L - j(X_m + X_L)}{[(R_m + R_L)^2 + (X_m + X_L)^2]^{1/2}}, \quad (5.8)$$

in which $Z_m = R_m + jX_m$ is the no-load mechanical impedance of the transducer, and

$$\phi_m = \tan^{-1} \frac{-(X_m + X_L)}{R_m + R_L}, \quad -90^\circ \leq \phi_m \leq 90^\circ. \quad (5.9)$$

In this report we measure all angles relative to 2β . The sign of ϕ_m is determined in the simple case of one degree of freedom as follows: the sum $X_m + X_L$ is negative when mechanical stiffness exceeds mechanical inertia in the loaded transducer, and positive when inertia predominates. From Eq. 5.9 it is seen that when stiffness predominates, ϕ_m is positive, and that when inertia predominates, ϕ_m is negative. When $\omega \rightarrow 0$, $\phi_m \rightarrow 90^\circ$, and when $\omega \rightarrow \infty$, $\phi_m \rightarrow -90^\circ$.

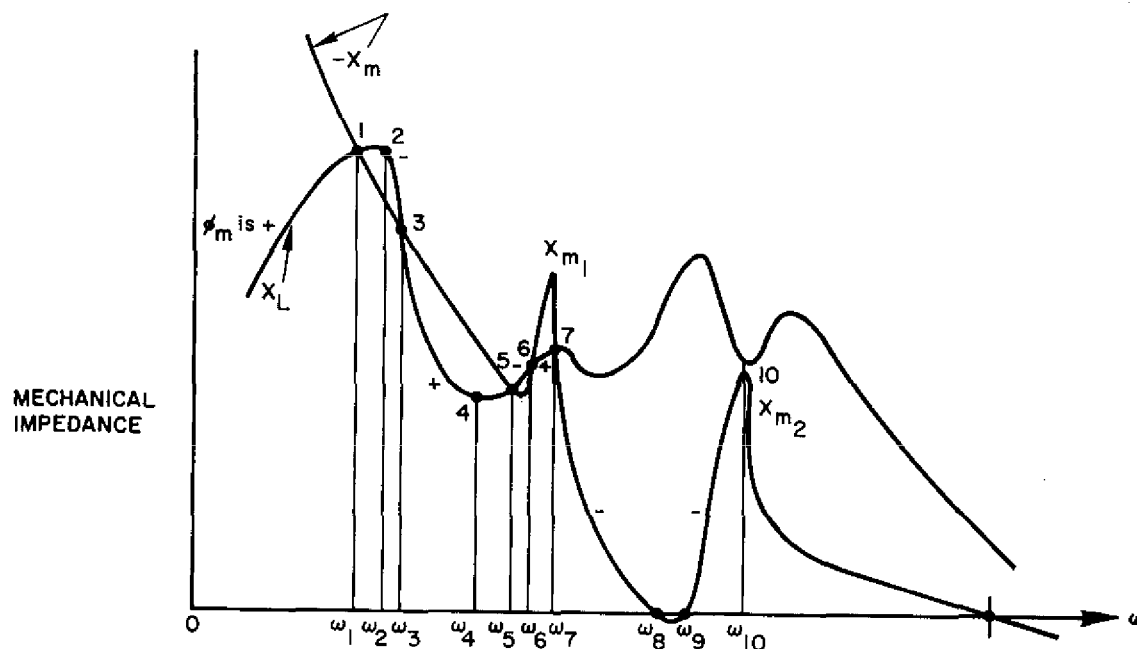
5.2.2 X_m -plus- X_L Plots

Equations 5.6 through 5.9 describe the motional effect of the mechanical vibration of the ring core on the electrical terminals, including resonance. As noted in Section 5.1.3, a frequency of *mechanical resonance* is defined as that frequency of forced drive of the shell for which the phase angle ϕ_m is 0. For a true elastic continuum (such as a magnetostrictive metal shell in a fluid medium) the number of frequencies of mechanical resonance is indefinitely large. To determine the first few of these conveniently, it is useful to superimpose plots of X_m and X_L versus frequency on a single coordinate plane, and visually note points where $X_m + X_L$ falls to 0.

The calculation of X_m is performed as follows: The ring shell is driven in forced vibration in the presence of a load. At a given frequency of forced drive, the resultant shell velocities store kinetic energy, and shell deformations store strain energy. The difference between these two energies multiplied by ω and divided by a velocity normalization factor is X_m . The method of calculation of these quantities and the normalization factor follows in Section 5.3.

The calculation of X_L is performed in accordance with the formulas found in Section 9 of Part 1 [1].

When X_m and X_L are available, it is convenient to plot the negative of X_m and overlay it with a plot of X_L . A typical overlay of $-X_m$ and X_L is shown in Fig. 31.

Fig. 31 — Plot of X_m plus X_L

This plot, as can be seen from Eq. 5.9, may also be used to identify sign changes in the phase ϕ_m under the assumption that $R_m + R_L$ is positive. The significance of the $-X_m$ and X_L curves, and the selected frequencies ω_1 to ω_{10} , are as follows:

- The $-X_m$ curve begins with a maximum (say X_{m_0}) at $\omega \rightarrow 0$, and shows a diminishing trend as ω is increased, except for recurrent peaks $-X_{m_1}$, $-X_{m_2}$, Each maximum corresponds to a different spatial pattern of displacement of the shell (independent of amplitude).
- The X_L curve begins at $X_L = 0$ at $\omega = 0$ and shows thereafter a succession of peak and valleys as ω increases. When $X_L \geq X_m$, we say the shell is load (cavity) controlled.
- In the region $\omega < \omega_1$ it is seen that $-X_m > X_L$. This condition indicates that stiffness reactance in radial displacement dominates the reactance of the system of shell and fluid. Since stiffness reactance is negative (in this report) ϕ_m is positive.
- At $\omega = \omega_1$ the sum $X_m + X_L$ is 0. The reactance X_m is predominantly stiffness in uniform radial motion, and the load reactance X_L is predominantly inertial. Since the phase ϕ_m approaching ω_1 is positive, we identify ω_1 as a frequency of mechanical resonance controlled by the water load, in nearly uniform radial motion.
- At $\omega = \omega_2$ the transducer is water-load (cavity) controlled and the phase ϕ_m is negative.

- At $\omega = \omega_3$ the sum $X_m + X_L$ is again 0 and the phase ϕ_m approaching ω_3 is negative. Hence ω_3 is a frequency of small motion in the uniform radial pattern of displacement.
- At $\omega = \omega_4$ the phase ϕ_m is again positive and motion with the spatial displacement of the pattern of peak X_m is increasing in amplitude. The transducer is stiffness controlled.
- At $\omega = \omega_5$ there is a frequency of mechanical resonance with an associated spatial pattern of displacement which is different from that at $\omega = \omega_1$.
- Between ω_5 and ω_6 the transducer is water-load or inertia controlled. The phase here is negative. Between ω_6 and ω_7 the transducer is stiffness controlled again and the phase is positive.
- At ω_7 the phase ϕ_m switches back to negative and remains negative throughout ω_8, ω_9 , and ω_{10} . Between ω_8 and ω_9 the shell reactance is predominantly inertial whereas between ω_9 and ω_{10} it becomes a stiffness reactance once more with an associated shell motion of a second mode (peak at X_{m_2}).
- At ω_{10} the sum $X_m + X_L$ is small but not 0. The phase ϕ_m remains negative between ω_9 and ω_{10} , although it rapidly changes in magnitude. We call ω_{10} a *nonresonant water-controlled mode*.

5.3 Strain and Kinetic Energy Formulas

As noted in Section 5.2.2, the calculation of both X_m and X_L require special methods in the case of a magnetostrictive shell. These are discussed now. The mathematical model of EIGSHIP is based on the assumption of axisymmetric motion. In determining strain energy (U) and kinetic energy (T) of the shell, and from them the mechanical reactance X_m , we use the formulas of Sharma [6] for the special case of axisymmetric motion. Thus the relevant EIGSHIP formulas (using symbols given in Table 1) are

$$\text{strain energy: } U = \frac{Y(1-k^2\chi_R)ab2\pi}{(1-\nu^2)} \left\{ \int_{-\ell/2}^{\ell/2} \left[\frac{\partial u}{\partial x} \left(\frac{\partial u}{\partial x} \right)^* + \frac{w w^*}{a^2} + \frac{2\nu}{a} \frac{\partial u}{\partial x} w^* \right] dx \right. \\ \left. + \frac{b^2}{12a^2} \int_{-\ell/2}^{\ell/2} \left[a^2 \frac{\partial^2 w}{\partial x^2} \left(\frac{\partial^2 w}{\partial x^2} \right)^* + \frac{w w^*}{a^2} - 2a \frac{\partial u}{\partial x} \left(\frac{\partial^2 w}{\partial x^2} \right)^* \right] dx \right\}$$

and

$$\text{kinetic energy: } T = 2\pi\rho ab \int_{-\ell/2}^{\ell/2} \left[\left(\frac{\partial u}{\partial t} \right)^2 + \left(\frac{\partial w}{\partial t} \right)^2 \right] dx.$$

The symbols u and w represent displacement in the axial and radial directions respectively. The factor $(1 - k^2 \chi_R)$ is due to constant-current drive. It is not present for constant-voltage drive. Also rms values are assumed in these formulas, which cause them to differ from those in Sharma by a factor of 2. From U and T the inertial and stiffness reactances are obtained as follows:

$$\text{medium inertial reactance } ZKN = j\omega T/VNM$$

and

$$\text{Shell Stiffness Reactance } ZST = j\omega U/VNM,$$

where VNM is a velocity normalization factor. EIGSHIP (described in Section 7) obtains integrals for U and T using an expansion of u and w [1, pp. 19ff] in terms of modal shapes and integrating the modal shapes analytically. VNM itself is calculated using band velocities:

$$VNM = \sum_{\substack{i \\ \text{all bands}}} v_i v_i^* A_i / [4\pi a(\ell + b)],$$

where v_i represents the numerical value of normal velocity on the i th band as calculated by EIGSHIP and A_i represents the area of the i th band.

6. AN ELECTRIC-IMPEDANCE ANALYSIS OF THE ACOUSTIC PERFORMANCE OF RING C

The methods of X -vs- R plots, and X_m -plus- X_L plots described in Section 5 can be applied to each of the Figs. 2 through 28 to obtain an interpretation of the theoretical and experimental data of our models. We will illustrate the use of these methods by making a complete electromechanical analysis of ring C. This particular ring is selected because it shows a wealth of elastic and piezomagnetic responses over the frequency range 1 to 20 kHz.

The physical dimensions of ring C together with its elastic and electromagnetic properties are given in Table 1. The electroacoustic performance of this underwater sound transducer as predicted by theory, and as measured by experiment, are found in the following plots and graphs:

- Predicted total electric impedance in water, Fig. 32;
- Measured total electric impedance in water, Fig. 33;
- Predicted and measured constant-current transmitting response, Fig. 22;

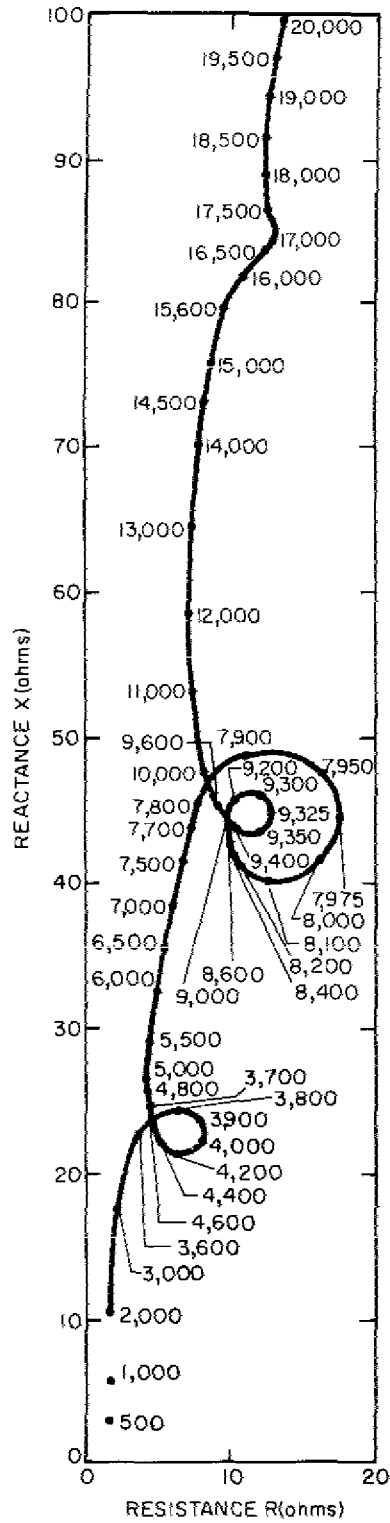


Fig. 32 -- Theoretical total electric impedance (Z_{ee}) of ring C in water

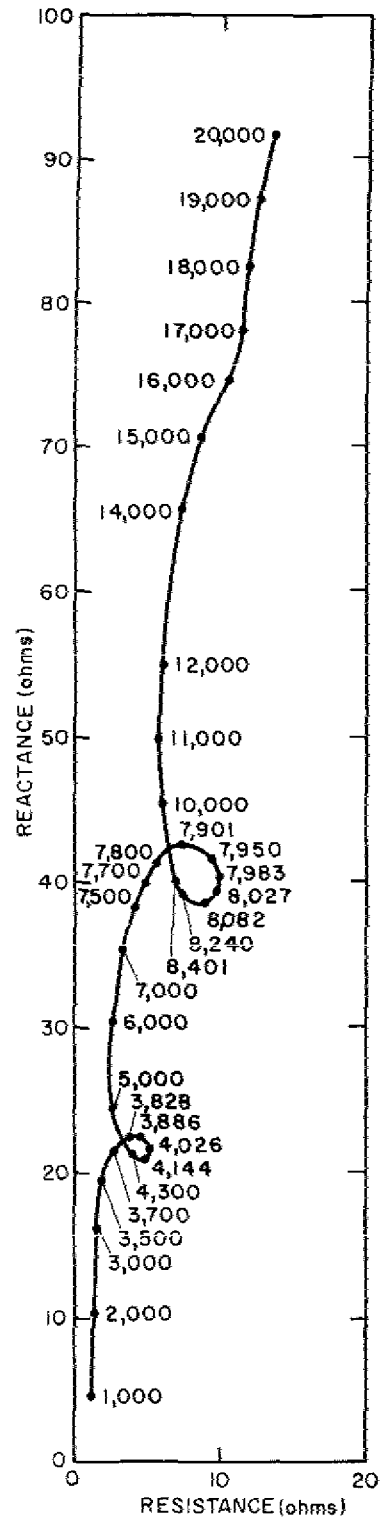


Fig. 33 -- Experimental total electrical impedance of ring C in water

- Predicted and measured far-field radiation patterns at 4.0, 8.0, 12, 14, and 15.8 kHz, Fig. 25;
- Predicted total electrical reactance and resistance in water, Fig. 7b;
- Predicted radiation loading, Fig. 13a;
- Predicted relative pressure magnitude distributions on the transducer surface, Fig. 26;
- Predicted total electrical reactance and resistance in air, Fig. 4b;
- Predicted motional electric impedance in water, Fig. 34. Each motional value has been rotated (as described in Section 5.1.3) by the angle 2β (twice the value of the hysteresis and eddy-current angle at the appropriate frequency);
- Predicted mechanical reactance in water, Fig. 10;
- Predicted surface velocity in air and water, Figs. 27 and 29.

Although the general theoretical basis for predicting the performance of ring C is detailed in Part 1 [1], a more explicit elucidation of the particular results of computation contained in the plots and graphs just listed is needed because of the complexity of the predictions. This follows. To assure better understanding we will adhere to the definitions and concepts of analysis developed in Section 5.

6.1 EIGSHIP Prediction of Surface Velocity

The interpretation of the electroacoustic performance of ring C requires a graphical display of the absolute magnitude of the (spatially averaged) radial and axial surface velocities versus frequency both in air and in water as predicted by EIGSHIP. These are found in Figs. 27 and 28 along with the radial surface velocities predicted by the Butterworth and Smith model. An additional graph, which displays the predicted acoustic power radiated versus frequency for both the EIGSHIP model and the Butterworth and Smith model, is shown in Fig. 16. These graphs will be used in the following discussions.

6.2 Computer Determination of Resonant Frequencies in Air and Calculation of EIGSHIP Input Data

We consider first the predicted total electrical reactance and resistance of ring C in air, Fig. 4b. For the condition of free vibration our elastic resonances are predicted by EIGSHIP in the frequency range 0 to 40 kHz. These are listed here accompanied by sketches of their predominant elastic shapes (center to one end in the length direction):

$f_1 = 9231$ Hz,

$f_2 = 9972$ Hz,

$f_3 = 21,452$ Hz,

$f_4 = 23,510$ Hz.

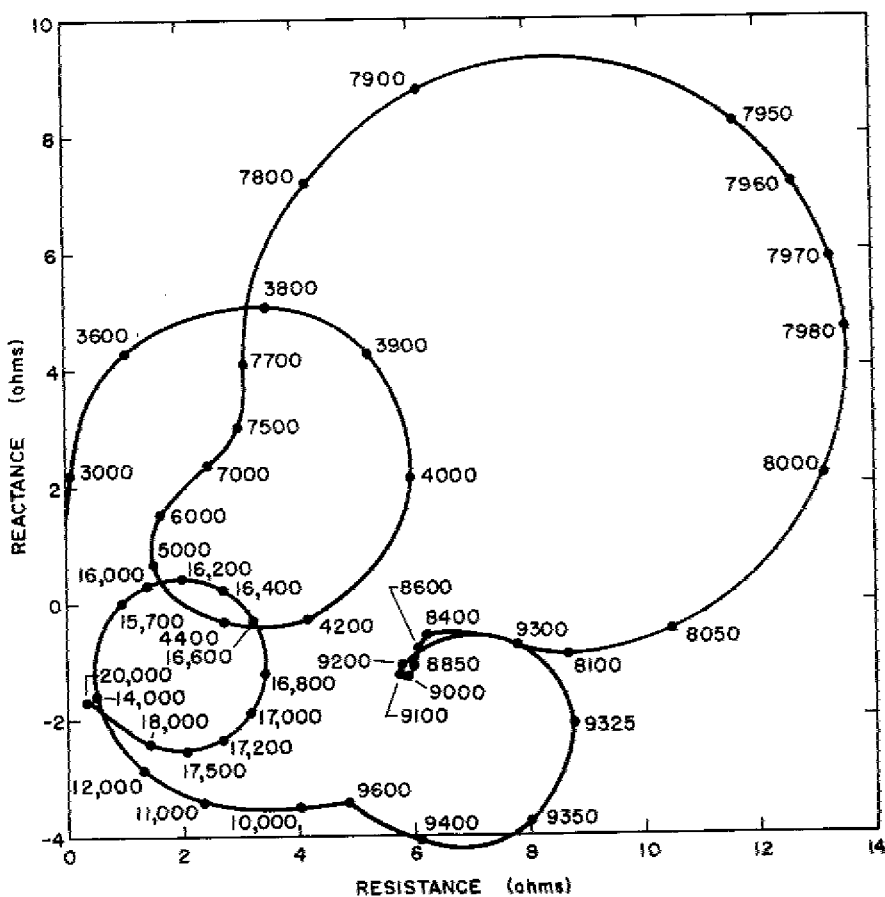
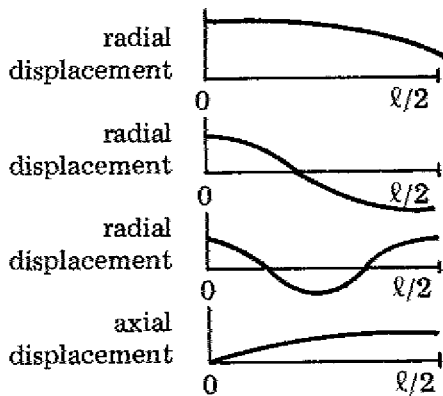


Fig. 34 -- Theoretical motional electric impedance of ring C in water (Z_{motw}), adjusted by multiplying Z_{motw} by $e^{j2\beta}$

As noted in Section 3, the measured total reactance and total resistance in air are used to obtain needed values of parameters to serve as input to EIGSHIP. In particular, by drawing the lower frequency slope to the reactance curve, one obtains the magnetic permeability μ . In addition, by constructing the electrical motional impedance diagram in air, one obtains a value for the hysteresis and eddy-current dip angle 2β and obtains the mechanical Q at constant current. These values serve as EIGSHIP input data.

The displacement curves of ring C in water are shown in Fig. 35. They were obtained by EIGSHIP, from reference surface velocities in water as calculated from EIGSHIP with constant-current drive, by first dividing the velocity magnitude by the appropriate frequencies to obtain displacement. The angle variation was accounted for by arbitrarily setting the phase of the displacement at the first band (near the center of the shell) to 0 so that the magnitude represented the actual displacement, and adjusting displacements on the other eight bands accordingly. The phase difference between those bands that have positive displacements and those bands that have negative displacements is nearly 180° except possibly for displacements of relatively small magnitude, so that the positions of the modes illustrated in curves for 9340 Hz and 7960 Hz vary little over one cycle of motion and the displacement at the end of the shell effectively represents the maximum displacement of the end over the cycle of motion.

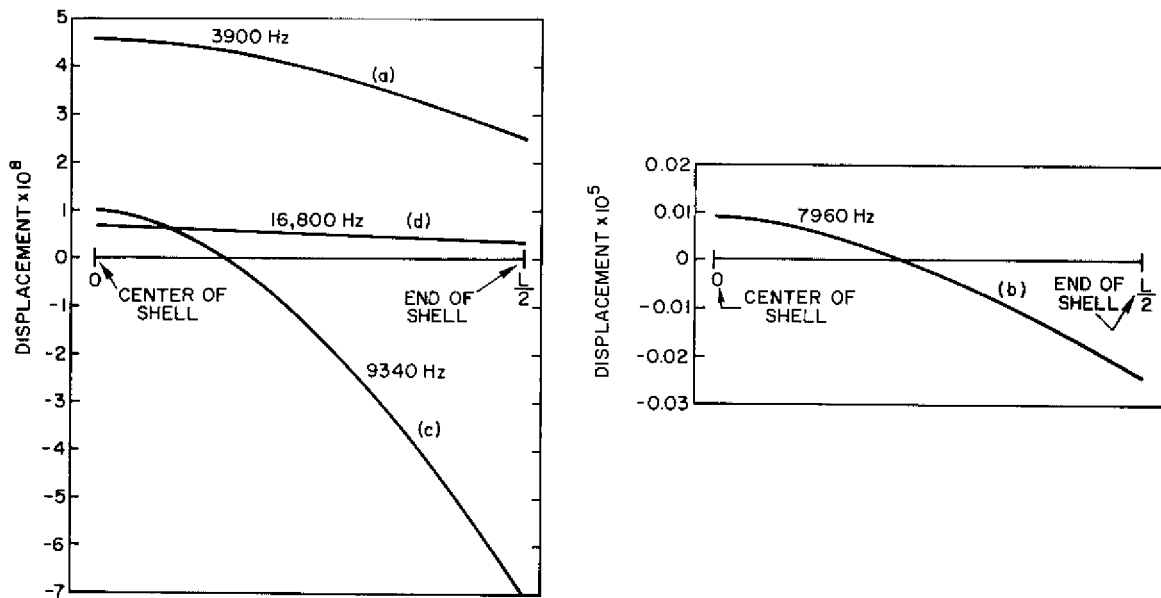


Fig. 35 — Radial displacement as predicted by EIGSHIP of the reference surface of ring C in water plotted along the length of the shell from the middle to the end for four discrete frequencies

6.3 Predicted Total Electrical Impedance and Its Theoretical Significance

The predicted total electrical impedance $Z_{tot} = R_{tot} + jX_{tot}$ in water is shown in Fig. 32. This is a plot of X_{tot} vs R_{tot} with frequency as parameter. It shows several frequency ranges where the motion of the ring in water noticeably alters the electrical impedance of the simple coil wound on a nickel core. These ranges are 3500 to 4500 Hz, 7500 to 8600 Hz, 8600 to 10,000 Hz, and 13,000 to 18,000 Hz. These are the ranges of immediate interest, and we shall analyze them in accordance with the definitions and concepts of Section 5. To this end we use the $-X_m + X_L$ diagram (Fig. 10), the electrical motional impedance diagram (Fig. 34), the radiation load diagram (Fig. 13a), and various far-field pressure patterns (Fig. 25).

6.3.1 Electrical Impedance Disturbance in the Vicinity of 4 kHz

In Fig. 34 the predicted motional impedance vector increases to a peak magnitude of $|Z_{mot}| \approx 7$ electrical ohms at a frequency of ≈ 3900 Hz. The motional resistance is almost a maximum as well, thus leading to the conclusion that the frequency in the vicinity of 3900 Hz is a point of (local) maximum (effective) axial and radial surface velocities, as well as maximum transmitting response. The curve of radial displacement (Fig. 35) is similar to the deformation shape of the first air radial mode (sketched in Section 6.2). It exhibits bending but has no nodes. The point of zero motional phase angle (Fig. 34) is approximately 4180 Hz. In the range 4180 to 4600 Hz the motional phase angle is negative (Fig. 10), indicating inertial control of the motion. At 5000 Hz the (effective) surface velocities (axial and radial) are small because of the high impedance of the transducer-medium system. At 5400 Hz the radiation reactance drops to zero and then become negative, remaining so until 7000 Hz.

We interpret the impedance disturbance near 4000 Hz as follows: The elastic cylinder-water complex is a combination of an elastic ring which views an unbounded medium on three sides (outside surface and two ends); surrounding-within itself a cylindrical rod of water which views the medium at its two water ends. The elastic ring acting as a dynamic radiator of sound develops an inertial reactance of the medium to its own motion. Its self-reactance is that of a *stiffness* ($-X_m$ curve in Fig. 10). The cylindrical rod of water when vibrating generates a self-impedance which is the sum of a stiffness of the fluid acting as a rod and an inertial reactance of the radiation mass accompanying the squirting of fluid from the ends. In accordance with numerical calculation it can be shown that a cylindrical rod of water for the dimensions of ring C and the ring wall impedance actually present is in "longitudinal half-wave resonance" at a frequency near 4200 Hz [7]. In this resonant state the longitudinal stiffness cancels the inertial radiation mass of the water rod, leaving only the inertial reactance of the medium on the exterior surfaces of the ring and the stiffness reactance of the ring itself. Figure 10 shows that the two latter reactances cancel at approximately 4100 Hz. From this we conclude that near 4 kHz the ring radial velocity will be a maximum, the transmitting response (Fig. 22) in the radial plane will peak due to the momentary existence of a maximum in radial motion and in electrical resistance (Fig. 34), and the transmitting

response in the axial direction (Fig. 22) will peak due to the relatively large axial motion of the ends of the interior water rod vibrating in longitudinal motion.

As the frequency increases beyond 4.6 kHz, the medium reactance drops. This is interpreted as due to the accession of cavity stiffness in the *radial direction* (Fig. 10) and the detuning of the longitudinal mode of rod vibration. Both effects sharply reduce the system motion. At 5.4 kHz the radial stiffness of the water in the cavity begins to dominate the reactance (Fig. 10). This condition of negative reactance continues with increasing frequency until it itself begins to be canceled by the inception of a new mode of motion of the ring as the frequency of 7 kHz is approached. As described in the next subsection this new deformation shape couples with the medium to generate an inertial reactance of the medium which soon dominates the radial stiffness of the fluid cylinder, producing an inertial reactance of the system beginning at 7 kHz.

6.3.2 *Electrical Impedance Disturbance in the Vicinity of 8 kHz*

In the vicinity 7960 Hz the motional impedance rises to a peak magnitude of $|Z_{mot}| \approx \sqrt{(13.6)^2 + (7.2)^2} = 14.5$ electrical ohms at positive phase of approximately 30° (Fig. 34). Since this maximization occurs in the vicinity of a (local) maximum value of motional resistance, the frequency 7960 Hz is a (local) point of maximum (effective) transducer velocity (Fig. 28). The curve of radial displacement (Fig. 35) shows that there are two nodes at symmetrical positions approximately 0.2 λ from the center, with the radial displacement at the ends of the cylinder having about twice the magnitude of the center displacement. The point of zero motional phase is at $f_3 \approx 8040$ Hz (Fig. 34), with an associated magnitude of motional impedance of 11.4 ohms. In the frequency range 8200 to 9300 Hz the net mechanical reactance is small, the motional phase angle is negative, and the magnitude of motional impedance varies from 6 to 8 ohms (Fig. 34).

We interpret the impedance disturbance near 8000 Hz as follows: From Fig. 10 it is noted that the radiation reactance reaches an (inertial) maximum at 8000 Hz, then drops to near 0 at 9000 Hz. The radiation resistance (Fig. 13a) is small at 8000 Hz, and rises to a maximum at 9000 Hz. We say that this reactance sequence follows the *reactance-resistance* sequence at 4000 Hz and hence that the cavity reactance again becomes small at 8000 Hz. The remaining external inertial reactance of the ring cancels the stiffness of the ring, thus generating the large motional impedance effect noted. This cancellation is effectively present over the (wide) band of frequencies from 8000 to 8800 Hz.

An important feature of the dynamical motion near 8000 Hz is the marked increase in stiffness (decrease in stiffness) during a frequency sweep when the radial deformation involving the two nodes (7960-Hz curve in Fig. 35) supercedes the nonmodal radial deformation associated with 4 Hz (3900-Hz curve in Fig. 35). This increase in stiffness is seen in Fig. 10 as a vertical perturbation of the $-X_m$ curve for the ring at 8000 Hz. It is also seen in Fig. 34 in the region between 6000 and 7700 Hz, where the motional impedance curve reverses its curvature. The sudden increase in stiffness of a new modal

shape causes the surface pressure distribution to radically change, as shown in Fig. 26, from a maximum at the center at 7800 Hz to a minimum at the center at 8000 Hz, with the result that there is a transient drop in radiation to the far field, appearing in the predicted transmitting response as a 3-dB dip between 7600 and 7800 Hz (Fig. 22). The higher frequency side of this dip is very closely followed by a rise in motional impedance as the high- Q two-node modal motion takes over that peaks at ≈ 7960 Hz (Fig. 34). The large radial transmitting response (Fig. 22) at 8000 Hz is attributable to the coincidence of the cancellation of stiffness of the ring and inertia of the medium plus the pronounced reduction in cavity reactance.

In the vicinity of 9200 Hz the radiation resistance peaks, attributable to a cavity-type longitudinal mode. This peaking leads to the prediction that the axial transmitting response will also rise (Fig. 22).

The maximization at 7960 has just been noted to correspond to a (radial) deformation curve featuring a pair of symmetrical nodes located 0.2ℓ from the center. Starting at 8600 Hz (Fig. 34) the deformation shape begins to change, and at 9340 Hz the pair of displacement nodes is symmetrically located approximately 0.1ℓ from the center (Fig. 35), making the ring more stiff. This increased stiffness makes $-X_m$ less negative (less inertial). The motional effect therefore rises again (Fig. 34), reaching a maximum at 9340 Hz, where the motional impedance has a magnitude of 9 electrical ohms. Since the mechanical Q of this mode exceeds 80, we predict a rapid perturbation of the planar transmitting response, in which the magnitude of perturbation is small because the motion of the ring is controlled by residual reactance (Fig. 10), rather than by resistance.

6.3.3 *Electrical Impedance Disturbance Above 14 kHz*

In Fig. 34 the motional impedance vector at 14 kHz is approximately 1.7 ohms in magnitude at an angle of approximately -72° with a motional resistance component of 0.2 electrical ohm. The motion of the ring is small, and the associated reactance is highly inertial. As the frequency is increased, the radiation reactance drops to 0 at 15.5 kHz (Fig. 10) and then becomes negative, that is, changes from inertial to stiffness reactance. At $f = 15.7$ kHz the motional phase angle is 0. Between 15.7 and 16.5 kHz the elastic ring exhibits inertial reactance while the medium exhibits stiffness, with stiffness predominating (Fig. 10). Hence the motional phase angle is positive in this range. At 16.5 kHz (Fig. 10) the ring inertia overcomes the cavity stiffness and the phase angle switches back to negative. At 16.8 kHz the electrical motional impedance vector reaches a maximum magnitude of about 3.7 electrical ohms (Fig. 34). At 18 kHz the ring inertia still predominates over the cavity stiffness, and the total reactance is large (Fig. 10). This indicates little motion of the radiating surfaces. At the frequency of maximum electrical motional impedance (16.8 kHz) the shape of radial deformation is similar to the shape at 4 kHz (Fig. 35).

We interpret the electrical impedance disturbance in the range 14 to 18 kHz as follows: From Fig. 13a the reactance-resistance peaking sequence is similar to the same sequence at 4 kHz. Hence we must consider the dynamical response of the ring to be

strongly related to the effects of the water in the cavity. Between 10 and 14 kHz the ring-medium system is *highly reactive because the medium and the elastic ring are both inertial in behavior* (Fig. 10). This accounts for the steep decline of the ring transmitting response in *both* the radial and axial directions (Fig. 22). In addition, at a frequency of 13,742 Hz the radiation to the far field exhibits a minimum in the radial direction, as will be explained in the next subsection. Thus the *radiated power* in the axial direction (the real power delivered by the transducer to the far field) is at a minimum in the vicinity of 14 kHz. We conclude that both near-field effects (as exhibited by the small surface velocity) and far-field effects (as exhibited by the near-zero radial radiation) control the decline in the radial transmitting response in this region. Between 15 and 16 kHz however the medium reactance plunges from a highly inertial to a highly stiffness controlled reactance (Fig. 10). This switch in reactance is due to the onset of radial stiffness of the water in the cavity. At 15.7 kHz this radial stiffness cancels the ring (elastic) inertia, *thereby setting the ring free* to begin its motion. Between 15.7 and 16.5 kHz the motion rises rapidly, bringing the motional phase to 0 at ≈ 16.5 kHz (Fig. 34). At 16.8 kHz the electrical motional impedance vector reaches a maximum magnitude. At this frequency both the radial and axial transmitting responses are at their maximum values. *The interior fluid of the cavity is in a form of radial resonance corresponding to low-impedance boundary walls* (Section 6.3.5). At 19 kHz the ring (elastic) inertia and the medium load inertia are both again combining to impose a reactive load on the transducer and a corresponding negative electrical motional phase angle, resulting in a great diminution of its vibratory motion and near-vanishing electrical resistance.

6.4 Far-Field Radiation Predictions in Simple-Model Cases

6.4.1 Zeros of Far-Field Radiation in the Radial Direction

The far-field radiation predictions of EIGSHIP are based on the analysis of Part 1 [1]. Simpler models can be used in most cases to good approximation, and discussion of them will illuminate the radiation of sound by a free flooded ring.

One technique is to model the elastic-ring shell as a circular ring of radiating dipoles, since at specific frequencies the magnetostrictive shell has the characteristics of such a ring. We will explore the zeros of this model. The directivity function of a distribution of sources $dQ(x)$ located on a circle of radius a is known to be [8]

$$\bar{D}(\theta) = \frac{1}{Q} \int e^{jk\rho \sin\theta \cos\varphi} dQ$$

Letting $dQ = Q_0 a d\varphi$ and setting $Q = 2\pi a Q_0$, one sees that

$$\bar{D}(\theta) = J_0(ka \sin \gamma)$$

in which θ is the angle between the normal to the plane of the circle and radius vector to the observation point. The far-field pressure \bar{P} is then given by

$$\bar{P} = \bar{P}_0 \bar{D} ,$$

in which \bar{P}_0 is the maximum far-field pressure. When the sources are dipoles with a moment arm Δa units long, the far-field pressure is modeled as

$$p = S_\omega e^{jkr} \frac{(-jk\rho c)}{4\pi r} \left\{ J_0(ka \sin \theta) - J_0 [k(a + \Delta a) \sin \theta] \right\} ,$$

in which S_ω is the monopole source strength. For small $\Delta ka \sin \theta$ we expand $J_0[k(a + \Delta a) \sin \theta]$ in a Taylor series:

$$J_0[k(a+\Delta a) \sin \theta] = J_0(ka \sin \theta) - J_1(ka \sin \theta)\Delta ka \sin \theta + \dots$$

To first order in $\Delta ka \sin \theta$,

$$p \approx D_\omega \sin \theta j \frac{e^{jkr}}{4\pi r} k^2 \rho c J_1(ka \sin \theta),$$

where $D_\omega = S_\omega \Delta a$ is the dipole source strength. In this approximation the far field is always 0 on the axis of the ring and is 0 for any angle θ where

$$J_1(ka \sin \theta) = 0.$$

The first root of $J_1(r) = 0$ is $r = 3.83$. Hence the far-field pressure is 0 in those directions for which

$$\sin \theta = \frac{3.83}{ka} = \frac{3.83c}{\omega a} = \frac{3.83}{2\pi f} \left(\frac{c}{a} \right).$$

At $\theta = 90^\circ$ the first zero occurs at frequency f_1 , where

$$f_1 = \frac{3.83}{2\pi} \left(\frac{c}{a} \right).$$

Higher order zeros of far-field radiation in the radial direction (mainly $\theta = 90^\circ$) coincide with the zeros of $J_1(r)=0$. This simple model therefore accounts for the quasi-periodic appearance of radiation nulls in the radial direction. Its validity however is limited, as can be seen by its dependence on a single coordinate (namely r) in a vibration pattern which is two dimensional (axial and radial). For these more complicated two-dimensional deformation patterns the full power of EIGSHIP must be used.

6.4.2 *Confined-Fluid-Cylinder Modes*

A second technique is to model the elastic-ring shell as a fluid-filled cylinder in which progressive waves are propagating. This model illuminates the theory of radiation from a free flooded shell in those cases in which the length of the shell is equal to or greater than the wavelength of sound in the fluid. Since this model deals only with the elasticity of the fluid but not of the shell, its validity is also limited. It does however provide insight into the conditions of fluid motion in the cavity. A brief account of the relevant theory is presented in this section.

A *confined* fluid cylinder of circular shape, radius a , can propagate acoustic waves in the axial (z) direction, in which the wave motion can be described by the displacement potential ϕ (dimensions: m^2), at harmonic time $e^{j\omega t}$. The acoustic pressure satisfies the equation of state $p = -\rho \partial^2 \phi / \partial t^2$. Let u_r ($= \partial \phi / \partial r$), u_θ ($= \partial \phi / r \partial \theta$), and u_z ($= \partial \phi / \partial z$), be the radial, tangential and axial wave displacements, and let c_d be the speed of sound of the *unconfined medium*. If K_d is the transverse *spatial* wavenumber, and ω/c_d is the temporal propagation constant, then for axisymmetrical wave motion the wave equation for the potential can be factored into a product of radial waves and axial waves with separation constants K_d^2 and $(\omega/c_d)^2 - K_d^2 = k_z^2$ respectively. The classical solution is

$$\phi = A J_0(K_d r) e^{-jk_z z} e^{j\omega t} .$$

The wave numbers K_d are determined by the boundary conditions. For zero pressure at the boundary, K_d satisfies the equation $J_0(K_d a) = 0$, or $K_d^{(m)} = \alpha_m/a$, where α_m are the roots of $J_0(x) = 0$. The first three values of $K_d^{(m)}$ are

$$K_d^{(1)} = 2.40/a, K_d^{(2)} = 5.52/a, \text{ and } K_d^{(3)} = 8.65/a.$$

The phase velocity is

$$c_p^{(m)} = \omega/k_0 = \omega / \left[\left(\omega^2/c_d^2 \right) - K_d^{(m)2} \right]^{1/2} .$$

When $K_d^{(m)2} \geq (\omega/c_d)^2$, that is, when $\omega \leq K_d c_d$, there is no propagation of the m th mode (it is evanescent). Thus there is no axial propagation in a pressure release waveguide at frequencies

$$\omega^{(1)} \leq 2.40/a c_d, \omega^{(2)} \leq 5.52/a c_d, \omega^{(3)} \leq 8.65/a c_d, \dots$$

In the case of a rigid waveguide, K_d satisfies the equation $J_1(K_d a) = 0$. The cases of no axial propagation then occur at frequencies

$$\omega^{(0)} \leq 0, \omega^{(1)} \leq 3.83/a c_d, \omega^{(2)} \leq 7.01/a c_d, \dots,$$

where $\omega^{(0)}$ is the plane-wave mode, which is seen to propagate at all frequencies. In the case of a free flooded magnetostrictive shell the interior cavity undergoes transverse

resonant motion at specific frequencies. Thus the cavity exhibits alternate stiffness and inertial reactance at successive frequencies, resulting in alternate peaks and valleys in radial radiation. These changes of reactance appear as a succession of loops on a plot of electrical reactance versus resistance in which frequency is a parameter.

6.5 Measurement of Experimental Curves of Total Impedance in Water

The total electrical impedance is the sum of the blocked impedance and the motional impedance. When the magnitude of these quantities is of the order of a few electrical ohms, their measurement in the NRL Acoustic Test Tank becomes difficult. A significant parameter in the capability of making the measurement is the ratio of the motional to the blocked impedance. Experience has shown that measurement of ratios of less than 10 percent are subject to errors. We will note a few such ratios as determined from EIGSHIP, choosing ring C as an example.

The magnitudes of blocked impedances $|Z_b|$ can be roughly estimated from the total electrical impedance of ring C in water given by Fig. 33, and the magnitudes of motional impedance can be predicted from the motional-impedance *perturbations* as calculated from EIGSHIP and shown in Fig. 34. These calculated impedance magnitudes and their ratios are listed in Table 2. The results in Figs. 33 and 34 permit the prediction that there will be at least two measurable loops on the experimental total impedance plot, namely, in the neighborhood of 4000 and 8000 Hz. Since in these regions the motional effect equals or exceeds 25 percent of the blocked effect, available instrumentation at the NRL Acoustic Test Tank is capable of recording these electrical impedances. In addition these predicted motional impedances pass through zero phase angles, thus guaranteeing the existence of a loop on the total impedance plot. In contrast the predicted motional impedance in the vicinity of 9300 Hz does not pass through zero phase. Thus it is predicted that it will not *per se* exhibit the presence of a loop on the total impedance curve but rather a perturbation (discussed in Section 5.1.4). Also, at 9300 Hz the motional impedance is less than 10 percent of the blocked value, and a perturbation due to it will result only in a local deformation of the impedance curve. In the vicinity of 17,000 Hz the motional impedance plot (Fig. 34) passes through zero phase. Hence a loop is predicted at this frequency. However the motional effect is less than 4 percent of the blocked value. The predicted loop will be small. In actual experiments the instrumentation at the NRL Acoustic Test Tank was incapable of resolving this small loop.

6.6 Transmitting Responses Predicted by EIGSHIP

The transmitting current response of a ring transducer is a simple linear function of the surface velocity. This velocity may be induced by an applied current at the electrical terminals of the transducer [1, Eq. 5.23]. It is also induced by an applied mechanical force of the medium at the mechanical terminals [1, Eqs. 5.1 and 5.2]. When both mechanical and electrical applied drives act simultaneously, the resultant surface velocity distribution exhibits more complex modal shapes than when either drive acts separately (Fig. 35). A direct measure of the mechanical motion in any mode is the electrical motional impedance measured at the electric terminals (Figs. 5, 6, 7, and 34). This quantity

Table 2 — Calculated Magnitudes of Blocked Impedances and Motional Impedances of Ring C in Water and the Ratios of These Magnitudes at Particular Frequencies

| Frequency (kHz) | $ Z_b $ (ohms) | $ Z_{motw} $ (ohms) | $ Z_{motw}/Z_b $ (%) |
|--------------------|-------------------|------------------------|-------------------------|
| 4 | 22 | 6.5 | 30 |
| 8 | 42 | 10.5 | 25 |
| 9.3 | 44 | 4 | 9 |
| 17 | 77 | 3 | 3.9 |

is known to be proportional to the square of the transduction (or force) factor and the mechanical admittance [5, Eq. 4.3, and 1, Eq. 5.5]. In a ring transducer the force factor is proportional to the product κh (Appendix E, Section E3). Below mechanical resonance (in any mode) the mechanical admittance is small; hence the mechanical motion is small in the conventional range of linear force motion and the electrical impedance is predominantly that of an electric coil. The radiation field is controlled by the modal stiffness of the elastic structure. At frequencies of maximum transmitting response the motion is a maximum for the particular mode. The magnitude of motion is then determined by the mechanical resistance (predominantly of the water load) and by the magnitude of the product $\kappa^2 h^2$. Thus the prediction of frequencies of maximum transmitting response of EIGSHIP depends on the prediction of two quantities: the mechanical resistance and the magnitude of the product $\kappa^2 h^2$ (Appendix E, end of Section E3).

6.6.1 Dependence on Mechanical Resistance

At frequencies of maximum surface velocities under loaded conditions the mechanical resistance is a sum of (a) the coupled hysteresis and eddy current losses in the magnetic circuit specified by the complex transduction factor, (b) the purely elastic losses specified by the complex Young's modulus, and (c) the acoustic radiation resistance. It is assumed that terms (a) and (b) are accounted for with sufficient accuracy in the EIGSHIP prediction of radial transmitting response. Term (c) is discussed in Section 6.6.4.

6.6.2 Dependence on the Product $\kappa^2 h^2$

The reversible magnetic susceptibility that appears in the product κh is related to the reversible permeability μ by the formula $\kappa = \mu - \mu_0$ (Appendix E, Section E1). The quantity μ is measured directly from a low frequency impedance measurement on the mechanically free (nonstressed) ring. It is assumed that this quantity is known with sufficient accuracy. We are thus left with the determination of the magnitude of the piezomagnetic constant h . This constant is in general a tensor quantity, the number of whose components depend on geometric and electric coil configurations. By definition h is the ratio of applied mechanical stress to magnetic flux density. In the lowest air

mode of a magnetostrictive ring the applied stress is tangential: $T = T_{\theta\theta}$. Hence at any one instant in dynamic motion the ring is assumed either in uniform elastic tension or in compression, and the induced magnetization is uniform on the cross-sectional area of the ring. Thus the predicted h is assumed to be $h_{\theta\theta}$. This constant is measured from dynamic responses of the ring in air, that is, under conditions of no load at the mechanical terminals. Thus measured, the magnitude $h_{\theta\theta}$ can be used to predict the relation of stress to flux density in all situations where the stress in the ring shell consists of one component ($= T_{\theta\theta}$) which is uniform across the shell thickness.

When the rings are driven in water at their resonant frequencies, they exhibit modal shapes corresponding to bending (Fig. 35). This bending is due to load-induced forces applied at the mechanical terminals, which in air were effectively open circuited. In bending, the magnetic flux due to the positive stress of tension is partially canceled by the oppositely directed flux due to the negative stress of compression and is nonuniformly distributed in the axial direction. Thus, while the electrical terminals supply a steady current to produce a uniform magnetic field in the ring, the forces at the mechanical terminals induce magnetic fluxes oppositely directed across the thickness and nonuniformly distributed along the length. The ratio of stress to flux density is thus no longer $h_{\theta\theta}$, as measured in air, but a necessarily *smaller* number due to partial cancellation and nonuniform distribution. In effect the medium adds a pair of mechanical terminals not present in air. The coefficient $h_{\theta\theta}$ (originally determined from air data) is thus effectively multiplied by an additional fraction accounting for flow of (coupled) energy through the mechanical terminals of flexure. In water therefore, the transducer is operating with several mechanical terminals (including flexure), rather than two (longitudinal and radial) as in air. The equivalent circuit of the ring may be generalized to show this (Fig. 36). In air the piezoconstant $h_{\theta\theta}$ directs the flow of energy through the path $\phi_{12} \rightarrow \phi_{34} \rightarrow$ radial. In water a *smaller* piezoconstant h directs the flow of energy through the path $\phi_{12} \rightarrow \phi_{36} \rightarrow \phi_{64} \rightarrow$ "radial."

The experimental results in water substantiate this reduction of $h_{\theta\theta}$ under loaded conditions. We first choose ring C and examine Figs. 7a, 7b, and 35. At 9.3 kHz (Figs. 7b and 35c) the prediction of EIGSHIP shows a barrel mode. This is based on the value of $h_{\theta\theta}$ measured in air. In actual experiment (Fig. 7a) no motional effect appears; that is, the flow of energy through the flexure terminals is too small to be measured. Again, the reactive motional impedance of the "first radial mode" at 8 kHz predicted by EIGSHIP (Figs. 7b and Fig. 35b) is larger than that actually measured (Fig. 7a). Here again the value of $\mu^2 h^2$ is too high, since it was based on air data, obtained when only two mechanical terminals are present. From this discussion on ring C it will be seen that the current transmitting responses predicted by EIGSHIP over the frequency ranges at which the flexure modes occur will exhibit peaks (Fig. 22) of higher magnitude than measured, indicating greater motion than actually occurs. This conclusion is also evident in the responses of ring B, as predicted and is measured (Figs. 6 and 21).

6.6.3 Effect of Cavity-Mode Radiation

Although ring flexure accounts in the main for the differences between measured and predicted responses, another response requires discussion. This is the "cavity mode"

6.7 Axial Constant-Current Transmitting-Response Curves

6.7.1 *Comparison of Theoretical and Measured Responses*

Figures 20, 21, and 22 show comparisons of theoretical and measured transmitting current responses of rings A, B, and C respectively (Table 1). We will discuss here the axial response curves. Convenient bases for comparison of two curves of theoretical and experimental response are general trends, critical maxima and minima, and magnitude (or level).

The general trends of the two curves for rings A, B, and C agree with each other; that is, the curves rise and fall in rough unison. The theoretical curves of rings A and C show more local maxima and minima than experiment, but they tend to seek the trends of the experimental response upon recovery.

In ring A (Fig. 20) the maxima of the two curves occur near to each other in frequency (approximately 7.6 kHz). The minima of the curves are widely separated, the interval being estimated at 1 kHz. In ring B the first maximum in both curves occurs at about the same frequency (5.8 kHz), at which the 3-dB bandwidth is about 1 kHz in both cases. The theoretical curve shows a sharp maximum at 13.8 kHz, and the experimental curves show poorly defined maxima at 13.5 kHz and 12.8 kHz. In ring C the first maximum in both curves occurs at approximately the same frequency (4 kHz), but the 3-dB bandwidth of the experimental curve is 0.8 kHz, in contrast to the theoretical-curve bandwidth of 0.6 kHz. A second maximum-minimum is theoretically predicted over a narrow frequency range of about 100 Hz centered at 7.8 Hz. The experimental curve shows no evidence of this prediction. Beyond 14 kHz both curves show sharp minima, the theoretical curve predicting one at 14.8 kHz, but the experimental curve displaying one at 15.7 kHz.

Levels of transmitting responses are best compared at frequencies at which peaks occur. In ring A the theoretical curve is 4 dB higher than the experimental curve as measured near the peaking frequency of 7.6 kHz. In ring B the theoretical peak level at 5.8 kHz is approximately 9 dB higher than that actually measured. In ring C the theoretical value is again higher by 9 dB than the experimental curve at the peaking frequency of 3.8 kHz.

6.7.2 *Effects of Alterations in the Internal Support Structure and Coil Windings*

This sharp discrepancy between experimental and predicted levels at the first cavity mode in rings A, B, and C was initially attributable to three factors: the uncertain prediction of ring surface velocities, insufficient accuracy in the electroacoustic conversion parameters, and the deleterious effects of the ring internal support in hindering the motion of the contained fluid. Since the third cause could be mathematically investigated

by the use of EIGSHIP, an analysis was performed and reproduced here as Appendix F. There it is shown that the shell annulus surface pressure is the dominant factor in axial radiation.

Since the effect of shell annulus surface pressure on axial response was the most susceptible to experimental check, we choose a convenient ring (ring B) for experimental trial. In ring B we replaced the internal support structure by an exterior temporary support consisting of an acoustically transparent net of nylon string. In addition we reduced the number of coil windings to 48 turns (simultaneously increasing the bias current to maintain the same ampere-turn excitation as before). With these alterations in support structure and coil winding in place we made standard transmitting response curves and far-field radiation patterns for comparison with earlier tests on ring B.

We consider the axial transmitting current response first (Fig. 37). The test result for the nylon-string-supported ring B (called NS ring B for convenience) showed dramatic improvement over the old ring B (Fig. 21) in the frequency range between 4 kHz and 13 kHz. It is seen (Fig. 37) that NS ring B and the EIGSHIP prediction agree well both in slope and peak magnitude from 4 kHz to 6.5 kHz. Between 6.5 kHz and 9 kHz EIGSHIP predicts a lower response than shown by experiment. However at 9.5 kHz the agreement becomes good again and continues good to 13 kHz. At 14 kHz a second dramatic change occurs. Here the experimentally observed null of ring B (Fig. 21) has vanished in the response of NS ring B, only to reappear at 17 kHz. Thus replacement of the internal support by an external support and redesign of the coil structure shifts the axial transmitting null from 14 kHz to 17 kHz. However further experiments involving the addition of 96 turns of wire arranged arbitrarily around NS ring B resulted in the elimination of the null at 17 kHz. We thus are led to consider the occurrence of a null at precisely 17 kHz in the NS ring B as a fortuitous result, unpredictably dependent on coil arrangement, acoustic wavelength, and dynamic damping of the shell.

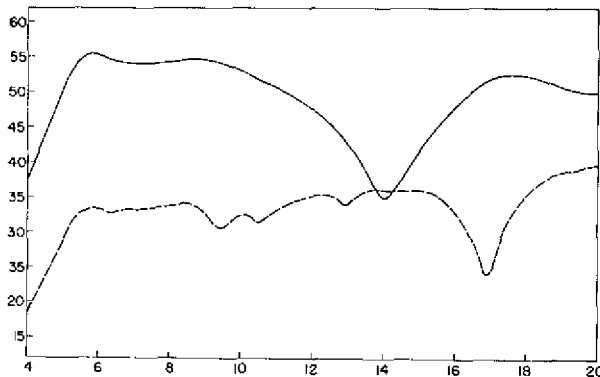


Fig. 37 — Transmitting current response at 1 meter in the plane of the ring and on the axis of the ring when driven at 1 ampere for ring B without the internal support structure (replaced by a nylon-string support) and with fewer coil windings, for comparison with the results in Fig. 21.

The axial transmitting response of NS ring B tends to bear out the main conclusion of Appendix F, which is that axial response is mainly affected by the shell annulus surface pressure. It is apparent that this buildup of acoustic pressure is a low-level phenomenon and is therefore highly sensitive to neighboring obstacles, support structures, coil windings, etc., as is demonstrated by the preceding experiment. Cancellation of the radiation from the annulus, hence the appearance of an axial transmitting null, will consequently be highly sensitive to the presence of neighboring obstacles, transducers, etc. Cancellation will also depend strongly on the precise distribution of radial shell velocity on the inside and outside *lateral* surfaces of the shell, since these velocities (and their phases) likewise determine the annulus surface pressure buildup.

We next consider the NS ring B radial transmitting response as shown in Fig. 37. By comparison with the radial response of ring B (Fig. 21) it is seen that the alteration of support structure and coil winding arrangement has had little effect on the radial response in the frequency range from 4 kHz to 20 kHz. The only noticeable change occurs in the depth of the experimental null which occurs at 14 kHz, the NS ring B showing a depth of 21 dB below radial peak response as compared with 34 dB shown by ring B. This difference in the depth of the null is considered unimportant. Additional experiments have shown that the depth of the null depends on several arbitrary test conditions such as misalignment of source and receiver axes and lack of symmetry in the physical construction of the ring-coil assembly.

We conclude from the comparison of NS ring B and EIGSHIP that predictions of EIGSHIP are in good agreement over most of the frequency range and that any disagreements are of minor importance and are traceable to unmodelable elements in the ring structure such as ring supports and coil windings.

7. THE COMPUTER PROGRAM EIGSHIP

The computer program EIGSHIP (listed in Appendix A) numerically calculates the acoustic performance characteristics of a free-flooded magnetostrictive ring shell whose mathematical modeling is described in Part 1 [1]. It is written in CDC 3600 Fortran for the CDC 3800 computer at the Naval Research Laboratory. Data input to program EIGSHIP (in the form of punched input cards) includes ring shell dimensions and magnetostrictive properties, electric-coil-winding dimensions, and external fluid medium properties. The output of EIGSHIP for each frequency input consists of ring shell normal surface velocities and electrical and mechanical impedances in both air and water. In addition computer output of performance of the submerged ring includes surface acoustic pressures, transmitting responses, and, if desired, a radiation directivity pattern. A complete set of numerical output data for air and underwater acoustic performance can be obtained in less than 15 seconds for one frequency.

The computer program EIGSHIP consists of a main program (called EIGSHIP) and several subroutines. The program consists of two distinct sections: input and introductory calculations, and basic acoustic performance calculations and output.

7.1 Input and Introductory Calculations

The function of the input and introductory-calculation section is to read in all data cards necessary to describe the ring shell and to obtain thickness correction factors, modal frequencies, and modal shape factors needed for the basic calculations performed in the second of the two program sections.

7.1.1 Data Cards

A diagram of the arrangement of data cards for EIGSHIP is shown in Fig. 38. A detailed description of each data card follows.

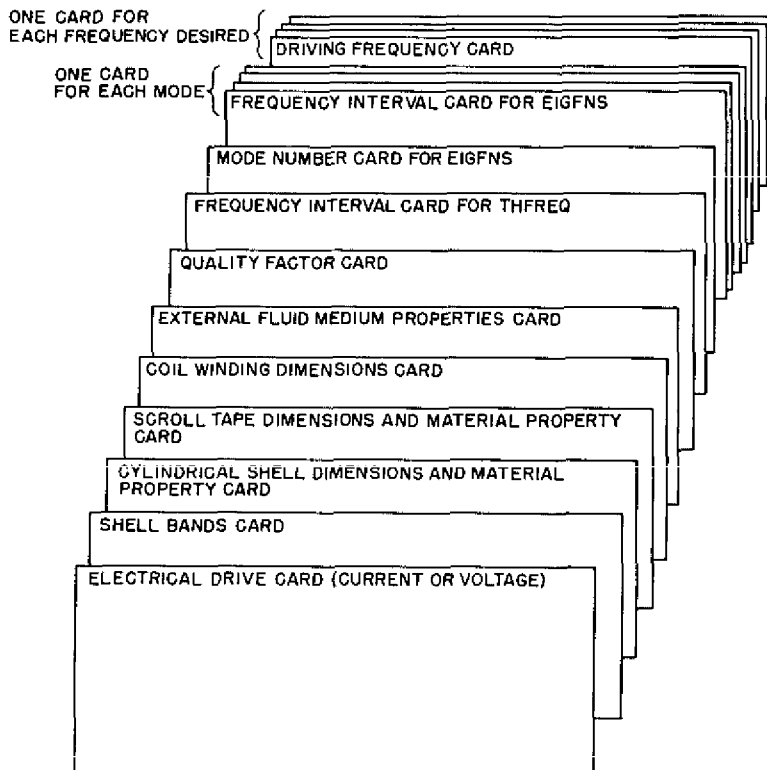


Fig. 38 — Data cards for the computer program EIGSHIP

Electrical Drive Card

| <u>Variables</u> | <u>Format</u> | <u>Column</u> | <u>Description</u> |
|------------------|--------------------|---------------|--|
| ICRT | I1 | 1 | 0 if constant-voltage drive; 1 if constant-current drive. |
| DRIVE | C(E9.5,E10.5) 2-20 | | Complex value of electric drive; it is a value of voltage if ICRT = 0 or a value of current if ICRT = 1. |

Shell Bands Card

| <u>Variables</u> | <u>Format</u> | <u>Column</u> | <u>Description</u> |
|------------------|---------------|---------------|--|
| JMAXH | I5 | 1-5 | One-half the number of sidebands into which the shell is divided. The maximum value allowed is 10. |
| IMAX | I5 | 6-10 | Number of endbands describing top (and bottom) of the shell. The maximum value allowed is 10. |

Comments: The shell is divided into $2 \times JMAXH$ bands of equal area on the inside surface, $2 \times JMAXH$ bands of equal area on the outside surface, and $IMAX$ bands of equal thickness (radial dimension) on the top and bottom and labeled as shown in Fig. 39 for the specific case of $JMAXH = 4$ and $IMAX = 3$. Only the top half of the shell need be modeled due to geometrical and input electrical drive symmetry. The labeling in Fig. 39 follows that of the computer program SHIP [9], which is the main subroutine in the second of the two sections of the program EIGSHIP.

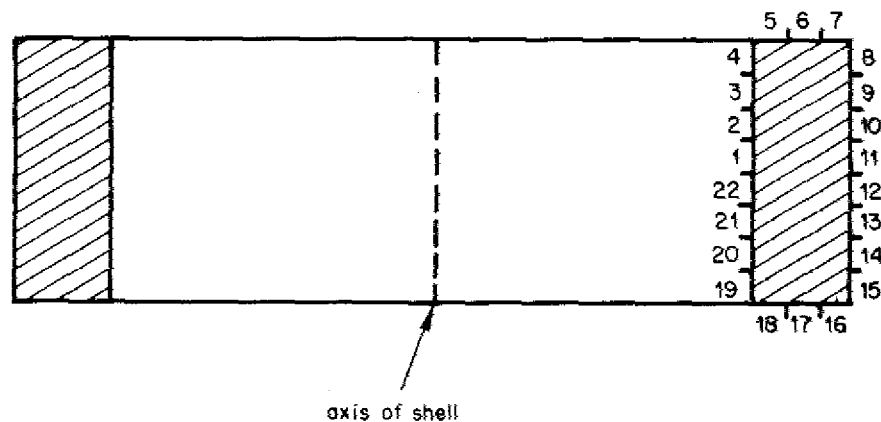


Fig. 39 — Numbering of the bands on a cylindrical shell for eight sidebands and three top (and bottom) endbands

Cylindrical Shell Dimensions and Material Property Card

| <u>Variables</u> | <u>Format</u> | <u>Column</u> | <u>Description</u> |
|------------------|---------------|---------------|---|
| RMEAN | E10.5 | 1-10 | Mean radius of shell, a . |
| THK | E10.5 | 11-20 | Radial dimension (thickness) of shell, b . |
| LTH | E10.5 | 21-30 | Axial dimension (length) of shell, l . |
| RHO | E10.5 | 31-40 | Material density, ρ . |
| NU | E10.5 | 41-50 | Poisson's ratio of material, ν . |
| Y | E10.5 | 51-60 | Young's modulus at constant magnetic induction, Y . |

Scroll Tape Dimensions and Material Property Card

| <u>Variables</u> | <u>Format</u> | <u>Column</u> | <u>Description</u> |
|------------------|---------------|---------------|---|
| THST | E10.5 | 1-10 | Scroll lamination thickness, t . |
| RES | E10.5 | 11-20 | Resistivity, ρ_e . |
| URS | E10.5 | 21-30 | Relative magnetic permeability at constant strain, $\mu^{RS} = \mu^S / \mu^0$. |
| HTT | E10.5 | 31-40 | Piezomagnetic stress constant, $h_{\theta\theta} = h_{22}$. |
| DIP | E10.5 | 41-50 | Either -2β if IHYS = 0 or $-\eta$ if IHYS = 1. |
| IHYS | I1 | 51 | 0 or 1. |

Comments: Two methods of describing hysteresis losses are available, corresponding to IHYS = 0 and 1. If IHYS = 0, then DIP is interpreted as -2β , the negative angle measured as the total dip angle from the constant-current motional impedance circle in air (Fig. 40). If IHYS = 1, then DIP is interpreted as η , the negative angle which describes the lag between magnetic flux and magnetic intensity [1, Section 7].

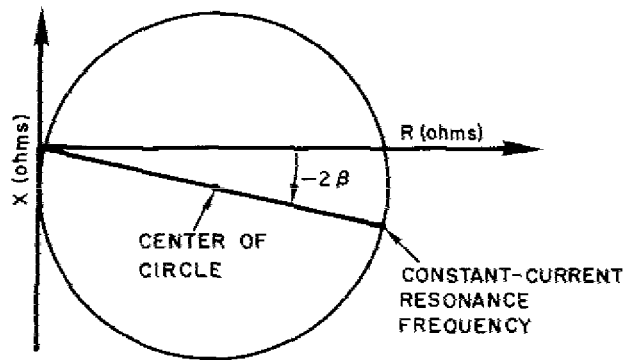


Fig. 40 — Motional impedance circle

Coil Winding Dimensions Card

| <u>Variables</u> | <u>Format</u> | <u>Column</u> | <u>Description</u> |
|------------------|---------------|---------------|---|
| NTRN | I10 | 1-10 | Number of turns of wire wound toroidally around the ring. |
| THC | E10.5 | 11-20 | Radial dimension of the coil (Fig. 41). |
| LC | E10.5 | 21-30 | Axial dimension of the coil (Fig. 41). |
| REL | E10.5 | 31-40 | Copper loss in the coil, R^l . |

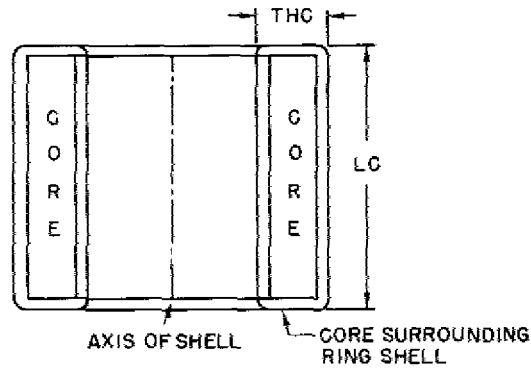


Fig. 41 — Definition of THC and LC

External Fluid Medium Properties Card

| <u>Variables</u> | <u>Format</u> | <u>Column</u> | <u>Description</u> |
|------------------|---------------|---------------|---------------------------------------|
| RHOF | E10.5 | 1-10 | Density of the external fluid. |
| CF | E10.5 | 11-20 | Speed of sound in the external fluid. |

Quality Factor Card

| <u>Variables</u> | <u>Format</u> | <u>Column</u> | <u>Description</u> |
|------------------|---------------|---------------|--|
| Q | E10.5 | 1-10 | Quality factor for the lowest mode, either for constant current if ICRT = 1 or for constant voltage if ICRT = 0. |

Frequency Interval Card for THFREQ

| <u>Variables</u> | <u>Format</u> | <u>Column</u> | <u>Description</u> |
|------------------|---------------|---------------|--|
| FR(1) | F10.5 | 1-10 | Lower limit of the frequency interval. |
| FR(2) | F10.5 | 11-20 | Upper limit of the frequency interval. |

Comments: An explanation of this input card appears in Section 7.1.3.

Mode Number Card for EIGFNS

| <u>Variables</u> | <u>Format</u> | <u>Column</u> | <u>Description</u> |
|------------------|---------------|---------------|--|
| NBRFNS | I1 | 1 | Number of modes to be used in the modal expansion of g_{ij} . The maximum value allowed is 9. Also JMAXH must be greater than or equal to NBRFNS (shell bands card). |

Frequency Interval Card for EIGFNS

| <u>Variables</u> | <u>Format</u> | <u>Column</u> | <u>Description</u> |
|------------------|---------------|---------------|--|
| FR(1) | F10.5 | 1-10 | Lower limit of the frequency interval. |

| <u>Variables</u> | <u>Format</u> | <u>Column</u> | <u>Description</u> |
|------------------|---------------|---------------|--|
| FR(2) | F10.5 | 11-20 | Upper limit of the frequency interval. |
| IMG | I1 | 25 | 1 if the imaginary part of the determinant (discussed in Section 7.1.2) is used blank otherwise. |

Comments: An explanation of this input appears in Section 7.1.2.

Driving Frequency Card

| <u>Variables</u> | <u>Format</u> | <u>Column</u> | <u>Description</u> |
|------------------|---------------|---------------|--|
| FREQ | F10.5 | 1-10 | Frequency for which performance characteristics are desired. |
| IAIR | I5 | 11-15 | 0 if air and water calculations are desired or 1 if only air calculations are desired. |
| IFD | I5 | 16-20 | Integer number indicating the number of equally spaced points along a 90° arc from 0° (in the radial direction) to 90° (on axis) at which normalized far-field pressures in decibels are calculated (Fig. 42). If IFD = 0, no far-field points are calculated. |

Comments: The first driving-frequency input should be close to the constant-current resonance frequency corresponding to the lowest radial mode (ring mode) in air, because the resistance $R_m''(\omega_1)$ in this program is calculated according to Eqs. 6.21 or 6.22 of Part 1 [1] with $Q_n^r \equiv Q_1^r$ or $Q_n^E \equiv Q_1^E$ and remains fixed thereafter for all driving frequencies. For most cases, if this resonance frequency is not obtained by experiment, an approximate value for this frequency f_1 can be obtained by using the equation

$$f_1 = \sqrt{(1-k^2)} F_1 \quad (7.1)$$

where k is the low-frequency material coupling coefficient and F_1 is the "frequency" corresponding to the lowest radial mode of free (elastic) vibration. F_1 appears as an output of subroutine EIGFNS. Subsequent construction of a motional impedance circle in air enables f_1 to be obtained more accurately. Another reason for choosing the first driving

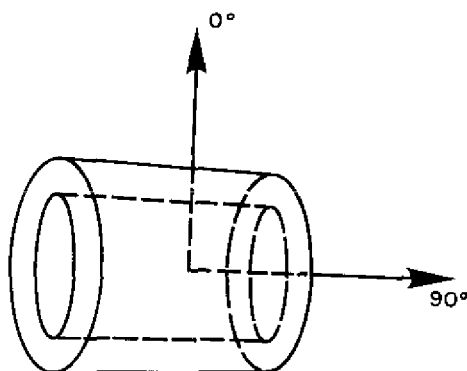


Fig. 42 — Definition of the angle used in describing the far field

frequency to be f_1 is that the hysteresis factor is calculated from a knowledge of the total dip angle occurring in the air motional impedance circle for constant-current drive.

7.1.2 Modal Calculations

Frequencies and accompanying modes of free vibration of a dissipationless shell are required [1, Section 3]. Specifically modal displacement shapes for radial and axial displacement (but not for tangential displacement, because the input drive is considered uniform in the circumferential direction) are obtained in subroutine EIGFNS. The calculation follows the analysis developed in Part 1 [1, Eqs. 4.36ff] with appropriate reduction to two unknown directions.

The method of interval halving is used to converge to the nontrivial solution of the homogeneous boundary-condition matrix equation appearing in the analysis (Appendix C). Thus for each modal frequency a frequency interval is required which (a) contains the desired modal frequency and (b) is such that the boundary condition matrix determinant passes through 0 exactly once in the interval. For numerical application, requirement (b) is replaced by the following requirement: A frequency interval is required which is such that the real part or imaginary part of the boundary-condition-matrix determinant changes sign exactly once in the interval, with the sign change being due to a passage through 0. Such an interval will be called a valid interval.

Valid intervals are obtained in two steps. The first step is to examine the determinant of the matrix formed in EIGFNS as a function of frequency. Computer program DTRMNT (Appendix B) along with its one required subroutine CUBIC performs the necessary examination. This program is simply an abbreviated version of subroutine EIGFNS which calculates and prints the determinant of the boundary-condition matrix as a function of frequency. Two types of input cards are required for computer program DTRMNT. The first input card is the cylindrical shell dimensions and material property card. Following this card are any number of input cards corresponding to the input statement

```
READ 9,K1,K2,K3
```

```
9 FORMAT (3I5).
```

The Fortran statements

```
DO 666 IFR = K1, K2, K3
```

```
FREQ = IFR
```

appearing in DTRMNT indicate that the determinant is calculated for frequencies in the interval from K1 Hz to K2 Hz in steps of K3 Hz. (The statement `FREQ = IFR` can be replaced with the statement `FREQ = IFR*C`, where C is a constant. This circumvents limits on integer numbers allowed in DO statements.) From the resultant printout one can determine potentially valid intervals by examining sign changes in the real or imaginary part of the determinant as a function of frequency.

The second step for obtaining valid intervals consists of checking all potentially valid intervals by employing calculations performed in subroutine EIGFNS. This is accomplished by converting subroutine EIGFNS to an independent program which can then be run externally to program EIGSHIP. Appendix C describes the method of conversion. The new deck may now be called program EIGFNS and is run with its one required subroutine CUBIC as a complete program. The input to the program consists of a cylindrical shell dimensions and material property card, a mode number card which defines NBRFNS, and the appropriate number of frequency interval cards (NBRFNS frequency interval cards with the digit 1 placed in column 25 if the imaginary part of the boundary-condition determinant is to be used for frequency locations or with column 25 left blank if the real part of the determinant is used.)

The output of EIGFNS is used to determine valid intervals and identify the mode shapes. If the sign change of the boundary-condition determinant (specifically the sign change of the real or imaginary part) is due to a passing through 0, then the frequency interval is valid. This will be reflected by the output variables RT1 and RT2 having nearly the same value say to several significant digits and also by the value of the determinant at the resonant frequency being approximately nine orders of magnitude less than the larger of the determinants evaluated at the interval frequencies (Appendix C). However, if the determinant passes through infinity when changing sign, then RT1 will not equal RT2 and the determinant at the "supposed" resonant frequency will not be smaller than the determinants evaluated at the interval frequencies. Thirty interval halvings are used, which provides sufficient convergence for valid intervals.

The relative magnitudes of axial displacement shapes and radial displacement shapes (scaled, not absolute values) determine whether the motion is predominantly axial or radial. Examination of the predominant motion as a function of axial position reveals the shape of the predominant motion: first radial mode (no nodes), second radial mode (two symmetric nodes), etc.

Figure 43 shows various mode shapes as calculated for a particular set of shell parameters for free-free end boundary conditions. Only the shape of the predominant motion is depicted and labeled, although both axial and radial displacements occur at every frequency. Symmetric or even mode shapes are calculated. The displacement of half the shell is shown. These curves describe the motion of the reference surface of the shell (Fig. 44 shows the labeling of the reference surface bands).

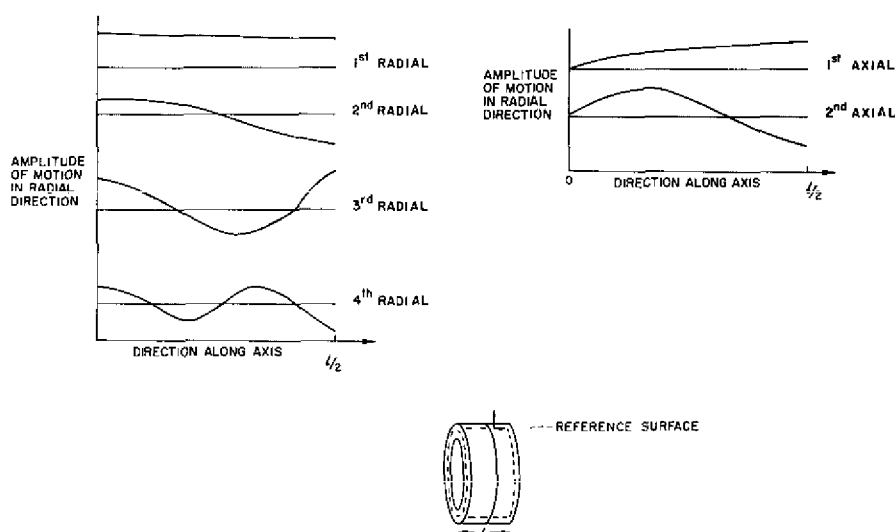


Fig. 43 — Even mode shapes for free-free end boundary conditions

Frequencies of several modes of the elastic vibration of cylindrical shells for six cylinder dimensions are presented in Table 3. Each frequency is labeled according to the dominant motion occurring. For a given thickness the number of modes occurring below 100 kHz increases as the length increases. Also, for a given length the spread between radial modes increases when the thickness is doubled.

Examination of mode shapes predicted for a set of shell parameters is necessary to ensure that all modes within an interval have been located. For example suppose the use of DTRMNT followed by EIGFNS yields four resonant frequencies, f_1 , f_2 , f_3 , and f_4 where $f_1 < f_2 < f_3 < f_4$, with corresponding mode shapes first radial, third radial, first axial, and fourth radial respectively. One should suspect that the frequency corresponding to the mode shape second radial has been overlooked. A more careful scan of frequencies between f_1 and f_3 with DTRMNT and EIGFNS is required.

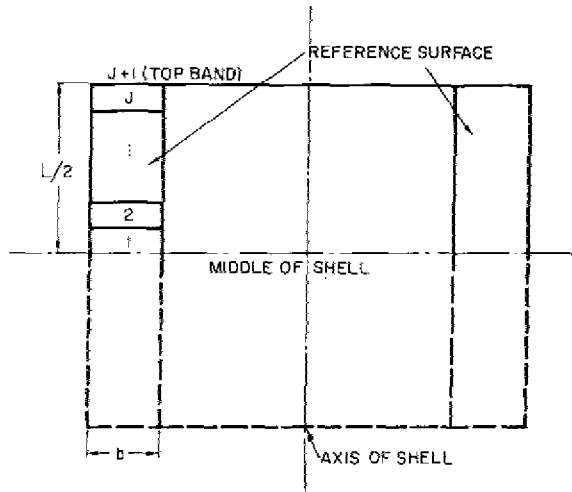


Fig. 44 — Labeling of reference surface bands

Table 3 — Frequencies of Mode Shapes as a Function of Length and Thickness (for fixed material parameters $\rho = 8400 \text{ kg/m}^3$, $Y = 2.02 \times 10^{11} \text{ N/m}^2$, $\nu = 0.3$, and $a = 6.5725 \text{ cm}$)

| Thick-ness (mm) | Length (mm) | Frequencies of Resonant Modes (Hz) | | | | | |
|-----------------|-------------|------------------------------------|------------|------------|------------|-----------|-----------|
| | | 1st Radial | 2nd Radial | 3rd Radial | 4th Radial | 1st Axial | 2nd Axial |
| 6.4 | 19.4 | 11876 | 90679 | — | — | — | — |
| | 38.8 | 11863 | 25381 | — | — | 66308 | — |
| | 77.6 | 11807 | 13096 | 32534 | 75889 | 33349 | 99370 |
| 12.8 | 19.4 | 11890 | — | — | — | — | — |
| | 38.8 | 11878 | 46284 | — | — | 66499 | — |
| | 77.6 | 11821 | 16245 | 61650 | — | 33379 | 99529 |

Program EIGFNS prints out the normalized inner products of mode shapes as a numerical check of orthogonality of modes after all desired mode shapes have been obtained.

7.1.3 Thickness Correction Factors

Thickness correction factors $f(A)$ and $f(B)$ [1, Eqs. 9.2ff] are obtained in subroutine THFREQ. This subroutine is used to obtain scaled radial displacements of the ring along its thickness, that is, displacements as a function of radial distance from the inner radius to the outer radius. The displacements are obtained at the frequency corresponding to the ring mode (radial mode shape with no nodes). The frequency interval used as input (frequency interval card for THFREQ) may be identical with the frequency interval used in EIGFNS for this mode shape, since both subroutines are attempting to obtain the same frequency.

The correct resonant frequency is obtained as the frequency which minimizes a particular determinant [1, Eqs. 9.2ff]. The method of interval halving is again used. A check on the validity of the resonant frequency obtained can be made by examining output of THFREQ (Appendix D). At the correct resonant frequency the value of the determinant will be about eight orders of magnitude less than the larger of the two determinants corresponding to the initial frequency interval. Also the values of $R1$ and $R2$ (defined in Appendix D) will agree to several digits.

The frequency obtained from subroutine THFREQ should be close to the ring mode frequency obtained from program EIGFNS.

7.2 Basic Performance Characteristics Calculation and Output

The second of the two distinct sections of computer program EIGSHIP contains the numerical calculation of various performance characteristics of the magnetostrictive ring shell and the output of the program. The calculations are based on equations derived in Part 1 [1]. In what follows the quantities being described are presented in the order in which they appear in the output format listed as Output Data (Appendix D).

7.2.1 First Page of Output: Radial Velocity and B and S Model

Radial Velocity

Radial velocity (VELBS) as calculated from a Butterworth and Smith analysis is presented first in the output. For constant-current drive

$$\text{VELBS} = \psi I \left\{ j\omega\rho b + \frac{Rm''}{2\pi a\ell} + \frac{Yb}{\omega a^2} [k^2\chi_I + j(k^2\chi_R - 1)] + T \right\}, \quad (7.2)$$

where $T = 0$ in air and

$$T = \frac{1}{J} \sum_m^J \sum_n^J j\omega \mathcal{G}(m,n) \text{ in water}, \quad (7.3)$$

in which $\mathcal{G}(m,n)$ is given by Eq. 9.1 of Part 1 [1], and where

$$\psi = \frac{h_{22}\mu^s b N \chi}{2\pi a^2},$$

as given by Eq. 5.9 of Part 1. The radial velocity VELBS is followed on the first page of the output by NRL EIGSHIP velocities (VEL(k)). For constant-current drive

$$\text{VEL}(k) + \sum_{\ell}^J \sum_r^{J+1} j\omega g_{m3}(k,\ell) \mathcal{G}(\ell,r) \text{VEL}(r) = \psi I \sum_{\ell}^J g_{m3}[k,\ell], \quad (7.4)$$

with $\mathcal{G} = 0$ in air [1, Eq. 5.2]. Here and in Eq. 7.2, $m = 1$ when k refers to an endband and $m = 3$ when k refers to a sideband. In these equations J is the number of sidebands on half the ring shell. J corresponds to the input quantity JMAXH. The labeling of bands is depicted in Fig. 44.

For constant-voltage drive

$$\begin{aligned} \text{VELBS} = \frac{\psi E}{Z_b} \bigg/ \left\{ j\omega \rho b + R_m'' + \frac{R_m'}{2\pi a \ell} + \frac{Y_b}{\omega a^2} [k^2 \chi_I + j(k^2 \chi_R - 1)] \right. \\ \left. + \frac{\psi^2 2\pi a \ell}{Z_b} + T \right\} \end{aligned} \quad (7.5)$$

where T is defined as before, and, in accordance with Eq. 5.6 of Part 1,

$$\begin{aligned} \text{VEL}(k) + \sum_{\ell}^J \sum_r^{J+1} j\omega g_{m3}(k,\ell) \mathcal{G}(\ell,r) \text{VEL}(r) \\ + \frac{\psi^2}{Z_b} \sum_{\ell}^J g_{m3}[k,\ell] \sum_r^{J+1} A_r \text{VEL}(r) = \frac{\psi E}{Z_b} \sum_{\ell}^J j\omega g_{m3}(k,\ell), \end{aligned} \quad (7.6)$$

where a_j is the area of the j th band. The velocities VEL(k) refer to bands on the reference surface of the shell.

Output of Butterworth and Smith Model

Various characteristics as calculated using a Butterworth and Smith analysis are now obtained. For constant-current drive

$$\text{electrical power} \equiv PIN = |I|^2 ZEE, \quad (7.7)$$

$$\text{radiation impedance} \equiv ZRAD = \frac{2\pi a \ell}{J} \sum_i^J \sum_{\ell}^J \mathcal{G}(i, \ell), \quad (7.8)$$

$$\begin{aligned} \text{power conversion efficiency} \equiv ETA = & \frac{\text{Re}(ZRAD) |ZEM|^2}{|ZM+ZL|^2} \left\{ \text{Re}(ZEL+ZC) \right. \\ & \left. + [\text{Re}^2(ZEM) - \text{Im}^2(ZEM)] \text{Re}(ZM+ZL) + 2\text{Re}(ZEM) \text{Im}(ZEM) \right\}. \end{aligned} \quad (7.9)$$

$$\text{motional impedance in air} \equiv ZMOTA = (ZEM)^2 / ZM \quad (7.10)$$

(given in Part 1 as Eq. 7.12),

$$\text{electrical impedance in air} \equiv ZEA = ZB + ZMOTA, \quad (7.11)$$

$$\text{motional impedance in water} \equiv ZMOTW = (ZEM)^2 / (ZM + ZRAD), \quad (7.12)$$

and

$$\text{electrical impedance in water} \equiv ZEE = ZB + ZMOTW. \quad (7.13)$$

For constant-voltage drive

$$\text{electrical power} \equiv PIN = |E|^2 YEE, \quad (7.14)$$

$$\text{radiation impedance} \equiv ZRAD = \text{same as Eq. 7.8}$$

$$\text{power conversion efficiency} \equiv ETA = \text{same as Eq. 7.9}$$

$$\text{motional admittance in air} \equiv YMOTA = -(YB \cdot ZEM)^2 / (ZM + ZEM^2 YB), \quad (7.15)$$

$$\text{electrical admittance in air} \equiv YEA = YB + YMOTA, \quad (7.16)$$

$$\text{motional admittance in water} \equiv YMOTW = -(YB + ZEM)^2 / (ZM + ZEM^2 YB + ZRAD), \quad (7.17)$$

$$\text{electrical admittance in water} \equiv YEE = YB + YMOTW. \quad (7.18)$$

Variables (in addition to $ZRAD$ and ETA) common to both constant-current drive and constant-voltage drive are

$$\text{core impedance} \equiv ZC = \frac{j\omega N^2 \mu^S \chi b \ell}{2\pi a} \quad (7.19)$$

(given in Part 1 as Eq. 7.2),

$$\text{copper loss leakage impedance} \equiv ZEL = REL + \frac{j\omega N^2 \mu_0}{2\pi a} (A_{\text{coil}} - A_{\text{core}}) \quad (7.20)$$

(given in Part 1 as Eq. 8.5),

$$\text{transduction coefficient} \equiv ZEM = 2\pi a \ell \psi = \frac{h_{\theta\theta} b \ell N \mu^S \chi}{a} \quad (7.21)$$

(given in Part 1 as Eq. 7.11),

$$\text{electrochemical coupling coefficient} \equiv K = \frac{h_{\theta\theta}^2 |\mu^S|}{Y}, \quad (7.22)$$

$$\text{electromechanical impedance} \equiv ZMP = j \frac{2\pi b \ell K^2 Y \chi}{a\omega}, \quad (7.23)$$

and

$$\text{mechanical impedance} \equiv ZMPP = RMPP + j \left(\frac{2\pi a \ell \rho b \omega - 2\pi b \ell Y}{a\omega} \right). \quad (7.24)$$

For constant-current drive [1, Eq. 6.21]

$$RMPP = \frac{\omega_1 M_s}{Q_1^I} - \text{Re} \left\{ ZMP(\omega_1) \right\}, \quad (7.25)$$

and for constant-voltage drive [1, Eq. 6.22]

$$RMPP = \frac{\Omega_1 M_s}{Q_1^E} + \text{Re} \left\{ \frac{(ZEL)(ZEM)^2}{(ZC)(Zb)} \right\} \text{ ref (6.22)} \quad (7.26)$$

The factor *CHI* (χ) is defined as follows [1, equation following 7.8]:

$$\text{eddy-current factor} = CHI = \chi = \frac{\tanh\left(\frac{j\omega_1 \mu_h \pi t^2}{2\rho_e}\right)^{1/2}}{\left(\frac{j\omega_1 \mu_h \pi t^2}{2\rho_e}\right)^{1/2}} \quad (7.27)$$

in which μ_h is the complex hysteresis term, assumed to be independent of frequency. If the hysteresis angle is known, it may be used directly as input to program EIGSHIP. Otherwise input to EIGSHIP calls for the total dip angle as measured from the constant-current motional impedance circle in air (Fig. 40). With this angle denoted by 2β the factor representing both hysteresis and eddy-current losses, $\bar{\mu}$, is defined as

$$\bar{\mu} \equiv |\bar{\mu}| e^{-j2\beta} = \mu^S e^{-j\eta} \chi = \mu_h \chi . \quad (7.28)$$

The hysteresis factor μ_h is assumed to have known magnitude μ^S but unknown angle η . The angle η is obtained by solving

$$\mu_h = \frac{\bar{\mu}}{\chi(\mu_h)} \quad (7.29)$$

[1, Eqs. 7.6 and 7.7] for the complex number μ_h . Finally χ is redefined so that it contains all angle information:

$$\chi = \chi e^{j\eta} = \text{Re}(\chi) - j\text{Im}(\chi). \quad (7.30)$$

The final Butterworth and Smith type quantity is, for constant-current drive,

$$\text{total open-circuit mechanical impedance} \equiv ZMOC = ZM = ZMP + ZMPP \quad (7.31)$$

or, for constant-voltage drive,

$$\text{total short-circuit mechanical impedance} \equiv ZMSC = ZM + (ZEM)^2/ZB \quad (7.32)$$

7.2.2 Second Page of Output: EIGSHIP MODEL

Thickness correction factors are used to obtain shell surface velocities from the reference surface velocities found from Eq. 7.4 or 7.6. Surface pressures are then calculated using the NRL computer program SHIP [1, Section 9]. The numbering of bands is shown in Fig. 39. Normal surface velocities and acoustic pressures for the "upper" half of the shell surface are displayed on the second page of the output.

Modal contributions to air and water impedances displayed next represent the expansion of motional impedance in terms of the modal shape functions used in the analysis.

Displayed next in the output are

$$\text{electrical power} \equiv PIN = |I|^2 ZEE \text{ (constant current)} \quad (7.33)$$

$$= |E|^2 YEE \text{ (constant voltage)} \quad (7.34)$$

and

$$\text{acoustic power} \equiv PA = \sum_j^{\text{all bands}} p_j v_j^* A_j, \quad (7.35)$$

where the asterisk means complex conjugate, p_j and v_j are the shell surface (not reference surface) pressure and surface velocity on the j th band, and A_j is the area of the j th band. This equation differs from Eq. 5.27 of Part 1 in that rms values are assumed in EIGSHIP. Also presented in the output is

$$\text{power conversion efficiency} \equiv EFF = \text{Re}(PA)/\text{Re}(PIN). \quad (7.36)$$

For constant-current drive the electrical motional impedance in air is, in accordance with Part 1 (Eqs. 5.24, 6.25, 6.32, and 6.64),

$$ZMOTA = \frac{j\omega 2\pi a \ell \psi^2}{\rho b} \sum_n^{NBRFNS} \frac{I_n}{N_n[\omega]_n}, \quad (7.37)$$

where $NBRFNS$ is the number of mode shapes used in the calculation. The total electrical impedance is

$$ZEA = ZB + ZMOTA \quad (7.38)$$

In water these quantities become

$$ZMOTW = 2\pi a \frac{\psi}{I} \left\{ 2b[VEL(j+1)] + \frac{\ell}{J} \sum_i^J VEL(i) \right\} \quad (7.39)$$

[1, Eqs. 5.24 and 6.42] and

$$ZEE = ZB + ZMOTW \quad (7.40)$$

Also, as given in Part 1 in the line following Eq. 6.42,

$$\text{blocked electrical impedance} \equiv ZB = ZEL + ZC. \text{ ref (6.42)} \quad (7.41)$$

For constant-voltage drive the electrical motional admittance in air is [1, Eqs. 5.26 and 6.23]

$$Y_{MOTA} = \frac{j\omega 2\pi a \ell \psi^2}{(ZB)^2 \rho b} \sum_n^{NBRFNS} \frac{I_n}{N_n [\Omega]_n} \quad (7.42)$$

The total electrical admittance is

$$YEA = YB + Y_{MOTA}. \quad (7.43)$$

In water, these quantities become

$$Y_{MOTW} = \frac{\psi 2\pi a}{ZB^*E} \left(2b^*VEL(J+1) + \frac{\ell}{J} \sum_i^J VEL(i) \right) \quad (7.44)$$

[1, Eq. 5.26],

$$YEE = YB + Y_{MOTW}, \quad (7.45)$$

and

$$YB = 1/ZB. \quad (7.46)$$

The two variables HL and ZL are common to constant-current drive and constant-voltage drive:

$$\text{radiation impedance} \equiv ZL = PA/VNM \quad (7.47)$$

in which the VNM is the normalizing factor defined in Section 5.3, and [1, Eq. 6.51]

$$\text{transduction coefficient} \equiv HL = \psi = \frac{h_{\theta\theta} b N \mu^S \chi}{2\pi a^2} \quad (7.48)$$

For constant-current drive the three quantities HR , TRP , and TRA take on the values

$$\text{magnetic field in coil} \equiv HR = NI/2\pi a, \quad (7.49)$$

$$\text{transmitting response in plane} \equiv TRP = 20 \log (FF0/|I|), \quad (7.50)$$

and

$$\text{transmitting response on axis} \equiv TRA = 20 \log (FF90/|I|), \quad (7.51)$$

where $FF0$ and $FF90$ are the far-field source level (referred to 1 meter) in the plane of the ring and in the axial direction respectively. The transmitting current response is expressed in dB relative to $1 N/m^2$ at 1 meter per ampere.

For constant-voltage drive

$$HR = E(YEE)N/2\pi a, \quad (7.52)$$

$$TRP = 20 \log (FF0/|E|), \quad (7.53)$$

and

$$TRA = 20 \log (FF90/|E|). \quad (7.54)$$

The quantities $FF0$ and $FF90$ are obtained from subroutine FARFLD, which calculates the far-field source level from the surface velocities and pressures. If the standard asymptotic form of the Green's function is used and the pressure and velocity are assumed constant over each band, the required integrations can be formed analytically.

The two quantities UH and UHE have the meanings

$$\text{permeability due to hysteresis} \equiv UH = \mu_h \quad (7.55)$$

(Eqs. 7.28ff) and

$$\text{total permeability} \equiv UHE = \bar{\mu} = \mu\chi(\mu_h) \quad (7.56)$$

[1, Eqs. 7.1ff].

The medium inertial reactance and shell stiffness reactance in air and water, ZKNA, ZSTA, ZKN, and ZST, are obtained from formulas discussed in Section 5.3.

If far-field beam patterns are required, an additional call to FARFLD

CALL FARFLD (IFD), IFD > 1

calculates and prints the far-field beam pattern at IFD + 1 points equally spaced between 0° and 90° . The results are given in dB referred to the value at 0° .

8. CONCLUSION TO PART 2

The computer program EIGSHIP has been used to generate the complete prediction of the electroacoustic response of three free-flooded magnetostrictive rings differing from each other principally in axial length. Physical models of these rings were constructed and were subjected to both in-air and in-water tests at NRL test facilities. Test data were compared with theoretical predictions on the several important performance parameters. It was found that EIGSHIP successfully predicts electroacoustic performance to within

reasonable tolerances. In addition to demonstrating the validity of the EIGSHIP model, this report also includes a detailed analysis of the test data using special analytic and graphical tools developed for this purpose. These tools are considered an important by-product of the research on the subject of magnetostrictive rings.

9. ACKNOWLEDGMENTS

The authors acknowledge the assistance given to them by the following members of the Acoustics Division: Dr. J. Sinsky, for help in obtaining the physical models; Mr. D. Dorsey, Mr. D. Gregan, and Mr. J. Neeley, for help in gathering test data; and Dr. L. Van Buren, for assistance in the analysis of the axial transmitting response.

10. REFERENCES AND BIBLIOGRAPHY

10.1 References

1. S. Hanish, R.V. Baier, B.J. King, and P.H. Rogers, "Electroacoustic Modeling of Magnetostrictive Shells and Rings, Part 1 — Mathematical Modeling," NRL Report 7767, Dec. 1974.
2. J. Chervenak, "A New NRL Acoustic Research Tank Facility," NRL Report 6822, Feb. 1969.
3. "The Design and Construction of Magnetostriction Transducers," Summary Technical Report of Division 6, NDRC Vol. 13, 1946, p. 69.
4. S. Butterworth and F.D. Smith, "The Equivalent Circuit of the Magnetostriction Oscillator," Proc. Phys. Soc. XLIII, 2, 166 (1931).
5. F.V. Hunt, *Electroacoustics*, Harvard University Press, Cambridge, Mass., 1954.
6. C.B. Sharma, "Calculation of Natural Frequencies of Fixed-Free Circular Cylindrical Shells," Jo. Sound and Vibration 35 (1), 55-76 (1974).
7. A.S. Merriweather, "The Modes of Vibration in Water of Ferroelectric Cylindrical Tubes Devoid of All Forms of Pressure-Release," NEL Technical Memorandum TM-501, Oct. 1961.
8. E. Skudrzyk, *The Foundations of Acoustics*, Springer-Verlag, New York, 1971, p. 600.
9. P.H. Rogers, "SHIP (Simplified-Helmholtz-Integral Program), A Fast Computer Program for Calculating the Acoustic Radiation and Radiation Impedance for Free-Flooded-Ring and Finite-Circular-Cylinder Sources," NRL Report 7240, June 1972.

10.2 BIBLIOGRAPHY

- W.S. Cramer, "Magnetostrictive Materials and Their Application to Underwater Sound Transducers," U.S. Navy Journal of Underwater Acoustics 17, 199 (Apr. 1967).
- E.A. Norfolk, Jr., and C.A. King, "Problems Encountered in the Repair and Maintenance of Magnetostrictive Sonar Transducers," U.S. Navy Journal of Underwater Acoustics 17, 215 (Apr. 1967).
- A.P. Edson, "Alloys for Magnetostriction Transducers," U.S. Navy Journal of Underwater Acoustics 17, 285 (Apr. 1967).
- F.G. Brockman, "Ferrites for Magnetostrictive Applications," U.S. Navy Journal of Underwater Acoustics 17, 319 (Apr. 1967).
- R.R. Whymark and K.E. Feith, "The Determination of Large Amplitude Properties of Magnetostrictive Nickel and Nickel Base Alloys in Transducer Design," Vol. II, Armour Research Foundation of Illinois Institute of Technology, Report ARF 1732-4, Feb. 1963.
- W.E. Lawrie et al., "High Power Magnetostrictors for Sonar Applications," Tracor document T-70-RV-5049-U, ONR Contract N00014-66-C-0119, Mar. 13, 1970.
- E.A. Neppiras, "New Magnetostrictive Materials and Transducers, I and II" J. Sound and Vibration 8 (No. 1), 408 and 431 (July 1968).
- R.R. Whymark, "Vibrations of a Magnetostrictive Tube," Tracor document RL/69-024-U, ONR Contract N000 14-66-C-0119, Mar. 17, 1969.
- O.N. Al'tgauzen, L.S. Bezuglaya, Z.N. Bulycheva, and O.V. Lyubelskaya, "Magnetic Properties of Alloys for Magnetostrictive Transducers," Sov. Phys. Acoust. 12 (No. 3), 249 (1967).
- R.S. Woollett, "Power Limitations of Sonic Transducers," IEEE Trans. Sonics and Ultrasonics Su-15 (No. 4), 218 (Oct. 1968).
- B.A. Wise, "Design of Nickel Magnetostriction Transducers," The International Nickel Co.
- Z. Jagodzinski, "On the Adequacy of Equivalent Circuits for Piezomagnetic Transducers," Acustica 21, 283 (1969).
- Y. Kikuchi and H. Shimizu, "On the 'B-Type' Resonance of Magnetostriction and Electrostriction Transducers," The Reports of the Research Institute of Electrical Communication, Tohoku Univ. 4B, 173-203 (1952).
- Y. Kikuchi, "Ultrasonic Transducers," Corona Publishing Co., Tokyo, 1969.

Y. Masiyama, "On the Magnetostriction of Iron-Nickel Alloys," *The Science Reports of the Tohoku Imperial Univ., First Series* **20**, 574-593 (1931).

J.A. Sinsky, "Acoustic Near-Field Measurements of a Free-Flooded Magnetostrictive Ring," *NRL Report* 7328, Dec. 1971.

J.A. Sinsky, "Comparison of a Cube-Textured-Nickel and a Nickel-200 Magnetostrictive Ring Transducer," *NRL Report* 7779, Aug. 1974.

R.S. Woollett, "Effective Coupling Factor of Single-Degree-of-Freedom Transducers," *J. Acoust. Soc. Am.* **40**, 1112 (1966).

R.S. Woollett, "Electromechanical Evaluation of Magnetostrictive Cylinders by Resonance-Antiresonance Measurements," *USL Report* 225, Dec. 1953.

R.S. Woollett, "Magnetostrictive Material Requirements for Sonar Transducers," *J. Underwater Acoustics* **20**, 679 (1970).

L.W. Camp, "Magnetostrictive Properties of low-Cobalt Nickel Alloys," *J. Underwater Acoustics* **10**, 95 (1960).

L.W. Camp, "Magnetostrictive Longitudinal Vibrators," *J. Underwater Acoustics* **17**, 245 (1967).

B.A. Wise, "Technology of Magnetostrictive Transducers Related to Material Requirements," *J. Underwater Acoustics* **20**, 691 (1970).

R.J. Bulmer, T.J. Meyers, and E.J. Parssinen, "Free-Flooding Magnetostrictive Scroll Transducers," *J. Underwater Acoustics* **17**, 251 (1967).

T.J. Meyers, "Evaluation of Low-Frequency, Broad-Band, Free-Flooding Magnetostrictive Scroll Transducers," *USL Report* 754, June 1966.

G.C. Connolly, "Performance Characteristics of the XU-1405 Free-Flooded Magnetostrictive Scroll Transducer," *USL Report* TD-12-308-73, July 1973.

C.M. van der Burgt, "Dynamical Physical Parameters of the Magnetostrictive Excitation of Extensional and Torsional Vibrations in Ferrites," *Philips Res. Rpt.* **8**, 91-132 (1953).

R.R. Whymark and J.M. Witting, "Resonant Displacement of Nickel and Permendur Magnetostrictors under Static Compressive Stress," *J. Acoust. Soc. Am.* **33**, (No. 12), 1720 (Dec. 1961).

C.A. Clark, "The Dynamic Magnetostriction of Nickel-cobalt Alloys," *British J. of Appl. Phys.* **7**, 355 (Oct. 1956).

R.R. Whymark, "A Nonlinear Design Technique for High Power Magnetostrictors," *Tracor document* 68/197-U, Jan. 1969.

J.A. Sinsky, "An Experimental Description of a Free-Flooded Finite-Length Radiating Magnetostrictive Ring Transducer," *NRL Report* 7887, June 1975.

Appendix A

COMPUTER LISTING OF EIGSHIP

```

PROGRAM EIGSHIP
TYPE COMPLEX CFM,CHI,CHIE,CUR,CURQ,DNM,DRIVE,E,G,GS,HL,HK,KSQ,MOL,
18MA,DMBKT,PA,PINB,PINF,RLML,S,SP,STR,UH,UHE,UHEF,VA,VES,VBSA,VEL,
2VELS,VG,VH,VING,VJ,VK,VL,YB,YEA,YEAF,YEE,YEEF,YMOTA,YMOTAF,
3YMOTW,YMOTWF,Z,ZB,ZC,ZEA,ZEAF,ZEE,ZEEF,ZEL,ZEM,ZKN,ZKNA,ZL,ZM,ZMA,
4ZMOC,ZMOT,ZMOTA,ZMOTAF,ZMOTW,ZMOTWF,ZMP,ZMPP,ZMSC,ZMW,ZRAD,ZSAC,
5ZST,ZSTA,ZTRM,ZZ
TYPE REAL LC,LTH,MSTAT,NA,NR,NU
DIMENSION AXEDGE(9),CFM(11),DNM(9),EOMEGA(9),FK(2),FRQ(9),
1G(30,30),GS(11,11),MOL(9),DMBKT(9),RD(9,10),RDIN(9,10),RINT(9),
2SP(60),STR(11,12),VA(11,12),VEL(11),VELS(60),VG(11,11),VH(11),
3VJ(11,11),VK(11,11),VL(11,11),ZMA(9),ZMW(9)
DIMENSION DMY(4200),DUM(3600),REST(5704)
COMMON/VNM/VNM
COMMON/5/VJ,VK,GS,STR,VA,VG,REST
COMMON/6/DUM,G,DMY
COMMON/INT/CFM,UX2I,UZI,WZI,UXWI,WXX2I,UXXXI
COMMON/VEL0/VELS/FF/ICOR,NPTS /LC/LCMAX,LCMAXH /FUD/PI,FM
COMMON/RAD/RIN,ROUT/BLK1/H,RMEAN,FK,PI/PIT/JMAX,JMAXH,IMAX
COMMON /YND/Y,NU,RHO,NDS/PA/PA,RHOCA/DIST/DIST
COMMON /RRCC/RRCC/FFPR/FF0,FF90/ANS/SP/FRK/FR
COMMON/MODES/FRQ,RO,RDIN,MBRFNS,THK,NDEM,AXEDGE,RINT
PI = 3.141592654
U0 = PI*4.E-7

C
C READ IN PARAMETERS.
C
READ 01,ICHT,DRIVE
61 FORMAT (I1,C(E9.5,E10.5))
READ 62,JMAXH,IMAX
62 FORMAT (2I5)
READ 63,RMEAN,THK,LTH,RHO,NU,Y
63 FORMAT (6E10.5)
READ 64,THST,RES,URS,HTT,DIP,IHYS
64 FORMAT (5F10.5,I1)
READ 65,NTRN,THC,LC,REL
65 FORMAT (110,3E10.5)
READ 66,RHOF,CF
66 FORMAT (2E10.5)
READ 67,G
67 FORMAT (E10.5)

C
C CALCULATE AUXILIARY PARAMETERS.
C
AREA = 2.*PI*RMEAN*LTH
NDEM = JMAXH
NDS = 2*IPAX+1
RRCC = RHOF*CF
DIPR = DIP*PI/360.
IF (IHYS.EQ.1) HSTAN = DIP
AM = THK*LTH

```

```

AC01L = THK*LC
NSQ = NTRN*NTRN
US = URS*U0
UHE = US*CMPLX(COSF(DIPR),SINF(DIPR))
H = LTH/2.
ROUT = RMEAN+THK/2.
RIN = RMEAN-THK/2.
MSTAT = 2.*PI*RMEAN*THK*LTH*RHO
ROM = ROUT/RMEAN
RIM = RIN/RMEAN
LCMAXH = JMAXH+JMAXH+IMAX
LCM1 = LCMAXH + 1
MXSIZE = JMAXH
MX1 = MXSIZE + 1
MXE = JMAXH + IMAX
MX2 = MX1 + 1
FC = 2.*RES/(PI*THST*THST)

C
C READ IN FREQUENCY INTERVAL FOR SUBROUTINE THFREQ.
C
READ 45,FR(1),FR(2)
45 FORMAT (2F10.5)
T1 = TIMELEFT(K)

C
C OBTAIN THICKNESS CORRECTION FACTORS FI AND FO FROM SUBROUTINE THFREQ.
C
CALL THFREQ
T2 = TIMELEFT(K)
TM = T1 - T2
PRINT 5000,TM
5000 FORMAT (/1X*TIME FOR THFREQ IS* F10.3/)
T1 = TIMELEFT(K)
FI = FO = 1.

C
C OBTAIN ELASTIC RESONANCE FREQUENCIES FRQ(), MODE SHAPES RD() AND
C AXEDGE(), AND INTEGRALS OF MODE SHAPES RDIN(,) AND RINT(,) FROM
C SUBROUTINE EIGFNS.
C
CALL EIGFNS
T2 = TIMELEFT(K)
TM = T1 - T2
PRINT 5001,TM
5001 FORMAT (/1X*TIME FOR EIGFNS IS* F10.3/)
DO 22 I = 1,NBRFNS
22 OMEGA(I) = 2.*PI*FRQ(I)

C
C PRINT INPUT PARAMETERS.
C
PRINT 1000
1000 FORMAT (1H158X *INPUT PARAMETERS*//35X *THIN WALLED ELASTIC CYLI
$NDRICAL TUBE MAGNETOSTRICTIVE MATERIAL*/52X

```

HANISH, KING, BAIER, AND ROGERS

```

$ *ALL UNITS ARE IN MKS SYSTEM*
  IF (ICRT.EQ.0) GO TO 1014
  CUR = DRIVE
  PRINT 1004,CUR
1004 FORMAT (/43X19HCURRENT DRIVE CUR = C(E14.6,E14.6))
  GO TO 1013
1014 E = DRIVE
  PRINT 1005,E
1005 FORMAT (/43X17MVOLTAGE DRIVE E =C(E14.6,E14.6))
1013 PRINT 1006,JMAXH,IMAX
1006 FORMAT (/751X28HNUMBER OF SIDE BANDS JMAXH =I3/51X
  $28HNUMBER OF END BANDS IMAX =I3)
  PRINT 1001,RMEAN,THK,LTH,RMO,NU,Y
1001 FORMAT (/750X *CYLINDER DIMENSIONS AND PROPERTIES*/732X11HMEAN RA
  $DIUS38X7HRMEAN =E14.6/
  $32X16HRADIAL THICKNESS35X5HTHK =E14.6/
  $32X12HAXIAL LENGTH39X5HLTH = E14.6/
  $32X7HDENSITY44X5HRHO =E14.6/
  $32X14HPPOISSONS RATIO38X4HNU =E14.6/
  $32X45HYOUNGS MODULUS AT CONSTANT MAGNETIC INDUCTION BX3HY =E14.6)
  PRINT 1002,THST,RES,URS,UO,US,HTT
1002 FORMAT (/748X *SCROLL TAPE DIMENSIONS AND PROPERTIES*/732X
  $9HTHICKNESS41X6HTHST =E14.6/32X11HRESISTIVITY40X5HRES =E14.6/
  $32X49HRELATIVE MAGNETIC PERMEABILITY AT CONSTANT STRAIN2X5HURS =
  $E14.6/32X26HPERMEABILITY OF FREE SPACE 26X4HUO =E14.6/
  $32X40HMAGNETIC PERMEABILITY AT CONSTANT STRAIN 12X4HUS =E14.6/
  $32X29HPIEZOMAGNETIC STRESS CONSTANT 22X5HHTT =E14.6)
  IF (IHYS.EQ.1) GO TO 56
  PRINT 57,DIP
  57 FORMAT (32X15HTOTAL DIP ANGLE 36X5HDIP =E14.6)
  GO TO 58
  56 PRINT 59,HSTAN
  59 FORMAT (32X16HHYSTERESIS ANGLE 33X7HHSTAN =E14.6)
  58 PRINT 1003,NTRN,THC,LC,REL
1003 FORMAT (/754X *COIL WINDING DIMENSIONS*/732X15HNUMBER OF TURNS35X
  $6HNTRN =I14/32X16HRADIAL THICKNESS35X5HTHC =E14.6/
  $32X12HAXIAL LENGTH40X4HLC =E14.6/
  $32X19HCOPPER LOSS IN COIL 32X5HREL =E14.6)
  PRINT 1007,RHOF,CF
1007 FORMAT (/750X *EXTERNAL FLUID MEDIUM PROPERTIES*/732X7HDENSITY43X
  $6HRHOF =E14.6/32X14HSPEED OF SOUND38X4HCF =E14.6)
  NDX = 0
C
C   DEFINE MODAL MASSES MDL().
C
  DO 1110 I = 1,NBRFNS
1110 MDL(I) = MSTAT
  49 NDX = NDX + 1
C
C   READ IN DRIVING FREQUENCY, AIR/WATER FLAG, AND FAR FIELD REQUEST.
C   NOTE THAT FIRST FREQUENCY READ IN MUST BE CONSTANT CURRENT RESONANCE

```

NRL REPORT 7964

```

C   FREQUENCY FOR FIRST RADIAL MODE.
C
  READ 50,FREQDR,IAIR,IFD
50  FORMAT (F10.5,2I5)
    IF (EOF,60) 51,52
52  OMEGA = 2.*PI*FREQDR
    FK = OMEGA/CF
    OMA = CMPLX(0.,OMEGA)
    IF (NDX,GT,1) GO TO 43
C
C   OBTAIN RMPP AND QE OR QI FOR USE AT ALL DRIVING FREQUENCIES. THIS
C   CALCULATION IS PERFORMED ONLY ONCE.
C
  UH = US
  IF (IHYS,EQ,1) GO TO 53
  DO 41 I = 1,16
  Z = CSQRT(FREQDR*UH/FC*(0.,1.))
  ZZ = CEXP(2.*Z)
  CHI = (ZZ-1.)/((ZZ+1.)*Z)
  CHA = CANG(CHI)
  HTRA = DIPR - CHA
41  UH = US*CMPLX(COSF(HTRA),SINF(HTRA))
    GO TO 54
53  HTRA = HSTAN*PI/180.
  UH = US*CMPLX(COSF(HTRA),SINF(HTRA))
  Z = CSQRT(FREQDR*UH/FC*(0.,1.))
  ZZ = CEXP(2.*Z)
  CHI = (ZZ-1.)/((ZZ+1.)*Z)
54  CHIE = CHI
  UHE = CHI*UH
  UG = CANG(UH)
  CHI = CHI*CMPLX(COSF(UG),SINF(UG))
  CHIR = REAL(CHI)
  CHII = -AIMAG(CHI)
  BKSQ = HTT*HTT*CAHS(UH)/Y
  SRTH = SQRTF(BKSQ)
  Z = CSQRT(FRQ(1)*UH/FC*(0.,1.))
  ZZ = CEXP(2.*Z)
  UHEE = (ZZ-1.)/((ZZ+1.)*Z)*UH
  XEL = EOMEGA(1)*NSQ*UO/(2.*PI*RMEAN)*(ACBTL-AM)
  ZEL = CMPLX(REAL,XEL)
  ZC = EOMEGA(1)*NSQ*UHEE*AM/(2.*PI*RMEAN)*(0.,1.)
  ZB = ZEL + ZC
  ZEM = HTT*AM*NTRN/RMEAN*UHEE
  ZTRM = ZEL*ZEM**2/(ZC*ZB)
  IF (ICRT,EQ,0) GO TO 31
  QI = 0
  RMPP = OMEGA*MSTAT/QI - EOMEGA(1)**2*MSTAT*BKSQ*CHII/OMEGA
  QE = EOMEGA(1)*MSTAT/(RMPP - REAL(ZTRM))
  GO TO 32
51  QE = 0

```

HANISH, KING, BAIER, AND ROGERS

```

RMPP = EOMEGA(1)*MSTAT/QE + REAL(ZTRM)
QI = OMEGA*MSTAT/(RMPP+EOMEGA(1)**2*MSTAT*BKSG*CHII/OMEGA)
C
C PRINT VALUES OF QE AND QI.
C
32 PRINT 1060,QE,QI
1060 FORMAT (/60X15HQUALITY FACTORS//32X16HCONSTANT VOLTAGE36X4HQE =
3E14.6/32X16HCONSTANT CURRENT36X4HQI =E14.6)
GO TO 46
C
C OBTAIN VARIOUS BUTTERWORTH AND SMITH QUANTITIES.
C
43 Z = CSQRT(FREQDR*UH/FC*(0.,1.))
ZZ = CEXP(2.*Z)
CHI = (ZZ-1.)/((ZZ+1.)*Z)
CHIE = CHI
UHE = CHI*UH
UG = CANG(UH)
CHI = CHI*CMPLX(COSF(UG),SINF(UG))
CHIR = REAL(CHI)
CHII = -AIMAG(CHI)
46 HL = HTI*THK*NTRN/(2.*PI*RMEAN**2)*UHE
XEL = OMEGA*NSQ*UU/(2.*PI*RMEAN)*(AC01L-AM)
ZEL = CMPLX(REL,XEL)
ZC = OMEGA*NSQ*UHE*AM/(2.*PI*RMEAN)*(0.,1.)
ZB = ZEL + ZC
YB = 1./ZB
ZEM = HTI*AM*NTRN/RMEAN*UHE
REM = REAL(ZEM)
XEM = AIMAG(ZEM)
ZMP = 2.*PI*AM*BKSG*Y/(PMEAN*OMEGA)*CMPLX(CHII,CHIR)
XMPP = 2.*PI*OMEGA*RH0*AM*RMEAN-2.*PI*AM*Y/(RMEAN*OMEGA)
RMP = REAL(ZMP)
ZMPP = CMPLX(RMPP,XMPP)
RZM = RMPP/(2.*PI*RMEAN*LTH)
ZM = ZMP + ZMPP
ZMOC = ZM
ZMSC = ZM + ZEM*ZEM/ZB
ZMOTA = ZEM*ZEM/ZM
ZEA = ZB + ZMOTA
YMOTA = -(YB*ZEM)**2/(ZM+ZEM*ZEM*YB)
YEA = YB + YMOTA
C
C OBTAIN INFLUENCE COEFFICIENTS VL(,) FOR CONSTANT CURRENT CASE.
C
ZTRM = RMPP - HL*HL*ZEL*AREA**2/(ZC*ZB)
S = (0.,0.)
DO 23 I = 1,NBRFNS
OMBKT(I) = EOMEGA(1)**2 - OMEGA**2 + OMA*ZTRM/MDL(I)
23 S = S + 2.*PI*RMEAN*RINT(I)*(2.*RINT(I)+2.*THK*AXEDGE(I))/(LTH/2.*
$OMBKT(I))

```

```

KSO = OMA*HL*HL*S/(CHI*ZC*RH0*THK)
DO 24 I = 1,NBRFNS
24 DNM(I) = LTH/2.*RH0*THK*(1. -KSO*CHI*ZC/ZB)*OMBKT(I)
DO 55 I = 1,MXSIZE
DO 55 J = 1,MXSIZE
VL(I,J) = (0.,0.)
DO 55 K = 1,NBRFNS
55 VL(I,J) = VL(I,J) + RD(K,I)*RDIN(K,J)/DNM(K)*OMA
DO 44 J = 1,MXSIZE
VL(MX1,J) = (0.,0.)
DO 44 K = 1,NBRFNS
44 VL(MX1,J) = VL(MX1,J) + AXEDGE(K)*RDIN(K,J)/DNM(K)*OMA
IF (ICRT.EQ.1) GO TO 400

```

```

C
C CALCULATE INFLUENCE MATRIX NEEDED FOR CONSTANT VOLTAGE CASE AND PLACE
C IN ARRAY VL(.).
C

```

```

DO 404 I = 1,MX1
DO 404 J = 1,MXSIZE
404 VK(I,J) = VL(I,J)
DO 403 I = 1,MX1
DO 403 J = 1,MX1
VJ(I,J) = (0.,0.)
DO 403 K = 1,MXSIZE
403 VJ(I,J) = VJ(I,J) + VL(I,K)
DO 408 I = 1,MX1
DO 408 J = 1,MXSIZE
408 VJ(I,J) = HL**2*AREA/JMAXH/ZB*VJ(I,J)
DO 409 I = 1,MX1
409 VJ(I,MX1) = HL**2*4.*PI*RMEAN*THK/ZB*VJ(I,MX1)
DO 407 I = 1,MX1
407 VJ(I,1) = VJ(I,1) + (1.,0.)
CALL CINV(VJ,MX1,11)
DO 412 I = 1,MX1
DO 412 J = 1,MXSIZE
VL(I,J) = (0.,0.)
DO 412 K = 1,MX1
412 VL(I,J) = VL(I,J) + VJ(I,K)*VK(K,J)

```

```

C
C OBTAIN NORMAL VELOCITIES VEL() IN AIR ON REFERENCE SURFACE BANDS.
C

```

```

400 DO 4 I = 1,MX1
VH(I) = (0.,0.)
DO 4 J = 1,MXSIZE
4 VH(I) = VH(I) + VL(I,J)
IF (ICRT.EQ.1) GO TO 11
DO 12 I = 1,MX1
12 VH(I) = VH(I)*HL*E/ZB
GO TO 13
11 DO 14 I = 1,MX1
14 VH(I) = VH(I)*CUR*HL

```

HANISH, KING, BAIER, AND ROGERS

```

13 DO 73 I = 1, MX1
73 VEL(I) = VH(I)
C
C      OBTAIN COEFFICIENTS OF VELOCITY EXPANSION IN MODE SHAPES CFM() FROM
C      SUBROUTINE MDS.
C
      CALL MDS(VA, STR, RD, NBRFNS, VEL, CFM)
C
C      USE COEFFICIENTS TO OBTAIN MODAL CONTRIBUTIONS TO MOTIONAL IMPEDANCE OR
C      ADMITTANCE ZMA(). SUM CONTRIBUTIONS TO OBTAIN TOTAL MOTIONAL IMPEDANCE
C      ZMOTAF OR ADMITTANCE YMOTAF.
C
      ZMOT = (0., 0.)
      DO 36 I = 1, NBRFNS
      ZMA(I) = CFM(I)*4.*PI*RMEAN*(RINT(I)+THK*AXEDGE(I))
36 ZMOT = ZMOT + ZMA(I)
      IF (ICRT.EQ.1) GO TO 37
      YMOTAF = -HL/(ZB*E)*ZMOT
      YFAF = YMOTAF + YB
      DO 33 I = 1, NBRFNS
33 ZMA(I) = ZMA(I)*HL/(ZB*E)
      GO TO 38
37 ZMOTAF = HL/CUR*ZMOT
      ZEAF = ZB + ZMOTAF
      DO 39 I = 1, NBRFNS
39 ZMA(I) = ZMA(I)*HL/CUR
C
C      CALCULATE BUTTERWORTH AND SMITH VELOCITY IN AIR VBSA.
C
38 ZSB = Y*THK/(OMEGA*RMEAN**2)
      ZSBC = ZSB*(BKSG*CH11 + (0., 1.)*(BKSG*CH1R-1.))
      VBSA = (ICRT*HL*CUR + (1-ICRT)*HL*E/ZB)/(OMEGA*RH0*THK*
      $(0., 1.) + R2M + ZSBC + (1-ICRT)*HL*HL*2.*PI*RMEAN*LTH/ZB)
      VBM = CABS(VBSA)
      VBA = CANG(VBSA)*180./PI
      IF (ICRT.EQ.0) GO TO 1018
C
C      PRINT ALL AIR VELOCITIES.
C
      PRINT 1020, CUR, FREQDR
1020 FORMAT (1H144X15HCURRENT DRIVE =C(E14.6,E14.6),15X11HFREQUENCY =
      $E14.6)
      GO TO 1019
1018 PRINT 1021, E, FREQDR
1021 FORMAT (1H144X15HVOLTAGE DRIVE =C(E14.6,E14.6),15X11HFREQUENCY =
      $E14.6)
1019 PRINT 1010
1010 FORMAT (/61X11HOUTPUT DATA)
      PRINT 1022
1022 FORMAT (/49X35HREFERENCE SURFACE VELOCITIES IN AIR//48X4HREAL
      $7X9HIMAGINARY7X9HMAGNITUDESX14HANGLE(DEGREES)/)

```

NRL REPORT 7964

```

PRINT 1023,VBSA,VBM,VBA
1023 FORMAT (1X21HBUTTERWORTH AND SMITH11X5HVELBS3X1H=C(E14.6,E14.6),
$E15.6,7XF9.3/)
I = 1
VELMG = CABS(VEL(I))
VELAN = CANG(VEL(I))*180./PI
PRINT 1011,1,VEL(I),VELMG,VELAN
1011 FORMAT (1X11HNRL EIGSHIP21X4HVEL(I2,3H) =C(E14.6,E14.6),E15.6,
$7XF9.3)
DO 87 I = 2, MX1
VELMG = CABS(VEL(I))
VELAN = CANG(VEL(I))*180./PI
87 PRINT 34,1,VEL(I),VELMG,VELAN
34 FORMAT (33X4HVEL(I2,3H) =C(E14.6,E14.6),E15.6,7XF9.3)
C
C OBTAIN INTEGRALS NECESSARY FOR CALCULATING SHELL STIFFNESS REACTANCE
C AND MEDIUM INERTIAL REACTANCE IN AIR FROM ENTRY POINT IMPD OF SUBROUTINE
C EIGFNS.
C
DO 878 I = 1,NBRFNS
878 CFM(I) = CFM(1)/DMA
CALL IMPD
C
C CALCULATE SHELL STIFFNESS REACTANCE ZSTA AND MEDIUM INERTIAL REACTANCE
C ZKNA IN AIR.
C
VNM = 2.*CABS(VEL(MX1))**2*RMEAN*THK
DO 881 I = 1,JMAXH
881 VNM = VNM + (RQUT*FO + RIN*FI)*CABS(VEL(I))**2*LTH/JMAXH
VNM = VNM/(2.*RMEAN*(LTH+THK))
ZSTA = 2.*PI*Y*RMEAN*THK/(1.-NU*NU)*(UX2I+W2I+UX*WI)
$+ PI/6.*(THK/RMEAN)**2*Y*RMEAN*THK/(1.-NU*NU)*(WXX2I+W2I-UX*WXX1)
ZSTA = 2.*ZSTA*DMA/VNM*(1.-BKSG*CHIR)
ZKNA = OMEGA**2*MSSTAT/LTH*2.*(U2I+W2I*RMEAN**2)/VNM*DMA
IF (LAIR.EQ.0) GO TO 88
C
C IF ONLY AIR RESULTS ARE DESIRED THEN PRINT ALL OUTPUT QUANTITIES.
C
PRINT 1025
IF (ICRT.EQ.0) GO TO 76
PRINT 1101,ZMOTA,ZEA
1101 FORMAT(29X25HMOTIONAL IMPEDANCE IN AIR 18X7HZMOTA =C(E14.6,E14.6)/
$29X27HELECTRICAL IMPEDANCE IN AIR 18X5HZEA =C(E14.6,E14.6))
GO TO 79
76 PRINT 1102,YMOTA,YEA
1102 FORMAT(29X26HMOTIONAL ADMITTANCE IN AIR 17X7HYMOTA =C(E14.6,E14.6)
$29X28HELECTRICAL ADMITTANCE IN AIR 17X5HYEA =C(E14.6,E14.6))
79 PRINT 1027,ZC,ZEL,ZEM,SRTB,ZMP,ZMPP,CHIE
IF (ICRT.EQ.0) GO TO 82
PRINT 1030,ZMOC
PRINT 1012

```

HANISH, KING, BAIER, AND ROGERS

```

      PRINT 1103,ZM0TAF,ZEAF,ZB
1103 FORMAT (29X25HMOTIONAL IMPEDANCE IN AIR 18X7HZM0TA =
      $C(E14.6,E14.6)/
      $29X27HELECTRICAL IMPEDANCE IN AIR 18X5HZEA =C(E14.6,E14.6)/
      $29X28HBLOCKED ELECTRICAL IMPEDANCE 18X4HZB =C(E14.6,E14.6))
      GO TO 86
      82 PRINT 1040,ZMSC
      PRINT 1012
      PRINT 1104,YM0TAF,YEAF,YB
1104 FORMAT (29X26HMOTIONAL ADMITTANCE IN AIR 17X7HYM0TA =
      $C(E14.6,E14.6)/
      $29X28HELECTRICAL ADMITTANCE IN AIR 17X5HYEA =C(E14.6,E14.6)/
      $29X29HBLOCKED ELECTRICAL ADMITTANCE 17X4HYB =C(E14.6,E14.6))
      86 PRINT 1105,HL,UH,UHE,ZKNA,ZSTA
1105 FORMAT(29X24HTRANSDUCTION COEFFICIENT 22X4HHL =C(E14.6,E14.6)/
      $29X30HPERMEABILITY DUE TO HYSTERESIS 16X4HUH =C(E14.6,E14.6)/
      $29X18HTOTAL PERMEABILITY27X5HUHE =C(E14.6,E14.6)/
      $29X29HMEDIUM INERTIAL REACTANCE AIR 15X6HZKNA =C(E14.6,E14.6)/
      $29X29HSHELL STIFFNESS REACTANCE AIR 15X6HZSTA =C(E14.6,E14.6))
      TM = TIMELEFT(K)
      PRINT 98,TM
      98 FORMAT (1X4HTIME FB.2)
C
C      GO BACK TO READ ANOTHER DRIVING FREQUENCY.
C
      GO TO 49
C
C      CONTINUE CALCULATIONS FOR WATER BY OBTAINING TRUE SURFACE RADIATION
C      GREENS FUNCTION G(,) FROM SUBROUTINE SHIP AND THEN CALCULATING REFERENCE
C      SURFACE GREENS FUNCTION GS(,).
C
      88 CALL SHIP
      DO 71 I = 1,MXSIZE
      DO 71 J = 1,MXSIZE
      71 GS(I,J) = (G(I,J)*RIM-G(LCM1-I,J)*ROM)*F1 + (G(LCM1-I,LCM1-J)*ROM
      $-G(I,LCM1-J)*RIM)*F0
      DO 75 I = 1,MXSIZE
      GS(I,MX1) = (0.,0.)
      DO 75 J = MX1,MXE
      75 GS(I,MX1) = GS(I,MX1) + G(LCM1-1,J)*ROM - G(I,J)*RIM
      DO 74 I = 1,MX1
      DO 74 J = 1,MX1
      VG(I,J) = (0.,0.)
      DO 74 K = 1,MXSIZE
      74 VG(I,J) = VG(I,J) + VL(I,K)*GS(K,J)
      DO 72 I = 1,MX1
      72 VG(I,I) = VG(I,I) + (1.,0.)
      DO 198 I = 1,MX1
      DO 198 J = 1,MX1
      198 VA(I,J) = VG(I,J)
      DO 199 I = 1,MX1

```


HANISH, KING, BAIER, AND ROGERS

```

C
  RML = REAL(ZM+ZRAD)
  AIML = AIMAG(ZM+ZRAD)
  ETA = REAL(ZRAD)*(REM*REM + XEM*XEM)/((REL + REAL(ZC))*(RML*RML +
  $AIML*AIML) + (REM*REM - XEM*XEM)*RML + 2.*REM*XEM*AIML)
  PRINT 1025
1025 FORMAT (/57X21HBUTTERWORTH AND SMITH/85X4HREAL7X9HIMAGINARY/)
  IF (ICRT.EQ.0) GO TO 1016
  ZMOTW = ZEM*ZEM/(ZM+ZRAD)
  ZEE = ZB + ZMOTW
  PINB = CABS(CUR)**2*ZEE
  PRINT 1026,PINB,ZRAD,ETA,ZMOTA,ZEA,ZMOTW,ZEE
1026 FORMAT (29X16HELECTRICAL POWER 29X5HPIN =C(E14.6,E14.6)/
  $29X19HRADIATION IMPEDANCE 25X6HZRAD =C(E14.6,E14.6)/
  $29X27HPOWER CONVERSION EFFICIENCY 18X5HETA =E14.6/
  $29X25HMOTIONAL IMPEDANCE IN AIR 18X7HZMOTA =C(E14.6,E14.6)/
  $29X27HELECTRICAL IMPEDANCE IN AIR 18X5HZEA =C(E14.6,E14.6)/
  $29X27HMOTIONAL IMPEDANCE IN WATER 16X7HZMOTW =C(E14.6,E14.6)/
  $29X29HELECTRICAL IMPEDANCE IN WATER 16X5HZEE =C(E14.6,E14.6))
  GO TO 1017
1016 YMOTW = -(YB*ZEM)**2/(ZM+ZEM*ZEM*YB+ZRAD)
  YEE = YB + YMOTW
  PINB = CABS(E)**2*YEE
  PRINT 1036,PINB,ZRAD,ETA,YMOTA,YEA,YMOTW,YEE
1036 FORMAT (29X16HELECTRICAL POWER 29X5HPIN =C(E14.6,E14.6)/
  $29X19HRADIATION IMPEDANCE 25X6HZRAD =C(E14.6,E14.6)/
  $29X27HPOWER CONVERSION EFFICIENCY 18X5HETA =E14.6/
  $29X26HMOTIONAL ADMITTANCE IN AIR 17X7HYMOTA =C(E14.6,E14.6)/
  $29X28HELECTRICAL ADMITTANCE IN AIR 17X5HYEA =C(E14.6,E14.6)/
  $29X28HMOTIONAL ADMITTANCE IN WATER 15X7HYMOTW =C(E14.6,E14.6)/
  $29X30HELECTRICAL ADMITTANCE IN WATER 15X5HYEE =C(E14.6,E14.6))
1017 PRINT 1027,ZC,ZEL,ZEM,SRIB,ZMP,ZMPP,CHIE
1027 FORMAT (29X14HCORE IMPEDANCE 32X4HZC =C(E14.6,E14.6)/
  $29X30HCOPPER LOSS, LEAKAGE IMPEDANCE 15X5HZEL =C(E14.6,E14.6)/
  $29X24HTRANSDUCTION COEFFICIENT 21X5HZEM =C(E14.6,E14.6)/
  $29X38HELECTROMECHANICAL COUPLING COEFFICIENT 9X3HK =E14.6/
  $29X27HELECTROMECHANICAL IMPEDANCE 18X5HZMP =C(E14.6,E14.6)/
  $29X20HMECHANICAL IMPEDANCE 24X6HZMPP =C(E14.6,E14.6)/
  $29X19HEDDY CURRENT FACTOR 25X6HCHIE =C(E14.6,E14.6))
  IF (ICRT.EQ.0) GO TO 1028
  PRINT 1030,ZMOC
1030 FORMAT (29X40HTOTAL MECHANICAL IMPEDANCE OPEN CIRCUIT 4X
  $6HZMOC =C(E14.6,E14.6))
  PRINT 1020,CUR,FREQDR
  GO TO 1039
1028 PRINT 1040,ZMSC
1040 FORMAT (29X41HTOTAL MECHANICAL IMPEDANCE SHORT CIRCUIT 3X
  $6HZMSC =C(E14.6,E14.6))
  PRINT 1021,E,FREQDR
1039 PRINT 1010
  PRINT 1012

```

NRL REPORT 7964

1012 FORMAT (/61X11HNRL EIGSHIP/)

C
C PRINT TRUE SURFACE PRESSURES AND VELOCITIES ON SURFACE BANDS.
C

PRINT 1041
1041 FORMAT (/61X12HRING SURFACE//28X17HSURFACE PRESSURES 47X
\$18HSURFACE VELOCITIES /1X4HBAND9X4HREAL7X9HIMAGINARY7X
\$9HMAGNITUDE3X14HANGLE(DEGREES)11X4HREAL7X9HIMAGINARY7X
\$9HMAGNITUDE3X14HANGLE(DEGREES)/)
DO 78 I = 1,LCMAXH
SPM = CABS(SP(I))
SPA = CANG(SP(I))*180./PI
VLM = CABS(VELS(I))
VLA = CANG(VELS(I))*180./PI
78 PRINT 1042,I,SP(I),SPM,SPA,VELS(I),VLM,VLA
1042 FORMAT (2X12,4XC(E14.6,E14.6),E15.6,2XF9.3,10XC(E14.6,E14.6),
\$E15.6,2XF9.3)

C
C PRINT MODAL CONTRIBUTIONS TO MOTIONAL IMPEDANCE OR ADMITTANCE.
C

IF (ICRT.EQ.0) GO TO 1053
DO 1032 I = 1,NBRFNS
1032 ZMW(I) = ZMW(I)*HL/CUR
PRINT 1031,(ZMA(I),ZMW(I),I=1,NBRFNS)
1031 FORMAT (/27X*MODAL CONTRIBUTIONS TO AIR IMPEDANCE*5X*MODAL CONTRIB
UTIONS TO WATER IMPEDANCE*/(31XC(E14.6,E14.6),15XC(E14.6,E14.6)))
GO TO 1054
1053 DO 1052 I = 1,NBRFNS
1052 ZMW(I) = ZMW(I)*HL/(ZB*E)
PRINT 1051,(ZMA(I),ZMW(I),I=1,NBRFNS)
1051 FORMAT (/27X*MODAL CONTRIBUTIONS TO AIR ADMITTANCE*5X*MODAL CONTRI
UTIONS TO WATER ADMITTANCE*/(31XC(E14.6,E14.6),15XC(E14.6,E14.6)))

C
C CALCULATE AND PRINT VARIOUS EIGSHIP OUTPUT QUANTITIES.
C

1054 EFF = REAL(PA)/REAL(PINF)
PRINT 1044,PINF,PA,EFF
1044 FORMAT (/29X16HELECTRICAL POWER 29X5HPIN =C(E14.6,E14.6)/
\$29X14HACOUSTIC POWER 32X4HPA =C(E14.6,E14.6)/
\$29X27HPOWER CONVERSION EFFICIENCY 18X5HEFF =E14.6)
CALL FARFLD(1)
IF (ICRT.EQ.0) GO TO 1048
PRINT 1045,ZMOTAF,ZEAF,ZMOTWF,ZEEF,ZB
1045 FORMAT (29X25HMOTIONAL IMPEDANCE IN AIR 18X7HZMOTA =
\$C(E14.6,E14.6)/
\$29X27HELECTRICAL IMPEDANCE IN AIR 18X5HZEA =C(E14.6,E14.6)/
\$29X27HMOTIONAL IMPEDANCE IN WATER 16X7HZMOTW =C(E14.6,E14.6)/
\$29X29HELECTRICAL IMPEDANCE IN WATER 16X5HZEE =C(E14.6,E14.6)/
\$29X28HBLOCKED ELECTRICAL IMPEDANCE 18X4HZB =C(E14.6,E14.6))
CHA = CABS(CUK)
TRP = 20.*ALOG10(EFF/CHA)

HANISH, KING, BAIER, AND ROGERS

```

    TRA = 20.*ALOG10(FF90/CHA)
    GO TO 1049
1048 PRINT 1055,YMOTAF,YEAF,YMOTWF,YEEF,YB
1055 FORMAT (29X26HMOTIONAL ADMITTANCE IN AIR 17X7HYMOTA =
    $C(E14.6,E14.6)/
    $29X28HELECTRICAL ADMITTANCE IN AIR 17X5HYEA =C(E14.6,E14.6)/
    $29X28HMOTIONAL ADMITTANCE IN WATER 15X7HYMOTW =C(E14.6,E14.6)/
    $29X30HELECTRICAL ADMITTANCE IN WATER 15X5HYEE =C(E14.6,E14.6)/
    $29X29HBLOCKED ELECTRICAL ADMITTANCE 17X4HYB =C(E14.6,E14.6))
    VTA = CABS(E)
    TRP = 20.*ALOG10(FF0/VTA)
    TRA = 20.*ALOG10(FF90/VTA)
1049 PRINT 1047,ZL,HL,HR,TRP,TRA,UH,UHE,ZKNA,ZSTA,ZKN,ZST
1047 FORMAT (29X19HRADIATION IMPEDANCE 27X4HZL =C(E14.6,E14.6)/
    $29X24HTRANSDUCTION COEFFICIENT 22X4HHL =C(E14.6,E14.6)/
    $29X22HMAGNETIC FIELD IN COIL 24X4HHR =C(E14.6,E14.6)/
    $29X35HTRANSMITTING RESPONSE IN PLANE (DB)10X5HTRP =E14.6/
    $29X32HTRANSMITTING RESPONSE AXIAL (DB) 13X5HTRA =E14.6/
    $29X30HPERMEABILITY DUE TO HYSTERESIS 16X4HUH =C(E14.6,E14.6)/
    $29X18HTOTAL PERMEABILITY27X5HUHE =C(E14.6,E14.6)/
    $29X29HMEDIUM INERTIAL REACTANCE AIR 15X6HZKNA =C(E14.6,E14.6)/
    $29X29HSHELL STIFFNESS REACTANCE AIR 15X6HZSTA =C(E14.6,E14.6)/
    $29X25HMEDIUM INERTIAL REACTANCE 20X5HZKN =C(E14.6,E14.6)/
    $29X25HSHELL STIFFNESS REACTANCE 20X5HZST =C(E14.6,E14.6))
C
C   CALCULATE AND PRINT RADIATION DIRECTIVITY PATTERN AT IFD+1 EQUALLY SPACED
C   ANGLES FROM SUBROUTINE FARFLD.
C
    IF (IFD.NE.0) CALL FARFLD(IFD)
    TM = TIMELEFT(K)
    PRINT 98,TM
C
C   GO BACK TO READ ANOTHER DRIVING FREQUENCY.
C
    GO TO 49
51 STOP
END

```

NRL REPORT 7964

```

SUBROUTINE BESL(X,BJ0,BJ1,Y0,Y1)
IF(X.GT.3.)GO TO 1
XT = (X*X)/9.
BJ0=(1. + XT*(-2.2499997 + XT*(1.2656208 + XT*( -.3163866 +
1 XT*(.0444479 + XT*(-.0039444 + XT*.0002100))))))
BJ1= X*(.5 +XT*(-.56249985 + XT*(.21093573 + XT*(-.03954289 +
1 XT*(.00443319 + XT*(-.00031761 + XT*.00001109))))))
RETURN
1 XT = 3./X
F0 = .79788456 +XT*(-.00000077 + XT*(-.00552740 + XT*(-.00009512
1 + XT*(.00137237 + XT*(-.00072805 + XT*.00014476))))))
F1 = .79788456 +XT*(.00000156 + XT*(.01659667 + XT*(.00017105 +
1 XT*(-.00249511 + XT*(.00113653 - .00020033*XT))))))
T0 = X-.78539816 + XT*(-.04166397 + XT*(-.00003954 + XT*(.00262573
1 + XT*(-.00054125 + XT*(-.00029333 + .00013558*XT))))))
T1= X - 2.35619449 + XT*(.12499612 + XT*(.00005650 +XT*(-.00637879
1 + XT*(.00074348 + XT*(.00079824 -.00029166*XT))))))
SX = SQRT(X)
SX = 1./SX
BJ0 = SX*F0*COS(T0)
BJ1 = SX*F1*COS(T1)
RETURN
END

```

```

SUBROUTINE BES1(X,BJ1)
IF(X.GT.3.)GO TO 1
XT = (X*X)/9.
BJ1= X*(.5 +XT*(-.56249985 + XT*(.21093573 + XT*(-.03954289 +
1 XT*(.00443319 + XT*(-.00031761 + XT*.00001109))))))
RETURN
1 XT = 3./X
F1 = .79788456 +XT*(.00000156 + XT*(.01659667 + XT*(.00017105 +
1 XT*(-.00249511 + XT*(.00113653 - .00020033*XT))))))
T1= X - 2.35619449 + XT*(.12499612 + XT*(.00005650 +XT*(-.00637879
1 + XT*(.00074348 + XT*(.00079824 -.00029166*XT))))))
SX = SQRT(X)
SX = 1./SX
BJ1 = SX*F1*COS(T1)
RETURN
ENTRY BES0
IF(X.GT.3.) GO TO 5
XT = (X*X)/9.
BJ1=(1. + XT*(-2.2499997 + XT*(1.2656208 + XT*( -.3163866 +
1 XT*(.0444479 + XT*(-.0039444 + XT*.0002100))))))
RETURN
5 XT = 3./X
F0 = .79788456 +XT*(-.00000077 + XT*(-.00552740 + XT*(-.00009512
1 + XT*(.00137237 + XT*(-.00072805 + XT*.00014476))))))
T0 = X-.78539816 + XT*(-.04166397 + XT*(-.00003954 + XT*(.00262573
1 + XT*(-.00054125 + XT*(-.00029333 + .00013558*XT))))))
SX = SQRT(X)
SX = 1./SX
BJ1 = SX*F0*COS(T0)
RETURN
END

```

HANISH, KING, BAIER, AND ROGERS

```

SUBROUTINE CALBES
DIMENSION PZ(20),PLZ(20),PR(20),PLR(20),XI(32),WF(32)
DIMENSION BI0(10,32),BI1(10,32),GI0(10,32),GI1(10,32)
DIMENSION GSO(10,32),GSI(10,32),BS0(10,32),BS1(10,32)
COMMON/BLKA/PR,PLR,PZ,PLZ/PIY/JMAX,JMAXH,IMAX/RCC/JTOP
COMMON/5/BTO(10,10,32),BT1(11,10,32),QZ(32,10),SIGMA(32),REST(128)
COMMON/6/GTO(10,10,32),GT1(11,10,32),RUST1(2880)
COMMON/TDY/NQD1,NQD2,NQD3/BOLD/GSO,GSI/BLK1/H,A,FK,PI/BLK2/XI,WF
COMMON/BLK3B/HI0,BI1/BOLD/GI0,GI1/TDY/FAST/BLK3/HS0,BS1
COMMON/RAD/RIN,ROUT/GGMS/GGMS
DIMENSION GGMS(10,32)
N=NQD1
FKFK = FK*FK
FKFAST = 2.*FAST*FK
DO 9 L=1,N
SIGMA(L) = XI(L) + 0.5 * FK
QZ(L,1) = FAST * (XI(L) + XI(L) - FK)
QQ = SIGMA(L) * SIGMA(L)
D = SQRT(FKFK - QQ)
GGMS(1,L) = D
T=D*ROUT $ TI = D*RIN
CALL BESL(T,BSJ0,BSJ1,Y0,YU)
CALL BESL(TI,BIJ0,BIJ1,Y0,YU)
BI0(1,L) = BIJ0 $ BI1(1,L) = BIJ1 * D
BS0(1,L) = BSJ0
BS1(1,L) = BSJ1 * D
BT1(1,1,L) = BIJ1 * HIN * WF(L) / D
BT1(IMAX + 1,1,L) = BSJ1 * ROUT * WF(L) / D
9 CONTINUE
DR15 ICE=2,JTOP
DR16 M=1,N
GZ(M,ICE) = QZ(M,ICE - 1) + FKFAST
RHO = QZ(M,ICE)
QQR = RHO*RHO
GMS = SQRT(QQR + FKFK)
GGMS(ICE,M) = GMS
TM = GMS*ROUT $ SM = RHO*ROUT
TIM = GMS*RIN $ SIM = RHO*RIN
CALL BESL(SM,GST0,GST1,Y1,Y2)
CALL BESL(TIM,GST0,BST1,YZ,YJ)
CALL BESL(SIM,GIT0,GIT1,YI,Y0)
CALL BESL(TIM,HIT0,BIT1,YK,Y0)
BI0(ICE,M) = HIT0 $ BI1(ICE,M) = BIT1 * GMS $ GI0(ICE,M) = GIT0
GI1(ICE,M) = GIT1
HS0(ICE,M) = BST0
BS1(ICE,M) = BST1 * GMS
GSO(ICE,M) = GST0
GSI(ICE,M) = GST1
BT1(1,ICE,M) = RIN * HIT1 * WF(M) / GMS
BT1(IMAX + 1,ICE,M) = ROUT * BST1 * WF(M) / GMS
GT1(1,ICE,M) = RIN * GIT1 * WF(M) / RHO

```

NRL REPORT 7964

```

GT1(IMAX + 1,ICE,M) = R0UT * GST1 * WF(M) / RH0
16 CONTINUE
15 CONTINUE
DDELR = (R0UT - RIN)/IMAX
DELK = .5*DDELK
RL = RIN - DDELK
DO 5 IMP=1,IMAX
RL = RL + DDELK
DO 1 L=1,N
O = GGMS(1,L)
T = D*PR(IMP)
T1 = D*(PR(IMP) - DELK)
CALL BES0(T,HT0(IMP,1,L))
IF(IMP.FQ.1) GO TO 1
CALL RES1(T1,BT1(IMP,1,L))
BT1(IMP,1,L) = BT1(IMP,1,L) * RL * WF(L) / D
1 CONTINUE
DO 5 ICE=2,JIMP
DO 6 M=1,N
RHO = QZ(M,ICE)
GMS = GGMS(ICE,M)
SM = RHO*PR(IMP) $ SM1 = RHO*(PR(IMP) - DELK)
TM = GMS*PR(IMP) $ TM1 = GMS*(PR(IMP) - DELK)
CALL BES0(TM,BT0(IMP,ICE,M))
CALL BES0(SM,GT0(IMP,ICE,M))
IF(IMP.EQ.1) GO TO 6
CALL RES1(TM1,HT1(IMP,ICE,M))
BT1(IMP,ICE,M) = BT1(IMP,ICE,M) * RL * WF(M) / GMS
CALL RES1(SM1,GT1(IMP,ICE,M))
GT1(IMP,ICE,M) = GT1(IMP,ICE,M) * RL * WF(M) / RHO
6 CONTINUE
5 CONTINUE
DO 20 ICE = 1, JIMP
DO 21 M = 1, N
DO 22 IMP = 1, IMAX
HT1(IMP,ICE,M) = BT1(IMP+1,ICE,M) - BT1(IMP,ICE,M)
IF(ICE .EQ. 1) GO TO 22
GT1(IMP,ICE,M) = GT1(IMP+1,ICE,M) - GT1(IMP,ICE,M)
22 CONTINUE
21 CONTINUE
20 CONTINUE
RETURN
END

```

00016600
00016700

00018700
00018800

00018900

HANISH, KING, BAIER, AND ROGERS

```

SUBROUTINE CALTRIG
COMMON/BLK2/XI,WF/BLK1/H,R,FK,PI/STORSCST/TBSIN,THCOS,THEXP
COMMON/TBY/NQD1,ISYM,ICOR/TIDY/FAST
DIMENSION TBSIN(32),THCOS(32),THEXP(32,10),XI(32),WF(32)
EQUIVALENCE (THCOS(1),TBEXP(1))
COMMON/FS/FKFK,FKFAST,TFK
COMMON/PIT/JMAX,JMAXH,IMAX/DEL/DELR,DELZ
COMMON/STORSCST/STSIN(32,21),STCOS(32,21)
DIMENSION STEMP(32),CTEMP(32),ETEMP(32,10)
COMMON/S/BT0(10,10,32),BT1(11,10,32),QZ(32,10),SIGMA(32),REST(128)
COMMON/B/GT0(10,10,32),STEXP(32,20,10)
EQUIVALENCE (STSIN(1),TSSIN(1)), (STCOS(1),TSCOS(1))
EQUIVALENCE (STEXP(1),TSEXP(1))
DIMENSION TSSIN(32,21),TSCOS(32,21),TSEXP(32,20,10)
FKFK = FK * FK & TFK = 0.25 * FK & FKFAST = 2.0 * FAST * FK
TPK = 0.25 * FKFAST
RTPKSQ = 1.0 / (TPK * TPK)
N = NQD1
A = H * H
DO 300 L = 1, N
  B = A * SIGMA(L)
  TBSIN(L) = SIN(B) * TFK
  THCOS(L) = COS(B) * TFK
300 CONTINUE
  A = -4.0 * FAST * H
  B = FK * A
  TBMULT = EXP(B)
  DO 301 M = 1, N
    H = A * SIGMA(M)
    THEXP(M,2) = EXP(H) * TPK
    DO 302 ICE = 3, 10
      THEXP(M,ICE) = TBEXP(M,ICE-1) * TBMULT
302 CONTINUE
301 CONTINUE
  RETURN
ENTRY STTRIG
  HZ = 0.5 * DELZ
  DO 350 L = 1, N
    A = HZ * SIGMA(L)
    STSIN(L,1) = SIN(A)
    STCOS(L,1) = COS(A)
    PRD = STSIN(L,1) * STCOS(L,1)
    STEMP(L) = PRD + PRD
    PRD = STCOS(L,1) * STCOS(L,1)
    CTEMP(L) = PRD + PRD - 1.0
    STSIN(L,1) = STSIN(L,1) * TFK
    STCOS(L,1) = STCOS(L,1) * TFK
    DO 351 IR = 2, JMAX
      STSIN(L,IR) = STSIN(L,IR-1) * CTEMP(L) + STCOS(L,IR-1) * STEMP(L)
      STCOS(L,IR) = STCOS(L,IR-1) * CTEMP(L) - STSIN(L,IR-1) * STEMP(L)
351 CONTINUE

```

```

350 CONTINUE
HZ = -HZ
STMULT = EXP(HZ * FKFAST)
DO 352 M = 1, N
STEXP(M,1,1) = EXP(HZ * QZ(M,1)) * TPK
DO 353 ICE = 2, 10
STEXP(M,1,ICE) = STEXP(M,1,ICE-1) * STMULT
ETEMP(M,ICE) = STEXP(M,1,ICE) * STEXP(M,1,ICE) * RTPKSG
DO 354 IR = 2, JMAX
STEXP(M,IR,ICE) = STEXP(M,IR-1,ICE) * ETEMP(M,ICE)
354 CONTINUE
353 CONTINUE
352 CONTINUE
RETURN
ENTRY SSTRIG
DO 370 L = 1, N
DO 371 J = 2, JMAX
STSIN(L,J-1) = (STSIN(L,J-1)-STSIN(L,J)) * WF(L) / SIGMA(L)
STCOS(L,J-1) = (STCOS(L,J-1)-STCOS(L,J)) * WF(L) / SIGMA(L)
DO 372 ICE = 2, 10
STEXP(L,J-1,ICE) = (STEXP(L,J-1,ICE)-STEXP(L,J,ICE)) * WF(L) /
$ QZ(L,ICE)
372 CONTINUE
371 CONTINUE
370 CONTINUE
RETURN
ENTRY TSTRIG
JMAXP = JMAX + 1
DO 400 L = 1, N
TSSIN(L,1) = 0.0
TSCOS(L,1) = TPK * WF(L) / SIGMA(L)
DO 401 J = 2, JMAXP
TSSIN(L,J) = TSSIN(L,J-1) * CTEMP(L) + TSCOS(L,J-1) * STEMP(L)
TSCOS(L,J) = TSCOS(L,J-1) * CTEMP(L) - TSSIN(L,J-1) * STEMP(L)
TSSIN(L,J-1) = TSSIN(L,J-1) - TSSIN(L,J)
TSCOS(L,J-1) = TSCOS(L,J-1) - TSCOS(L,J)
401 CONTINUE
400 CONTINUE
DO 402 M = 1, N
DO 403 ICE = 2, 10
TSEXP(M,1,ICE) = WF(M) * (1.0 - ETEMP(M,ICE)) * TPK / QZ(M,ICE)
DO 404 J = 2, JMAX
TSEXP(M,J,ICE) = TSEXP(M,J-1,ICE) * ETEMP(M,ICE)
404 CONTINUE
403 CONTINUE
402 CONTINUE
RETURN
END

```

HANISH, KING, BAIER, AND ROGERS

```

SUBROUTINE CFINT(A,B,C,X,ANS)
COMPLEX ARG1, ARG3, F1, F3
COMMON/ICE/ICE,NOEXI/JOE/JTOP1/SAVE/ISAVE,EXMZR,EXMZI
DIMENSION A1RG(2), A3RG(2), FF1(2), FF3(2), SAVER(2)
EQUIVALENCE (ARG1,A1RG), (ARG3,A3RG), (F1,FF1), (F3,FF3)
DATA (PII = 0.15915494309)
IF(ICE .LT. JTOP1) GO TO 400
FACT = 1.
IFLAG = 0
NFLAG = 0
GO TO 1
ENTRY CFONE
IF(ICE .LT. JTOP1) GO TO 400
FACT = 1. / X
IFLAG = 1
NFLAG = 0
GO TO 1
ENTRY CFZERO
IF(ICE .LT. JTOP1) GO TO 400
FACT = 1. / X
IFLAG = 1
NFLAG = 1
1 CONTINUE
FM = PII / SQRT(B * C)
A1RG(1) = A * X
A1RG(2) = - (B - C) * X
A3RG(1) = A1RG(1)
A3RG(2) = - (B + C) * X
IF(IFLAG .EQ. 1) GO TO 2
CALL EXI(ARG1,F1)
NSAVE = ISAVE * SAVER(1) = EXMZR $ SAVER(2) = EXMZI
CALL EXI(ARG3,F3)
GO TO 3
2 CALL EXI2(ARG3, F3)
ISAVE = NSAVE * EXMZR = SAVER(1) * EXMZI = SAVER(2)
CALL EXI2(ARG1, F1)
3 CONTINUE
IF(NFLAG .EQ. 0) ANS = FM * (FF1(2) + FF3(1))
IF(NFLAG .EQ. 1) ANS = FM * (FF1(1) + FF3(2))
ANS = ANS * FACT
RETURN
400 ANS = 0.0
RETURN
END

```

```

SUBROUTINE CINV(B,NS,ND)
C THIS SUBROUTINE PREPARES INPUT TO AND OUTPUT FROM SUBROUTINE MINC
C WHICH INVERTS MATRIX B(.,.).
TYPE COMPLEX B,D
DIMENSION B( ND,1),L(100),M(100)
DO 1 J = 1,NS
DO 1 I = 1,NS
1 B(I+NS*(J-1)) = B(I+ND*(J-1))
CALL MINC(B,NS,ND,D,L,M)
DO 2 JJ = 1,NS
J = NS+1-JJ
DO 2 II = 1,NS
I = NS+1-II
2 B(I+ND*(J-1)) = B(I+NS*(J-1))
RETURN
END

```

NRL REPORT 7964

```

SUBROUTINE COMPBES
THIS SUBROUTINE CALCULATES COMPLEX BESSEL FUNCTIONS FOR ORDER 0 AND 1 OF
THE FIRST KIND AND SECOND KIND FOR COMPLEX ARGUMENT X,Y. SUBROUTINE
COMPBES REQUIRES THE FIVE SUBROUTINES MLT, DVD, SRT, PSUBV, AND QSUBV.
TYPE REAL J0R,J0I,J1R,J1I,J0RPR,J0IPR,J1RPR,J1IPR
COMMON /BLK/ X,Y,J0R,J0I,J1R,J1I,Y0R,Y0I,Y1R,Y1I
XK1=1.414213562373
EULER=0.577215664901
PI=3.1415926536
TOL=5.0E-10
IF(ABS(X).GE.9.0.OR.ABS(Y).GE.9.0)GO TO 100
RH0=SQRT(X*X+Y*Y)
R0V=RH0/2.0
IF(RH0.NE.0.0)GO TO 1
J0R=1.0
J0I=J1R=J1I=Y0I=Y1I=0.0
Y0R=Y1R=-1.0E307
RETURN
SERIES
1 JC1=JC2=JC3=JC4=FIJ0=FXA=FXB=0.0
FRJ0=XKK=FACTOR=1.0
COSPHI=X/RH0
IF(COSPHI.GT.1.0)COSPHI=1.0
IF(COSPHI.LT.-1.0)COSPHI=-1.0
SINPHI=Y/RH0
PHI=ACOS(COSPHI)
IF(Y.LT.0.0)PHI=PI+PI-PHI
3 ANGLE=XKK*PHI*2.0
COS2KP=COS(ANGLE)
SIN2KP=SIN(ANGLE)
FACTOR=-FACTOR*R0V*R0V/(XKK*XKK)
A=FACTOR*COS2KP
B=FACTOR*SIN2KP
J0R=FRJ0+A
IF(J0R.EQ.0.0.OR.ABS(A/J0R).LT.TOL)JC1=1
J0I=FIJ0+B
IF(J0I.EQ.0.0.OR.ABS(B/J0I).LT.TOL)JC2=1
XA=FXA+XKK*A/R0V
IF(XA.EQ.0.0.OR.ABS((XA-FXA)/XA).LT.TOL)JC3=1
XB=FXB+XKK*B/R0V
IF(XB.EQ.0.0.OR.ABS((XB-FXB)/XB).LT.TOL)JC4=1
IF(JC1.EQ.1.AND.JC2.EQ.1.AND.JC3.EQ.1.AND.JC4.EQ.1)GO TO 2
XKK=XKK+1.0
JC1=JC2=JC3=JC4=0
FRJ0=J0R
FIJ0=J0I
FXA=XA
FXB=XB
GO TO 3
2 J1R=-SINPHI*XB-COSPHI*XA
J1I=SINPHI*XA-COSPHI*XB

```

```

XKK=1.0
JC5=JC6=FXZ=FXQ=0
XLR2=LOGF(R0V)
XMKP=-1.0
RTK=0.0
7 ANGLE=XKK*PHI*2.0
COSY=COS(ANGLE)
SINY=SIN(ANGLE)
XMKP=-XMKP*RHO*RHO/(4.0*XKK*XKK)
RTK=RTK+(1.0/XKK)
XZ=RTK*XMKP*COSY+FXZ
IF(XZ, EQ, 0.0, OR, ABS((XZ-FXZ)/XZ), LT, TOL) JC5=1
XQ=XMKP*RTK*SINY+FXQ
IF(XQ, EQ, 0.0, OR, ABS((XQ-FXQ)/XQ), LT, TOL) JC6=1
IF(JC5, EQ, 1, AND, JC6, EQ, 1) GO TO 4
XKK=XKK+1.0
JC5=JC6=0
FXZ=XZ
FXQ=XQ
GO TO 7
4 Y0R=(2.0/PI)*(J0R*(EULER+XLR2)-PHI*J0I+XZ)
Y0I=(2.0/PI)*(J0I*(EULER+XLR2)+PHI*J0R+XQ)
JC7=JC8=SKF=0
XKK=1.0
FKF=R0V
FXN=R0V*COSPHI
FXP=R0V*SINPHI
9 ANGLE=(XKK+XKK+1.0)*PHI
COSY2=COS(ANGLE)
SINY2=SIN(ANGLE)
FKF=-FKF*RHO*RHO/(4.0*XKK*(XKK+1.0))
SKF=SKF+1.0/XKK
SMK=(2.0*SKF+1.0/(XKK+1.0))*FKF
XN=SMK*COSY2+FXN
IF(XN, EQ, 0.0, OR, ABS((XN-FXN)/XN), LT, TOL) JC7=1
XP=SMK*SINY2+FXP
IF(XP, EQ, 0.0, OR, ABS((XP-FXP)/XP), LT, TOL) JC8=1
IF(JC7, EQ, 1, AND, JC8, EQ, 1) GO TO 5
XKK=XKK+1.0
JC7=JC8=0
FXN=XN
FXP=XP
GO TO 9
5 Y1R=(2.0*(J1R*(EULER+XLR2)-PHI*J1I-COSPHI/RHO)-XN)/PI
Y1I=(2.0*(J1I*(EULER+XLR2)+PHI*J1R+SINPHI/RHO)-XP)/PI
RETURN
C ASYMPTOTIC EXPANSION
100 IF(Y, GT, 0.0, OR, (Y, EQ, 0.0, AND, X, GT, 0.0)) GO TO 101
X=-X
Y=-Y
JEX=1

```

```

GO TO 102
101 JEX=0
102 SQ=X*X+Y*Y
RHQ2=SQRT(SQ)
SIN2=Y/RHQ2
IF(SIN2.LT.0.9999)SIN2=0.0
TMAI=2.0/(PI*SQ)
TMAR=TMAI*X
TMAI=TMAI*(-Y)
CALL SRT(TMAR,TMAI,AAI,AAI)
EY=EXP(Y)
EMY=EXP(-Y)
COSH1=SINH1=EY/2.0
COSH1PR=EMY/2.0
SINH1PR=-COSH1PR
SINR=SIN(X)
COSR=COS(X)
SCAO=COSR+SINR
BBR=COSH1*SCAO/XK1
BBRPR=COSH1PR*SCAO/XK1
BBI=SINH1*(COSR-SINR)/XK1
BBIPR=SINH1PR*(COSR-SINR)/XK1
CCR=COSH1*(SINR-COSR)/XK1
CCRPR=COSH1PR*(SINR-COSR)/XK1
CCI=SINH1*SCAO/XK1
CCIPR=SINH1PR*SCAO/XK1
CALL PSUBV(0.0,X,Y,DDR,DDI)
CALL PSUBV(1.0,X,Y,FFR,FFI)
CALL PSUBV(0.0,X,Y,EER,EI)
CALL PSUBV(1.0,X,Y,GGR,GGI)
CALL MLT(BBR,BBI,DDR,DDI,FRR,FRI)
CALL MLT(BBRPR,BBIPR,DDR,DDI,FRRPR,FRIPR)
CALL MLT(CCR,CCI,EER,EI,SER,SEI)
CALL MLT(CCRPR,CCIPR,EER,EI,SERPR,SEIPR)
THR=FRR-SER
THI=FRI-SEI
THRPR=FRRPR-SERPR
THIPR=FRIPR-SEIPR
CALL MLT(AAI,AAI,THR,THI,JOR,JOI)
CALL MLT(AAI,AAI,THRPR,THIPR,JORPR,JOIPR)
JOR=JOR+JORPR-SIN2*JORPR
JOI=JOI+JOIPR-SIN2*JOIPR
CALL MLT(CCR,CCI,FFR,FFI,FRR,FRI)
CALL MLT(CCRPR,CCIPR,FFR,FFI,FRRPR,FRIPR)
CALL MLT(BBR,BBI,GGR,GGI,SER,SEI)
CALL MLT(BBRPR,BBIPR,GGR,GGI,SERPR,SEIPR)
THR=FRR+SER
THI=FRI+SEI
THRPR=FRRPR+SERPR
THIPR=FRIPR+SEIPR
CALL MLT(AAI,AAI,THR,THI,J1R,J1I)

```

```

CALL MLT(AAR,AAI,THRPR,THIPR,J1RPR,J1IPR)
J1R=J1R+J1RPR-SIN2*J1RPR
J1I=J1I+J1IPR-SIN2*J1IPR
CALL MLT(CCR,CCI,DDR,DDI,FRR,FRI)
CALL MLT(CCRPR,CCIPR,DDR,DDI,FRRPR,FRIPR)
CALL MLT(BBR,bbI,EER,EEI,SER,SEI)
CALL MLT(BBRPR,bbIPR,EER,EEI,SERPR,SEIPR)
THR=FRR+SER
THI=FRI+SEI
THRPR=FRRPR+SERPR
THIPR=FRIPR+SEIPR
CALL MLT(AAR,AAI,THR,THI,YOR,YOI)
CALL MLT(AAR,AAI,THRPR,THIPR,YORPR,YOIPR)
YOR=YOR+YORPR+SIN2*YORPR
YOI=YOI+YOIPR+SIN2*YOIPR
CALL MLT(CCR,CCI,GGR,GGI,FRR,FRI)
CALL MLT(CCRPR,CCIPR,GGR,GGI,FRRPR,FRIPR)
CALL MLT(BBR,bbI,FFR,FFI,SER,SEI)
CALL MLT(BBRPR,bbIPR,FFR,FFI,SERPR,SEIPR)
THR=FRR-SER
THI=FRI-SEI
THRPR=FRRPR-SERPR
THIPR=FRIPR-SEIPR
CALL MLT(AAR,AAI,THR,THI,Y1R,Y1I)
CALL MLT(AAR,AAI,THRPR,THIPR,Y1RPR,Y1IPR)
Y1R=Y1R+Y1RPR+SIN2*Y1RPR
Y1I=Y1I+Y1IPR+SIN2*Y1IPR
IF(JEX.EQ.0)RETURN
J1=-J1
YOR=YOR-JOI-JOI
YOI=YOI+JOR+JOR
Y1R=-Y1R-J1I-J1I
Y1I=-Y1I+J1R+J1R
END

```

NRL REPORT 7964

SUBROUTINE CSSM

```

COMMON/ICE/ICE,NGEXI
DIMENSION SIV(10,20),IIV(10,20),SSV(10,20),ISV(10,20)
DIMENSION SIM(10,20),IIM(10,20),SSM(10,20),ISM(10,20)
TYPE COMPLEX SSV,SIV,ISV,IIV,SSM,SIM,ISM,IIM
DIMENSION PZ(20),PLZ(20),PR(20),PLR(20)
TYPE REAL IIV,IIRV,ISIV,ISRV,ISB,IIB,IIT,IST,III,IIR,ISI,ISR
DIMENSION SSH(10),IIB(10),SIB(10),ISB(10)
DIMENSION GSO(10,32),GS1(10,32),XI(32),WF(32),SUMT(10)
DIMENSION BSO(10,32),BS1(10,32)
DIMENSION BIO(10,32),BI1(10,32),GIO(10,32),GI1(10,32)
TYPE COMPLEX SS,II,YAKC,UMII,UMSS,UMIS
DIMENSION SST(10),IIT(10),SIT(10),IST(10),GGMS(10,32)
DIMENSION HUNT(10),DUNT(10),EXPF1(32)
COMMON/EPS/EPS
COMMON/RAD/RIN,ROUT,18Y/NGD1,NGD2,NGD3/JOE/JTOP/BOLD/GSO,GS1
COMMON/PIT/JMAX,JMAXH,IMAX/BLKA/PR,PLR,PZ,PLZ
COMMON/SSV/SSV/IIV/IIV/SIV/SIV/ISV/ISV/GGMS/GGMS
COMMON/BLKB/SSM/SIM/SIM/IIM/IIM/ISM/ISM/FS/FKFK,FKFAST,TFK
COMMON/BLKI/H,A,FK,PI/BLK2/XI,WF/BLK3/BSO,BS1/TIDY/FAST
COMMON/BOLD/GIO,GI1/BLK3B/BIO,BI1/DEL/DELR,DELZ
COMMON/S/BTO(10,10,32),BT1(11,10,32),QZ(32,10),SIGMA(32),REST(128)
COMMON/G/GTU(10,10,32),SSEXP(32,20,10)
COMMON/STORSCST/SSSIN(32,21),SSCOS(32,21)
N = NGD1
ARGP = .5*DELZ
ZERO = 0.0
TPK = .25*FKFAST
ZU = H - .5*DELZ
SSI=SSR=III=IIR=SII=SIR=ISI=ISR=0.
UMII = UMIS = UMSS = (0.0,0.0)
DO 1 L = 1,N
SIGMAP = ARGP*SIGMA(L)
EXPF1(L) = EXPF(-QZ(L,1)*ARGP)
TRIGFR = 2.*COS(SIGMAP) - 2.
TRIGFI = 2.*SIN(SIGMAP)
YAK = TFK*WF(L)/SIGMA(L)
YAKR = -YAK*TRIGFR
YAKI = YAK*TRIGFI
YAKC = CMPLX(YAKR,-YAKI)
SSI = SSI + BSO(1,L)*BS1(1,L)*YAKI
SSR = SSR + BSO(1,L)*BS1(1,L)*YAKR
IIR = IIR - BIO(1,L)*BI1(1,L)*YAKR
III = III - BIO(1,L)*BI1(1,L)*YAKI
SII = SII - BSO(1,L)*BI1(1,L)*YAKI
SIR = SIR - BSO(1,L)*BI1(1,L)*YAKR
ISI = ISI + BIO(1,L)*BS1(1,L)*YAKI
ISR = ISR + BIO(1,L)*BS1(1,L)*YAKR
UMII = UMII + YAKC*BIO(1,L)*BIO(1,L)
UMIS = UMIS + YAKC*BIO(1,L)*BSO(1,L)

```

00009400

HANISH, KING, BAIER, AND ROGERS

```

    UMSS = UMSS + YAKC*BSO(1,L)*BSO(1,L)
1 CONTINUE
    SUMT(1) = REAL(UMSS) $ BUMT(1) = REAL(UMII) $ DUMT(1) = REAL(UMIS)
    SST(1) = SSR $ IIT(1) = IIR $ SIT(1) = SIR $ IST(1) = ISH
    EXFACT = EXPF(-FKFAST*ARGP)
    DO 501 ICE = 2, 10
    SUMSS=SUMII=SUMSI = SUMIS = 0.
    SUMMIT = SUMMITB = SUMMITD = 0.
    DO 375 M=1,N
    EXPF1(M) = EXPF1(M)*EXFACT
    EXPF2 = 2.*(EXPF1(M) - 1.)
    YAK = -TPK*WF(M)
    YAKR = -EXPF2*YAK
    YAKRG = YAKR / QZ(M,ICE)
    YAK = YAK + YAK
    SUMSS = SUMSS + BSO(ICE,M) * BS1(ICE,M) * YAKRG
    SUMSS = SUMSS - GSO(ICE,M)*GS1(ICE,M)*YAKR
    SUMII = SUMII - BIO(ICE,M) * BI1(ICE,M) * YAKRG
    SUMII = SUMII + GIO(ICE,M)*GI1(ICE,M)*YAKR
    SUMSI = SUMSI - BSO(ICE,M) * BI1(ICE,M) * YAKRG
    SUMSI = SUMSI + GSO(ICE,M)*GI1(ICE,M)*YAK
    SUMIS = SUMIS + BIO(ICE,M) * BS1(ICE,M) * YAKRG
    SUMIS = SUMIS - GIO(ICE,M)*GS1(ICE,M)*YAK
    BSBS = BSO(ICE,M)*BSO(ICE,M)
    BIBS = BIO(ICE,M)*BSO(ICE,M)
    BIBI = BIO(ICE,M)*BIO(ICE,M)
    SUMMIT = SUMMIT + BSBS * YAKRG
    SUMMITB = SUMMITB + BIBI * YAKRG
    SUMMITD = SUMMITD + BIBS * YAKRG
375 CONTINUE
    SST(ICE) = SST(ICE-1) + SUMSS
    IIT(ICE) = IIT(ICE-1) + SUMII
    SIT(ICE) = SIT(ICE-1) + SUMSI
    IST(ICE) = IST(ICE-1) + SUMIS
    SUMT(ICE) = SUMT(ICE-1) + SUMMIT
    BUMT(ICE) = BUMT(ICE-1) + SUMMITB
501 DUMT(ICE) = DUMT(ICE-1) + SUMMITD
    AA = 4.*R0UT*R0UT
    P = ARGP
    PP = P*P
    DK = AA/(PP + AA)
    SDK = SQRT(DK)
    CF2 = -P*SDK*ELLIPK(DK)/(PI*AA)
    SSR = R0UT*(SST(JTOP) + CF2 + CF2)
    AA = RIN*RIN*4.
    DK = AA/(PP + AA)
    SDK = SQRT(DK)
    CF2 = -P*SDK*ELLIPK(DK)/(PI*AA)
    IIR = RIN*(IIT(JTOP) - CF2 - CF2)
    SSI = R0UT*SSI $ III = RIN*III $ SII = RIN*SII $ ISI = R0UT*IST
    ICE = 10

```

NRL REPORT 7964

```

FL = (ICE-1)*FKFAST
NOEXI = 0
CALL CFINT(ARGP,ROUT,RIN,FL,CFIS)
CALL CFINT(ARGP,RIN,ROUT,FL,CFP)          $          CFSI = -CFP
SIT(ICE) = SIT(ICE) + CFSI + CFSI
IST(ICE) = IST(ICE) + CFIS + CFIS
SIR = RIN*SIT(ICE) $ ISR = ROUT*IST(ICE)
ISR = ISR - 1.0
JM = 9
FLAM = FKFAST*JM
CALL CFZERO(ARGP,ROUT,ROUT,FLAM,CP)
CALL CFZERO(ZERO,ROUT,ROUT,FLAM,CM)
CF1 = 2*(CP-CM)
CALL CFZERO(ARGP,RIN,RIN,FLAM,CP)
CALL CFZERO(ZERO,RIN,RIN,FLAM,CM)
CF2 = 2*(CP-CM)
CALL CFZERO(ARGP,ROUT,RIN,FLAM,CP)
CALL CFZERO(ZERO,ROUT,RIN,FLAM,CM)
CF3 = -2*(CP-CM)
ANSR = SUMT(ICE) + CF1
ANSRB = BUMT(ICE) + CF2
ANSRD = DUMT(ICE) - CF3
QI = -AIMAG(UMI)
IIV(1,1) = RIN*CMPLX(ANSRB,QI)
QI = -AIMAG(UMIS)
ISV(1,1) = ROUT*CMPLX(ANSRD,QI)
SIV(1,1) = RIN*CMPLX(ANSRD,QI)
QI = -AIMAG(UHSS)
SSV(1,1) = ROUT*CMPLX(ANSR,QI)
IIM(1,1) = -CMPLX(IIR,III) + (0.5,0.0)
SSM(1,1) = -CMPLX(SSR,SSI) + (0.5,0.0)
SIM(1,1) = -CMPLX(SIR,SII)
ISM(1,1) = -CMPLX(ISR,ISI)
DO 06 J=2,JMAX
Z = PL2(J)
ARGP = ZO - Z - DELZ
ARGM = ZO - Z
SSI=SSR=III=IIR=SII=SIR=ISI=ISR=0.
SSIV=SSRV=IIIV=IIRV=SIIV=SIRV=ISIV=ISRV=0.
DO 01 L=1,N
YAKR = -SSCOS(L,J-1)
YAKI = SSSIN(L,J-1)
ISR = ISR + B10(1,L)*BS1(1,L)*YAKR
ISI = ISI + B10(1,L)*BS1(1,L)*YAKI
SIR = SIR - BS0(1,L)*BI1(1,L)*YAKR
SII = SII - BS0(1,L)*BI1(1,L)*YAKI
III = III - B10(1,L)*BI1(1,L)*YAKI
IIR = IIR - B10(1,L)*BI1(1,L)*YAKR
SSR = SSR + BS0(1,L)*BS1(1,L)*YAKR
SSI = SSI + BS0(1,L)*BS1(1,L)*YAKI
IIIV = IIIV + B10(1,L) * B10(1,L) * YAKI

```

HANISH, KING, BAIER, AND ROGERS

```

IIRV = IIRV + B10(1,L) * B10(1,L) * YAKR
ISRV = ISRV + B10(1,L) * BSO(1,L) * YAKR
ISIV = ISIV + B10(1,L) * BSO(1,L) * YAKI
SSRV = SSRV + BSO(1,L) * BSO(1,L) * YAKR
61 SSIV = SSIV + BSO(1,L) * BSO(1,L) * YAKI
SIIV = ISIV & SIRV = ISRV
FACT1 = PI * 0.5 / (R0UT - RIN)
FACT = 2. / (A*PI*ARGM)
SST(1) = SSR & IIT(1) = IIR & SIT(1) = SIR & IST(1) = ISR
SSB(1) = SSRV & IIB(1) = IIRV & SIB(1) = SIRV & ISB(1) = ISRV
ICE = 1
2 ICE = ICE + 1
SUMSS=SUMII=SUMSI = SUMIS = 0.
VUMSS = VUMII=VUMSI=VUMIS = 0.
DO 376 M=1,N
VAKR = SSEXPN(M,J-1,ICE)
VUMSS = VUMSS + BSO(ICE,M)*BSO(ICE,M)*VAKR
VUMIS = VUMIS + B10(ICE,M)*BSO(ICE,M)*VAKR
VUMII = VUMII + B10(ICE,M)*B10(ICE,M)*VAKR
SUMSI = SUMSI + BSO(ICE,M) * B11(ICE,M) * VAKR
SUMIS = SUMIS + B10(ICE,M) * B11(ICE,M) * VAKR
SUMSS = SUMSS + BSO(ICE,M) * B11(ICE,M) * VAKR
376 SUMII = SUMII + B10(ICE,M) * B11(ICE,M) * VAKR
VUMSI = VUMIS
SST(ICE) = SST(ICE-1) + SUMSS
IIT(ICE) = IIT(ICE-1) + SUMII
IST(ICE) = IST(ICE-1) + SUMIS
SIT(ICE) = SIT(ICE-1) + SUMSI
SSB(ICE) = SSB(ICE-1) + VUMSS
IIR(ICE) = IIR(ICE-1) + VUMII
ISB(ICE) = ISB(ICE-1) + VUMIS
SIB(ICE) = SIB(ICE-1) + VUMSI
FL = (ICE - 1)*PKFAST
FLT = FL + FACT1
ERFC = (FACT/FL)*(EXPF(-ARGP*FL) - EXPF(- ARGP*FLT))
ERFC = ERFC/SIT(ICE)
ERFC = ABS(ERFC)
IF(ERFC.LE.EPS) GO TO 3
IF(ICE.GE.10) GO TO 3
GO TO 2
3 SSI = R0UT*SSI & III = RIN*III & SII = RIN*SII & ISI = R0UT*ISI
N0EXI = 0
CALL CFINT(ARGM, RIN, R0UT, FL, CFM)
CALL CFINT(ARGP, RIN, R0UT, FL, CFP)
SIT(ICE) = SIT(ICE) - (CFP - CFM)
CALL CFINT(ARGP, RIN, RIN, FL, CFP)
N0EXI = 1
CALL CFZERO(ARGP, RIN, RIN, FL, CP)
N0EXI = 0
CALL CFINT(ARGM, RIN, RIN, FL, CFM)
N0EXI = 1

```

NRL REPORT 7964

```

CALL CFZERO(ARGM, RIN, RIN, FL, CM)
IIT(ICE) = IIT(ICE) - (CFP - CFM)
IIB(ICE) = IIB(ICE) + (CP - CM)
NOEXI = 0
CALL CFINT(ARGP, ROUT, ROUT, FL, CFP)
NOEXI = 1
CALL CFZERO(ARGP, ROUT, ROUT, FL, CP)
NOEXI = 0
CALL CFINT(ARGM, ROUT, ROUT, FL, CFM)
NOEXI = 1
CALL CFZERO(ARGM, ROUT, ROUT, FL, CM)
SST(ICE) = SST(ICE) + (CFP - CFM)
SSB(ICE) = SSB(ICE) + (CP - CM)
NOEXI = 0
CALL CFINT(ARGP, ROUT, RIN, FL, CFP)
NOEXI = 1
CALL CFZERO(ARGP, ROUT, RIN, FL, CP)
NOEXI = 0
CALL CFINT(ARGM, ROUT, RIN, FL, CFM)
NOEXI = 1
CALL CFZERO(ARGM, ROUT, RIN, FL, CM)
IST(ICE) = IST(ICE) + (CFP - CFM)
ISB(ICE) = ISB(ICE) + (CP - CM)
SIB(ICE) = SIB(ICE) + (CP - CM)
SSR = ROUT*SST(ICE) $ IIR = RIN*IIT(ICE)
SIR = RIN*SII(ICE) $ ISR = ROUT*IST(ICE)
SSIV = ROUT*SSIV $ IIV = RIN*IIV $ SIV = RIN*SIV
ISIV = ROUT*ISIV
SIRV = RIN*SIB(ICE) $ ISRV = ROUT*ISB(ICE)
SSRV = ROUT*SSB(ICE) $ IIRV = RIN*IIR(ICE)
SS = CMPLX(SSR, SSI) $ II = CMPLX(IIR, III)
SSM(1,J)=SS
ISM(1,J)=          CMPLX(ISR, ISI)
SIM(1,J)=          CMPLX(SIR, SII)
IIM(1,J)=II
SSV(1,J)=          -CMPLX(SSRV, SSIV)
IIV(1,J)=          -CMPLX(IIRV, IIIV)
ISV(1,J)=          -CMPLX(ISRV, ISIV)
SIV(1,J)=          -CMPLX(SIRV, SIV)
IF(J.GT.JMAXH) GO TO 66
SSM(J,1)=SSM(1,J) $ SSV(J,1)=SSV(1,J) $ ISM(J,1)=ISM(1,J)
SIM(J,1)=SIM(1,J) $ ISV(J,1)=ISV(1,J) $ IIM(J,1)=IIM(1,J)
IIV(J,1)=IIV(1,J) $ SIV(J,1)=SIV(1,J)
66 CONTINUE
DO 12 J=1, JMAX
JILT = JMAX-J+1
DO 11 M=2, JILT
IF(M.GT.JMAXH) GO TO 601
SSM(M,M+J-1) = SSM(1,J)
SSV(M,M+J-1) = SSV(1,J)
ISM(M,M+J-1) = ISM(1,J)

```

```
ISV(M,M+J-1) = ISV(1,J)
IIM(M,M+J-1) = IIM(1,J)
IIV(M,M+J-1) = IIV(1,J)
SIM(M,M+J-1) = SIM(1,J)
SIV(M,M+J-1) = SIV(1,J)
601 CONTINUE
IF(M+J-1.GT.JMAXH) GO TO 11
SSM(M+J-1,M) = SSM(1,J)
SSV(M+J-1,M) = SSV(1,J)
ISM(M+J-1,M) = ISM(1,J)
ISV(M+J-1,M) = ISV(1,J)
IIM(M+J-1,M) = IIM(1,J)
IIV(M+J-1,M) = IIV(1,J)
SIM(M+J-1,M) = SIM(1,J)
SIV(M+J-1,M) = SIV(1,J)
11 CONTINUE
12 CONTINUE
END
```

NRL REPORT 7964

```

SUBROUTINE CSTM
COMMON/ICE/ICE,NDEXI
TYPE COMPLEX STV,ITV,STM,ITM
COMMON/EPS/EPS/JOE/JTOP
COMMON/STV/STV/ITV/ITV/PJ/STM/ITM/ITM
COMMON/RAD/RIN,ROUT
DIMENSION ITM(20,10),ITV(20,10),STM(20,10),STV(20,10)
COMMON/BLKA/PR,PLR,PZ,PLZ/PIT/JMAX,JMAXH,IMAX
DIMENSION PZ(20),PLZ(20),PR(20),PLR(20),GGMS(10,32)
DIMENSION BSO(10,32),RSI(10,32),BIO(10,32),BII(10,32)
DIMENSION XI(32),WF(32),SUMV(10)
DIMENSION GSO(10,32),GSI(10,32),BUNT(10),SUMT(10),BUMV(10)
TYPE COMPLEX ANS,ANSB,VNS,VNSB
COMMON/FS/FKFK,FKFAST,TFK/GGMS/GGMS
COMMON/DEL/DELR,DELZ/BOLD/GSO,GSI/BLK1/H,A,FK,PI/BLK2/XI,WF
COMMON/5/BT0(10,10,32),BT1(11,10,32),QZ(32,10),SIGMA(32),REST(128)
COMMON/T0Y/H,NN,NNN/BLK3B/BIO,BII/BLK3/BSO,BS1/TIDY/FAST
COMMON/6/GT0(10,10,32),STEXP(32,20,10)
COMMON/STORSCST/STSIN(32,21),STCOS(32,21)
PIOTW0 = 0.5 * PI
R1 = A
HD = .5*DELR
DO 1000 JR=1,IMAX
R2 = PR(JR)
RL = R2 - HD
RU = R2 + HD
DO 1000 IR=1,JMAX
ARGP = H - PZ(IR)
SUMR=SUMI=SUMRB=SUMIB = VUMR=VUMI=VUMRB=VUMIB= 0.
DO 1 L =1,N
BU = BT1(JR,1,L)
VAK = BSO(1,L) * BU
VAKB = BIO(1,L) * BU
YAK = VAK * SIGMA(L)
YAKB = VAKB * SIGMA(L)
SUMR = SUMR - YAK * STCOS(L,IR)
SUMI = SUMI + YAK * STSIN(L,IR)
VUMR = VUMR - VAK * STSIN(L,IR)
VUMI = VUMI + VAK * STCOS(L,IR)
SUMRB = SUMRB - YAKB * STCOS(L,IR)
SUMIB = SUMIB + YAKB * STSIN(L,IR)
VUMRB = VUMRB - VAKB * STSIN(L,IR)
VUMIB = VUMIB + VAKB * STCOS(L,IR)
1 CONTINUE
R = R1
IF(R2.LE.R1) R = R2
IF(R.EQ.0.) R = DELR
FACT = 2./(R*PI*ARGP)
RM = R1
IF(R.EQ.R1) RM = R2
FACT1 = PIOTW0 / AMINI(ROUT - R2, R2 - RIN)
00009400

```

```

EFACT1 = 1.0 - EXPF(-ARGP * FACT1)
SUMT(1) = - SUMR
BUMT(1) = - SUMRB
SUMV(1) = VUMR $ BUMV(1) = VUMRB
FL = 0.0
ICE = 1
2 ICE = ICE + 1
VUMMIT = VUMMITB = 0.
SUMMIT = SUMMITB = 0.
DO 375 M=1,N
BU = STEXP(M,IR,ICE) * BT1(JR,ICE,M)
VAKR = BSO(ICE,M) * BU
VAKRB = BIO(ICE,M) * BU
SUMMIT = SUMMIT + VAKR * QZ(M,ICE)
SUMMITB = SUMMITB + VAKRB * QZ(M,ICE)
VUMMIT = VUMMIT + VAKR
VUMMITB = VUMMITB + VAKRB
375 CONTINUE
BUMV(ICE) = BUMV(ICE - 1) + VUMMITB
SUMV(ICE) = SUMV(ICE - 1) + VUMMIT
SUMT(ICE) = SUMT(ICE - 1) + SUMMIT
BUMT(ICE) = BUMT(ICE - 1) + SUMMITB
FL = FL + FKFAST
FLT = FL + FACT1
ERFC = ABS(FACT * RM * EFACT1 * EXPF(-ARGP * FL) / (FL*SUMT(ICE)))
IF(ERFC.LT.FPS) GO TO 3
IF(ICE.GE.JTOP) GO TO 3
GO TO 2
3 CONTINUE
ANSI = -SUMI
ANSR = SUMT(ICE)
ANSIB = - SUMIB $ ANSRB = BUMT(ICE)
NBEXI = 0
CALL CFINT(ARGP, RU, R0UT, FL, CFU)
CFST = RU * CFU
NBEXI = 1
CALL CFONE(ARGP, RU, R0UT, FL, CFU)
CFSTV = RU * CFU
NBEXI = 0
CALL CFINT(ARGP, RL, R0UT, FL, CFL)
CFST = CFST + (RL * CFL)
NBEXI = 1
CALL CFONE(ARGP, RL, R0UT, FL, CFL)
CFSTV = CFSTV + (RL * CFL)
NBEXI = 0
CALL CFINT(ARGP, RU, RIN, FL, CFU)
CFIT = RU * CFU
NBEXI = 1
CALL CFONE(ARGP, RU, RIN, FL, CFU)
CFITV = RU * CFU
NBEXI = 0

```

00011300

NRL REPORT 7964

```
CALL CFINT(ARGP, RL, RIN, FL, CFL)
CFIT = CFIT - (RL * CFL)
NEXI = 1
CALL CFONE(ARGP, RL, RIN, FL, CFL)
CFITV = CFITV - (RL * CFL)
ANSR = ANSR+CFST & ANSRB = ANSRB + CFIT
STM(IR, JR) = CMPLX(ANSR, ANSI)
ITM(IP, JR) = CMPLX(ANSRB, ANSIB)
SUMV(ICE) = SUMV(ICE) + CFSTV
BUMV(ICE) = BUMV(ICE) + CFITV
VNS = CMPLX(-SUMV(ICE), VUMI) & VNSB = CMPLX(-BUMV(ICE), VUMIB)
STV(IP, JR) = VNS & ITV(IR, JR) = VNSB
1000 CONTINUE
END
```

HANISH, KING, BAIER, AND ROGERS

```

SUBROUTINE CTBM
COMMON/EP51/EP5
COMMON/5/BT0(10,10,32),BT1(11,10,32),QZ(32,10),SIGMA(32),REST(128)
COMMON/6/GT0(10,10,32),GT1(11,10,32),RUST1(2880)
COMMON/BLK1/H,A,FK,PI/PIT/JMAX,JMAXH,IMAX/TTV/TTV/TIDY/FAST
COMMON/BLK2/XI,WF/TBY/NQD1,N2,N3/BLK3B/BI0,BI1/BLK3/BS0,BS1
COMMON/BLKA/PR,PLR,PZ,PLZ/DEL/DELR,DELZ/BOLD/GS0,GS1/HCC/JTAP
COMMON/FS/FKFK,FKFAST,TFK/TBV/TBV/UJ/TBM/GGMS/GGMS
DIMENSION PZ(20),PLZ(20),PR(20),PLR(20),TTV(10,10),TBM(10,10),
1 TBV(10,10),GGMS(10,32)
TYPE COMPLEX TTV,TBM,TBV
DIMENSION XI(32),WF(32),SUMT(10),GS0(10,32),GS1(10,32),UMT(10),
1BUMT(10),BS0(10,32),BS1(10,32),BI0(10,32),BI1(10,32)
COMMON/STORSCIB/TBSIN,TBCOS,TBEXP
DIMENSION TBSIN(32),TBCOS(32),TBEXP(32,10)
EQUIVALENCE (TBCOS(1),TBEXP(1))
TPK = 0.25 * FKFAST
PI0TW0 = 0.5 * PI $ TW0PI = PI + PI
N=NQD1
HD = .5*DELR
ARGP = H + H
DO 7 JR=1,IMAX
R2 = PR(JR)
RL = R2 - HD
RU = R2 + HD
DO 7 IR=1,IMAX
R1 = PR(IR)
UMI=SUMR=SUMI=SUMRB=SUMIB=0.
DO 1 L =1,N
YAK = BT0(IR,1,L) * BT1(JR,1,L)
VI = YAK * TBCOS(L)
VR = YAK * TBSIN(L)
SUMIB = SUMIB - VI
SUMRB = SUMRB + VR
SUMR = SUMR - VI * SIGMA(L)
SUMI = SUMI + VR * SIGMA(L)
1 UMI = UMI + YAK
UMI = UMI*TFK
R = R1
IF(R2.LE.R1) R = R2
IF(R.EQ.0.) R = DELR
FACT = 2./(R*PI*ARGP)
RM = R1
IF(R.EU.R1) RM = R2
FACT1 = PI0TW0 / ABS(ABS(R2-R1) - HD)
EFACT1 = 1.0 - EXPF(-FACT1 * ARGP)
UMT(1) = 0. $ SUMT(1) = -SUMR $ BUMT(1) = -SUMRB
FL = 0.0
ICE = 1
2 ICE = ICE + 1
UMMIT = SUMMIT = SUMMITB = 0.

```

00009400

NRL REPORT 7964

```

DO 375 M=1,N
YAKR = BT0(IR,ICE,M) * BT1(JR,ICE,M)
VAKR = YAKR - GT0(IR,ICE,M) * GT1(JR,ICE,M)
UMMIT = UMMIT + VAKR
ARTISTB = YAKR * TBEXP(M,ICE)
ARTIST = ARTISTB * OZ(M,ICE)
SUMMIT = SUMMIT + ARTIST
375 SUMMITH = SUMMITB + ARTISTB
SUMT(ICE) = SUMT(ICE-1) + SUMMIT
BUMT(ICE) = BUMT(ICE-1) + SUMMITB
UMT(ICE) = UMT(ICE-1) + TPK * UMMIT
FL = FL + FKFAST
ERFC = ABS(FACT * RM * EXPF(-ARCP * FL) * EFAC1 / (FL * SUMT(ICE)))
TESTER = ABS(1.0 - SUMT(ICE) / SUMT(ICE-1))
IF(TESTER.LT.EPS,AND.ERFC.LT.EPS) GO TO 3
IF(ICE.GE.JTOP) GO TO 3
GO TO 2
3 CONTINUE
ANSR = SUMT(ICE) $ ANSI = -SUMI
VNSI = -SUMIB $ VNSR = -BUMT(ICE)
TBM(IR,JR) = CMPLX(ANSR,ANSI) $ TBV(IR,JR) = CMPLX(VNSR,VNSI)
DK = 4.*R1*RU / ((R1 + RU) * (R1 + RU))
CU = (R1+RU)*ELLIPE(DK) + (RU-R1)*ELLIPK(DK)
DK = 4.*R1*RL / ((R1 + RL) * (R1 + RL))
CL = (R1+RL)*ELLIPE(DK) + (RL-R1)*ELLIPK(DK)
CF = (CU - CL) / TWOPI
ANSR = - UMT(ICE) - CF
7 TTV(IR,JR) = CMPLX(ANSR,UMI)
END

```

00011300

00012300

HANISH, KING, BAIER, AND ROGERS

SUBROUTINE CTSM

```

COMMON/ICE/ICE,NOEXI
TYPE COMPLEX TIV,TSV,TIM,TSM,ANS,ANSB,VNS,VNSB
DIMENSION TSM(10,20),TIM(10,20),TSV(10,20),TIV(10,20)
DIMENSION PZ(20),PLZ(20),PR(20),PLR(20)
COMMON/EPS/EPS/JOE/JTOP
COMMON/BLK1/H,A,FK,PI/RAO/RIN,RBUT/PIT/JMAX,JMAXH,IMAX/IJK/I,J
COMMON/TIM/TIM/BLK0/TSM/TIV/TIV/TSV/TSV/BLKA/PR,PLR,PZ,PLZ
DIMENSION BS0(10,32),BS1(10,32),EX(32)
DIMENSION B10(10,32),B11(10,32),G10(10,32),G11(10,32)
DIMENSION SUMTV(10),BUMTV(10),XI(32),WF(32),SUMT(10),BUMT(10)
DIMENSION GS0(10,32),GS1(10,32),GGMS(10,32)
COMMON/5/BT0(10,10,32),BT1(11,10,32),GZ(32,10),SIGMA(32),REST(128)
COMMON/6/G10(10,10,32),TSEXP(32,20,10)
COMMON/BBOLD/G10,G11/DEL/DELR,DELZ/HOLD/GS0,GS1
COMMON/BLK3/BS0,BS1/TIDY/FAST/FS/FKFK,FKFAST,FK
COMMON/BLK3R/B10,B11/TOY/NN,NNN/BLK2/XI,WF/GGMS/GGMS
COMMON/STORCST/TSSIN(32,21),TSCOS(32,21)
IPK = 0.25 * FKFAST
PIOTW0 = 0.5 * PI
EPS1 = 0.0001
DO 20 I=1,IMAX
R = PR(I)
IR = I
DO 20 J= 1,JMAX
Z = PLZ(J)
ARGP = H - Z - DELZ
IF(J.EQ. 1) ARGP = 0.0
ARGM = H - Z
SUMR=SUMI=SUMRB=SUMIB=SUMRV=SUMIV=SUMRBV=SUMIBV=0.
DO 1 L =1,N
TRIGFR = TSCOS(L,J) * BT0(IR,1,L)
TRIGFI = TSSIN(L,J) * BT0(IR,1,L)
SUMR = SUMR - TRIGFR * BS1(1,L)
SUMI = SUMI + TRIGFI * BS1(1,L)
SUMRB = SUMRB + TRIGFR * B11(1,L)
SUMIB = SUMIB - TRIGFI * B11(1,L)
SUMRV = SUMRV - TRIGFR * BS0(1,L)
SUMIV = SUMIV - TRIGFI * BS0(1,L)
SUMRBV = SUMRBV - TRIGFR * B10(1,L)
SUMIBV = SUMIBV - TRIGFI * B10(1,L)
1 CONTINUE
SUMT(1) = SUMR & BUMT(1) = SUMRB
SUMTV(1) = SUMRV & BUMTV(1) = SUMRBV
IF(J.EQ.1) GO TO 54321
FACT = 2./(*PI*ARGP)
54321 CONTINUE
FACT1 = PIOTW0 / AMINI(RBUT - R, R - RIN)
EFACT1 = 1.0 - EXPF(-ARGP * FACT1)
ANSTB = RIN*SUMRB

```

00009400

NRL REPORT 7964

```

ANST = ROUT*SUMR
FL = 0.0
ICE = 1
2 ICE = ICE + 1
SUMMIT=SUMMITB=VUMMIT=VUMMITB=0.
DO 375 M=1,N
GMR = BT0(IR,ICE,M) * TSEXP(M,J,ICE)
ARTIST = BS1(ICE,M) * GMR
ARTISTB = B11(ICE,M) * GMR
ARTISTV = GMR*BS0(ICE,M)
VRTISTB = GMR*B10(ICE,M)
VUMMIT = VUMMIT + ARTISTV
VUMMITB = VUMMITB + VRTISTB
IF(J.EQ.1) GO TO 93
GO TO 94
93 GS = GT0(IR,ICE,M)*WF(M) *TPK
GSGS = GS*GS1(ICE,M)
GSGSI = GS*GI1(ICE,M)
ARTIST = ARTIST - GSGS $ ARTISTB = ARTISTB - GSGSI
94 SUMMIT = SUMMIT + ARTIST
SUMMITB= SUMMITB - ARTISTB
375 CONTINUE
BUMT(ICE) = BUMT(ICE-1) + SUMMITB
SUMT(ICE) = SUMT(ICE-1) + SUMMIT
SUMTV(ICE) = SUMTV(ICE-1) + VUMMIT
BUMTV(ICE) = BUMTV(ICE-1) + VUMMITB
FL = FL + FKFAST
IF(J.EQ.1) GO TO 95
FLT = FL + FACT1
ERFC = ABS(FACT * EXPF(-ARGP * FL) * EFAC1 / (FL * SUMT(ICE)))
IF(ERFC.LT.EPS) GO TO 8
IF(ICE.GE.JT6P) GO TO 8
GO TO 2
95 ANSR = ROUT*SUMT(ICE) + .50
ANSRB = RIN*BUMT(ICE)
TESTER = ABS(1.0 - ANST / ANSR)
TESTERB = ABS(1.0 - ANSTB / ANSRB)
IF(ICE.GE.JT6P) GO TO 100
IF(TESTER.LT.EPS1.AND.TESTERB.LT.EPS1) GO TO 100
ANST = ANSR
ANSTB = ANSRB
GO TO 2
100 CONTINUE
N0EXI = 0
CALL CFINT(ARGM, ROUT, PR(IR), FL, CFM)
SUMT(ICE) = SUMT(ICE) - CFM
N0EXI = 1
CALL CFZER0(ARGM, ROUT, PR(IR), FL, CFM)
N0EXI = 0
CALL CFZER0(ARGP, ROUT, PR(IR), FL, CFP)
SUMTV(ICE) = SUMTV(ICE) + CFP - CFM

```

00011300

00012400

```

CALL CFINT(ARGM, RIN, PR(IR), FL, CFM)
BUMT(ICE) = BUMT(ICE) + CFM
NDEXI = 1
CALL CFZERO(ARGM, RIN, PR(IR), FL, CFM)
NDEXI = 0
CALL CFZERO(ARGP, RIN, PR(IR), FL, CFP)
BUMTV(ICE) = BUMTV(ICE) + CFP - CFM
GO TO 3
8 NDEXI = 0
CALL CFINT(ARGP, ROUT, PR(IR), FL, CFP)
SUMT(ICE) = SUMT(ICE) + CFP
NDEXI = 1
CALL CFZERO(ARGP, ROUT, PR(IR), FL, CFP)
SUMTV(ICE) = SUMTV(ICE) + CFP
NDEXI = 0
CALL CFINT(ARGM, ROUT, PR(IR), FL, CFM)
SUMT(ICE) = SUMT(ICE) - CFM
NDEXI = 1
CALL CFZERO(ARGM, ROUT, PR(IR), FL, CFM)
SUMTV(ICE) = SUMTV(ICE) - CFM
NDEXI = 0
CALL CFINT(ARGP, RIN, PR(IR), FL, CFP)
BUMT(ICE) = BUMT(ICE) - CFP
NDEXI = 1
CALL CFZERO(ARGP, RIN, PR(IR), FL, CFP)
BUMTV(ICE) = BUMTV(ICE) + CFP
NDEXI = 0
CALL CFINT(ARGM, RIN, PR(IR), FL, CFM)
BUMT(ICE) = BUMT(ICE) + CFM
NDEXI = 1
CALL CFZERO(ARGM, RIN, PR(IR), FL, CFM)
BUMTV(ICE) = BUMTV(ICE) - CFM
3 CONTINUE
ANS = CMPLX(SUMT(ICE), SUMI)
ANSB = CMPLX(BUMT(ICE), SUMIB)
VNS = CMPLX(-SUMTV(ICE), SUMIV)
VNSB = CMPLX(-BUMTV(ICE), SUMIBV)
TSM(I,J) = ANS*ROUT & TIM(I,J) = RIN*ANSB
TSV(I,J) = VNS*ROUT & TIV(I,J) = RIN*VNSB
IF(J,EQ,1) TSM(I,J) = TSM(I,J) + 0.500
20 CONTINUE
END

```

NRL REPORT 7964

```

SUBROUTINE CUBIC(A2,A1,A0,RT)
THIS SUBROUTINE SOLVES THE CUBIC EQUATION X**3 + A2*X**2 + A1*X + A0 = 0.
DIMENSION RT(6)
TYPE DOUBLE DR,QRSQD,QRR
RT(2) = RT(4) = RT(6) = 0.
AA = .8660254037
A23 = A2/3.
Q = A1/3. - A23*A23
R = (A1*A2-3.*A0)/6. - A23**3
QRSQ = Q**3 + R*R
IF (QRSQ)30,31,32
32 DR = DBLE(R)
QRSQD = Q**3 + DR*DR
QRR = DSQRT(QRSQD)
S1 = CUBERTF(SNGL(DR+QRR))
S2 = CUBERTF(SNGL(DR-QRR))
RT(1) = S1 + S2 - A23
RT(3) = RT(5) = -.5*(S1+S2) - A23
RT(4) = AA*(S1-S2)
RT(6) = -RT(4)
GO TO 10
30 QR = SQRTF(-QRSQ)
PHI = ATAN2(QR,R)/3.
Z = CUBERTF(SQRTF(R**2-QRSQ))
SPS = 2.*Z*COSF(PHI)
SMS = 2.*Z*SINF(PHI)
RT(1) = SPS - A23
RT(5) = -.5*SPS - A23 + AA*SMS
RT(3) = -.5*SPS - A23 - AA*SMS
GO TO 10
31 IF (R.EQ.0.) GO TO 33
SPS = 2.*CUBERTF(R)
RT(1) = SPS - A23
RT(3) = RT(5) = -.5*SPS - A23
GO TO 10
33 RT(1) = RT(3) = RT(5) = -A23
10 RETURN
END

```

```

SUBROUTINE DVD(XA,YA,XB,YB,XC,YC)
DENOM=XB*XB+YB*YB
XC=(XA*XB+YA*YB)/DENOM
YC=(YA*XB-XA*YB)/DENOM
END

```

HANISH, KING, BAIER, AND ROGERS

```

SUBROUTINE EIGFNS
C THIS SUBROUTINE CALCULATES ELASTIC RESONANCE FREQUENCIES FRQ(), MODAL
C SHAPES RD(,) AND AXEDGE(), AND INTEGRALS OF RADIAL MODAL SHAPES RDIN(,)
C AND RINT(). IT USES SUBROUTINE CUBIC.
C THE ENTRY POINT IMPO NEAR THE END OF THIS SUBROUTINE IS USED TO OBTAIN
C VARIOUS INTEGRALS NEEDED TO CALCULATE SHELL STIFFNESS REACTANCE AND
C MEDIUM INERTIAL REACTANCE.
TYPE COMPLEX AN,B,BU,BW,C1,C2,C3,C4,C5,C6,C7,C8,CFM,CU,CW,D,DN,DK,
10TD,DTRMNT,EE,EM,EN,EPM,EPP,G,RAR,RN,RT,RT1,RT2,RTR,SRT,T1,T2,TM,
2U,U2,UM,US,UX,UX2,UXM,UXW,UXWXX,W,W2,WM,WS,XXX,XXX2,XXXM
DIMENSION AA(9),AX(9,10),AXEDGE(9),B(3,3),BU(9,3),CW(9,3),CFM(11),
1CU(3),CW(3),DETR(2),EN(3),F(3),FR(2),FRQ(9),G(4),NA(9),NR(9),
2RAR(9,3),RD(9,10),RDIN(9,10),RINT(9),RT(3),RTR(3),TT(2)
TYPE REAL LTH,NA,NR,NU
EQUIVALENCE (TT,DK)
COMMON/INT/CFM,UX2I,UZI,WZI,UXWI,WXX2I,UXXXXI
COMMON/BLK1/HD2,RMEAN,FK,PI/YMD/Y,NU,RHO,NDS
COMMON/MODES/FRQ,RO,RDIN,NBRFNS,THK,NPTS,AXEDGE,RINT
NIT = 30
LTH = 2.*HD2
A = RMEAN
PRINT 19
19 FORMAT (1H144X*CALCULATION OF MODAL SHAPE FUNCTIONS*)
PRINT 20,A,THK,LTH,RHO,NU,Y
20 FORMAT (//56X*INPUT PARAMETERS*//29X11HMEAN RADIUS3BX
$7HRMEAN =E14.6/
$29X16HRADIAL THICKNESS35X5HTHK =E14.6/
$29X12HAXIAL LENGTH39X5HLTH = E14.6/
$29X7HDENSITY44X5HRHO =E14.6/
$29X14HPOISSONS RATIO38X4HNU =E14.6/
$29X45HYOUNGS MODULUS AT CONSTANT MAGNETIC INDUCTION 8X3HF =E14.6)
PRINT 5056
5056 FORMAT (//)
C
C READ IN NBRFNS, FREQUENCY INTERVALS, AND IMG FLAG.
C
READ 99,NBRFNS
99 FORMAT (I1)
DO 777 IJX = 1,NBRFNS
IX = IJX
IF (IX.GT.1) PRINT 5057
5057 FORMAT (1H1)
READ 9,FR(1),FR(2),IMG
9 FORMAT (2F10.5,4X11)
INX = 1
IT = 0
FREQ = FR(1)
PRINT 52
52 FORMAT (51X*INITIAL FREQUENCY INTERVAL*//)
42 CONTINUE
C

```

NRL REPORT 7964

```

C   CALCULATE BOUNDARY CONDITION MATRIX B(,) AND ITS DETERMINANT DTRMNT.
C
DELTA = RH0**A**A*(1.-NU**2)*FREQ**2/Y**4.*PI*PI
BETA = THK**2/(12.**A**A)
A2 = DELTA + 2.*NU
A1 = (1.-DELTA-NU*NU)/BETA + 1.
A0 = (DELTA-DELTA**2)/BETA + DELTA
CALL CUBIC(A2,A1,A0,RT)
DO 1 I = 1,3
SRJ = CSQRT(RT(I))
EN(I) = (RT(I)+DELTA)/(NU*SRT-BETA*SRT*RT(I))
D = SRT/A
RTR(I) = D
RAR(IX,I) = 0
EPP = CEXP(LTH/2.*D)
EPM = (1.,0.)/EPP
TM = BETA*EN(I)*RT(I)/A-NU/A*EN(I) + 0
B(1,I) = (EPP + EPM)*TM
TM = EN(I)*D*D/D/A
B(2,I) = (EPP + EPM)*TM
TM = EN(I)*D**3+D*D/A
1 B(3,I) = (EPP - EPM)*TM
DTRMNT = B(1)*B(5)*B(9) + B(4)*B(8)*B(3) + B(7)*B(2)*B(6) -
$B(3)*B(5)*B(7) - B(6)*B(8)*B(1) - B(9)*B(2)*B(4)
DET = REAL(DTRMNT)
IF (IMG.EQ.1) DET = AIMAG(DTRMNT)
IF (INX.LE.2) PRINT 50,FREQ,DTRMNT
50 FORMAT (23X*FREQUENCY =*E18.10,5X*DETERMINANT =*(E18.10,E18.10)/)
C
C   APPLY INTERVAL HALVING.
C
IF (INX.GE.3) GO TO 41
DETR(INX) = DET
INX = INX + 1
IF (INX.GE.3) GO TO 44
FREQ = FR(INX)
GO TO 42
41 IF (IT.GE.NIT) GO TO 43
IT = IT + 1
IF (DETR*DETR(1).GT.0.) GO TO 45
DETR(2) = DET
FR(2) = FREQ
GO TO 44
45 DETR(1) = DET
FR(1) = FREQ
44 IF (DETR(1)*DETR(2).GT.0.) GO TO 46
FREQ = .5*(FR(1)+FR(2))
GO TO 42
C
C   OBTAIN SCALED MODAL SHAPE COEFFICIENTS FOR AXIAL CU() AND RADIAL CW()
C   MOTION.

```

```

C
43 F(1) = A2
   F(2) = A1
   F(3) = A0
   FRQ(IX) = FREQ
   DN = B(1)/B(3)
   G(1) = B(4) - DN*B(6)
   G(3) = B(7) - DN*B(9)
   DN = B(2)/B(3)
   G(2) = B(5) - DN*B(6)
   G(4) = B(8) - DN*B(9)
   RT1 = -G(3)/G(1)
   RT2 = -G(4)/G(2)
   CU(1) = (-B(9)-B(6)*RT1)/B(3)
   CU(2) = RT1
   CU(3) = (1.,0.)
   C1 = (0.,0.)
   DO 31 I = 1,3
   CW(I) = CU(I)*EN(I)
31 C1 = C1 + CW(I)
   DO 215 I = 1,3
   CU(I) = CU(I)/C1
215 CW(I) = CW(I)/C1
   DO 210 I = 1,3
   BU(IX,I) = CU(I)
210 BW(IX,I) = CW(I)

C
C   PRINT OUT VALUES RT1 AND RT2 FOR USE IN CHECKING VALIDITY OF RESONANCE
C   FREQUENCIES AND MODAL SHAPES.
C
C   PRINT 60,RT1,RT2
60 FORMAT (/17X*CONVERGENCE CHECK*//5X5HRT1 =C(E18.10,E18.10)/5X5HRT2
I =C(E18.10,E18.10)/)

C
C   RESCALE MODAL SHAPES SO THAT THE INTEGRAL OF THE MODAL SHAPE OVER THE
C   ENTIRE LENGTH OF THE SHELL IS NUMERICALLY EQUAL TO THE LENGTH OF THE
C   SHELL. THEN PRINT SCALED MODAL SHAPES.
C
AN = (0.,0.)
RN = (0.,0.)
DO 21 I = 1,3
DO 21 J = 1,3
T1 = T2 = LTM
OR = RTR(I) + CONJG(RTR(J))
IF (TT(1)+TT(2).EQ.0.) GO TO 22
EPP = CEXP(DR*HD2)
EPM = (1.,0.)/EPP
T1 = (EPP-EPM)/OR
22 DR = RTR(I) - CONJG(RTR(J))
IF (TT(1)+TT(2).EQ.0.) GO TO 23
EE = CEXP(DR*HD2)

```


HANISH, KING, BAIER, AND ROGERS

```

EPM = (1.,0.)/EPP
305 RN = RN + CW(J)/RTR(J)*(EE-EM-EPP+EPM)*ANRM
304 PDIN(IX,1) = REAL(RN)
RN = (0.,0.)
DO 300 J = 1,3
EPP = CEXP(RTR(J)*LTH/2.)
EPM = (1.,0.)/EPP
300 RN = RN + CW(J)/RTR(J)*(EPP-EPM)*ANRM
RINT(IX) = REAL(RN)
PRINT 54
54 FORMAT (//54X*RESONANT FREQUENCY*/)
PRINT 50,FREQ,DTRMNT
777 CONTINUE
GO TO 7
46 PRINT 55
55 FORMAT (//10X*NO SIGN DIFFERENCE*)
STOP

C
C   CALCULATE AND PRINT INNER PRODUCTS OF MODAL SHAPES.
C
7 PRINT 8
8 FORMAT (//43X*NORMALIZED INNER PRODUCTS OF MODAL SHAPES*//42X
$12HMODAL SHAPES11X*VALUE OF INNER PRODUCT*/)
DO 95 K = 1,IX
KP = K + 1
DO 95 L = KP,IX
AN = (0.,0.)
RN = (0.,0.)
DO 96 I = 1,3
DO 96 J = 1,3
EPP = CEXP((RAR(K,I)+CONJG(RAR(L,J)))*HDZ)
EPM = (1.,0.)/EPP
EE = CEXP((RAR(K,I)-CONJG(RAR(L,J)))*HDZ)
EM = (1.,0.)/EE
AN = AN + BU(K,I)*CONJG(BU(L,J))*((EPP-EPM)/(RAR(K,I)
$+CONJG(RAR(L,J))) - (EE-EM)/(RAR(K,I)-CONJG(RAR(L,J))))
96 RN = RN + BW(K,I)*CONJG(BW(L,J))*((EPP-EPM)/(RAR(K,I)
$+CONJG(RAR(L,J))) + (EE-EM)/(RAR(K,I)-CONJG(RAR(L,J))))
REE = REAL(AN+RN)/SQRT((NA(K)+NR(K))*(NA(L)+NR(L)))
95 PRINT 97,K,L,REE
97 FORMAT (/44X12,* AND*12,18X12.4)
RETURN

C
C   CALCULATE VARIOUS INTEGRALS NEEDED TO OBTAIN SHELL STIFFNESS REACTANCE
C   AND MEDIUM INERTIAL REACTANCE.
C
ENTRY IMPD
DO 80 I = 1,NBRFNS
80 CFM(I) = CFM(I)*AA(I)
UX2 = UZ = W2 = UXX = WXX2 = UXWXX = (0.,0.)
DO 81 K = 1,NBRFNS

```

```

D0 81 L = 1,NBRFNS
C1 = C2 = C3 = C4 = C5 = C6 = (0.,0.)
D0 82 I = 1,3
D0 82 J = 1,3
T1 = T2 = LTH
DR = RAR(K,I) + CONJG(RAR(L,J))
IF (TT(1)+TT(2).EQ.0.) GO TO 83
EPP = CEXP(DR*HD2)
EPM = (1.,0.)/EPP
T1 = (EPP-EPM)/DR
83 DR = RAR(K,I) - CONJG(RAR(L,J))
IF (TT(1)+TT(2).EQ.0.) GO TO 84
EE = CEXP(DR*HD2)
EM = (1.,0.)/EE
T2 = (EE-EM)/DR
84 C1 = C1 + BU(K,I)*CONJG(BU(L,J))*RAR(K,I)*CONJG(RAR(L,J))*(T1+T2)
C2 = C2 + BU(K,I)*CONJG(BU(L,J))*(T1-T2)
C7 = BU(K,I)*CONJG(BU(L,J))*(T1+T2)
C3 = C3 + C7
C8 = BU(K,I)*CONJG(BU(L,J))*RAR(K,I)*(T1+T2)
C4 = C4 + C8
C5 = C5 + (RAR(K,I)*CONJG(RAR(L,J)))*2*C7
82 C6 = C6 + CONJG(RAR(L,J))*2*C8
UX2 = UX2 + CFM(K)*CONJG(CFM(L))*REAL(C1)
U2 = U2 + CFM(K)*CONJG(CFM(L))*REAL(C2)
W2 = W2 + CFM(K)*CONJG(CFM(L))*REAL(C3)
UXW = UXW + CFM(K)*CONJG(CFM(L))*REAL(C4)
WXX2 = WXX2 + CFM(K)*CONJG(CFM(L))*REAL(C5)
81 UXWXX = UXWXX - CFM(K)*CONJG(CFM(L))*REAL(C6)
UX2I = CABS(UX2)
U2I = CABS(U2)
W2I = CABS(W2)/(A*A)
UXW1 = REAL(UXW)*2.*NU/A
WXX2I = CABS(WXX2)*A*A
UXWXXI = REAL(UXWXX)*2.*A
END

```

HANISH, KING, BAIER, AND ROGERS

```

SUBROUTINE ERING
TYPE COMPLEX GM,ISM,SIM,ITM,TIM,IIM,SSM,TSM,STM,SBM,TBM,DM,HHOC,
$ANS,VT,V,VS,VI,ISV,SIV,ITV,IIV,SSV,TSV,STV,SBV,TBV,SUMJ,ITV
DIMENSION GM(30,60),DM(60,60),SSM(10,20),SSV(10,20),REST(6000),
1ISM(10,20),TBM(10,10),STM(20,10),ITV(10,10),TSV(10,20),TBV(10,10),
2STV(20,10),ISM(10,20),ITM(20,10),SIM(10,20),TIM(10,20),IIM(10,20)
3,ISV(10,20),SIV(10,20),ITV(20,10),IIV(10,20)
4,IIV(10,20),PLZ(20),PR(20),PLR(20),PZ(20)
COMMON/DEL/DELZ,DELZ/BLKA/PR,PLR,PZ,PLZ/LC/LCMAX,LCMAXH
COMMON/SSV/SSV/TSV/TSV/STV/STV/SBV/SBV/TBV/TBV/ITV/ITV
COMMON/ISV/ISV/SIV/SIV/ITV/ITV/IIV/IIV/IIV/IIV
COMMON/TIM/TIM/SIM/SIM/ISM/ISM/ITM/ITM/IIM/IIM
COMMON/BLKD/TSM/UJ/TBM/PJ/STM/BLKE/SSM/VEL/VS,VI/VELT/VT
COMMON/PII/JMAX,JMAXH,IMAX/RAD/RIN,ROUT/S/DM/6/GM,REST
COMMON/TIDY/FAST/RCC/JTOP/BLK1/H,A,FK,PI
FKA = FK*A $ DELZ = H/JMAXH $ DELR = (ROUT-RIN)/IMAX
DO 1 J=1,JMAXH
KC = JMAXH + 1 - J
PZ(J) = H + .5*DELZ - J*DELZ
PZ(KC) = -PZ(J)
PLZ(J) = PZ(J) - .5*DELZ
1 PLZ(KC) = PZ(KC) - .5*DELZ
DO 2 I=1,IMAX
2 PR(I) = RIN - .5*DELR + I*DELR
CALL CALBES
CALL CALTRIG
CALL CTBM
CALL STTRIG
CALL CSTM
CALL SSTRIG
CALL CSSM
CALL TSTRIG
CALL CTSM
DO 6000 I=1,LCMAXH
DO 6000 J=1,LCMAXH
6000 GM(I,J) = (0.0,0.0)
DM(I,J) = (0.0,0.0)
IF(RIN.EQ.0.) GO TO 80
DO 64 I=1,IMAX
DO 64 J= 1,IMAX
GM(JMAXH+I,JMAXH+J) = TTV(I,J)
64 CONTINUE
DO 31, I=1,JMAXH
KITE = JMAXH + 1 - I
DO 32 J=1,JMAXH
DM(I,J) = IIM(KITE,JMAXH+1-J)
GM(I,J) = IIV(KITE,JMAXH+1-J)
GM(I,LCMAX+1-J) = IIV(KITE,JMAXH+J)
32 DM(I,LCMAX+1-J) = IIM(KITE,JMAXH+J)
DO 33 J=1,IMAX
GM(I,JMAXH+J) = ITV(KITE,J)

```

NRL REPORT 7964

```

33 DM(I,JMAXH+J) = ITM(KITE,J)
D0 34 J=1,JMAX
GM(I,JMAXH+IMAX+J)= ISV(KITE,J)
34 DM(I,JMAXH+IMAX+J)= ISM(KITE,J)
D0 35 J=1,IMAX
GM(I,JMAXH+LCMAXH+J)= ITV(JMAX +1-KITE,IMAX+1-J)
35 DM(I,JMAXH+LCMAXH+J)= ITM(JMAX +1-KITE,IMAX+1-J)
31 CONTINUE
D0 36 I=1,IMAX
K00T = JMAXH+I
DM(K00T,K00T) = (0.5,0.0)
D0 37 J=1,JMAXH
KITE = JMAXH + 1 - J
GM(K00T,J)= TIV(I,KITE)
DM(K00T,J)= TIM(I,KITE)
GM(K00T,LCMAX +1-J)= TIV(I,JMAXH+J)
37 DM(K00T,LCMAX +1-J)= TIM(I,JMAXH+J)
D0 38 J=1,JMAX
GM(K00T,JMAXH+IMAX+J)= TSV(I,J)
38 DM(K00T,JMAXH+IMAX+J)= TSM(I,J)
D0 39 J=1,IMAX
GM(K00T,LCMAXH+JMAXH+J)= TBV(I,IMAX+1-J)
39 DM(K00T,LCMAXH+JMAXH+J)= TBM(I,IMAX+1-J)
36 CONTINUE
D0 40 I=1,JMAXH
K00T = JMAXH + IMAX + I
D0 41 J=1,JMAXH
KITE = JMAXH+1-J
GM(K00T,J) = SIV(I,KITE)
DM(K00T,J) = SIN(I,KITE)
DM(K00T,LCMAX+1-J)= SIM(I,JMAXH+J)
GM(K00T,LCMAX+1-J)= SIV(I,JMAXH+J)
41 CONTINUE
D0 42 J=1,IMAX
DM(K00T,JMAXH+LCMAXH+J)=STM(JMAX+1-I,IMAX+1-J)
GM(K00T,JMAXH+LCMAXH+J)=STV(JMAX+1-I,IMAX+1-J)
GM(K00T,JMAXH+J)= STV(I,J)
42 DM(K00T,JMAXH+J)= STM(I,J)
D0 43 J=1,JMAX
GM(K00T,JMAXH+IMAX+J) = SSV(I,J)
43 DM(K00T,JMAXH+IMAX+J) = SSM(I,J)
40 CONTINUE
RETURN
80 D0 84 I=1,IMAX
D0 84 J= 1,IMAX
84 GM(I,J) = TIV(I,J)
D0 71 I=1,IMAX
DM(I,I)= (0.5,0.0)
D0 72 J=1,JMAX
GM(I,IMAX+J) = TSV(I,J)
72 DM(I,IMAX+J) = TSM(I,J)

D0 71 J=1,IMAX
GM(I,JMAX + IMAX + J) = TBV(I,IMAX + 1 - J)
71 DM(I,JMAX + IMAX + J) = TBM(I,IMAX + 1 - J)
D0 73 I=1,JMAXH
K= IMAX + I
D0 74 J=1,IMAX
GM(K,J) = STV(I,J)
74 DM(K,J) = STM(I,J)
D0 75 J=1,JMAX
GM(K,IMAX + J) = SSV(I,J)
75 DM(K,IMAX + J) = SSM(I,J)
D0 73 J=1,IMAX
GM(K,JMAX+IMAX+J)= + STV(JMAX +1-I,IMAX + 1 -J)
73 DM(K,JMAX+IMAX+J)= + STM(JMAX +1-I,IMAX + 1 -J)
END

```

```

SUBROUTINE EXI(Z,ANS)
COMPLEX Z, ANS
COMPLEX ZZ, AANS
DIMENSION B(2), SUM(2)
EQUIVALENCE (ZZ,B), (AANS,SUM)
COMMON/SAVE/ISAVE,EXMZR,EXMZI
DIMENSION FACT(40)
DATA (ISTORE = 0), (PIGTWO = 1.5707963268)
IF(ISTORE .EQ. 1) GO TO 410
DO 320 N = 1, 40
FACT(N) = - FLOAT(N - 1) / FLOAT(N * N)
320 CONTINUE
ISTORE = 1
410 CONTINUE
K = 1
GAMMA = 0.5772156649
ZZ = Z
B1B1 = B(1) * B(1)
B2B2 = B(2) * B(2)
U = B1B1 + B2B2
IF(U.GT.100.0) GO TO 400
ISAVE = 0
IF(B1B1 .GT. B2B2) SU = B(1) + 0.5 * B2B2 / B(1)
IF(B1B1 .LE. B2B2) SU = ABS( B(2) + 0.5 * B1B1 / B(2) )
EN = 6.0 + 3.5 * SU
NN = EN
IF(NN .GT. 40) NN = 40
SUM(1) = -B(1) $ SUM(2) = -B(2)
TERMR = -B(1) $ TERMI = -B(2)
DO 300 N = 2, NN
X = (TERMR*B(1) - TERMI*B(2)) * FACT(N)
Y = (TERMR*B(2) + TERMI*B(1)) * FACT(N)
TERMR = X
TERMI = Y
SUM(1) = SUM(1) + TERMR
SUM(2) = SUM(2) + TERMI
300 CONTINUE
ELNRZ = 0.5 * ALOG(U)
IF(B(1) .NE. 0.0) ELNIZ = ATAN(B(2) / B(1))
IF(B(1) .EQ. 0.0) ELNIZ = SIGN(PIGTWO, B(2))
SUM(1) = -GAMMA - ELNRZ - SUM(1)
SUM(2) = -ELNIZ - SUM(2)
ANS = AANS
RETURN
400 CONTINUE
ISAVE = 1
ONEBU = 1.0 / U
SUM(1) = 1.0 $ SUM(2) = 0.0
TERMR = 1.0 $ TERMI = 0.0
EEMEE = 0.0
DO 310 N = 1, 4

```

```
SUBROUTINE EXI2(Z,ANS)
```

```
COMMON/SAVE/ISAVE,EXMZR,EXMZI/ICE/ICE,NDEXI
```

```
COMPLEX Z,ANS
```

```
COMPLEX ZZ, AANS
```

```
DIMENSION B(2), A(2)
```

```
EQUIVALENCE (ZZ,B), (AANS,A)
```

```
AANS = ANS
```

```
ZZ = Z
```

```
K = 1
```

```
TEST1 = REAL(ZZ)
```

```
TEST2 = AIMAG(ZZ)
```

```
IF(TEST1 .EQ. 0.0 .AND. TEST2 .EQ. 0.0) GO TO 1
```

```
IF(NDEXI .EQ. 0) CALL EXI(ZZ, AANS)
```

```
X = A(1)*B(1) - A(2)*B(2)
```

```
Y = A(1)*B(2) + A(2)*B(1)
```

```
IF(ISAVE .EQ. 1) GO TO 400
```

```
E = EXP(-B(1))
```

```
EXMZR = E * COS(B(2))
```

```
EXMZI = -E * SIN(B(2))
```

```
400 CONTINUE
```

```
A(1) = EXMZR - X
```

```
A(2) = EXMZI - Y
```

```
ANS = AANS
```

```
RETURN
```

```
1 A(1) = 1.0
```

```
A(2) = 0.0
```

```
ANS = AANS
```

```
RETURN
```

```
END
```

```
EMMEE = EMMEE + 1.0
```

```
FFF = EMMEE * ONE00
```

```
X = - FFF * (TERMR*B(1) + TERMI*B(2))
```

```
Y = FFF * (TERMR*B(2) - TERMI*B(1))
```

```
TERMR = X
```

```
TERMI = Y
```

```
SUM(1) = SUM(1) + TERMR
```

```
SUM(2) = SUM(2) + TERMI
```

```
310 CONTINUE
```

```
E = EXP(-B(1))
```

```
X = E * COS(B(2))
```

```
Y = -E * SIN(B(2))
```

```
EXMZR = X
```

```
EXMZI = Y
```

```
FACTR = (X * B(1) + Y * B(2)) * ONE00
```

```
FACTI = (Y * B(1) - X * B(2)) * ONE00
```

```
X = FACTR * SUM(1) - FACTI * SUM(2)
```

```
Y = FACTR * SUM(2) + FACTI * SUM(1)
```

```
SUM(1) = X
```

```
SUM(2) = Y
```

```
ANS = AANS
```

```
RETURN
```

```
END
```

HANISH, KING, BAIER, AND ROGERS

```

SUBROUTINE FARFLD(NPTS)
C THIS PROGRAM CALCULATES THE FAR FIELD PRESSURE DISTRIBUTION IN
C DB REFERENCED TO 0 DEGREES (RADIAL DIRECTION) FOR NPTS+1 EQUALLY
C SPACED ANGLES FROM 0 DEGREES TO 90 DEGREES (AXIAL DIRECTION).
COMMON/FFANGL/ FFUAN,FF90AN
DIMENSION PTOP(10),PINS(20),POUT(20),ANS(60)
COMMON/LC/LCMAX,LCMAXH/RAD/RIN,ROUT/ANS/ANS
COMMON/BLK1/H,A,FK,PI/DEL/DELR,DELZ/BLKA/PR,PLR,PZ,PLZ
COMMON/PIT/JMAX,JMAXH,IMAX/VEL/VEL/RRCC/RRCC/FFPR/FF0,FF90
TYPE COMPLEX FF1,FFT,FFT0,RHOC,ADDIT1,SUM1,FFVT,FFVS,BJI,BJOUT,CEP
1,CEM,PTOP,PINS,POUT,ANS,I,SUM,ADDIT,ARG1,VEL,PBOT,VINS,VOUT,VTOP,
2 VBOT
DIMENSION VEL(60),PBOT(10),VINS(20),VOUT(20),VTOP(10),VBOT(10)
DIMENSION PZ(20),PLZ(20),PR(20),PLR(20)
DATA(ALICE= 8.685889638)
IF (NPTS.EQ.1) GO TO 42
PRINT 43
43 FORMAT (//S4X28HFARFIELD PATTERN AT INFINITY//39X*0 DEGREES IS BRO
$ADSIDE. 90 DEGREES IS IN AXIAL DIRECTION,*/43X*ANGLE*12X*PRESSURE
$ IN DB*3X*PHASE ANGLE OF PRESSURE*/)
42 I = (0.,1.) $ RHOC = RRCC*I
DO = 1./((2.*NPTS) $ DELTH = DO*PI $ DELTHD = 180.*DO
NPI = NPTS-1 $ JMAXT = JMAXH
IF(HIN.EQ.0.) JMAXH = 0
DO 2 J=1,IMAX
PBOT(J) = ANS(LCMAX - JMAXH + 1 - J)
VBOT(J) = VEL(LCMAX - JMAXH + 1 - J)
VTOP(J) = VEL(JMAXH + J)
2 PTOP(J) = ANS(JMAXH+J)
DO 3 J=1,JMAXT
POUT(J) = ANS(IMAX+JMAXH+J)
VOUT(J) = VEL(IMAX+JMAXH+J)
VOUT(JMAX + 1 - J) = VEL( LCMAX + 1 - JMAXH - IMAX - J)
3 POUT(JMAX + 1 - J) = ANS( LCMAX + 1 - JMAXH - IMAX - J)
JMAXH = JMAXT
IF(RIN.EQ.0.) GO TO 966
DO 965 J=1,JMAXH
PINS(J) = ANS(JMAXH+1-J)
VINS(J) = VEL(JMAXH+1-J)
VINS(JMAX+1 - J) = VEL(LCMAX - JMAXH + J)
965 PINS(JMAX+1 - J) = ANS(LCMAX - JMAXH + J)
GO TO 970
966 DO 969 J=1,JMAX
VINS(J) = (0.0,0.0)
969 PINS(J) = (0.0,0.0)
970 FFI = .5*FK*DELZ
RR = FK*ROUT $ RI = FK*RIN
CALL HESL(RR,RS0,BJ0,Y0,Y1) $ CALL HESL(RI,RSI,BJI,Y1,Y0)
RS = RS0*ROUT $ SI = SSI*RIN
BJI = RIN*BJI $ BJOUT = ROUT*BJ0
BSI=RS0=0.
203 BJOUT = BJOUT + I*RS0 $ BJI = BJI + I*RSI
SUM = (0.0,0.0)
DO 37 K=1,JMAX
ADDIT = (BJOUT*POUT(K) - BJI*PINS(K))
ADDIT1= RHOC*(VINS(K)*BI + VOUT(K)*BR)
ADDIT = ADDIT - ADDIT1
37 SUM = SUM + ADDIT
FFI = FFI*SUM $ FFVT = (0.0,0.0)

```

NRL REPORT 7964

```

DO 38 K=1,IMAX
RL = PR(K) - .5*DELR $ RU = RL + DELR
TU = FK*RU $ TL = FK*RL
CALL BES1(TU,BU) $ CALL BES1(TL,BL)
38 FFVT = FFVT - (VTOP(K) + VBOT(K))*(RU*BU - RL*BL)
FF0 = CABS(FFI + FFVT*.5*RHO)
FF0AN = CANG(FFI + FFVT*.5*RHO)*180./PI
DEG = 0.0 $ FF0M = 0.0
IF(NPTS.GT.1) PRINT 33, DEG,FF0M,FF0AN
DO 1 J=1,NPTS
THEIA = J*DELTH
IF(J.EQ.NPTS) THEIA = 8999.*PI/18000.
COSTH = COS(THETA) $ SINTH = SIN(THETA)
ARGI = -I*FK*SINTH
TT = RI*COSTH
CALL BESL(TT,RS),BJ1,Y0,Y1
BI = RI*HSI
TT = RO*COSTH
CALL BESL(TT,RS2),BJ2,Y0,Y1
BJI = RI*BJ1 $ BJO1 = RO*BJ2 $ B0 = RO*BS2
BJO1 = BJO1*COSTH
BJI = BJI*COSTH
207 FFI = .5*I*(CEXP(ARGI*DELZ) - 1.)/SINTH
SUM = (0.0,0.0)
DO 4 K=1,JMAX
CEM = CEXP(ARGI*PLZ(K))
ADDIT = (RJO1*POUT(K) - BJI*PINS(K))*CEM
ADDIT1 = (VOUT(K)*B0 + VINS(K)*BI)*RHO*CEM
4 SUM = SUM + ADDIT -ADDIT1
FFI = FFI*SUM
SUM = (0.0,0.0)
FFTB = .5/COSTH
ARGI = I*FK*H*SINTH
CEM = CEXP(-ARGI)
CEP = CONJG(CEM)
DO 5 K=1,IMAX
RU = PR(K) + .5*DELR $ RL = PR(K) - .5*DELR
TT = FK*RU*COSTH $ TTL = FK*RL*COSTH
CALL BES1(TT,BU) $ CALL BES1(TTL,BL)
RUBL = RU*BU - RL*BL
ADDIT = -I*SINTH*(PBOT(K)*CEP - PTOP(K)*CEM)
ADDIT1 = RHO*(VTOP(K)*CEM + VBOT(K)*CEP)
5 SUM = SUM + (ADDIT - ADDIT1)*RUBL
FFTB = SUM*FFTB
FFM = CABS(FFI + FFTB)
FFAN = CANG(FFI + FFTB)*180./PI
IF(J.EQ.NPTS) FF0 = FFM
IF(J.EQ.NPTS) FF0AN = FFAN
DEG = J*DELTH
FFM = ALICE*LOGF(FFM/FF0)
IF (NPTS.EQ.1) GO TO 1
PRINT 33, DEG,FFM,FFAN
53 FORMAT (26X3F22.2)
1 CONTINUE
END

```

HANISH, KING, BAIER, AND ROGERS

```

FUNCTION FN(X)
DIMENSION AK(4),BK(4),AE(4),BE(4),A(4),B(4)
DIMENSION FA(4),FB(4),GA(4),GB(4)
DATA (FA=38.027264,265.187033,335.677320,38.102495)
DATA (FB=40.021433,322.624911,570.236280,157.105423)
DATA (GA = 42.242855,302.757865,352.018498,21.821899)
DATA (GB=48.196927,482.485984,1114.978885,449.690326)
DATA (F2=-.250000000),(F4=0.010416667),(F6=-.000231481)
DATA (F8=0.000003100),(F10=-.000000028),(F3=-.055555556)
DATA (F5=0.001666667),(F7=-.000028345),(F9=0.000000306),(F11=
1-.000000002)
DATA (AK= 0.09666344259,0.03590092383,0.03742563713,0.01451196212)
DATA (BK=0.12498593597,0.06880248576,0.03328355346,0.00441787012)
DATA (AE=0.44325141463,0.06260601220,0.04757383546,0.01736506451)
DATA (BE=0.24998368310,0.09200180037,0.04069967526,0.00526449639)
  ENTRY CI
  IFLAG = 1
  IF(X.LT.1.) GO TO 1
27 XX=XX*X
  FDEN = FB(4) + XX*(FB(3) + XX*(FB(2) + XX*(FB(1) + XX)))
  FNUM = FA(4) + XX*(FA(3) + XX*(FA(2) + XX*(FA(1) + XX)))
  F = FNUM/(X*FDEN)
  GNUM = GA(4) + XX*(GA(3) + XX*(GA(2) + XX*(GA(1) + XX)))
  GDEN = GB(4) + XX*(GB(3) + XX*(GB(2) + XX*(GB(1) + XX)))
  G = GNUM/(XX*GDEN)
  IF(IFLAG.EQ.0) GO TO 28
  FN = F*SIN(X) - G*COS(X)
  RETURN
1 XX = X*X
  CH = XX*(F2 + XX*(F4 + XX*(F6 + XX*(F8 + XX*(F10 )))))
  GAMMA = .577215664
  FN = GAMMA + LOGF(X) + CH
  RETURN
  ENTRY SI
  IFLAG = 0
  IF(X.LT.1.) GO TO 29
  GO TO 27
28 FN = - F*COS(X) - G*SIN(X)
  RETURN
29 XX = X*X
  PI = 3.1415926536
  SH = X*(1. + XX*(F5 + XX*(F5 + XX*(F7 + XX*(F9 + XX*(F11))))))
  FN = SH - .5*PI
  RETURN
  ENTRY ELLIPK
  HOLDA=1.38629436112 & HOLDB = 0.5
  DO 2 J=1,4
  A(J) = AK(J)
2 B(J) = BK(J)
  GO TO 4
  ENTRY ELLIPE
  HOLDA = 1.0
  HOLDB = 0.0
  DO 3 J=1,4
  A(J) = AE(J)
3 B(J) = BE(J)
4 Q = QM = 1. - X
  FACT = LOGF(1./Q)
  DO 11 J=1,4
  HOLDA = HOLDA + A(J)*Q
  HOLDB = HOLDB + B(J)*Q
11 Q = Q*QM
  FN = HOLDA + HOLDB*FACT
  END

```

NRL REPORT 7964

```

SUBROUTINE GGC
TYPE DOUBLE W,X
COMMON/BLK1/H,A,FK,PI/TNY/NQD1,LL,MM/BLK2/X1,WF
DIMENSION XI(32),WF(32),W(31),X(31)
DATA (PI = 3.14159265359)
DATA(X = 0.1488743389816310000, 0.4333953941292470000,
* 0.6794095682990240000,0.8650633666889850000,
* 0.9739065285171720000,
* 0.0765265211334973337550000,0.2277858511416450780800000,
* 0.3737060887154195606730000,0.5108670019508270980040000,
* 0.6360536807265150254530000,0.7463319064601507926140000,
* 0.8391169718222188233950000, 0.9122344282513259058660000,
* 0.963971927279137912680000,0.9931285991850949247860000,
* 0.997263861849481563540000, 0.985611511545268335400000,
* 0.964762255587506430770000, 0.934906075937739689170000,
* 0.896321155766052123960000, 0.849367613732569970130000,
* 0.794483795967942406960000, 0.732182118740289680380000,
* 0.663044266930215200970000, 0.587715757240762329040000,
* 0.506899908932229390020000, 0.421351276130635345360000,
* 0.331868602282127649770000, 0.239287362252137074540000,
* 0.144471961582796493480000, 0.483076656877383162340-001)
DATA(W= 0.2955242247147530000, 0.2692667193099960000,
* 0.2190863625159820000, 0.1494513491505810000,
* 0.0666713443086880000,
* 0.1527533871307258506980000,0.1491729864726037467880000,
* 0.1420961093183820513290000,0.1316886384491766268980000,
* 0.1181945319615184173120000, 0.1019301198172404350370000,
* 0.0832767415767047487250000,0.062672048334109063570000,
* 0.0400014298003869413310000, 0.0176140071391521163120000,
* 0.70186100094700960040-002, 0.162743947309056700050-001,
* 0.253920053092620594550-001, 0.342738629130214331020-001,
* 0.428358980222266806560-001, 0.509980592623761762960-001,
* 0.586840934785355471450-001, 0.658222227763618468370-001,
* 0.723457941088485062250-001, 0.781938957870703064710-001,
* 0.833119242269467552220-001, 0.876520930044038111420-001,
* 0.911736786957638847120-001, 0.938443990808045656390-001,
* 0.956387200792748594190-001, 0.965400685147278005660-001)
PFK = 0.5 * FK
NRL = NQD1/2 $ NBL = 0
IF(NQD1.EQ.20) NBL = 5
IF(NQD1.EQ.32) NBL = 15
DO 111 I=1,NBL
K = I + NBL
XI(I) = X(K) * PFK
WF(I) = W(K)
XI(I + NBL) = - X(K) * PFK
111 WF(I + NBL) = W(K)
RETURN
ENTRY TIME
TIMER = TIMELEFT(K)
PRINT 1, TIMER
1 FORMAT(* TIME LEFT *F10.3* SECONDS*//)
RETURN
END

```

09000200
00000500
00000700
00000800
00000900
00001000
00001100
00001200
00001300
00001400
00001500
00001600
00001700
00001800
00001900
00002000
00002100
00002400

HANISH, KING, BAIER, AND ROGERS

```

SUBROUTINE MOS(VA,STR,RD,NF,NPTS,VVV,ANS)
C THIS SUBROUTINE OBTAINS THE COEFFICIENTS OF VELOCITY EXPANSION ANS
C IN TERMS OF MODAL SHAPES.
TYPE COMPLEX ANS,STR,VA,VVV
DIMENSION ANS(11),RD(9,10),STR(11,1),VA(11,1),VVV(11)
PI = 3.141592654
NN = NF + 1
K = 0
N3 = NPTS/NF
DO 300 J = 1,NPTS,N3
K = K + 1
IF (K,GT,NF) GO TO 301
VA(K,NN) = -VVV(J)
DO 300 I = 1,NF
300 VA(K,I) = RD(I,J)
301 CALL SIMEX(VA,11,STR,NF,ANS)
END

```

```

SUBROUTINE MINC(A,N,ND,D,L,M)
TYPE COMPLEX A,D,BIGA,BIGAI,HOLD,B
EQUIVALENCE(B,C)
DIMENSION C(2),C1(2)
EQUIVALENCE(BIGA,C1)
DIMENSION A( ND,1),L(1),M(1)
D= (1.0,0.0)
NK = -N
DO 80 K=1,N
NK = NK+N
L(K) = K
M(K) = K
KK = NK+K
BIGA = A(KK)
BIGC = ABS(C1(1))
IF(ABS(C1(2)).GT.BIGC) BIGC = ABS(C1(2) )
DO 20 J=K,N
IZ = N*(J-1)
DO 20 I=K,N
IJ = IZ + I
B = A(IJ)
IF(BIGC-ABS(C(1))) 101,102,102
101 BIGC = ABS(C(1))
GO TO 15
102 IF(BIGC-ABS(C(2))) 103,20,20
103 BIGC = ABS(C(2))
15 BIGA = A(IJ)
L(K) = I
M(K) = J
20 CONTINUE
500 CONTINUE
BIGAI = (1.0,0.0)/BIGA
J=L(K)
IF(J=K) 35,35,25
25 KI = K-N
DO 30 I=1,N
KI = KI+N
HOLD = -A(KI)
JI = KI -K+J
A(KI)=A(JI)
30 A(JI) = HOLD
35 I=M(K)
IF(I=K) 45,45,38
38 JP= N*(I-1)
DO 40 J=1,N
JK = NK+J
JI = JP+J
HOLD = -A(JK)
A(JK) = A(JI)
40 A(JI) = HOLD
45 IF(C1(1).EQ.0..AND.C1(2).EQ.0.)46,48

```

HANISH, KING, BAIER, AND ROGERS

```

46 D= 0.0
   PRINT 222,D
222 FORMAT (/5X*DETERMINANT OF MATRIX BEING SOLVED BY MINC IS*F6.2)
   STOP
48 DO 55 I=1,N
   IF(I-K) 50,55,50
50 IK = NK + I
   A(IK) = -BIGAI*A(IK)
55 CONTINUE
   DO 65 I=1,N
   IK = NK+1
   HOLD = A(IK)
   IJ = I-N
   DO 65 J=1,N
   IJ = IJ+N
   IF(I,EQ,K,OR,J,EQ,K) GO TO 65
62 KJ = IJ -I +K
   A(IJ) = HOLD*A(KJ) + A(IJ)
65 CONTINUE
   KJ = K-N
   DO 75 J=1,N
   KJ = KJ + N
   IF(J-K) 70,75,70
70 A(KJ) = BIGAI*A(KJ)
75 CONTINUE
   D = D*BIGA
   A(KK) = BIGAI
80 CONTINUE
   K = N
100 K = K-1
   IF(K) 150,150,105
105 I= L(K)
   IF(I-K) 120,120,108
108 JQ = N*(K-1)
   JR = N*(I-1)
   DO 110 J=1,N
   JK = JQ+J
   HOLD = A(JK)
   JI = JR+J
   A(JK) = -A(JI)
110 A(JI) = HOLD
120 J=M(K)
   IF(J-K) 100,100,125
125 KI = K-N
   DO 130 I=1,N
   KI = KI +N
   HOLD = A(KI)
   JI = KI-K+J
   A(KI) = -A(JI)
130 A(JI)=HOLD
   GO TO 100

150 RETURN
   END

```

NRL REPORT 7964

```

SUBROUTINE MLT(XA,YA,XB,YB,XC,YC)
XC=XA*XB-YA*YB
YC=XA*YB+YA*XB
END

```

```

SUBROUTINE PSUBV(V,XR,XI,DR,DI)
EPS=5.0E-11
K9=K10=0
HOLDR=HOLDI=1.0E307
CALL MLT(XR,XI,XR,XI,XSR,XSI)
AK=0.0
FVS=4.0*V*V
AR=FORPVR=1.0
AI=FORPVI=0.0
C BEGIN ITERATION WITH AK=1
3 AK=AK+1.0
FACN=(FVS-(4.0*AK-1.0)**2)*(FVS-(4.0*AK-3.0)**2)
FACDR=-2.0*AK*(2.0*AK-1.0)*64.0
FACDI=FACDR*XSI
FACDR=FACDR*XSR
BR=AR*FACN
BI=AI*FACN
CALL DVD(BR,BI,FACDR,FACDI,AR,AI)
IF(K9)7,2,7
2 DR=AR+FORPVR
IF(DR.EQ.0.0.OR.ABS(AR/DR).LT.EPS)GO TO 11
IF(ABS(AR).LE.HOLDR)GO TO 6
DR=FORPVR
11 K9=1
GO TO 7
6 FORPVR=DR
HOLDR=ABS(AR)
7 IF(K10)10,8,10
8 DI=AI+FORPVI
IF(DI.EQ.0.0.OR.ABS(AI/DI).LT.EPS)GO TO 12
IF(ABS(AI).LE.HOLDI)GO TO 9
DI=FORPVI
12 K10=1
GO TO 10
9 FORPVI=DI
HOLDI=ABS(AI)
10 IF(K9.EQ.1.AND.K10.EQ.1)RETURN
GO TO 3
END

```

HANISH, KING, BAIER, AND ROGERS

```

SUBROUTINE QSUBV(V,XR,XI,ER,EI)
EPS=5.0E-11
K9=K10=0
HOLDR=HOLDI=1.0E307
CALL MLT(XR,XI,XR,XI,XSR,XSI)
AK=1.0
FVS=4.0*V*V
UPR=FVS-1.0
UPI=0.0
DER=8.0*XR
DEI=8.0*X1
CALL DVD(UPR,UPI,DER,DEI,AR,AI)
FORQVR=AR
FORQVI=AI
C BEGIN ITERATION WITH AK=2 BECAUSE FIRST TERM IS NOT SAME AS FACTOR
3 AK=AK+1.0
FACN=(FVS-(4.0*AK-3.0)**2)*(FVS-(4.0*AK-5.0)**2)
FACDR=-(2.0*AK-1.0)*(2.0*AK-2.0)*64.0
FACDI=FACDR*XSI
FACDR=FACDR*XSR
BR=AR*FACN
BI=AI*FACN
CALL DVD(BR,BI,FACDR,FACDI,AR,AI)
IF(K9)7,2,7
2 ER=AR+FORQVR
IF(ER.EQ.0.0.OR.ABS(AR/ER).LT.EPS)GO TO 11
IF(ABS(AR).LE.HOLDR)GO TO 6
ER=FORQVR
11 K9=1
GO TO 7
6 FORQVR=ER
HOLDR=ABS(AR)
7 IF(K10)10,8,10
8 EI=AI+FORQVI
IF(EI.EQ.0.0.OR.ABS(AI/EI).LT.EPS)GO TO 12
IF(ABS(AI).LE.HOLDI)GO TO 9
EI=FORQVI
12 K10=1
GO TO 10
9 FORQVI=EI
HOLDI=ABS(AI)
10 IF(K9.EQ.1.AND.K10.EQ.1)RETURN
GO TO 3
END

```

```

SUBROUTINE SHIP
C THIS SUBROUTINE OBTAINS THE TRUE SURFACE RADIATION GREENS FUNCTION G(,).
DIMENSION G(30,30)
COMMON/VNM/VNM
TYPE COMPLEX G,PA
TYPE COMPLEX V,SUMJ,RHOC,ANS,VEL,DM,GM,VEL1,ANS1,ANS2
DIMENSION REST(4200),ANS(60),V(30),VEL(60),GM(30,60),DM(60,60)
1,VEL1(30),PZ(20),PLZ(20),PR(20),PLR(20),ANS1(30),ANS2(30),AREA(60)
COMMON/RRCC/RRCC
COMMON/LC/LCMAX,LCMAXH/BLKA/PR,PLR,PZ,PLZ/RCC/JTOP
COMMON/TOY/NQD1,ISYM,NQD3/PIT/JMAX,JMAXH,IMAX
COMMON/BLK1/H,A,FK,PI/DEL/DELR,DELZ
COMMON/PA/PA,RHOCA
COMMON/RAD/RIN,ROUT/MX0/JMXT,MX0/5/DM/ANS/ANS/VELO/VEL
COMMON/6/GM,G,REST/TIDY/FAST/EPS/EPS/EPS1/EPS1/JOE/JTOP1
COMMON/AREA/AREA/NOPR/NOPR/PQR/PQR
DATA(NQD1 = 32),(PI = 3.14159265359),(EPS = 0.001),(EPS1 = 0.0001)
DATA(JTOP1 = 10),(JTOP = 10)
ISYM = 1
LCMAXH = JMAXH + JMAXH + IMAX $ LCMAX = LCMAXH + LCMAXH
JMAX = JMAXH + JMAXH
A = .5*(RIN+ROUT)
FAST = PI * NQD1 / (8.0 * FK * (ROUT + PI * H))
CALL GQC
CALL ERING
RHOC = FK*RRCC*(0.,-1.)
DO 14 J=1,LCMAXH
11 ANS1(J)= ANS2(J) = (0.0,0.0)
DO 14 I=1,LCMAXH
DM(I,J) = DM(I,J) + DM(I, LCMAX + 1 -J)
GM(I,J) = GM(I,J) + GM(I, LCMAX + 1 -J)
GM(I,J) = RHOC*GM(I,J)
14 CONTINUE
CALL CINV(DM,LCMAXH,60)
DO 246 I=1,LCMAXH
DO 246 J=1,LCMAXH
G(I,J) = (0.0,0.0)
DO 7 K=1,LCMAXH
7 G(I,J) = G(I,J) + DM(I,K)*GM(K,J)
246 CONTINUE
RETURN
ENTRY FIELD
DO 746 J=1,LCMAXH
VEL(LCMAX+1-J) = VEL(J)
ANS(J) = (0.0,0.0)
DO 10 K=1,LCMAXH
10 ANS(J) = ANS(J) + G(J,K)*VEL(K)
746 ANS(LCMAX+1-J) = ANS(J)
DO 537 J=1,JMAXH
AREA(J) = DELZ*RIN
537 AREA(JMAXH+IMAX+J) = DELZ*ROUT
DO 538 J=1,IMAX
538 AREA(JMAXH+J)= PR(J)*DELR
DO 539 J=1,LCMAXH
539 AREA(LCMAX + 1 - J) = AREA(J)
SUMJ = (0.0,0.0)
DO 401 J=1,LCMAX
SUMJ= SUMJ + ANS(J)*AREA(J)*CONJG(VEL(J))
401 CONTINUE
AREAT = A*( H + H + ROUT - RIN)
AREAT = AREAT + AREAT
PA = SUMJ*2.*PI
RHOCA = AREAT*2.*PI*RRCC
SUMJ = (0.,0.)
DO 402 I = 1,LCMAX
402 SUMJ = SUMJ + ABS(VEL(I))*2*AREA(I)
VNM = SUMJ/AREAT
END

```

HANISH, KING, BAIER, AND ROGERS

```

SUBROUTINE SIMCX(ORIG,NN,MAT,MCT,ANS)
C THIS SUBROUTINE SOLVES SIMULTANEOUS EQUATIONS REPRESENTED BY AUGMENTED
C MATRIX ORIG(,) WHOSE AUGMENTED COLUMN IS MINUS THE RIGHT HAND SIDE OF THE
C SIMULTANEOUS EQUATIONS.
TYPE COMPLEX MAT,ORIG,ANS,B0,B2,B4,B6,B8,B10,B11,B13,B15,CC,CC2,B500002300
1,SUM 00002400
EQUIVALENCE(B2,C),(CC,CX),(CC2,CX2) 00002500
DIMENSION MAT(MCT,1),ORIG(NN,1),ANS(MCT),C(2),CX(2),CX2(2) 00002600
15 FORMAT(25H THIS MATRIX IS SINGULAR/) 00002800
B11=(1.0,0.0) 00003800
MT=MCT+1 00004000
C PUT ORIGINAL MATRIX INTO MAT 00004200
NCT = ICT = M1
DO 2 J=1,ICT 00004400
DO 2 I=1,MCT 00004500
MAT(I,J)=ORIG(I,J) 00004600
2 CONTINUE 00004700
JCT=MCT-1
DO 3 J=1,JCT 00005900
KK=J+1 00006000
JV=J
CC=MAT(J,J) 00009500
IF(CX(1).EQ.0.0.AND.CX(2).EQ.0.0)11,12 00009600
11 IF(JV.EQ.MCT)13,14
13 PRINT15 00009800
RETURN 00009900
14 JV=JV+1 00010000
CC2=MAT(JV,J) 00010100
IF(CX2(1).EQ.0.0.AND.CX2(2).EQ.0.0)11,16 00010200
16 DO 17 JJ=J,JJ 00010300
B6=MAT(J,JJ) 00010400
MAT(J,JJ)=MAT(JV,JJ) 00010500
17 MAT(JV,JJ)=B6 00010600
B11=-B11 00010700
12 JSING=JSING-1 00010800
DO 4 K=KK,MCT
B8=MAT(K,J)/MAT(J,J) 00006300
DO 5 L=J,NCT 00006400
B10=B8*MAT(J,L) 00006500
5 MAT(K,L)=MAT(K,L)-B10 00006600
4 CONTINUE 00006700
C VALUE OF DETERMINANT 00006800
3 B11=B11*MAT(J,J) 00006900
B11=B11*MAT(MCT,MCT) 00007000
LOW=-MCT 00007100
MO=-1 00007110
C TO DO ONE OR MORE BACK SOLUTIONS 00007200
DO 6 MINC=MT,NCT 00007300
JFIN=MCTS IX=0 00007400
C BACK SOLUTION 00007500
DO 6 INM=LOW,MO 00007600
M=IABS(INM) 00007700
B0=-MAT(M,MINC) 00007800
B2=MAT(M,M) 00007900
B4=(0.0,0.0) 00008000
IF(IX) 7,22,7 00008100
22 IX=IX+1 00008200
GO TO 8 00008300
7 M02=-JFIN 00008400
DO 9 INN=LOW,M02 00008500
N=IABS(INN) 00008600
9 B4=B4+MAT(M,N)*MAT(N,MINC) 00008700
B0=B0-B4 00008800
JFIN=JFIN-1 00008810
8 IF(C(1).EQ.0.0.AND.C(2).EQ.0.0)13,29 00008900
29 MAT(M,MINC)=ANS(M)=B0/B2 00009000
6 CONTINUE 00009100
RETURN 00012900
END 00014900

```

NRL REPORT 7964

```

SUBROUTINE SOLVE(MCT,MAT,DET,RR,RATIO)
THIS SUBROUTINE OBTAINS THE DETERMINANT DET OF MATRIX MAT. IT ALSO
CALCULATES COEFFICIENT RATIOS RR AND RATIO().
DIMENSION MAT(4,4),RATIO(3)
TYPE REAL MAT
JCT = MCT - 2
DO 4 J=1,JCT
  KK=J+1
  IF (MAT(J,J).EQ.0.) 11,12
11 PRINT 50,J,J,MAT(J,J)
50 FORMAT (//10X4HMAT(I1,1H,I1,3H) =E14.6 ,2X7HTR0UBLE)
  STOP
12 DO 4 K = KK,MCT
  BB=MAT(K,J)/MAT(J,J)
  DO 4 L=J,MCT
  B10=BB*MAT(J,L)
  MAT(K,L)=MAT(K,L)-B10
4 CONTINUE
DET = MAT(1,1)*MAT(2,2)*(MAT(3,3)*MAT(4,4)-MAT(4,3)*MAT(3,4))
RR = -MAT(4,4)/MAT(4,3)
RATIO(3) = -MAT(3,4)/MAT(3,3)
RATIO(2) = -(MAT(2,3)*RATIO(3) + MAT(2,4))/MAT(2,2)
RATIO(1) = -(MAT(1,2)*RATIO(2) + MAT(1,3)*RATIO(3) + MAT(1,4))
S/MAT(1,1)
RETURN
END

```

170

200

220

```

SUBROUTINE SRT(XA,YA,XC,YC)
SS=SQRT(XA*XA+YA*YA)
XC=SQRT(ABS((SS+XA)/2.0))
IF(XA)1,2,1
2 YC=-XC
RETURN
1 YC=YA/(2.0*XC)
END

```

HANISH, KING, BAIER, AND ROGERS

```

SUBROUTINE THFREQ
C THIS SUBROUTINE OBTAINS THICKNESS CORRECTION FACTORS F1 AND F0. IT ALSO
C CALCULATES SCALED DISPLACEMENTS ALONG THE THICKNESS OF THE SHELL IN BOTH
C RADIAL AND AXIAL DIRECTIONS.
TYPE REAL IM,IJO,IJ1,IY0,IY1
COMMON /BLK/R,IM,RJO,IJU,RJ1,IJ1,RY0,IY0,RY1,IY1
COMMON /RAD/B,A/BLK1/H,AZ,FK,PI/YMD/Y,NU,RHO,NDS/FUD/F1,F0
COMMON /FRK/FR
TYPE REAL KAPPA,LAMBDA,NU,LTH
DIMENSION C(4,4),RATIO(3),FR(2),DETR(2),XMAG(15)
COMMON/AA/OMBRSQ,AB,ALPHA,BETA,DD,TT,C1SQ,RATIO
NIT = 30
PI2 = PI/2
LTH = H*H
PRINT 51
51 FORMAT (1H140X*CALCULATION OF THICKNESS CORRECTION FACTORS*)
PRINT 1,A,B,LTH,RHO,NU,Y
1 FORMAT (//56X*INPUT PARAMETERS*//29X*OUTER RADIUS*
$38X6HROUT =E14.6/
$29X*INNER RADIUS*39X5HRIN =E14.6/
$29X12HAXIAL LENGTH39X5HLTH = E14.6/
$29X7HDENSITY44X5HRHO =E14.6/
$29X14HPOISSONS RATIO38X4HNU =E14.6/
$29X45HYOUNGS MODULUS AT CONSTANT MAGNETIC INDUCTION 8X3HY =E14.6)
C
C CALCULATE BOUNDARY CONDITION MATRIX C(.). OBTAIN BESSEL FUNCTIONS FROM
C SUBROUTINE COMPHES.
C
KAPPA = PI/SQRTF(12.)
LAMBDA = Y*NU/((1.+NU)*(1.-NU-NU))
G = Y/(2.+NU+NU)
OMBRSQ = PI*PI*(LAMBDA+G+G)/(4.*H*H*RHO)
C1SQ = (LAMBDA+G+G)/RHO
C2SQ = G/RHO
C3SQ = 4.*G*(LAMBDA+G)/(RHO*(LAMBDA+G+G))
ALPHA = C1SQ/C3SQ
BETA = C2SQ/C3SQ
INX = 1
IT = 0
FREQ = FR(1)
PRINT 52
52 FORMAT (//51X*INITIAL FREQUENCY INTERVAL*//)
42 CONTINUE
22 OMSQ = (2.*PI*FREQ)**2
R0 = OMSQ/OMBRSQ
AR = ALPHA + BETA
PSI = SQRTF((AR*R0-1.)**2 + 4.*ALPHA*BETA*R0*(1.-R0))
DD = 1.5*(KAPPA/H)**2/BETA
D1SQ = DD*(AR*R0-1.+PSI)
D1 = SQRTF(D1SQ)
D2SQ = DD*(PSI+1.-AR*R0)

```

NRL REPORT 7964

```

D2 = SQRT(D2SQ)
TT = H*(LAMBDA+2.*G)/(KAPPA*LAMBDA)
SIG1 = TT*(D1SQ+0MSQ/C1SQ)
SIG2 = -TT*(D2SQ+0MSQ/C1SQ)
XSI = D2/D1
GA = D1*A
Z = B/A
ETA = 0MSQ/(2.*C1SQ*D1SQ)
TA = ALPHA*ETA*GA/BETA
TC = TA*Z
R = GA
IM = 0.
CALL COMPBES
C(1,1) = RJ1 - TA*RJ0
C(1,3) = RY1 - TA*RY0
C(3,1) = RJ1
C(3,3) = RY1
R = 0.
IM = XSI*GA
CALL COMPBES
C(1,2) = -XSI*IJ1 - TA*RJ0
C(1,4) = XSI*PI2*IY1 + TA*PI2*RY0
C(3,2) = -SIG2/SIG1*XSI*IJ1
C(3,4) = SIG2/SIG1*XSI*PI2*IY1
R = Z*GA
IM = 0.
CALL COMPBES
C(2,1) = RJ1 - TC*RJ0
C(2,3) = RY1 - TC*RY0
C(4,1) = RJ1
C(4,3) = RY1
R = 0.
IM = Z*XSI*GA
CALL COMPBES
C(2,2) = -XSI*IJ1 - TC*RJ0
C(2,4) = XSI*PI2*IY1 + TC*PI2*RY0
C(4,2) = -SIG2/SIG1*XSI*IJ1
C(4,4) = SIG2/SIG1*XSI*PI2*IY1
C
C OBTAIN DETERMINANT DAT, COEFFICIENT RATIOS RATIO(), AND COEFFICIENT
C RATIO RR FROM SUBROUTINE SOLVE.
C
C CALL SOLVE (4,C,DAT,RR,RATIO)
C
C PRINT INITIAL FREQUENCY INTERVAL.
C
C IF (INX.LE.2) PRINT 18,FREQ,DAT
18 FORMAT (37X11HFREQUENCY =E12.4,5X13HDETERMINANT =E12.4//)
C
C PERFORM INTERVAL HALVING.
C

```

HANISH, KING, BAIER, AND ROGERS

```

      IF (INX.GE.3) GO TO 41
      DETR(INX) = DAT
      IF (INX.NE.2) GO TO 46
      IF (DAT*DETR(1).LT.0) GO TO 46
      PRINT 55
55  FORMAT (//10X*INITIAL FREQUENCIES NOT VALID*//)
      STOP
46  INX = INX + 1
      IF (INX.GE.3) GO TO 44
      FREQ = FR(INX)
      GO TO 42
41  CONTINUE
      IF (IT.GE.NIT) GO TO 43
      IT = IT + 1
      IF (DAT*DETR(1).GT.0) GO TO 45
      DETR(2) = DAT
      FR(2) = FREQ
      GO TO 44
45  DETR(1) = DAT
      FR(1) = FREQ
44  FREQ = .5*(FR(1)+FR(2))
      GO TO 42

C
C   PRINT RESONANT FREQUENCY, DETERMINANT, AND RATIOS FOR CHECKING VALIDITY
C   OF RESONANT FREQUENCY.
C
43  PRINT 53
53  FORMAT (//55X*RESONANT FREQUENCY*//)
      PRINT 18,FREQ,DAT
      PRINT 30,RATIO(3),RR
30  FORMAT (/6X*CONVERGENCE CHECK*//5X4HR1 =E16.6/5X4HR2 =E16.6)

C
C   CALCULATE AND PRINT SCALED DISPLACEMENTS IN RADIAL AND AXIAL
C   DIRECTIONS VR AND VZ.
C
      BR = (A-B)/10.
      AW = B - BR
      PRINT 9
9  FORMAT (//29X*SCALED DISPLACEMENTS ALONG THICKNESS FROM INNER RADI
1US TO OUTER RADIUS*//36X*POSITION*10X*RADIAL DISPLACEMENT*6X
2*AXIAL DISPLACEMENT*//)
      DO 7 I = 1,11
      AR = AR + BR
      R = D1*AR
      IM = 0.
      CALL COMPHES
      VR = -RATIO(1)*D1*RJ1 - RATIO(3)*D1*RY1
      VZ = RATIO(1)*SIG1*RJU + RATIO(3)*SIG1*RYO
      R = 0.
      IM = D2*AW
      CALL COMPHES

```

NRL REPORT 7964

```
VR = VR + RATIO(2)*D2*IJ1 - D2*PI2*IY1  
VZ = VZ + RATIO(2)*SIG2*PJ0 - SIG2*PI2*RY0  
XMAG(I) = VR  
7 PRINT 8,AR,VR,VZ  
8 FORMAT (21X3(8XE16.4))
```

C
C
C

CALCULATE AND PRINT THICKNESS CORRECTION FACTORS FI AND FO.

```
FI = XMAG(1)/XMAG(6)  
FO = XMAG(11)/XMAG(6)  
PRINT 91,FI,FO  
91 FORMAT (//50X*THICKNESS CORRECTION FACTORS*//42X4HF1 =E16.6,  
*5X4HF2 =E16.6)  
21 RETURN  
END
```

Appendix B

COMPUTER LISTING OF DTRMNT AND A SAMPLE INPUT AND OUTPUT

The program DTRMNT is listed on the next page, and a sample output follows on the subsequent pages. The sample input is

```
.06587      .00685      .09055      8400.      .3          1.26E11
  0  900    10
 905 1040    5
1060 6000   20
```

Note the inclusion of the Fortran statement $FREQ = IFR \times 10$ in the program listing. A listing of subroutine CUBIC appears in Appendix A.

The input and resultant output used to describe the use of program EIGSHIP in this appendix and in Appendixes C and D is that of ring C. An examination of the output yields five potentially valid intervals:

9200 to 9250 Hz,
9950 to 10,000 Hz,
21,400 to 21,600 Hz,
23,400 to 23,600 Hz,
48,600 to 48,800Hz.

Four of these frequency intervals have been identified by examining the real part of the determinant. The frequency interval 9950 to 10,000 Hz was identified by examining the imaginary part of the determinant.

NRL REPORT 7964

```

PROGRAM DETRMNT
DIMENSION B(3,3),EN(3),RT(3)
TYPE REAL LTH,NU
TYPE COMPLEX B,CHK,D,DTRMNT,EN,EPM,EPP,RT,SRT,TM,RTR
READ 63,RMEAN,THK,LTH,RHO,NU,Y
63 FORMAT (6E10.5)
PI = 3.141592654
A = RMEAN
PRINT 20,A,THK,LTH,RHO,NU,Y
20 FORMAT (1H155*INPUT PARAMETERS*//29X11HMEAN RADIUS38X
$7HRMEAN =E14.6/
$29X16HRADIAL THICKNESS35X5HTHK =E14.6/
$29X12HAXIAL LENGTH39X5HSLTH = E14.6/
$29X7HODENSITY44X5HRO =E14.6/
$29X14HPOISSONS RATIO38X4HNU =E14.6/
$29X45HYOUNGS MODULUS AT CONSTANT MAGNETIC INDUCTION 8X3HY =E14.6)
PRINT 5056
5056 FORMAT (//)
88 CONTINUE
READ 9,K1,K2,K3
9 FORMAT (3I5)
IF (EOF,60)87,89
89 CONTINUE
INX = 1
IT = 0
42 CONTINUE
DO 666 IFR = K1,K2,K3
FREQ = IFR
FREQ = IFR*10.
DELTA = RHO*A*A*(1.-NU**2)*FREQ**2/Y*4.*PI*PI
BETA = THK**2/(12.*A*A)
A2 = DELTA + 2.*NU
A1 = (1.-DELTA-NU*NU)/BETA + 1.
A0 = (DELTA-DELTA**2)/BETA + DELTA
CALL CUBIC(A2,A1,A0,RT)
DO 1 I = 1,3
SRT = CSQRT(RT(I))
EN(I) = (RT(I)+DELTA)/(NU*SRT-BETA*SRT*RT(I))
D = SRT/A
EPP = CEXP(LTH/2,*D)
EPM = (1.,0.)/EPP
TM = BETA*EN(I)*RT(I)/A-NU/A*EN(I) + D
B(1,I) = (EPP + EPM)*TM
TM = EN(I)*D*D+D/A
B(2,I) = (EPP + EPM)*TM
TM = EN(I)*D**3+D*D/A
1 B(3,I) = (EPP - EPM)*TM
DTRMNT = B(1)*B(5)*B(9) + B(4)*B(8)*B(3) + B(7)*B(2)*B(6) -
$B(3)*B(5)*B(7) - B(6)*B(8)*B(1) - B(9)*B(2)*B(4)

666 PRINT 100,FREQ,DTRMNT
100 FORMAT (31X11HFREQUENCY =E12.4,5X13HDETERMINANT =C(E12.4,E12.4))
GO TO 88
87 STOP
END

```

HANISH, KING, BAIER, AND ROGERS

INPUT PARAMETERS

| | |
|---|----------------------|
| MEAN RADIUS | RMEAN = 6,587000-002 |
| RADIAL THICKNESS | TKK = 6,850000-003 |
| AXIAL LENGTH | LTM = 9,095000-002 |
| DENSITY | RHO = 8,400000-003 |
| POISSONS RATIO | NU = 3,800000-001 |
| YOUNGS MODULUS AT CONSTANT MAGNETIC INDUCTION | Y = 1,240000+011 |

| | | |
|------------------------|--------------------------|-------------|
| FREQUENCY = 0,0000+000 | DETERMINANT = 1,8190+011 | 1,8554+000 |
| FREQUENCY = 1,0000+002 | DETERMINANT = 7,5380+013 | -1,2976+003 |
| FREQUENCY = 2,0000+002 | DETERMINANT = 1,5038+014 | 3,5721+002 |
| FREQUENCY = 3,0000+002 | DETERMINANT = 2,2343+014 | 2,2881+003 |
| FREQUENCY = 4,0000+002 | DETERMINANT = 2,9976+014 | 4,9736+001 |
| FREQUENCY = 5,0000+002 | DETERMINANT = 3,7338+014 | -1,1480+003 |
| FREQUENCY = 6,0000+002 | DETERMINANT = 4,4613+014 | 4,2514+003 |
| FREQUENCY = 7,0000+002 | DETERMINANT = 5,1784+014 | -1,2886+003 |
| FREQUENCY = 8,0000+002 | DETERMINANT = 5,8834+014 | -1,1514+004 |
| FREQUENCY = 9,0000+002 | DETERMINANT = 6,5747+014 | 6,0493+003 |
| FREQUENCY = 1,0000+003 | DETERMINANT = 7,2507+014 | -4,8731+003 |
| FREQUENCY = 1,1000+003 | DETERMINANT = 7,9099+014 | 1,6930+003 |
| FREQUENCY = 1,2000+003 | DETERMINANT = 8,5507+014 | -8,5603+003 |
| FREQUENCY = 1,3000+003 | DETERMINANT = 9,1719+014 | -1,0823+003 |
| FREQUENCY = 1,4000+003 | DETERMINANT = 9,7718+014 | -9,0518+003 |
| FREQUENCY = 1,5000+003 | DETERMINANT = 1,0349+015 | -5,3950+003 |
| FREQUENCY = 1,6000+003 | DETERMINANT = 1,0903+015 | 3,8324+003 |
| FREQUENCY = 1,7000+003 | DETERMINANT = 1,1432+015 | -1,4438+004 |
| FREQUENCY = 1,8000+003 | DETERMINANT = 1,1935+015 | -3,4365+003 |
| FREQUENCY = 1,9000+003 | DETERMINANT = 1,2411+015 | -1,7965+003 |
| FREQUENCY = 2,0000+003 | DETERMINANT = 1,2859+015 | -2,0488+004 |
| FREQUENCY = 2,1000+003 | DETERMINANT = 1,3278+015 | -1,1492+003 |
| FREQUENCY = 2,2000+003 | DETERMINANT = 1,3667+015 | -1,2546+004 |
| FREQUENCY = 2,3000+003 | DETERMINANT = 1,4026+015 | -3,8052+003 |
| FREQUENCY = 2,4000+003 | DETERMINANT = 1,4354+015 | -2,0513+004 |
| FREQUENCY = 2,5000+003 | DETERMINANT = 1,4650+015 | -5,0780+003 |
| FREQUENCY = 2,6000+003 | DETERMINANT = 1,4915+015 | 9,3800+002 |
| FREQUENCY = 2,7000+003 | DETERMINANT = 1,5147+015 | -1,8475+003 |
| FREQUENCY = 2,8000+003 | DETERMINANT = 1,5347+015 | -1,4500+003 |
| FREQUENCY = 2,9000+003 | DETERMINANT = 1,5514+015 | 1,7500+002 |
| FREQUENCY = 3,0000+003 | DETERMINANT = 1,5648+015 | -1,1186+004 |
| FREQUENCY = 3,1000+003 | DETERMINANT = 1,5749+015 | 7,5570+003 |
| FREQUENCY = 3,2000+003 | DETERMINANT = 1,5818+015 | 2,1360+004 |
| FREQUENCY = 3,3000+003 | DETERMINANT = 1,5855+015 | 7,5100+003 |
| FREQUENCY = 3,4000+003 | DETERMINANT = 1,5859+015 | 8,7920+003 |
| FREQUENCY = 3,5000+003 | DETERMINANT = 1,5832+015 | 2,5980+003 |
| FREQUENCY = 3,6000+003 | DETERMINANT = 1,5774+015 | -2,8810+003 |
| FREQUENCY = 3,7000+003 | DETERMINANT = 1,5686+015 | 3,7600+003 |
| FREQUENCY = 3,8000+003 | DETERMINANT = 1,5568+015 | -2,1290+003 |
| FREQUENCY = 3,9000+003 | DETERMINANT = 1,5420+015 | -7,6180+003 |
| FREQUENCY = 4,0000+003 | DETERMINANT = 1,5245+015 | 2,4782+004 |
| FREQUENCY = 4,1000+003 | DETERMINANT = 1,5043+015 | 1,4825+004 |
| FREQUENCY = 4,2000+003 | DETERMINANT = 1,4814+015 | -1,4815+004 |
| FREQUENCY = 4,3000+003 | DETERMINANT = 1,4560+015 | -1,0132+004 |
| FREQUENCY = 4,4000+003 | DETERMINANT = 1,4283+015 | -2,4498+004 |
| FREQUENCY = 4,5000+003 | DETERMINANT = 1,3983+015 | -2,4286+004 |
| FREQUENCY = 4,6000+003 | DETERMINANT = 1,3661+015 | -2,2944+004 |
| FREQUENCY = 4,7000+003 | DETERMINANT = 1,3320+015 | -1,2854+004 |
| FREQUENCY = 4,8000+003 | DETERMINANT = 1,2960+015 | 2,8600+002 |
| FREQUENCY = 4,9000+003 | DETERMINANT = 1,2584+015 | -4,5980+003 |
| FREQUENCY = 5,0000+003 | DETERMINANT = 1,2191+015 | 1,1528+004 |
| FREQUENCY = 5,1000+003 | DETERMINANT = 1,1785+015 | -2,3250+004 |
| FREQUENCY = 5,2000+003 | DETERMINANT = 1,1366+015 | 2,1630+004 |
| FREQUENCY = 5,3000+003 | DETERMINANT = 1,0937+015 | 1,9136+004 |
| FREQUENCY = 5,4000+003 | DETERMINANT = 1,0498+015 | 6,2960+003 |

NRL REPORT 7964

| | | | | |
|-------------|------------|---------------|-------------|-------------|
| FREQUENCY # | 5,5000+003 | DETERMINANT # | 1.0052+015 | 6.5340+003 |
| FREQUENCY # | 5,6000+003 | DETERMINANT # | 9.6004+014 | 1.6780+004 |
| FREQUENCY # | 5,7000+003 | DETERMINANT # | 9.1445+014 | -6.4300+003 |
| FREQUENCY # | 5,8000+003 | DETERMINANT # | 8.6861+014 | -1.2940+004 |
| FREQUENCY # | 5,9000+003 | DETERMINANT # | 8.2269+014 | -7.9640+003 |
| FREQUENCY # | 6,0000+003 | DETERMINANT # | 7.7686+014 | -1.1352+004 |
| FREQUENCY # | 6,1000+003 | DETERMINANT # | 7.3128+014 | 6.0920+003 |
| FREQUENCY # | 6,2000+003 | DETERMINANT # | 6.8610+014 | 5.3680+003 |
| FREQUENCY # | 6,3000+003 | DETERMINANT # | 6.4148+014 | -5.0700+003 |
| FREQUENCY # | 6,4000+003 | DETERMINANT # | 5.9757+014 | 4.3660+003 |
| FREQUENCY # | 6,5000+003 | DETERMINANT # | 5.5451+014 | -7.2920+003 |
| FREQUENCY # | 6,6000+003 | DETERMINANT # | 5.1246+014 | 6.6560+003 |
| FREQUENCY # | 6,7000+003 | DETERMINANT # | 4.7153+014 | 1.7040+003 |
| FREQUENCY # | 6,8000+003 | DETERMINANT # | 4.3187+014 | 3.0580+003 |
| FREQUENCY # | 6,9000+003 | DETERMINANT # | 3.9357+014 | 2.9700+002 |
| FREQUENCY # | 7,0000+003 | DETERMINANT # | 3.5677+014 | 1.9670+003 |
| FREQUENCY # | 7,1000+003 | DETERMINANT # | 3.2155+014 | 3.1400+002 |
| FREQUENCY # | 7,2000+003 | DETERMINANT # | 2.8800+014 | 7.4800+002 |
| FREQUENCY # | 7,3000+003 | DETERMINANT # | 2.5622+014 | -2.2630+003 |
| FREQUENCY # | 7,4000+003 | DETERMINANT # | 2.2626+014 | -2.8560+003 |
| FREQUENCY # | 7,5000+003 | DETERMINANT # | 1.9820+014 | -4.9020+003 |
| FREQUENCY # | 7,6000+003 | DETERMINANT # | 1.7206+014 | -1.9290+002 |
| FREQUENCY # | 7,7000+003 | DETERMINANT # | 1.4790+014 | -3.0315+003 |
| FREQUENCY # | 7,8000+003 | DETERMINANT # | 1.2572+014 | -2.6880+003 |
| FREQUENCY # | 7,9000+003 | DETERMINANT # | 1.0553+014 | -3.3713+002 |
| FREQUENCY # | 8,0000+003 | DETERMINANT # | 8.7335+013 | 6.4569+002 |
| FREQUENCY # | 8,1000+003 | DETERMINANT # | 7.1103+013 | 1.3400+003 |
| FREQUENCY # | 8,2000+003 | DETERMINANT # | 5.6799+013 | -1.2395+003 |
| FREQUENCY # | 8,3000+003 | DETERMINANT # | 4.4372+013 | 5.3000+001 |
| FREQUENCY # | 8,4000+003 | DETERMINANT # | 3.3754+013 | 2.0945+003 |
| FREQUENCY # | 8,5000+003 | DETERMINANT # | 2.4859+013 | -5.4400+002 |
| FREQUENCY # | 8,6000+003 | DETERMINANT # | 1.7590+013 | -6.3800+002 |
| FREQUENCY # | 8,7000+003 | DETERMINANT # | 1.1827+013 | -3.0200+002 |
| FREQUENCY # | 8,8000+003 | DETERMINANT # | 7.4379+012 | -7.1000+001 |
| FREQUENCY # | 8,9000+003 | DETERMINANT # | 4.2683+012 | -1.0000+001 |
| FREQUENCY # | 9,0000+003 | DETERMINANT # | 2.1429+012 | -2.9000+001 |
| FREQUENCY # | 9,0500+003 | DETERMINANT # | 1.4087+012 | -5.2000+001 |
| FREQUENCY # | 9,1000+003 | DETERMINANT # | 8.5469+011 | 6.2000+001 |
| FREQUENCY # | 9,1500+003 | DETERMINANT # | 4.4681+011 | -2.5000+001 |
| FREQUENCY # | 9,2000+003 | DETERMINANT # | 1.4758+011 | 3.0000+000 |
| FREQUENCY # | 9,2500+003 | DETERMINANT # | -8.1181+010 | -2.5000+000 |
| FREQUENCY # | 9,3000+003 | DETERMINANT # | -2.7136+011 | 2.0000+000 |
| FREQUENCY # | 9,3500+003 | DETERMINANT # | -4.4048+011 | -5.0000+001 |
| FREQUENCY # | 9,4000+003 | DETERMINANT # | -5.8790+011 | 5.0000+001 |
| FREQUENCY # | 9,4500+003 | DETERMINANT # | -6.9546+011 | -8.0000+000 |
| FREQUENCY # | 9,5000+003 | DETERMINANT # | -7.2690+011 | -9.0000+000 |
| FREQUENCY # | 9,5500+003 | DETERMINANT # | -6.0924+011 | -1.1000+001 |
| FREQUENCY # | 9,6000+003 | DETERMINANT # | 0.0000+000 | -3.1600+011 |
| FREQUENCY # | 9,6500+003 | DETERMINANT # | 3.6242+001 | -9.7741+011 |
| FREQUENCY # | 9,7000+003 | DETERMINANT # | 0.0000+000 | -1.4709+012 |
| FREQUENCY # | 9,7500+003 | DETERMINANT # | 0.0000+000 | -1.8764+012 |
| FREQUENCY # | 9,8000+003 | DETERMINANT # | -3.5604+002 | -2.1435+012 |
| FREQUENCY # | 9,8500+003 | DETERMINANT # | -3.5209+002 | -2.1752+012 |
| FREQUENCY # | 9,9000+003 | DETERMINANT # | 0.0000+000 | -1.8137+012 |
| FREQUENCY # | 9,9500+003 | DETERMINANT # | -3.7589+002 | -7.8809+011 |
| FREQUENCY # | 1,0000+004 | DETERMINANT # | -1.1262+003 | 1.4423+012 |
| FREQUENCY # | 1,0050+004 | DETERMINANT # | -1.3879+003 | 6.3317+012 |
| FREQUENCY # | 1,0100+004 | DETERMINANT # | -2.0350+003 | 2.2607+013 |
| FREQUENCY # | 1,0150+004 | DETERMINANT # | 3.1929+013 | 2.1802+003 |
| FREQUENCY # | 1,0200+004 | DETERMINANT # | 2.8765+013 | 0.0000+000 |
| FREQUENCY # | 1,0250+004 | DETERMINANT # | 3.1684+013 | 0.0000+000 |
| FREQUENCY # | 1,0300+004 | DETERMINANT # | 3.6378+013 | 1.0715+003 |
| FREQUENCY # | 1,0350+004 | DETERMINANT # | 4.2208+013 | 0.0000+000 |
| FREQUENCY # | 1,0400+004 | DETERMINANT # | 4.9012+013 | 5.7433+002 |
| FREQUENCY # | 1,0600+004 | DETERMINANT # | 8.5701+013 | -3.4720+002 |
| FREQUENCY # | 1,0800+004 | DETERMINANT # | 1.3914+014 | 1.6738+003 |

HANISH, KING, BAIER, AND ROGERS

| | | | | | | |
|-----------|---|------------|-------------|---|-------------|-------------|
| FREQUENCY | * | 1,1000+004 | DETERMINANT | * | 2,1233+014 | 1,9986+003 |
| FREQUENCY | * | 1,1200+004 | DETERMINANT | * | 3,0840+014 | -2,7075+003 |
| FREQUENCY | * | 1,1400+004 | DETERMINANT | * | 4,3134+014 | -3,8670+003 |
| FREQUENCY | * | 1,1600+004 | DETERMINANT | * | 5,8398+014 | -5,3433+003 |
| FREQUENCY | * | 1,1800+004 | DETERMINANT | * | 7,6993+014 | -1,4367+004 |
| FREQUENCY | * | 1,2000+004 | DETERMINANT | * | 9,9250+014 | -1,8259+004 |
| FREQUENCY | * | 1,2200+004 | DETERMINANT | * | 1,2549+015 | -1,9445+004 |
| FREQUENCY | * | 1,2400+004 | DETERMINANT | * | 1,5600+015 | -1,5393+004 |
| FREQUENCY | * | 1,2600+004 | DETERMINANT | * | 1,9106+015 | -1,9200+004 |
| FREQUENCY | * | 1,2800+004 | DETERMINANT | * | 2,3091+015 | -1,2822+004 |
| FREQUENCY | * | 1,3000+004 | DETERMINANT | * | 2,7575+015 | -2,8477+004 |
| FREQUENCY | * | 1,3200+004 | DETERMINANT | * | 3,2575+015 | 1,8199+004 |
| FREQUENCY | * | 1,3400+004 | DETERMINANT | * | 3,8101+015 | 8,2453+004 |
| FREQUENCY | * | 1,3600+004 | DETERMINANT | * | 4,4159+015 | -9,6643+004 |
| FREQUENCY | * | 1,3800+004 | DETERMINANT | * | 5,0748+015 | -1,1285+005 |
| FREQUENCY | * | 1,4000+004 | DETERMINANT | * | 5,7860+015 | -6,5874+004 |
| FREQUENCY | * | 1,4200+004 | DETERMINANT | * | 6,5481+015 | -1,5267+005 |
| FREQUENCY | * | 1,4400+004 | DETERMINANT | * | 7,3589+015 | -1,7568+005 |
| FREQUENCY | * | 1,4600+004 | DETERMINANT | * | 8,2152+015 | -5,7173+004 |
| FREQUENCY | * | 1,4800+004 | DETERMINANT | * | 9,1130+015 | -6,5084+004 |
| FREQUENCY | * | 1,5000+004 | DETERMINANT | * | 1,0048+016 | 5,4258+004 |
| FREQUENCY | * | 1,5200+004 | DETERMINANT | * | 1,1013+016 | 6,0635+004 |
| FREQUENCY | * | 1,5400+004 | DETERMINANT | * | 1,2003+016 | 6,7514+004 |
| FREQUENCY | * | 1,5600+004 | DETERMINANT | * | 1,3009+016 | 0,0000+000 |
| FREQUENCY | * | 1,5800+004 | DETERMINANT | * | 1,4023+016 | 0,0000+000 |
| FREQUENCY | * | 1,6000+004 | DETERMINANT | * | 1,5035+016 | 0,0000+000 |
| FREQUENCY | * | 1,6200+004 | DETERMINANT | * | 1,6035+016 | -3,1128+005 |
| FREQUENCY | * | 1,6400+004 | DETERMINANT | * | 1,7011+016 | -1,9414+005 |
| FREQUENCY | * | 1,6600+004 | DETERMINANT | * | 1,7951+016 | -5,5621+005 |
| FREQUENCY | * | 1,6800+004 | DETERMINANT | * | 1,8843+016 | 6,0043+005 |
| FREQUENCY | * | 1,7000+004 | DETERMINANT | * | 1,9672+016 | -3,2263+005 |
| FREQUENCY | * | 1,7200+004 | DETERMINANT | * | 2,0425+016 | 1,0201+006 |
| FREQUENCY | * | 1,7400+004 | DETERMINANT | * | 2,1087+016 | 7,3512+005 |
| FREQUENCY | * | 1,7600+004 | DETERMINANT | * | 2,1644+016 | 1,6142+004 |
| FREQUENCY | * | 1,7800+004 | DETERMINANT | * | 2,2081+016 | -9,7648+004 |
| FREQUENCY | * | 1,8000+004 | DETERMINANT | * | 2,2384+016 | 8,6229+005 |
| FREQUENCY | * | 1,8200+004 | DETERMINANT | * | 2,2539+016 | 1,4525+006 |
| FREQUENCY | * | 1,8400+004 | DETERMINANT | * | 2,2532+016 | 5,8766+005 |
| FREQUENCY | * | 1,8600+004 | DETERMINANT | * | 2,2331+016 | 6,2317+005 |
| FREQUENCY | * | 1,8800+004 | DETERMINANT | * | 2,1985+016 | 0,0000+000 |
| FREQUENCY | * | 1,9000+004 | DETERMINANT | * | 2,1426+016 | 1,8375+006 |
| FREQUENCY | * | 1,9200+004 | DETERMINANT | * | 2,0665+016 | -4,3802+005 |
| FREQUENCY | * | 1,9400+004 | DETERMINANT | * | 1,9699+016 | -1,4693+006 |
| FREQUENCY | * | 1,9600+004 | DETERMINANT | * | 1,8526+016 | 0,0000+000 |
| FREQUENCY | * | 1,9800+004 | DETERMINANT | * | 1,7148+016 | 5,0689+005 |
| FREQUENCY | * | 2,0000+004 | DETERMINANT | * | 1,5571+016 | 1,0281+006 |
| FREQUENCY | * | 2,0200+004 | DETERMINANT | * | 1,3806+016 | 0,0000+000 |
| FREQUENCY | * | 2,0400+004 | DETERMINANT | * | 1,1868+016 | -1,4498+006 |
| FREQUENCY | * | 2,0600+004 | DETERMINANT | * | 9,7790+015 | -1,4610+006 |
| FREQUENCY | * | 2,0800+004 | DETERMINANT | * | 7,5679+015 | -1,1233+006 |
| FREQUENCY | * | 2,1000+004 | DETERMINANT | * | 5,2702+015 | -1,6390+006 |
| FREQUENCY | * | 2,1200+004 | DETERMINANT | * | 2,9297+015 | -7,5556+005 |
| FREQUENCY | * | 2,1400+004 | DETERMINANT | * | 3,9893+014 | -7,4929+005 |
| FREQUENCY | * | 2,1600+004 | DETERMINANT | * | -1,6595+015 | -5,5593+005 |
| FREQUENCY | * | 2,1800+004 | DETERMINANT | * | -3,7726+015 | -7,1378+005 |
| FREQUENCY | * | 2,2000+004 | DETERMINANT | * | -5,6557+015 | -1,6562+006 |
| FREQUENCY | * | 2,2200+004 | DETERMINANT | * | -7,2116+015 | -1,1503+006 |
| FREQUENCY | * | 2,2400+004 | DETERMINANT | * | -8,3299+015 | -8,8056+005 |
| FREQUENCY | * | 2,2600+004 | DETERMINANT | * | -8,8853+015 | 7,7945+005 |
| FREQUENCY | * | 2,2800+004 | DETERMINANT | * | -8,7372+015 | -2,5734+006 |
| FREQUENCY | * | 2,3000+004 | DETERMINANT | * | -7,7281+015 | -3,1693+006 |
| FREQUENCY | * | 2,3200+004 | DETERMINANT | * | -5,6831+015 | -1,6592+005 |
| FREQUENCY | * | 2,3400+004 | DETERMINANT | * | -2,4082+015 | 0,0000+000 |
| FREQUENCY | * | 2,3600+004 | DETERMINANT | * | 2,3108+015 | 1,1417+005 |
| FREQUENCY | * | 2,3800+004 | DETERMINANT | * | 8,7090+015 | -6,2979+006 |
| FREQUENCY | * | 2,4000+004 | DETERMINANT | * | 1,7044+016 | -1,2984+006 |

NRL REPORT 7964

| | | |
|------------------------|--------------------------|-------------|
| FREQUENCY * 2,4200+004 | DETERMINANT * 2,7597+016 | =8,3915+006 |
| FREQUENCY * 2,4400+004 | DETERMINANT * 4,0674+016 | =1,4789+006 |
| FREQUENCY * 2,4600+004 | DETERMINANT * 5,6607+016 | 0,0000+000 |
| FREQUENCY * 2,4800+004 | DETERMINANT * 7,5755+016 | =1,4394+007 |
| FREQUENCY * 2,5000+004 | DETERMINANT * 9,8506+016 | 4,4126+006 |
| FREQUENCY * 2,5200+004 | DETERMINANT * 1,2528+017 | 9,3410+006 |
| FREQUENCY * 2,5400+004 | DETERMINANT * 1,5651+017 | 0,0000+000 |
| FREQUENCY * 2,5600+004 | DETERMINANT * 1,9270+017 | 8,2780+006 |
| FREQUENCY * 2,5800+004 | DETERMINANT * 2,3434+017 | 3,4938+007 |
| FREQUENCY * 2,6000+004 | DETERMINANT * 2,8200+017 | 1,7289+007 |
| FREQUENCY * 2,6200+004 | DETERMINANT * 3,3624+017 | 1,9356+007 |
| FREQUENCY * 2,6400+004 | DETERMINANT * 3,9768+017 | =2,2478+007 |
| FREQUENCY * 2,6600+004 | DETERMINANT * 4,6699+017 | 1,9801+007 |
| FREQUENCY * 2,6800+004 | DETERMINANT * 5,4486+017 | 2,5784+007 |
| FREQUENCY * 2,7000+004 | DETERMINANT * 6,3200+017 | 0,0000+000 |
| FREQUENCY * 2,7200+004 | DETERMINANT * 7,2921+017 | 2,1019+007 |
| FREQUENCY * 2,7400+004 | DETERMINANT * 8,3727+017 | 1,2116+007 |
| FREQUENCY * 2,7600+004 | DETERMINANT * 9,5706+017 | 0,0000+000 |
| FREQUENCY * 2,7800+004 | DETERMINANT * 1,0895+018 | =5,4258+007 |
| FREQUENCY * 2,8000+004 | DETERMINANT * 1,2354+018 | 1,3974+007 |
| FREQUENCY * 2,8200+004 | DETERMINANT * 1,3958+018 | 2,2141+007 |
| FREQUENCY * 2,8400+004 | DETERMINANT * 1,5718+018 | =1,3803+008 |
| FREQUENCY * 2,8600+004 | DETERMINANT * 1,7644+018 | =7,4558+007 |
| FREQUENCY * 2,8800+004 | DETERMINANT * 1,9746+018 | =1,7884+007 |
| FREQUENCY * 2,9000+004 | DETERMINANT * 2,2037+018 | 6,5768+006 |
| FREQUENCY * 2,9200+004 | DETERMINANT * 2,4528+018 | =4,6490+008 |
| FREQUENCY * 2,9400+004 | DETERMINANT * 2,7231+018 | 7,9099+006 |
| FREQUENCY * 2,9600+004 | DETERMINANT * 3,0158+018 | =1,7307+007 |
| FREQUENCY * 2,9800+004 | DETERMINANT * 3,3323+018 | 0,0000+000 |
| FREQUENCY * 3,0000+004 | DETERMINANT * 3,6739+018 | 6,1739+007 |
| FREQUENCY * 3,0200+004 | DETERMINANT * 4,0419+018 | 1,1232+007 |
| FREQUENCY * 3,0400+004 | DETERMINANT * 4,4378+018 | 2,4439+007 |
| FREQUENCY * 3,0600+004 | DETERMINANT * 4,8629+018 | =1,5065+008 |
| FREQUENCY * 3,0800+004 | DETERMINANT * 5,3186+018 | 1,4409+007 |
| FREQUENCY * 3,1000+004 | DETERMINANT * 5,8066+018 | 1,5619+007 |
| FREQUENCY * 3,1200+004 | DETERMINANT * 6,3282+018 | =1,4813+008 |
| FREQUENCY * 3,1400+004 | DETERMINANT * 6,8849+018 | 9,6812+007 |
| FREQUENCY * 3,1600+004 | DETERMINANT * 7,4783+018 | 3,5253+005 |
| FREQUENCY * 3,1800+004 | DETERMINANT * 8,1098+018 | 3,7732+005 |
| FREQUENCY * 3,2000+004 | DETERMINANT * 8,7812+018 | =1,8518+008 |
| FREQUENCY * 3,2200+004 | DETERMINANT * 9,4937+018 | 2,1555+005 |
| FREQUENCY * 3,2400+004 | DETERMINANT * 1,0249+019 | 9,3380+007 |
| FREQUENCY * 3,2600+004 | DETERMINANT * 1,1049+019 | 1,9533+008 |
| FREQUENCY * 3,2800+004 | DETERMINANT * 1,1894+019 | 2,9016+008 |
| FREQUENCY * 3,3000+004 | DETERMINANT * 1,2787+019 | 5,5727+005 |
| FREQUENCY * 3,3200+004 | DETERMINANT * 1,3728+019 | 3,2312+008 |
| FREQUENCY * 3,3400+004 | DETERMINANT * 1,4720+019 | 3,4058+008 |
| FREQUENCY * 3,3600+004 | DETERMINANT * 1,5763+019 | 5,3820+008 |
| FREQUENCY * 3,3800+004 | DETERMINANT * 1,6859+019 | 1,8926+008 |
| FREQUENCY * 3,4000+004 | DETERMINANT * 1,8009+019 | 3,0417+008 |
| FREQUENCY * 3,4200+004 | DETERMINANT * 1,9214+019 | 5,2620+008 |
| FREQUENCY * 3,4400+004 | DETERMINANT * 2,0476+019 | 2,1956+008 |
| FREQUENCY * 3,4600+004 | DETERMINANT * 2,1795+019 | 6,8832+008 |
| FREQUENCY * 3,4800+004 | DETERMINANT * 2,3173+019 | 2,4052+008 |
| FREQUENCY * 3,5000+004 | DETERMINANT * 2,4609+019 | 2,5245+008 |
| FREQUENCY * 3,5200+004 | DETERMINANT * 2,6106+019 | 3,9087+008 |
| FREQUENCY * 3,5400+004 | DETERMINANT * 2,7663+019 | 2,7584+008 |
| FREQUENCY * 3,5600+004 | DETERMINANT * 2,9280+019 | 4,2180+008 |
| FREQUENCY * 3,5800+004 | DETERMINANT * 3,0959+019 | 0,0000+000 |
| FREQUENCY * 3,6000+004 | DETERMINANT * 3,2700+019 | 2,2672+008 |
| FREQUENCY * 3,6200+004 | DETERMINANT * 3,4501+019 | 3,2774+008 |
| FREQUENCY * 3,6400+004 | DETERMINANT * 3,6363+019 | 3,4154+008 |
| FREQUENCY * 3,6600+004 | DETERMINANT * 3,8286+019 | 2,0969+008 |
| FREQUENCY * 3,6800+004 | DETERMINANT * 4,0269+019 | 1,2971+009 |
| FREQUENCY * 3,7000+004 | DETERMINANT * 4,2311+019 | 0,0000+000 |
| FREQUENCY * 3,7200+004 | DETERMINANT * 4,4410+019 | 2,4995+008 |

HANISH, KING, BAIER, AND ROGERS

| | | |
|------------------------|---------------------------|-------------|
| FREQUENCY * 3,7400+004 | DETERMINANT * 4,6566+019 | 1,0951+009 |
| FREQUENCY * 3,7600+004 | DETERMINANT * 4,8776+019 | 4,2143+008 |
| FREQUENCY * 3,7800+004 | DETERMINANT * 5,1039+019 | 0,0000+000 |
| FREQUENCY * 3,8000+004 | DETERMINANT * 5,3352+019 | -4,6264+008 |
| FREQUENCY * 3,8200+004 | DETERMINANT * 5,5713+019 | 2,2959+008 |
| FREQUENCY * 3,8400+004 | DETERMINANT * 5,8119+019 | -4,9538+008 |
| FREQUENCY * 3,8600+004 | DETERMINANT * 6,0566+019 | 0,0000+000 |
| FREQUENCY * 3,8800+004 | DETERMINANT * 6,3051+019 | 0,0000+000 |
| FREQUENCY * 3,9000+004 | DETERMINANT * 6,5569+019 | 0,0000+000 |
| FREQUENCY * 3,9200+004 | DETERMINANT * 6,8116+019 | 2,8133+008 |
| FREQUENCY * 3,9400+004 | DETERMINANT * 7,0698+019 | -9,8210+008 |
| FREQUENCY * 3,9600+004 | DETERMINANT * 7,3327+019 | -4,2407+008 |
| FREQUENCY * 3,9800+004 | DETERMINANT * 7,5981+019 | 0,0000+000 |
| FREQUENCY * 4,0000+004 | DETERMINANT * 7,8491+019 | -9,0412+008 |
| FREQUENCY * 4,0200+004 | DETERMINANT * 8,1100+019 | -6,4766+008 |
| FREQUENCY * 4,0400+004 | DETERMINANT * 8,3702+019 | -1,1726+009 |
| FREQUENCY * 4,0600+004 | DETERMINANT * 8,6289+019 | -1,6484+009 |
| FREQUENCY * 4,0800+004 | DETERMINANT * 8,8952+019 | 3,1255+008 |
| FREQUENCY * 4,1000+004 | DETERMINANT * 9,1382+019 | 7,5767+008 |
| FREQUENCY * 4,1200+004 | DETERMINANT * 9,3869+019 | -7,2681+008 |
| FREQUENCY * 4,1400+004 | DETERMINANT * 9,6305+019 | 0,0000+000 |
| FREQUENCY * 4,1600+004 | DETERMINANT * 9,8677+019 | -9,0174+008 |
| FREQUENCY * 4,1800+004 | DETERMINANT * 1,0097+020 | 1,8923+009 |
| FREQUENCY * 4,2000+004 | DETERMINANT * 1,0319+020 | 0,0000+000 |
| FREQUENCY * 4,2200+004 | DETERMINANT * 1,0530+020 | -3,2375+009 |
| FREQUENCY * 4,2400+004 | DETERMINANT * 1,0730+020 | -4,6054+009 |
| FREQUENCY * 4,2600+004 | DETERMINANT * 1,0917+020 | 0,0000+000 |
| FREQUENCY * 4,2800+004 | DETERMINANT * 1,1090+020 | -2,4521+009 |
| FREQUENCY * 4,3000+004 | DETERMINANT * 1,1248+020 | -3,9675+009 |
| FREQUENCY * 4,3200+004 | DETERMINANT * 1,1388+020 | -1,7497+009 |
| FREQUENCY * 4,3400+004 | DETERMINANT * 1,1510+020 | -3,0498+009 |
| FREQUENCY * 4,3600+004 | DETERMINANT * 1,1611+020 | -1,6995+009 |
| FREQUENCY * 4,3800+004 | DETERMINANT * 1,1689+020 | 2,1593+008 |
| FREQUENCY * 4,4000+004 | DETERMINANT * 1,1743+020 | 4,3287+008 |
| FREQUENCY * 4,4200+004 | DETERMINANT * 1,1771+020 | 0,0000+000 |
| FREQUENCY * 4,4400+004 | DETERMINANT * 1,1770+020 | 0,0000+000 |
| FREQUENCY * 4,4600+004 | DETERMINANT * 1,1739+020 | 0,0000+000 |
| FREQUENCY * 4,4800+004 | DETERMINANT * 1,1675+020 | -6,6334+009 |
| FREQUENCY * 4,5000+004 | DETERMINANT * 1,1577+020 | -2,5961+009 |
| FREQUENCY * 4,5200+004 | DETERMINANT * 1,1441+020 | -2,0854+008 |
| FREQUENCY * 4,5400+004 | DETERMINANT * 1,1265+020 | 0,0000+000 |
| FREQUENCY * 4,5600+004 | DETERMINANT * 1,1048+020 | -2,8932+009 |
| FREQUENCY * 4,5800+004 | DETERMINANT * 1,0786+020 | -9,2993+009 |
| FREQUENCY * 4,6000+004 | DETERMINANT * 1,0477+020 | -4,2384+009 |
| FREQUENCY * 4,6200+004 | DETERMINANT * 1,0118+020 | -4,4385+009 |
| FREQUENCY * 4,6400+004 | DETERMINANT * 9,7069+019 | -4,6196+009 |
| FREQUENCY * 4,6600+004 | DETERMINANT * 9,2403+019 | -4,8089+009 |
| FREQUENCY * 4,6800+004 | DETERMINANT * 8,7155+019 | 4,0192+007 |
| FREQUENCY * 4,7000+004 | DETERMINANT * 8,1298+019 | 0,0000+000 |
| FREQUENCY * 4,7200+004 | DETERMINANT * 7,4802+019 | 1,3752+008 |
| FREQUENCY * 4,7400+004 | DETERMINANT * 6,7636+019 | -6,2329+007 |
| FREQUENCY * 4,7600+004 | DETERMINANT * 5,9771+019 | 0,0000+000 |
| FREQUENCY * 4,7800+004 | DETERMINANT * 5,1175+019 | -1,2187+010 |
| FREQUENCY * 4,8000+004 | DETERMINANT * 4,1819+019 | -1,2607+010 |
| FREQUENCY * 4,8200+004 | DETERMINANT * 3,1670+019 | -1,3117+010 |
| FREQUENCY * 4,8400+004 | DETERMINANT * 2,0697+019 | -6,7913+009 |
| FREQUENCY * 4,8600+004 | DETERMINANT * 8,8675+018 | -2,1154+010 |
| FREQUENCY * 4,8800+004 | DETERMINANT * -3,8497+018 | -7,2952+009 |
| FREQUENCY * 4,9000+004 | DETERMINANT * -1,7487+019 | -7,5453+009 |
| FREQUENCY * 4,9200+004 | DETERMINANT * -3,2076+019 | -7,8538+009 |
| FREQUENCY * 4,9400+004 | DETERMINANT * -4,7650+019 | -2,8488+010 |
| FREQUENCY * 4,9600+004 | DETERMINANT * -6,4240+019 | -8,4302+009 |
| FREQUENCY * 4,9800+004 | DETERMINANT * -8,1877+019 | -2,6190+010 |
| FREQUENCY * 5,0000+004 | DETERMINANT * -1,0059+020 | -9,4133+009 |
| FREQUENCY * 5,0200+004 | DETERMINANT * -1,2042+020 | -1,4487+010 |
| FREQUENCY * 5,0400+004 | DETERMINANT * -1,4139+020 | 0,0000+000 |

NRL REPORT 7964

| | | | | |
|-------------|------------|---------------|-------------|-------------|
| FREQUENCY # | 5,0600+004 | DETERMINANT # | -1,6353+020 | 1,0009+010 |
| FREQUENCY # | 5,0800+004 | DETERMINANT # | -1,8687+020 | 1,5530+010 |
| FREQUENCY # | 5,1000+004 | DETERMINANT # | -2,1144+020 | -1,1503+010 |
| FREQUENCY # | 5,1200+004 | DETERMINANT # | -2,3727+020 | -1,8194+009 |
| FREQUENCY # | 5,1400+004 | DETERMINANT # | -2,6438+020 | 1,0185+009 |
| FREQUENCY # | 5,1600+004 | DETERMINANT # | -2,9280+020 | 1,7695+010 |
| FREQUENCY # | 5,1800+004 | DETERMINANT # | -3,2256+020 | -2,5105+009 |
| FREQUENCY # | 5,2000+004 | DETERMINANT # | -3,5368+020 | -4,1500+009 |
| FREQUENCY # | 5,2200+004 | DETERMINANT # | -3,8617+020 | -4,5568+009 |
| FREQUENCY # | 5,2400+004 | DETERMINANT # | -4,2007+020 | -1,3355+010 |
| FREQUENCY # | 5,2600+004 | DETERMINANT # | -4,5539+020 | 2,0683+010 |
| FREQUENCY # | 5,2800+004 | DETERMINANT # | -4,9214+020 | -1,4602+010 |
| FREQUENCY # | 5,3000+004 | DETERMINANT # | -5,3034+020 | 2,1966+010 |
| FREQUENCY # | 5,3200+004 | DETERMINANT # | -5,7001+020 | 2,2626+010 |
| FREQUENCY # | 5,3400+004 | DETERMINANT # | -6,1116+020 | 1,8302+010 |
| FREQUENCY # | 5,3600+004 | DETERMINANT # | -6,5378+020 | 2,3982+010 |
| FREQUENCY # | 5,3800+004 | DETERMINANT # | -6,9790+020 | -5,7885+009 |
| FREQUENCY # | 5,4000+004 | DETERMINANT # | -7,4350+020 | -6,2139+009 |
| FREQUENCY # | 5,4200+004 | DETERMINANT # | -7,9060+020 | -6,6597+009 |
| FREQUENCY # | 5,4400+004 | DETERMINANT # | -8,3919+020 | 0,0000+000 |
| FREQUENCY # | 5,4600+004 | DETERMINANT # | -8,8925+020 | -3,0602+010 |
| FREQUENCY # | 5,4800+004 | DETERMINANT # | -9,4079+020 | 8,1288+009 |
| FREQUENCY # | 5,5000+004 | DETERMINANT # | -9,9379+020 | 0,0000+000 |
| FREQUENCY # | 5,5200+004 | DETERMINANT # | -1,0482+021 | 3,4114+010 |
| FREQUENCY # | 5,5400+004 | DETERMINANT # | -1,1041+021 | 9,8019+009 |
| FREQUENCY # | 5,5600+004 | DETERMINANT # | -1,1613+021 | -1,3101+010 |
| FREQUENCY # | 5,5800+004 | DETERMINANT # | -1,2199+021 | -1,3434+010 |
| FREQUENCY # | 5,6000+004 | DETERMINANT # | -1,2799+021 | 1,1711+010 |
| FREQUENCY # | 5,6200+004 | DETERMINANT # | -1,3411+021 | -1,3003+010 |
| FREQUENCY # | 5,6400+004 | DETERMINANT # | -1,4036+021 | 3,9134+010 |
| FREQUENCY # | 5,6600+004 | DETERMINANT # | -1,4673+021 | 1,3870+010 |
| FREQUENCY # | 5,6800+004 | DETERMINANT # | -1,5321+021 | 5,5048+010 |
| FREQUENCY # | 5,7000+004 | DETERMINANT # | -1,5980+021 | 1,5461+010 |
| FREQUENCY # | 5,7200+004 | DETERMINANT # | -1,6649+021 | 2,6937+010 |
| FREQUENCY # | 5,7400+004 | DETERMINANT # | -1,7327+021 | 4,3908+010 |
| FREQUENCY # | 5,7600+004 | DETERMINANT # | -1,8015+021 | 2,6687+010 |
| FREQUENCY # | 5,7800+004 | DETERMINANT # | -1,8710+021 | 3,8080+010 |
| FREQUENCY # | 5,8000+004 | DETERMINANT # | -1,9411+021 | 2,0023+010 |
| FREQUENCY # | 5,8200+004 | DETERMINANT # | -2,0119+021 | 2,1043+010 |
| FREQUENCY # | 5,8400+004 | DETERMINANT # | -2,0832+021 | 3,0734+010 |
| FREQUENCY # | 5,8600+004 | DETERMINANT # | -2,1549+021 | 4,6399+010 |
| FREQUENCY # | 5,8800+004 | DETERMINANT # | -2,2268+021 | 2,4338+010 |
| FREQUENCY # | 5,9000+004 | DETERMINANT # | -2,2988+021 | 2,6601+010 |
| FREQUENCY # | 5,9200+004 | DETERMINANT # | -2,3709+021 | 5,3484+010 |
| FREQUENCY # | 5,9400+004 | DETERMINANT # | -2,4428+021 | 0,0000+000 |
| FREQUENCY # | 5,9600+004 | DETERMINANT # | -2,5144+021 | 1,8615+010 |
| FREQUENCY # | 5,9800+004 | DETERMINANT # | -2,5855+021 | 8,4633+009 |
| FREQUENCY # | 6,0000+004 | DETERMINANT # | -2,6560+021 | 0,0000+000 |

Appendix C

COMPUTOR LISTING OF EIGFNS AND A SAMPLE INPUT AND OUTPUT

The program EIGFNS is listed on the next five pages, followed by a sample output: that of ring C. The sample input is

```
.06587      .00685      .09055      8400.      .38          1.26E11
5
9200.      9250.
9950.      10000.      1
21400.     21500.
23400.     23600.
48600.     48800.
```

A listing of subroutine CUBIC, which program EIGFNS requires, appears in Appendix A. Program EIGFNS differs from subroutine CUBIC in the following ways: all common cards have been removed, a READ statement and FORMAT statement corresponding to that of the cylindrical shell dimensions and material property card have been added, the Fortran statements $PI = 3.141592654$ and $NPTS = 9$ have been added, and the return statement preceding the statement entry IMPD has been replaced by an END statement and all cards following the statement have been removed. The value of NPTS may be changed. It represents the number of equally spaced points along half of the ring shell at which values of the mode shapes are to be calculated and printed. The purpose of program EIGFNS is to obtain the modal shape factors of ring C. Thus the frequency intervals found from program DETRMNT are used as input quantities for program EIGFNS. The digit 1 in column 25 of the second frequency-interval card indicates that the imaginary part of the boundary condition determinant is to be used to obtain the second resonance frequency.

Examination of the output shows that all five frequency intervals are indeed valid intervals. The interval halving converges to a resonant frequency for each frequency interval, as can be verified by comparing the value of the determinant at the resonant frequency to the values of the determinant at the endpoints of the input frequency and observing that the quantities RT1 and RT2 agree to several significant digits. The two quantities RT1 and RT2 are ratios of elements in the second and third rows respectively of the three-by-three matrix M_{ij} , where $M_{21} = M_{31} = 0$. This matrix is obtained by an equivalence transformation of the three-by-three boundary-condition matrix discussed in the last paragraph on the next page.

The mode shapes can be determined by examining the scaled displacements which due to symmetry are calculated for half the length of the shell. From the output, Table C1 can be constructed.

Table C1 — Mode Shapes and Resonant Frequencies for Ring C

| Resonant Frequency (Hz) | Mode Shape Number | Predominant Motion | Mode Shape | Number of Nodes in Half of Shell |
|-------------------------|-------------------|--------------------|------------|----------------------------------|
| 9230.9 | 1 | Radial | 1st Radial | 0 |
| 9972.1 | 2 | Radial | 2nd Radial | 1 |
| 21452.2 | 3 | Radial | 3rd Radial | 2 |
| 23510.2 | 4 | Axial | 1st Axial | 1 |
| 48740.9 | 5 | Radial | 4th Radial | 3 |

The displacements are for only half of the shell. For example the mode shapes for 9972.1 Hz and 23510.2 Hz are shown in Fig. C1.

A numerical check of the orthogonality of the calculated mode shapes is provided as the final printout of EIGFNS. The mode shapes are numbered in the order in which they were calculated (Table C1). The ten real numbers at the end of the printout under the heading "Value of Inner Product" represent the inner products of the orthonormal mode shapes listed under the heading "Modal Shapes."

The particular equations used in program EIGFNS are special cases of those found in Part 1, Eqs. 4.40ff. As stated earlier, only radial and axial displacements are considered. In addition symmetric free-free end boundary conditions are assumed. These conditions cause Eq. 4.43 of Part 1 to become a cubic equation whose roots are the squares of the separation constants. Similarly Eq. 4.48 of Part 1 is reduced to a three-by-three boundary-condition matrix equation in the three unknown displacement amplitude coefficients. It is the determinant of this matrix which must have the value 0 for nontrivial solutions of the displacement amplitudes to exist.

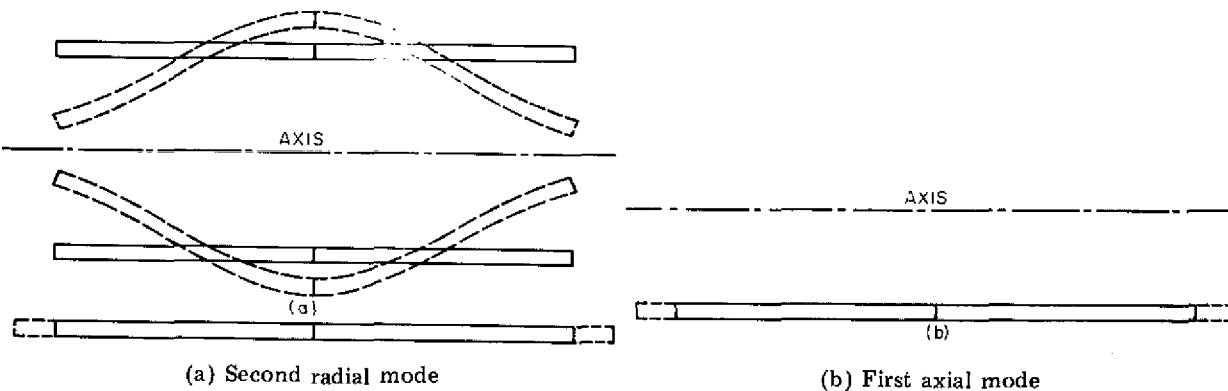


Fig. C1 — Undeformed surface (solid lines) and motion of ring shell (dashed lines) in the second radial mode and the first axial mode. The amplitudes of the motions are exaggerated for clarity.

HANISH, KING, BAIER, AND ROGERS

```

PROGRAM EIGFNS
TYPE COMPLEX AN,B,BU,BW,C1,C2,C3,C4,C5,C6,C7,C8,CFM,CU,CW,D,DN,DR,
1DTD,DTRMNT,EE,EM,EN,EPM,EPP,G,RAR,RN,RT,RT1,RT2,RTR,SRT,T1,T2,TM,
2U,U2,UM,US,UX,UX2,UXM,UXW,UXWX,W,W2,WM,WS,WXX,WXX2,WXXM
DIMENSION AA(9),AX(9,10),AXEDGE(9),B(3,3),BU(9,3),BW(9,3),CFM(11),
1CU(3),CW(3),DETR(2),EN(3),F(3),FR(2),FRQ(9),G(4),NA(9),NR(9),
2RAR(9,3),RD(9,10),RDIN(9,10),RINT(9),RT(3),RTR(3),TT(2)
TYPE REAL LTH,NA,NR,NU
EQUIVALENCE (TT,DR)
READ 63,RMEAN,THK,LTH,RHO,NU,Y
63 FORMAT (6E10.5)
PI = 3.141592654
NPTS = 9
HD2 = LTH/2.
NIT = 30
LTH = 2.*HD2
A = RMEAN
PRINT 19
19 FORMAT (1H144X*CALCULATION OF MODAL SHAPE FUNCTIONS*)
PRINT 20,A,THK,LTH,RHO,NU,Y
20 FORMAT (/56X*INPUT PARAMETERS*/29X11HMEAN RADIUS38X
37HRMEAN =E14.6/
$29X16HRADIAL THICKNESS35X5HCHK =E14.6/
$29X12HAXIAL LENGTH39X5HLTH = E14.6/
$29X7HDENSITY44X5HRHO =E14.6/
$29X14HPOISSONS RATIO38X4HNU =E14.6/
$29X45HYOUNGS MODULUS AT CONSTANT MAGNETIC INDUCTION 8X3HY =E14.6)
PRINT 5056
5056 FORMAT (//)
C
C READ IN NBRFNS, FREQUENCY INTERVALS, AND IMG FLAG.
C
HEAD 99,NBRFNS
99 FORMAT (I1)
DO 777 IXX = 1,NBRFNS
IX = IXX
IF (IX.GT.1) PRINT 5057
5057 FORMAT (1H1)
READ 9,FR(1),FR(2),IMG
9 FORMAT (2F10.5,4XI1)
INX = 1
IT = 0
FREQ = FR(1)
PRINT 52
52 FORMAT (51X*INITIAL FREQUENCY INTERVAL*//)
42 CONTINUE
C
C CALCULATE BOUNDARY CONDITION MATRIX B(,) AND ITS DETERMINANT DTRMNT.
C
DELTA = RHO*A*A*(1.-NU**2)*FREQ**2/Y*4.*PI*PI
BETA = THK**2/(12.*A*A)

```

```

A2 = DELTA + 2.*NU
A1 = (1.-DELTA-NU*NU)/BETA + 1.
A0 = (DELTA-DELTA**2)/BETA + DELTA
CALL CUBIC(A2,A1,A0,RT)
DO 1 I = 1,3
SRT = CSQRT(RT(I))
EN(I) = (RT(I)+DELTA)/(NU*SRT-BETA*SRT*RT(I))
D = SRT/A
RTR(I) = D
RAR(IX,I) = D
EPP = CEXP(LTH/2.*D)
EPM = (1.,0.)/EPP
TM = BETA*EN(I)*RT(I)/A-NU/A*EN(I) + D
B(1,I) = (EPP + EPM)*TM
TM = EN(I)*D*D+D/A
B(2,I) = (EPP + EPM)*TM
TM = EN(I)*D**3+D*D/A
1 B(3,I) = (EPP - EPM)*TM
DTRMNT = B(1)*B(5)*B(9) + B(4)*B(8)*B(3) + B(7)*B(2)*B(6) -
SB(3)*B(5)*B(7) - B(6)*B(8)*B(1) - B(9)*B(2)*B(4)
DET = REAL(DTRMNT)
IF (IMG.EQ.1) DET = AIMAG(DTRMNT)
IF (INX.LE.2) PRINT 50,FREQ,DTRMNT
50 FORMAT (23X*FREQUENCY =*E18.10,5X*DETERMINANT =*C(E18.10,E18.10)/)
C
C C
C APPLY INTERVAL HALVING.
IF (INX.GE.3) GO TO 41
DETR(INX) = DET
INX = INX + 1
IF (INX.GE.3) GO TO 44
FREQ = FR(INX)
GO TO 42
41 IF (IT.GE.NIT) GO TO 43
IT = IT + 1
IF (DET*DETR(1).GT.0.) GO TO 45
DETR(2) = DET
FR(2) = FREQ
GO TO 44
45 DETR(1) = DET
FR(1) = FREQ
44 IF (DETR(1)*DETR(2).GT.0.) GO TO 46
FREQ = .5*(FR(1)+FR(2))
GO TO 42
C
C C
C OBTAIN SCALED MODAL SHAPE COEFFICIENTS FOR AXIAL CU() AND RADIAL CW()
MOTION.
43 F(1) = A2
F(2) = A1
F(3) = A0

```

```

FRQ(IX) = FREQ
DN = B(1)/B(3)
G(1) = B(4) - DN*B(6)
G(3) = B(7) - DN*B(9)
DN = B(2)/B(3)
G(2) = B(5) - DN*B(6)
G(4) = B(8) - DN*B(9)
RT1 = -G(3)/G(1)
RT2 = -G(4)/G(2)
CU(1) = (-B(9)-B(6)*RT1)/B(3)
CU(2) = RT1
CU(3) = (1.,0.)
C1 = (0.,0.)
DO 31 I = 1,3
CW(I) = CU(I)*EN(I)
31 C1 = C1 + CW(I)
DO 215 I = 1,3
CU(I) = CU(I)/C1
215 CW(I) = CW(I)/C1
DO 210 I = 1,3
BU(IX,I) = CU(I)
210 BW(IX,I) = CW(I)
C
C PRINT OUT VALUES RT1 AND RT2 FOR USE IN CHECKING VALIDITY OF RESONANCE
C FREQUENCIES AND MODAL SHAPES.
C
C PRINT 60,RT1,RT2
60 FORMAT (/17X*CONVERGENCE CHECK*//5X5HRT1 =C(E18.10,E18.10)/5X5HRT2
1 =C(E18.10,E18.10)/)
C
C RESCALE MODAL SHAPES SO THAT THE INTEGRAL OF THE MODAL SHAPE OVER THE
C ENTIRE LENGTH OF THE SHELL IS NUMERICALLY EQUAL TO THE LENGTH OF THE
C SHELL. THEN PRINT SCALED MODAL SHAPES.
C
AN = (0.,0.)
RN = (0.,0.)
DO 21 I = 1,3
DO 21 J = 1,3
T1 = T2 = LTH
DR = RTR(I) + CONJG(RTR(J))
IF (TT(1)+TT(2).EQ.0.) GO TO 22
EPP = CEXP(DR*HD2)
EPM = (1.,0.)/EPP
T1 = (EPP-EPM)/DR
22 DR = RTR(I) - CONJG(RTR(J))
IF (TT(1)+TT(2).EQ.0.) GO TO 23
EE = CEXP(DR*HD2)
EM = (1.,0.)/EE
T2 = (EE-EM)/DR
23 AN = AN + CU(I)*CONJG(CU(J))*(T1-T2)
21 RN = RN + CW(I)*CONJG(CW(J))*(T1+T2)

```

NRL REPORT 7964

```

NA(IX) = CABS(AN)
NR(IX) = CABS(RN)
ANRM = SQRTF(HD2/(NA(IX)+NR(IX)))
AA(IX) = ANRM
XL2 = -LTH/(4.*NPTS)
XL1 = -2.*XL2
PRINT 18,IX
18 FORMAT (/24X*SCALED DISPLACEMENTS ALONG LENGTH FROM NEAR CENTER TO
$ END FOR MODAL SHAPE NUMBER*I2)
PRINT 53
53 FORMAT (/31X*POSITION ALONG AXIS*5X*AXIAL DISPLACEMENT*8X
1*RADIAL DISPLACEMENT*/)
DO 61 I = 1,NPTS
X = XL2 + I*XL1
U = W = (0.,0.)
DO 62 J = 1,3
EPP = CEXP(RTR(J)*X)
EPM = (1.,0.)/EPP
U = U - CU(J)*(EPP-EPM)*ANRM
62 W = W + CW(J)*(EPP+EPM)*ANRM
AX(IX,I) = REAL(U)
RD(IX,I) = REAL(W)
61 PRINT 35,X,AX(IX,I),RD(IX,I)
35 FORMAT (33XE12.4,13XE12.4,13XE12.4)
X = LTH/2.
U = (0.,0.)
W = (0.,0.)
DO 65 J = 1,3
EPP = CEXP(RTR(J)*X)
EPM = (1.,0.)/EPP
U = U - CU(J)*(EPP-EPM)*ANRM
65 W = W + CW(J)*(EPP+EPM)*ANRM
AXEDGE(IX) = REAL(U)
WRL = REAL(W)
PRINT 36,X,AXEDGE(IX),WRL
36 FORMAT (20X12HEND OF SHELL 1XE12.4,13XE12.4,13XE12.4)
C
C CALCULATE INTEGRALS OF RADIAL MODAL SHAPES RDIN(,) AND RINT(,).
C
DO 304 I = 1,NPTS
BG = LTH/(2.*NPTS)*(I-1)
ED = LTH/(2.*NPTS)*I
RN = (0.,0.)
DO 305 J = 1,3
EE = CEXP(RTR(J)*ED)
EM = (1.,0.)/EE
EPP = CEXP(RTR(J)*BG)
EPM = (1.,0.)/EPP
305 RN = RN + CW(J)/RTR(J)*(EE-EM-EPP+EPM)*ANRM
304 RDIN(IX,I) = REAL(RN)
RN = (0.,0.)

```

HANISH, KING, BAIER, AND ROGERS

```

      DO 300 J = 1,3
      EPP = CEXP(RTR(J)*LTH/2.)
      EPM = (1.,0.)/EPP
300  RN = RN + CW(J)/RTR(J)*(EPP-EPM)*ANRM
      RINT(IX) = REAL(RN)
      PRINT 54
      54 FORMAT (//54X*RESONANT FREQUENCY*/)
      PRINT 50,FREQ,DIRMNT
777  CONTINUE
      GO TO 7
      46 PRINT 55
      55 FORMAT (//10X*NO SIGN DIFFERENCE*)
      STOP
C
C      CALCULATE AND PRINT INNER PRODUCTS OF MODAL SHAPES.
C
      7 PRINT 8
      8 FORMAT (//43X*NORMALIZED INNER PRODUCTS OF MODAL SHAPES*//42X
      $12HMODAL SHAPES11X*VALUE OF INNER PRODUCT*/)
      DO 95 K = 1,IX
      KP = K + 1
      DO 95 L = KP,IX
      AN = (0.,0.)
      RN = (0.,0.)
      DO 96 I = 1,3
      DO 96 J = 1,3
      EPP = CEXP((RAR(K,I)+CONJG(RAR(L,J)))*HD2)
      EPM = (1.,0.)/EPP
      EE = CEXP((RAR(K,I)-CONJG(RAR(L,J)))*HD2)
      EM = (1.,0.)/EE
      AN = AN + BU(K,I)*CONJG(BU(L,J))*((EPP-EPM)/(RAR(K,I)
      $+CONJG(RAR(L,J))) - (EE-EM)/(RAR(K,I)-CONJG(RAR(L,J))))
96  RN = RN + BW(K,I)*CONJG(BW(L,J))*((EPP-EPM)/(RAR(K,I)
      $+CONJG(RAR(L,J))) + (EE-EM)/(RAR(K,I)-CONJG(RAR(L,J))))
      REE = REAL(AN+RN)/SQRTF((NA(K)+NR(K))*(NA(L)+NR(L)))
95  PRINT 97,K,L,REE
97  FORMAT (/44XI2,* AND*I2,18XE12.4)
      END

```

NRL REPORT 7964

CALCULATION OF MODAL SHAPE FUNCTIONS

INPUT PARAMETERS

| | |
|---|----------------------|
| MEAN RADIUS | RMEAN = 6.587000-002 |
| RADIAL THICKNESS | THK = 6.850000*003 |
| AXIAL LENGTH | LTH = 9.055000-002 |
| DENSITY | RHO = 8.400000*003 |
| POISSONS RATIO | NU = 3.800000*001 |
| YOUNGS MODULUS AT CONSTANT MAGNETIC INDUCTION | Y = 1.260000*011 |

INITIAL FREQUENCY INTERVAL

| | |
|------------------------------|---|
| FREQUENCY = 9.2000000000+003 | DETERMINANT = 1.4758412297+011 3.0000000000+000 |
| FREQUENCY = 9.2500000000+003 | DETERMINANT = -8.1180624343+010 -2.5000000000+000 |

CONVERGENCE CHECK

RT1 = -9.6492114249-001 -2.8453988025-001
 RT2 = -9.6492113422-001 -2.8453991075-001

SCALED DISPLACEMENTS ALONG LENGTH FROM NEAR CENTER TO END FOR MODAL SHAPE NUMBER 1

| POSITION ALONG AXIS | AXIAL DISPLACEMENT | RADIAL DISPLACEMENT |
|-------------------------|--------------------|---------------------|
| 2.5153-003 | -1.9493-002 | 1.0951+000 |
| 7.5458-003 | -5.8236-002 | 1.0850+000 |
| 1.2576-002 | -9.0255-002 | 1.0653+000 |
| 1.7607-002 | -1.3309-001 | 1.0366+000 |
| 2.2637-002 | -1.0832-001 | 9.9995-001 |
| 2.7668-002 | -2.0155-001 | 9.5671-001 |
| 3.2699-002 | -2.3245-001 | 9.0822-001 |
| 3.7729-002 | -2.6074-001 | 8.5582-001 |
| 4.2760-002 | -2.8619-001 | 8.0067-001 |
| END OF SHELL 4.5275-002 | -2.9780-001 | 7.7234-001 |

RESONANT FREQUENCY

FREQUENCY = 9.2309360562+003 DETERMINANT = -1.7480000000+003 5.0000000000-001

HANISH, KING, BAIER, AND ROGERS

INITIAL FREQUENCY INTERVAL

FREQUENCY = 9.9500000000+003 DETERMINANT = -3.7589339280+002 -7.8809049566+011
 FREQUENCY = 1.0000000000+004 DETERMINANT = -1.1262014239+003 1.4422802469+012

CONVERGENCE CHECK

RT1 = 6.0377914453-008 -1.0032617641+002
 RT2 = 2.0367965386-005 -1.0032644568+002

SCALED DISPLACEMENTS ALONG LENGTH FROM NEAR CENTER TO END FOR MODAL SHAPE NUMBER 2

| POSITION ALONG AXIS | AXIAL DISPLACEMENT | RADIAL DISPLACEMENT |
|-------------------------|--------------------|---------------------|
| 2.5153-003 | -1.8358-002 | 1.0798+000 |
| 7.5458-003 | -5.3357-002 | 9.7140-001 |
| 1.2576-002 | -8.3299-002 | 7.6042-001 |
| 1.7607-002 | -1.0513-001 | 4.5795-001 |
| 2.2637-002 | -1.1625-001 | 7.9348-002 |
| 2.7668-002 | -1.1461-001 | -3.5728-001 |
| 3.2699-002 | -9.8832-002 | -8.3282-001 |
| 3.7749-002 | -6.8156-002 | -1.3294+000 |
| 4.2780-002 | -2.2423-002 | -1.8325+000 |
| END OF SHELL 4.5275-002 | 6.0092-003 | -2.0834+000 |

RESONANT FREQUENCY

FREQUENCY = 9.9721327873+003 DETERMINANT = -4.4730690927+002 5.7891250000+003

NRL REPORT 7964

INITIAL FREQUENCY INTERVAL

FREQUENCY = 2.140000000+004 DETERMINANT = 5.9892971634+014 -7.4929310489+005
 FREQUENCY = 2.160000000+004 DETERMINANT = -1.6594993292+015 -5.5553264695+005

CONVERGENCE CHECK

RT1 = -2.2294435570+000 -2.2/45607875-010
 RT2 = -2.2294442519+000 -7.8158865315-011

SCALED DISPLACEMENTS ALONG LENGTH FROM NEAR CENTER TO END FOR MODAL SHAPE NUMBER 3

| POSITION ALONG AXIS | AXIAL DISPLACEMENT | RADIAL DISPLACEMENT |
|-------------------------|--------------------|---------------------|
| 2.5153-003 | -2.2109-002 | 1.3622+000 |
| 7.5458-003 | -5.7402-002 | 8.7842-001 |
| 1.2576-002 | -6.9204-002 | 8.8436-002 |
| 1.7607-002 | -5.1623-002 | -7.1581-001 |
| 2.2647-002 | -9.7289-003 | -1.2316+000 |
| 2.7668-002 | 4.2082-002 | -1.2505+000 |
| 3.2699-002 | 8.4850-002 | -7.2554-001 |
| 3.7729-002 | 1.0147-001 | 2.2694-001 |
| 4.2760-002 | 8.1612-002 | 1.3979+000 |
| END OF SHELL 4.5275-002 | 5.7182-002 | 2.0051+000 |

RESONANT FREQUENCY

FREQUENCY = 2.1452177284+004 DETERMINANT = -6.8792320000+006 1.7449277752+003

HANISH, KING, BAIER, AND ROGERS

INITIAL FREQUENCY INTERVAL

FREQUENCY = 2.3400000000+004 DETERMINANT = -2.4081510578+015 0.0000000000+000
 FREQUENCY = 2.3600000000+004 DETERMINANT = 2.3108087401+015 1.1416680523+005

CONVERGENCE CHECK

RT1 = 1.6697974351-003 -2.2+86525478+014
 RT2 = 1.6697972977-003 -4.2109582353-014

SCALED DISPLACEMENTS ALONG LENGTH FROM NEAR CENTER TO END FOR MODAL SHAPE NUMBER 4

| POSITION ALONG AXIS | AXIAL DISPLACEMENT | RADIAL DISPLACEMENT |
|-------------------------|--------------------|---------------------|
| 2.5153-003 | 1.2155-001 | 2.3861-001 |
| 7.5458-003 | 3.6067-001 | 2.4563-001 |
| 1.2576-002 | 5.8813-001 | 2.5361-001 |
| 1.7647-002 | 7.9687-001 | 2.5296-001 |
| 2.2637-002 | 9.8073-001 | 2.3448-001 |
| 2.7668-002 | 1.1346+000 | 1.9320-001 |
| 3.2699-002 | 1.2544+000 | 1.3039-001 |
| 3.7749-002 | 1.3370+000 | 5.2825-002 |
| 4.2760-002 | 1.3800+000 | -3.0708-002 |
| END OF SHELL 4.5275-002 | 1.3862+000 | -7.2699-002 |

RESONANT FREQUENCY

FREQUENCY = 2.3510248522+004 DETERMINANT = 7.7762560000+006 1.1095852999+003

NRL REPORT 7964

INITIAL FREQUENCY INTERVAL

FREQUENCY = 4.8600000000+004 DETERMINANT = 8.8675063271+018 -2.1154400636+010
 FREQUENCY = 4.8800000000+004 DETERMINANT = -3.8497032762+018 -7.2951901306+009

CONVERGENCE CHECK

RT1 = -5.5491958654+000 1.1629896573-010
 RT2 = -5.5491973395+000 -2.0252976303-007

SCALED DISPLACEMENTS ALONG LENGTH FROM NEAR CENTER TO END FOR MODAL SHAPE NUMBER 5

| POSITION ALONG AXIS | AXIAL DISPLACEMENT | RADIAL DISPLACEMENT |
|-------------------------|--------------------|---------------------|
| 2.5153-003 | -2.9506+002 | 1.2533+000 |
| 7.5458-003 | -6.1715-002 | 1.8418-001 |
| 1.2576-002 | -3.6590-002 | -1.0429+000 |
| 1.7647-002 | 2.0893-002 | -1.3835+000 |
| 2.2637-002 | 7.6153-002 | -5.5322-001 |
| 2.7668-002 | 6.4761-002 | 7.2407-001 |
| 3.2699-002 | 1.2986-002 | 1.3187+000 |
| 3.7729-002 | -4.5934-002 | 6.1943-001 |
| 4.2760-002 | -5.4989-002 | -1.0475+000 |
| END OF SHELL 4.5275-002 | -3.3943-002 | -2.0019+000 |

HANISH, KING, BAIER, AND ROGERS

RESONANT FREQUENCY

FREQUENCY = 4.8740939653+004 DETERMINANT = -3.2372162560+010 -7.2296313120+009

NORMALIZED INNER PRODUCTS OF MODAL SHAPES

| MODAL SHAPES | VALUE OF INNER PRODUCT |
|--------------|------------------------|
|--------------|------------------------|

| | |
|---------|-------------|
| 1 AND 2 | 1.0228-004 |
| 1 AND 3 | -2.4281-005 |
| 1 AND 4 | -2.7792+005 |
| 1 AND 5 | 2.6956-005 |
| 2 AND 3 | 3.6235-005 |
| 2 AND 4 | -7.1936-006 |
| 2 AND 5 | -5.3285-005 |
| 3 AND 4 | -1.2823+005 |
| 3 AND 5 | 3.2401-005 |
| 4 AND 5 | -8.6597-007 |

Appendix D

SAMPLE INPUT AND RESULTANT OUTPUT OF PROGRAM EIGSHIP

As stated in the preceding appendixes, the input used here describes ring C. Four driving frequencies are used in the input: 8850 Hz, which is the constant-current resonance frequency corresponding to the lowest radial mode in air; 4000 Hz, which corresponds to the lowest cavity mode in water; 7960 Hz, which is approximately the second-radial-mode resonant frequency in water; and 12,000 Hz, for which a far-field pattern is calculated. Four mode shapes have been used in the computation. (The mode shape at 48,740.9 Hz has been omitted due to the relatively large frequency at which it occurs.)

The sample input is

```

1  .015
   9   4
.06587   .00685   .09055   8400.   .38   1.26E11
   2.032E-4   7.58E-8 18.   2.30E7   -7.5
       144   .023   .11   1.6
1000.   1485.
69.
8000.   11000.
4
9200.   9250.
9950.   10000.   1
21400.   21600.
23400.   23600.
8850.
4000.
7960.
12000.   45

```

The sample output is found on page 157. The first page of output consists of print-out from subroutine THFREQ. A large input frequency interval has been used, although the frequency interval 9000 to 9500 Hz could have been used. Subroutine THFREQ is capable of calculating only the ring mode and the first thickness mode. Therefore one can use a large frequency interval as input. The validity of the resonant frequency is assured by noting that the determinant at the resonant frequency is seven orders of magnitude less than the determinant at 8000 Hz and that $R1$ and $R2$ agree to six significant digits. The quantities $R1$ and $R2$ are analogous to the quantities $RT1$ and $RT2$ of subroutine EIGFNS; that is, they are ratios of elements of a reduced matrix which is equivalent to the four-by-four boundary condition matrix whose determinant must be 0 for nontrivial solutions of coefficients to exist [1, Eqs. 9.2ff]. Scaled displacements along the thickness of the ring

for 11 equally spaced positions from the inner radius to the outer radius are provided. The middle or sixth point represents the middle of the ring (reference surface). Thickness correction factors FI and FO , referred to as $f(A)$ and $f(B)$ in Part 1, are calculated as

$$FI = \frac{\text{radial displacement at reference surface}}{\text{radial displacement at inner surface}}$$

and

$$FO = \frac{\text{radial displacement at reference surface}}{\text{radial displacement at outer surface}}.$$

The three pages of output following the first page contain output of subroutine EIGFNS. This output is identical to the output of program EIGFNS explained in Appendix C.

The page following output of subroutine EIGFNS contains the rest of the input quantities needed to describe the ring being analyzed. All quantities printed are input quantities with the exception of three: the permeability of free space, UO , which is a constant, the magnetic permeability at constant strain, US , which is the product of URS and UO , and one of the quality factors. The quality factor which is not included in the input is calculated from either Eq. 6.21 or Eq. 6.22 of Part 1.

These output pages just described are printed out once for each complete problem run. The output pages which follow these appear for every driving frequency input.

NRL REPORT 7964

CALCULATION OF THICKNESS CORRECTION FACTORS

INPUT PARAMETERS

| | |
|---|---------------------|
| OUTER RADIUS | ROUT = 6.929500+002 |
| INNER RADIUS | RIN = 6.244500+002 |
| AXIAL LENGTH | LTH = 9.055000+002 |
| DENSITY | RHO = 8.400000+003 |
| POISSONS RATIO | NU = 3.800000+001 |
| YOUNGS MODULUS AT CONSTANT MAGNETIC INDUCTION | Y = 1.260000+011 |

INITIAL FREQUENCY INTERVAL

| | |
|------------------------|---------------------------|
| FREQUENCY = 870000+003 | DETERMINANT = 3.2964+002 |
| FREQUENCY = 171000+004 | DETERMINANT = -5.2280+001 |

RESONANT FREQUENCY

| | |
|------------------------|---------------------------|
| FREQUENCY = 972186+003 | DETERMINANT = -2.0275+007 |
|------------------------|---------------------------|

CONVERGENCE CHECK

| | |
|------|---------------|
| F1 = | -4.195874+000 |
| F2 = | -4.195874+000 |

SCALED DISPLACEMENTS ALONG THICKNESS FROM INNER RADIUS TO OUTER RADIUS

| POSITION | RADIAL DISPLACEMENT | AXIAL DISPLACEMENT |
|------------|---------------------|--------------------|
| 6.2445+002 | -8.5140+001 | 2.8740+001 |
| 6.3130+002 | -8.4813+001 | 2.8739+001 |
| 6.3815+002 | -8.4496+001 | 2.8735+001 |
| 6.4500+002 | -8.4187+001 | 2.8729+001 |
| 6.5185+002 | -8.3885+001 | 2.8722+001 |
| 6.5870+002 | -8.3592+001 | 2.8715+001 |
| 6.6555+002 | -8.3305+001 | 2.8708+001 |
| 6.7240+002 | -8.3026+001 | 2.8701+001 |
| 6.7925+002 | -8.2754+001 | 2.8695+001 |
| 6.8610+002 | -8.2487+001 | 2.8692+001 |
| 6.9295+002 | -8.2227+001 | 2.8690+001 |

THICKNESS CORRECTION FACTORS

| | | | |
|------|--------------|------|--------------|
| F1 = | 17018917+000 | F0 = | 97836790+001 |
|------|--------------|------|--------------|

TIME MSR IMPREQ IS 2.158

HANISH, KING, BAIER, AND ROGERS

CALCULATION OF MODAL SHAPE FUNCTIONS

INPUT PARAMETERS

| | |
|---|----------------------|
| MEAN RADIUS | RMEAN = 6,587000+002 |
| RADIAL THICKNESS | THK = 6,850000-003 |
| AXIAL LENGTH | LTH = 9,055000+002 |
| DENSITY | RHO = 8,400000+003 |
| POISSONS RATIO | NU = 3,800000-001 |
| YOUNGS MODULUS AT CONSTANT MAGNETIC INDUCTION | Y = 1,240000+011 |

INITIAL FREQUENCY INTERVAL

| | | |
|------------------------------|---------------------------------|-------------------|
| FREQUENCY = 9,2000000000+003 | DETERMINANT = 1,4758412297+011 | 3,0000000000+000 |
| FREQUENCY = 9,2500000000+003 | DETERMINANT = -8,1180624343+010 | -2,5000000000+000 |

CONVERGENCE CHECK

RT1 = *9,6492114249+001 *2,6253788023+001
 RT2 = *9,6492113422+001 *2,6253991073+001

SCALED DISPLACEMENTS ALONG LENGTH FROM NEAR CENTER TO END FOR MODAL SHAPE NUMBER 1

| POSITION ALONG AXIS | AXIAL DISPLACEMENT | RADIAL DISPLACEMENT |
|-------------------------|--------------------|---------------------|
| 2,5153+003 | -1,9493+002 | 1,0951+000 |
| 7,5458+003 | -5,8236+002 | 1,0850+000 |
| 1,2576+002 | -9,6255+002 | 1,0653+000 |
| 1,7607+002 | -1,3309+001 | 1,0346+000 |
| 2,2637+002 | -1,6832+001 | 9,9999+001 |
| 2,7668+002 | -2,0155+001 | 9,5671+001 |
| 3,2699+002 | -2,3245+001 | 9,0822+001 |
| 3,7729+002 | -2,6074+001 | 8,5582+001 |
| 4,2760+002 | -2,8619+001 | 8,0067+001 |
| END OF SHELL 4,5275+002 | -2,9780+001 | 7,7234+001 |

RESONANT FREQUENCY

| | | |
|------------------------------|--------------------------------|------------------|
| FREQUENCY = 9,2309360582+003 | DETERMINANT = 1,7480000000+003 | 5,0000000000+001 |
|------------------------------|--------------------------------|------------------|

NRL REPORT 7964

INITIAL FREQUENCY INTERVAL

FREQUENCY = 9,9500000000+003 DETERMINANT = *3,7589339280+002 -7,8809049566+011
 FREQUENCY = 1,0000000000+004 DETERMINANT = *1,1262014239+003 1,4422802469+012

CONVERGENCE CHECK

FT1 = 4,0377914453+008 =1,6832617641+002
 FT2 = 2,0367905386+009 =1,6832644568+002

SCALED DISPLACEMENTS ALONG LENGTH FROM NEAR CENTER TO END FOR MODAL SHAPE NUMBER 2

| POSITION ALONG AXIS | AXIAL DISPLACEMENT | RADIAL DISPLACEMENT |
|-------------------------|--------------------|---------------------|
| 2,5153+003 | -1,8358+002 | 1,0798+000 |
| 7,5458+003 | -5,3357+002 | 9,7140+001 |
| 1,2978+002 | -8,3299+002 | 7,8042+001 |
| 1,7607+002 | -1,0513+001 | 4,5795+001 |
| 2,2637+002 | -1,1625+001 | 7,9348+002 |
| 2,7668+002 | -1,1461+001 | -3,5726+001 |
| 3,2699+002 | -9,8832+002 | -8,3282+001 |
| 3,7729+002 | -6,8156+002 | -1,3294+000 |
| 4,2760+002 | -2,2423+002 | -1,8325+000 |
| END OF SHELL 4,5275+002 | 6,0092+003 | -2,0534+000 |

RESONANT FREQUENCY

FREQUENCY = 9,9721327873+003 DETERMINANT = *4,4730690927+002 5,7891250000+003

INITIAL FREQUENCY INTERVAL

FREQUENCY = 2,1400000000+004 DETERMINANT = 5,9892971634+014 -7,4929310489+005
 FREQUENCY = 2,1600000000+004 DETERMINANT = *1,6594993252+015 -5,5553264695+005

CONVERGENCE CHECK

FT1 = *2,2294435570+000 =2,2745607875+010
 FT2 = *2,2294442519+000 =7,8198865315+011

SCALED DISPLACEMENTS ALONG LENGTH FROM NEAR CENTER TO END FOR MODAL SHAPE NUMBER 3

| POSITION ALONG AXIS | AXIAL DISPLACEMENT | RADIAL DISPLACEMENT |
|-------------------------|--------------------|---------------------|
| 2,5153+003 | -2,2109+002 | 1,3622+000 |
| 7,5458+003 | -5,7402+002 | 8,7842+001 |
| 1,2576+002 | -6,9204+002 | 8,8436+002 |
| 1,7607+002 | -5,1623+002 | -7,1581+001 |
| 2,2637+002 | -9,7289+003 | -1,2316+000 |
| 2,7668+002 | 4,2862+002 | -1,2505+000 |
| 3,2699+002 | 6,4850+002 | -7,2554+001 |
| 3,7729+002 | 1,0147+001 | 2,2694+001 |
| 4,2760+002 | 8,1612+002 | 1,3979+000 |
| END OF SHELL 4,5275+002 | 5,7182+002 | 2,0051+000 |

RESONANT FREQUENCY

FREQUENCY = 2,1452177284+004 DETERMINANT = *6,8792320000+006 1,7449277752+003

HANISH, KING, BAIER, AND ROGERS

INITIAL FREQUENCY INTERVAL

FREQUENCY = 2,340000000+004 DETERMINANT = +2,4081510578+015 0,0000000000+000
 FREQUENCY = 2,3600000000+004 DETERMINANT = 2,3108087+01+015 1,1416880523+005

CONVERGENCE CHECK

RT1 = 1,6697974351+003 = 2,2486525478+014
 RT2 = 1,6697972977+003 = 4,2109582353+014

SCALED DISPLACEMENTS ALONG LENGTH FROM NEAR CENTER TO END FOR MODAL SHAPE NUMBER 4

| POSITION ALONG AXIS | AXIAL DISPLACEMENT | RADIAL DISPLACEMENT |
|-------------------------|--------------------|---------------------|
| 2,5153+003 | 1,2155+001 | 2,3441+001 |
| 7,5458+003 | 3,6067+001 | 2,4563+001 |
| 1,2576+002 | 3,8813+001 | 2,5361+001 |
| 1,7607+002 | 7,9687+001 | 2,5296+001 |
| 2,2637+002 | 9,8073+001 | 2,3448+001 |
| 2,7668+002 | 1,1346+000 | 1,9320+001 |
| 3,2699+002 | 1,2544+000 | 1,3039+001 |
| 3,7729+002 | 1,3370+000 | 5,2825+002 |
| 4,2760+002 | 1,3800+000 | -3,0708+002 |
| END OF SHELL 4,5275+002 | 1,3882+000 | -7,2699+002 |

RESONANT FREQUENCY

FREQUENCY = 2,3510248522+004 DETERMINANT = 7,7762560000+006 1,1095852999+003

NORMALIZED INNER PRODUCTS OF MODAL SHAPES

| MODAL SHAPES | VALUE OF INNER PRODUCT |
|--------------|------------------------|
| 1 AND 2 | 1,0228+004 |
| 1 AND 3 | +2,4281+005 |
| 1 AND 4 | +2,7792+005 |
| 2 AND 3 | 3,6235+005 |
| 2 AND 4 | +7,1936+006 |
| 3 AND 4 | +1,2823+005 |

TIME FOR SIGFAS IS 3,168

NRL REPORT 7964

INPUT PARAMETERS

THIN WALLED ELASTIC CYLINDRICAL TUBE MAGNETOSTRICTIVE MATERIAL
ALL UNITS ARE IN MKS SYSTEM

CURRENT DRIVE CUR = 1.500000+002 +0.000000+000

NUMBER OF SIDE BANDS JMAXH = 9
NUMBER OF END BANDS JMAX = 4

CYLINDER DIMENSIONS AND PROPERTIES

| | |
|---|----------------------|
| MEAN RADIUS | RMEAN = 6.987000+002 |
| RADIAL THICKNESS | THK = 6.850000+003 |
| AXIAL LENGTH | LTH = 9.055000+002 |
| DENSITY | RHO = 8.400000+003 |
| POISSONS RATIO | NU = 3.800000+001 |
| YOUNGS MODULUS AT CONSTANT MAGNETIC INDUCTION | Y = 1.260000+011 |

SCROLL TAPE DIMENSIONS AND PROPERTIES

| | |
|---|---------------------|
| THICKNESS | THST = 2.032000+004 |
| RESISTIVITY | RES = 7.580000+008 |
| RELATIVE MAGNETIC PERMEABILITY AT CONSTANT STRAIN | URS = 1.800000+001 |
| PERMEABILITY OF FREE SPACE | UO = 1.256637+006 |
| MAGNETIC PERMEABILITY AT CONSTANT STRAIN | US = 2.261947+005 |
| PIEZOMAGNETIC STRESS CONSTANT | HTT = 2.300000+007 |
| TOTAL DIP ANGLE | DIP = -7.900000+000 |

COIL WINDING DIMENSIONS

| | |
|---------------------|--------------------|
| NUMBER OF TURNS | NTRN = 144 |
| RADIAL THICKNESS | THC = 2.300000+002 |
| AXIAL LENGTH | LC = 1.100000+001 |
| COPPER LOSS IN COIL | REL = 1.600000+000 |

EXTERNAL FLUID MEDIUM PROPERTIES

| | |
|----------------|---------------------|
| DENSITY | RHOF = 1.000000+003 |
| SPEED OF SOUND | CF = 1.485000+003 |

QUALITY FACTORS

| | |
|------------------|-------------------|
| CONSTANT VOLTAGE | QE = 9.651961+001 |
| CONSTANT CURRENT | QI = 6.900000+001 |

CURRENT DRIVE * 1.500000+002 =0.000000+000

FREQUENCY * 8.490000+003

OUTPUT DATA

REFERENCE SURFACE VELOCITIES IN AIR

| | REAL | IMAGINARY | MAGNITUDE | ANGLE(DEGREES) |
|-----------------------|---------------|---------------|--------------|----------------|
| BUTTERWORTH AND SMITH | | | | |
| VELBS # | 3.681621+003 | 2.720922+003 | 4.577963+003 | 36.466 |
| NRL EIGSKIP | | | | |
| VEL(1) # | 4.002941+003 | +3.292159+003 | 5.182842+003 | +39.435 |
| VEL(2) # | 3.979429+003 | +3.270538+003 | 5.150949+003 | +39.415 |
| VEL(3) # | 3.933122+003 | +3.228002+003 | 5.088167+003 | +39.377 |
| VEL(4) # | 3.865405+003 | +3.165919+003 | 4.996439+003 | +39.319 |
| VEL(5) # | 3.778237+003 | +3.086216+003 | 4.878505+003 | +39.243 |
| VEL(6) # | 3.674009+003 | +2.991241+003 | 4.737704+003 | +39.151 |
| VEL(7) # | 3.555353+003 | +2.883570+003 | 4.577717+003 | +39.044 |
| VEL(8) # | 3.424902+003 | +2.765766+003 | 4.402208+003 | +38.922 |
| VEL(9) # | 3.285016+003 | +2.640093+003 | 4.214431+003 | +38.788 |
| VEL(10) # | +1.116228+003 | 9.140282+004 | 1.442710+003 | 140.688 |

REFERENCE SURFACE VELOCITIES IN WATER

| | REAL | IMAGINARY | MAGNITUDE | ANGLE(DEGREES) |
|-----------------------|---------------|---------------|--------------|----------------|
| BUTTERWORTH AND SMITH | | | | |
| VELBS # | 1.329727+004 | -1.300042+005 | 1.336067+004 | -5.284 |
| NRL EIGSKIP | | | | |
| VEL(1) # | 1.387953+004 | 3.071356+005 | 1.421529+004 | 12.478 |
| VEL(2) # | 1.366009+004 | 2.573982+005 | 1.390048+004 | 10.671 |
| VEL(3) # | 1.330413+004 | 1.568632+005 | 1.339429+004 | 6.724 |
| VEL(4) # | 1.294726+004 | 4.677148+007 | 1.294939+004 | 0.207 |
| VEL(5) # | 1.272852+004 | -1.978341+005 | 1.288134+004 | -8.635 |
| VEL(6) # | 1.274053+004 | -4.454054+005 | 1.349666+004 | -19.269 |
| VEL(7) # | 1.299815+004 | -7.282247+005 | 1.489909+004 | -29.260 |
| VEL(8) # | 1.343867+004 | -1.033103+004 | 1.695876+004 | -37.391 |
| VEL(9) # | 1.395674+004 | -1.346519+004 | 1.939339+004 | -43.973 |
| VEL(10) # | +3.961726+005 | 8.761420+006 | 4.037450+005 | 167.530 |

BUTTERWORTH AND SMITH

| | REAL | IMAGINARY |
|---|----------------------|---------------|
| ELECTRICAL POWER | PIN # 2.324844+003 | 1.002743+002 |
| RADIATION IMPEDANCE | ZRAD # 7.718155+004 | +0.015966+003 |
| POWER CONVERSION EFFICIENCY | ETA # 5.926194+001 | |
| MOTIONAL IMPEDANCE IN AIR | ZM0TA # 1.806453+002 | 1.140455+002 |
| ELECTRICAL IMPEDANCE IN AIR | ZEA # 1.847947+002 | 1.616282+002 |
| MOTIONAL IMPEDANCE IN WATER | ZM0TW # 6.183219+000 | +1.016300+000 |
| ELECTRICAL IMPEDANCE IN WATER | ZEE # 1.033264+001 | +4.456638+001 |
| CORE IMPEDANCE | ZC # 2.549428+000 | 3.889673+001 |
| COPPER LOSS, LEAKAGE IMPEDANCE | ZEL # 1.600000+000 | 6.889948+000 |
| TRANSDUCTION COEFFICIENT | ZEM # 7.019966+002 | +4.601130+001 |
| ELECTROMECHANICAL COUPLING COEFFICIENT | K # 3.081653+001 | |
| ELECTROMECHANICAL IMPEDANCE | ZMP # 8.303988+002 | 1.266943+004 |
| MECHANICAL IMPEDANCE | ZMPP # 9.297808+002 | +1.415777+004 |
| EDDY CURRENT FACTOR | CHIE # 9.956287+001 | +5.675778+002 |
| TOTAL MECHANICAL IMPEDANCE OPEN CIRCUIT | ZMOC # 1.760179+003 | +1.488334+003 |

CURRENT DRIVE = 1.500000-002 = 0.000000+000

FREQUENCY = 8.450000+003

OUTPUT DATA

NRL EIGSHIP

RING SURFACE

| BAND | REAL | IMAGINARY | SURFACE PRESSURES | ANGLE(DEGREES) | MAGNITUDE | ANGLE(DEGREES) | REAL | IMAGINARY | SURFACE VELOCITIES | MAGNITUDE | ANGLE(DEGREES) |
|------|--------------|--------------|-------------------|----------------|---------------|----------------|--------------|---------------|--------------------|-----------|----------------|
| 1 | 5.849370+001 | 1.466432+002 | 1.198848+002 | 119.1205 | -1.413583+004 | -3.126229+005 | 1.447852+004 | -1.447852+004 | 1.447852+004 | -167.522 | |
| 2 | 6.106493+001 | 1.528876+002 | 1.194306+002 | 120.5116 | -1.391304+004 | -2.621645+005 | 1.419786+004 | -1.419786+004 | 1.419786+004 | -169.329 | |
| 3 | 6.146173+001 | 1.182655+002 | 1.182655+002 | 123.087 | -1.355749+004 | -1.597379+005 | 1.364435+004 | -1.364435+004 | 1.364435+004 | -171.276 | |
| 4 | 6.194253+001 | 9.183369+001 | 1.145922+002 | 126.791 | -1.318741+004 | -4.763756+007 | 1.318709+004 | -1.318709+004 | 1.318709+004 | -173.793 | |
| 5 | 6.253660+001 | 6.833633+001 | 1.117333+002 | 131.384 | -1.296421+004 | -2.014874+009 | 1.311987+004 | -1.311987+004 | 1.311987+004 | -171.165 | |
| 6 | 6.328194+001 | 7.218890+001 | 1.046888+002 | 136.405 | -1.297745+004 | -4.536530+005 | 1.374658+004 | -1.374658+004 | 1.374658+004 | -160.731 | |
| 7 | 6.428491+001 | 9.304227+001 | 9.304227+001 | 140.978 | -1.323383+004 | -7.417933+005 | 1.517496+004 | -1.517496+004 | 1.517496+004 | -150.740 | |
| 8 | 6.546524+001 | 4.73777+001 | 7.35269+001 | 142.892 | -1.368352+004 | -1.052233+004 | 1.724664+004 | -1.724664+004 | 1.724664+004 | -145.449 | |
| 9 | 6.683686+001 | 3.93377+001 | 4.065891+001 | 128.247 | -1.421318+004 | -1.571336+004 | 1.975246+004 | -1.975246+004 | 1.975246+004 | -134.027 | |
| 10 | 6.835564+001 | 1.720265+001 | 6.133303+001 | 15.080 | -3.961726+005 | -8.761420+006 | 4.057450+005 | -4.057450+005 | 4.057450+005 | -167.530 | |
| 11 | 7.049589+001 | 7.547827+000 | 7.802807+001 | 5.495 | -3.961726+005 | -8.761420+006 | 4.057450+005 | -4.057450+005 | 4.057450+005 | -167.530 | |
| 12 | 7.249336+001 | 1.542422+001 | 9.245049+001 | 0.096 | -3.961726+005 | -8.761420+006 | 4.057450+005 | -4.057450+005 | 4.057450+005 | -167.530 | |
| 13 | 1.021659+002 | 4.140422+000 | 1.062808+002 | -2.664 | 3.961726+005 | 8.761420+006 | 4.057450+005 | -4.057450+005 | 4.057450+005 | -167.530 | |
| 14 | 1.151559+002 | 2.190990+001 | 1.822535+002 | 8.780 | 3.961726+005 | 8.761420+006 | 4.057450+005 | -4.057450+005 | 4.057450+005 | -167.530 | |
| 15 | 2.068339+002 | 3.128933+001 | 2.096763+002 | 9.412 | 1.321934+004 | -1.101642+004 | 1.667418+004 | -1.667418+004 | 1.667418+004 | -43.551 | |
| 16 | 2.151876+002 | 4.196427+001 | 2.192221+002 | 11.009 | 1.278600+004 | -7.163393+005 | 1.465592+004 | -1.465592+004 | 1.465592+004 | -26.260 | |
| 17 | 2.154872+002 | 4.748322+001 | 2.20567+002 | 12.427 | 1.253259+004 | -4.381359+005 | 1.327638+004 | -1.327638+004 | 1.327638+004 | -19.249 | |
| 18 | 2.117598+002 | 5.33591+001 | 2.181320+002 | 13.887 | 1.252787+004 | -1.946853+005 | 1.267111+004 | -1.267111+004 | 1.267111+004 | -8.835 | |
| 19 | 2.064822+002 | 5.988077+001 | 2.144861+002 | 15.401 | 1.273395+004 | -4.600812+007 | 1.273603+004 | -1.273603+004 | 1.273603+004 | -0.207 | |
| 20 | 2.033688+002 | 6.628233+001 | 2.108846+002 | 16.834 | 1.308700+004 | -1.543303+005 | 1.317765+004 | -1.317765+004 | 1.317765+004 | 4.724 | |
| 21 | 1.974440+002 | 6.995915+001 | 2.075758+002 | 17.975 | 1.343714+004 | -2.931972+005 | 1.367361+004 | -1.367361+004 | 1.367361+004 | 10.671 | |
| 22 | 1.953415+002 | 6.878476+001 | 2.061202+002 | 18.611 | 1.365300+004 | -3.021228+005 | 1.398328+004 | -1.398328+004 | 1.398328+004 | 12.478 | |

MODAL CONTRIBUTIONS TO AIR IMPEDANCE

MODAL CONTRIBUTIONS TO WATER IMPEDANCE

| | |
|--------------|---------------|
| 1.565173+002 | =1.458314+002 |
| 6.942791+001 | =5.198684+001 |
| 4.643685+004 | =2.182220+004 |
| 1.568287+001 | =1.073646+001 |

| | | |
|------|----------------|----------------|
| PIN | = 2.248311+003 | 9.826975+003 |
| PA | = 1.333346+003 | 2.043810+004 |
| EPF | = 5.931321+001 | |
| ZMBA | = 1.573688+002 | -1.464780+002 |
| ZEA | = 1.635183+002 | -1.008933+002 |
| ZETA | = 5.843069+000 | -1.907232+000 |
| ZEB | = 9.992495+000 | 4.367545+001 |
| ZB | = 4.149426+000 | 4.588268+001 |
| ZL | = 6.492379+004 | 9.950509+003 |
| HL | = 1.873179+004 | -1.1227746+003 |
| HR | = 5.218987+000 | 0.000000+000 |
| TRP | = 6.032511+001 | 4.73 |
| TRA | = 4.103012+001 | -33.68 |
| UH | = 2.621665+005 | +1.923649+007 |
| UHE | = 2.250886+005 | -1.475309+006 |
| ZKNA | = 0.000000+000 | 1.322986+005 |
| ZSTA | = 0.000000+000 | 1.303584+005 |
| ZKN | = 0.000000+000 | 1.317135+005 |
| ZST | = 0.000000+000 | 1.340854+005 |

| | |
|-------------------------------------|--|
| ELECTRICAL POWER | |
| ACOUSTIC POWER | |
| POWER CONVERSION EFFICIENCY | |
| MOTIONAL IMPEDANCE IN AIR | |
| ELECTRICAL IMPEDANCE IN AIR | |
| MOTIONAL IMPEDANCE IN WATER | |
| ELECTRICAL IMPEDANCE IN WATER | |
| BLOCKED ELECTRICAL IMPEDANCE | |
| RADIATION IMPEDANCE | |
| TRANSDUCTION COEFFICIENT | |
| MAGNETIC FIELD IN COIL | |
| TRANSMITTING RESPONSE IN PLANE (DB) | |
| TRANSMITTING RESPONSE AXIAL (DB) | |
| PERMEABILITY DUE TO HYSTERESIS | |
| TOTAL PERMEABILITY | |
| MEDIUM INERTIAL REACTANCE AIR | |
| SHELL STIFFNESS REACTANCE AIR | |
| MEDIUM INERTIAL REACTANCE | |
| SHELL STIFFNESS REACTANCE | |

TIME 301.00

CURRENT DRIVE = 1.500000+002 =0.000000+000

FREQUENCY = 4.000000+003

OUTPUT DATA

REFERENCE SURFACE VELOCITIES IN AIR

| | REAL | IMAGINARY | MAGNITUDE | ANGLE (DEGREES) |
|-----------------------|---------------|---------------|--------------|-----------------|
| BUTTERWORTH AND SMITH | | | | |
| VELBS # | 2.127730+006 | 4.929812+005 | 4.934402+005 | 87.529 |
| NRL EIGSHIP | | | | |
| VEL(1) # | 2.175762+006 | 4.960875+005 | 4.965644+005 | 87.489 |
| VEL(2) # | 2.174553+006 | 4.959998+005 | 4.964762+005 | 87.490 |
| VEL(3) # | 2.172013+006 | 4.957958+005 | 4.962713+005 | 87.492 |
| VEL(4) # | 2.167884+006 | 4.954130+005 | 4.958871+005 | 87.494 |
| VEL(5) # | 2.161760+006 | 4.947486+005 | 4.952206+005 | 87.496 |
| VEL(6) # | 2.153095+006 | 4.936566+005 | 4.941260+005 | 87.503 |
| VEL(7) # | 2.141242+006 | 4.919566+005 | 4.924223+005 | 87.508 |
| VEL(8) # | 2.125544+006 | 4.894558+005 | 4.899171+005 | 87.513 |
| VEL(9) # | 2.105466+006 | 4.859880+005 | 4.864439+005 | 87.519 |
| VEL(10) # | -5.962812+007 | -1.326174+005 | 1.327514+005 | -92.574 |

REFERENCE SURFACE VELOCITIES IN WATER

| | REAL | IMAGINARY | MAGNITUDE | ANGLE (DEGREES) |
|-----------------------|---------------|---------------|--------------|-----------------|
| BUTTERWORTH AND SMITH | | | | |
| VELBS # | 1.321838+004 | 6.554983+005 | 1.475443+004 | 26.377 |
| NRL EIGSHIP | | | | |
| VEL(1) # | 1.665892+004 | 4.218061+005 | 1.718464+004 | 14.209 |
| VEL(2) # | 1.638501+004 | 4.231669+005 | 1.692264+004 | 14.481 |
| VEL(3) # | 1.584245+004 | 4.258193+005 | 1.640473+004 | 15.045 |
| VEL(4) # | 1.504371+004 | 4.296140+005 | 1.564913+004 | 15.938 |
| VEL(5) # | 1.401126+004 | 4.343080+005 | 1.466894+004 | 17.222 |
| VEL(6) # | 1.277935+004 | 4.395604+005 | 1.351418+004 | 18.981 |
| VEL(7) # | 1.139288+004 | 4.449511+005 | 1.223094+004 | 21.333 |
| VEL(8) # | 9.902437+005 | 4.500301+005 | 1.087708+004 | 24.440 |
| VEL(9) # | 8.355104+005 | 4.543983+005 | 9.510812+005 | 25.540 |
| VEL(10) # | -3.619904+008 | -1.165948+005 | 3.803043+005 | -162.147 |

BUTTERWORTH AND SMITH

| | REAL | IMAGINARY | |
|---|---------|--------------|---------------|
| ELECTRICAL POWER | PIN # | 1.916903+003 | 5.294731+003 |
| RADIATION IMPEDANCE | ZRAD # | 6.118398+004 | 1.802687+005 |
| POWER CONVERSION EFFICIENCY | ETA # | 6.948364+001 | |
| MOTIONAL IMPEDANCE IN AIR | ZM0YA # | 1.793732+001 | 2.312101+000 |
| ELECTRICAL IMPEDANCE IN AIR | ZEA # | 2.384660+000 | 2.297835+001 |
| MOTIONAL IMPEDANCE IN WATER | ZM0YW # | 6.314282+000 | 2.865884+000 |
| ELECTRICAL IMPEDANCE IN WATER | ZEE # | 8.519369+000 | 2.353214+001 |
| QERE IMPEDANCE | ZC # | 6.052872+001 | 1.764436+001 |
| QEMPER LOSS, LEAKAGE IMPEDANCE | ZEL # | 1.600000+000 | 3.021897+000 |
| TRANSDUCTION COEFFICIENT | ZEM # | 7.045489+002 | -2.416945+001 |
| ELECTROMECHANICAL COUPLING COEFFICIENT | K # | 3.081653+001 | |
| ELECTROMECHANICAL IMPEDANCE | ZMP # | 9.650997+002 | 2.813303+004 |
| MECHANICAL IMPEDANCE | ZMPP # | 9.297808+002 | -2.424252+005 |
| EDDY CURRENT FACTOR | CHIE # | 9.989829+001 | -2.576640+002 |
| TOTAL MECHANICAL IMPEDANCE OPEN CIRCUIT | ZMOC # | 1.894881+003 | -2.142922+005 |

CURRENT DRIVE = 1.500000+002 =0.000000+000

FREQUENCY = 4.000000+003

OUTPUT DATA

NRL EIGSHIP

RING SURFACE

| BAND | SURFACE PRESSURES | | | | SURFACE VELOCITIES | | | |
|------|-------------------|---------------|--------------|----------------|--------------------|---------------|--------------|----------------|
| | REAL | IMAGINARY | MAGNITUDE | ANGLE(DEGREES) | REAL | IMAGINARY | MAGNITUDE | ANGLE(DEGREES) |
| 1 | +1.874576+002 | +7.603693+002 | 8.025688+002 | -103.507 | +1.696740+004 | -4.296168+005 | 1.750285+004 | -165.791 |
| 2 | +1.867707+002 | +7.699172+002 | 7.922473+002 | -103.636 | +1.668841+004 | -4.318028+005 | 1.723599+004 | -165.519 |
| 3 | +1.854018+002 | +7.490488+002 | 7.716527+002 | -103.902 | +1.613580+004 | -4.337042+005 | 1.670850+004 | -164.955 |
| 4 | +1.833996+002 | +7.178131+002 | 7.408619+002 | -104.329 | +1.532227+004 | -4.375692+005 | 1.593483+004 | -164.062 |
| 5 | +1.806521+002 | +6.762052+002 | 6.999205+002 | -104.998 | +1.427071+004 | -4.423501+005 | 1.494057+004 | -162.778 |
| 6 | +1.772805+002 | +6.240254+002 | 6.487188+002 | -105.859 | +1.301598+004 | -4.476998+005 | 1.376442+004 | -161.019 |
| 7 | +1.732200+002 | +5.605313+002 | 5.866861+002 | -107.173 | +1.160385+004 | -4.531904+005 | 1.245747+004 | -158.667 |
| 8 | +1.683710+002 | +4.834469+002 | 5.119274+002 | -109.202 | +1.008580+004 | -4.583634+005 | 1.107859+004 | -155.560 |
| 9 | +1.623278+002 | +3.843793+002 | 4.172503+002 | -112.899 | +8.509816+005 | -4.628125+005 | 9.686925+005 | -151.460 |
| 10 | +1.551437+002 | +2.703525+002 | 2.990224+002 | -125.698 | +3.619904+005 | +1.165948+005 | 3.803043+005 | -162.147 |
| 11 | +1.474539+002 | +1.439674+002 | 2.279219+002 | -130.246 | +3.619904+005 | +1.165948+005 | 3.803043+005 | -162.147 |
| 12 | +1.436837+002 | +1.067482+002 | 1.997400+002 | -138.001 | +3.619904+005 | +1.165948+005 | 3.803043+005 | -162.147 |
| 13 | +1.404509+002 | +7.647908+002 | 1.792118+002 | -143.284 | +3.619904+005 | +1.165948+005 | 3.803043+005 | -162.147 |
| 14 | +1.370854+002 | +1.449139+001 | 1.378492+002 | 173.966 | 8.218740+005 | 4.469820+005 | 9.355585+005 | 28.540 |
| 15 | +1.365499+002 | +6.827617+001 | 1.526679+002 | 153.435 | 9.740819+005 | 4.426851+005 | 1.069954+004 | 24.440 |
| 16 | +1.363452+002 | +1.058387+002 | 1.726032+002 | 142.179 | 1.120694+004 | 4.376891+005 | 1.203132+004 | 21.333 |
| 17 | +1.362556+002 | +1.049043+002 | 1.917414+002 | 135.286 | 1.257077+004 | 4.323863+005 | 1.329361+004 | 19.981 |
| 18 | +1.362108+002 | +1.057842+002 | 2.084887+002 | 130.793 | 1.378258+004 | 4.272196+005 | 1.442953+004 | 17.222 |
| 19 | +1.361846+002 | +1.056408+002 | 2.222519+002 | 127.789 | 1.479818+004 | 4.226022+005 | 1.538978+004 | 15.938 |
| 20 | +1.361671+002 | +1.055889+002 | 2.327475+002 | 125.806 | 1.558388+004 | 4.186695+005 | 1.613699+004 | 14.048 |
| 21 | +1.361561+002 | +1.054185+002 | 2.398178+002 | 124.593 | 1.611759+004 | 4.162604+005 | 1.664644+004 | 14.481 |
| 22 | +1.361503+002 | +2.017266+002 | 2.433732+002 | 124.016 | 1.638703+004 | 4.149218+005 | 1.690417+004 | 14.209 |

MODAL CONTRIBUTIONS TO AIR IMPEDANCE
1.698307+001 2.173457+000
1.923206+003 2.529790+002
3.951658+004 5.828797+005
1.365385+003 2.023534+002

MODAL CONTRIBUTIONS TO WATER IMPEDANCE
6.101155+000 1.709766+000
+7.458810+002 3.246179+002
+2.914539+004 8.016967+005
6.248900+002 1.605546+002

ELECTRICAL POWER
ACOUSTIC POWER
POWER CONVERSION EFFICIENCY
MOTIONAL IMPEDANCE IN AIR
ELECTRICAL IMPEDANCE IN AIR
MOTIONAL IMPEDANCE IN WATER
ELECTRICAL IMPEDANCE IN WATER
BLOCKED ELECTRICAL IMPEDANCE
RADIATION IMPEDANCE
TRANSDUCTION COEFFICIENT
MAGNETIC FIELD IN COIL
TRANSMITTING RESPONSE IN PLANE (DB)
TRANSMITTING RESPONSE AXIAL (DB)
PERMEABILITY DUE TO HYSTERESIS
TOTAL PERMEABILITY
MEDIUM INERTIAL REACTANCE AIR
SHELL STIFFNESS REACTANCE AIR
MEDIUM INERTIAL REACTANCE
SHELL STIFFNESS REACTANCE

PIN = 1.866162+003 5.045539+003
PA = 1.437786+003 3.975826+003
EFF = 7.704511+001
ZMOTA = 1.731233+001 2.219048+000
ZEA = 2.378410+000 2.288530+001
ZMOTW = 6.088765+000 1.758363+000
ZEE = 8.294052+000 2.242462+001
ZB = 2.205287+000 2.066825+001
ZL = 7.471810+004 2.066132+005
HL = 1.879988+004 +6.449274+002
HR = 5.218987+000 0.000000+000
TRP = 6.155933+001 89.24
TRA = 3.904547+001 +119.49
UH = 2.261869+005 +1.923649+007
UHE = 2.259069+005 -7.749705+007
ZKNA = 0.000000+000 5.937865+004
ZSTA = 0.000000+000 2.874709+005
ZKN = 0.000000+000 5.952918+004
ZST = 0.000000+000 2.884540+005

TIME 284.30

165

NRL REPORT 7964

CURRENT DRIVE = 1.500000+002 =0.000000+000

FREQUENCY = 7.960000+003

OUTPUT DATA

REFERENCE SURFACE VELOCITIES IN AIR

| | REAL | IMAGINARY | MAGNITUDE | ANGLE(DEGREES) |
|-----------------------|------------------------|--------------|--------------|----------------|
| BUTTERWORTH AND SMITH | VELBS # 4.047920+002 | 3.895957+004 | 3.886308+004 | 82.835 |
| NRL EIGSHIP | VEL(1) * 5.828169+006 | 4.347354+004 | 4.386247+004 | 82.364 |
| | VEL(2) * 5.807462+005 | 4.338550+004 | 4.374272+004 | 82.371 |
| | VEL(3) * 5.766414+005 | 4.312050+004 | 4.350436+004 | 82.383 |
| | VEL(4) * 5.705731+005 | 4.277063+004 | 4.314953+004 | 82.401 |
| | VEL(5) * 5.626414+005 | 4.230866+004 | 4.268116+004 | 82.425 |
| | VEL(6) * 5.529699+005 | 4.173806+004 | 4.210277+004 | 82.453 |
| | VEL(7) * 5.416987+005 | 4.106266+004 | 4.141843+004 | 82.485 |
| | VEL(8) * 5.289762+005 | 4.028701+004 | 4.063280+004 | 82.520 |
| | VEL(9) * 5.149480+005 | 3.941628+004 | 3.975123+004 | 82.557 |
| | VEL(10) * 1.642388+005 | 1.222518+004 | 1.233501+004 | -97.652 |

REFERENCE SURFACE VELOCITIES IN WATER

| | REAL | IMAGINARY | MAGNITUDE | ANGLE(DEGREES) |
|-----------------------|-------------------------|---------------|--------------|----------------|
| BUTTERWORTH AND SMITH | VELBS # 1.062768+004 | 3.421775+005 | 1.116499+004 | 17.847 |
| NRL EIGSHIP | VEL(1) * 7.014835+004 | -8.889962+005 | 7.070942+004 | -172.777 |
| | VEL(2) * -6.044770+004 | -6.643985+005 | 6.081174+004 | -173.728 |
| | VEL(3) * -4.185982+004 | -2.327629+005 | 4.192448+004 | -178.817 |
| | VEL(4) * 1.584693+004 | 3.740587+005 | 1.628242+004 | 166.719 |
| | VEL(5) * 1.576190+004 | 1.115578+004 | 1.931033+004 | 35.200 |
| | VEL(6) * 5.109226+004 | 1.949249+004 | 5.468434+004 | 20.883 |
| | VEL(7) * 0.850241+004 | 2.836410+004 | 9.293653+004 | 17.770 |
| | VEL(8) * 1.267573+003 | 3.746425+004 | 1.321778+003 | 16.466 |
| | VEL(9) * 1.650775+003 | 4.658586+004 | 1.715250+003 | 15.759 |
| | VEL(10) * 6.889583+005 | 3.821535+005 | 7.878482+005 | +150.984 |

BUTTERWORTH AND SMITH

| | REAL | IMAGINARY |
|---|----------------------|---------------|
| ELECTRICAL POWER | PIN # 1.972851+003 | 9.524926+003 |
| RADIATION IMPEDANCE | ZRAD # 8.634603+004 | +7.194860+003 |
| POWER CONVERSION EFFICIENCY | EPA # 5.455845+001 | |
| MOTIONAL IMPEDANCE IN AIR | ZMOTA # 3.350879+000 | 1.792514+001 |
| ELECTRICAL IMPEDANCE IN AIR | ZEA # 7.045323+000 | 5.895317+001 |
| MOTIONAL IMPEDANCE IN WATER | ZMOTW # 5.073780+000 | 1.304967+000 |
| ELECTRICAL IMPEDANCE IN WATER | ZEW # 8.768225+000 | 4.233300+001 |
| CORE IMPEDANCE | ZC # 2.094445+000 | 3.501446+001 |
| COPPER LOSS, LEAKAGE IMPEDANCE | ZEL # 1.600000+000 | 6.013576+000 |
| TRANSDUCTION COEFFICIENT | ZEM # 7.025864+002 | +4.202631+001 |
| ELECTROMECHANICAL COUPLING COEFFICIENT | K # 3.081653+001 | |
| ELECTROMECHANICAL IMPEDANCE | ZMP # 8.432833+002 | 1.409782+004 |
| MECHANICAL IMPEDANCE | ZMP # 9.297808+002 | -4.120613+004 |
| EDDY CURRENT FACTOR | CMIE # 9.964163+001 | +5.110198+002 |
| TOTAL MECHANICAL IMPEDANCE OPEN CIRCUIT | ZMOC # 1.773064+003 | -2.710530+004 |

CURRENT DRIVE = 1,500000-002 = 0,000000+000

FREQUENCY = 1,200000+004

OUTPUT DATA

NRL EIGSHIP

HING SURFACE

| BAND | SURFACE PRESSURES | | | | SURFACE VELOCITIES | | | |
|------|-------------------|---------------|--------------|-----------------|--------------------|---------------|--------------|-----------------|
| | REAL | IMAGINARY | MAGNITUDE | ANGLE (DEGREES) | REAL | IMAGINARY | MAGNITUDE | ANGLE (DEGREES) |
| 1 | +6,144814+001 | 2,936967+000 | 6,151829+001 | 177,264 | +3,883814+005 | 5,072916+005 | 6,388934+005 | 127,438 |
| 2 | +6,406989+001 | 2,887946+000 | 6,410724+001 | 178,044 | +3,758581+005 | 5,277891+005 | 6,479434+005 | 125,456 |
| 3 | +6,680641+001 | 6,739235+001 | 6,880971+001 | 179,439 | +3,916915+005 | 5,656000+005 | 6,660257+005 | 121,873 |
| 4 | +7,471972+001 | +1,430078+000 | 7,473749+001 | +178,750 | +3,174842+005 | 6,152645+005 | 6,923487+005 | 117,294 |
| 5 | +8,026419+001 | +4,740495+000 | 8,070353+001 | +176,633 | +2,752881+005 | 6,705567+005 | 7,248654+005 | 119,320 |
| 6 | +8,490515+001 | +8,659642+000 | 8,534561+001 | +174,176 | +2,272862+005 | 7,260863+005 | 7,608287+005 | 107,382 |
| 7 | +8,614914+001 | +1,238592+001 | 8,718289+001 | +171,168 | +1,755021+005 | 7,784613+005 | 7,979993+005 | 109,705 |
| 8 | +8,230761+001 | +1,898327+001 | 8,446838+001 | +167,013 | +1,215912+005 | 8,266319+005 | 8,355266+005 | 94,368 |
| 9 | +6,948997+001 | +2,597655+001 | 7,418650+001 | +159,503 | +6,673125+006 | 8,713102+005 | 8,738619+005 | 94,380 |
| 10 | +3,758837+001 | +3,988498+001 | 5,479228+001 | +133,287 | +8,976790+006 | 2,214333+005 | 2,389372+005 | 112,067 |
| 11 | +3,521600+001 | +4,512387+001 | 5,586640+001 | +129,474 | +8,976790+006 | 2,214333+005 | 2,389372+005 | 112,067 |
| 12 | +3,261358+001 | +4,566252+001 | 5,976679+001 | +125,034 | +8,976790+006 | 2,214333+005 | 2,389372+005 | 112,067 |
| 13 | +2,700697+001 | +4,760638+001 | 5,473339+001 | +119,566 | +8,976790+006 | 2,214333+005 | 2,389372+005 | 112,067 |
| 14 | 2,557165+001 | +5,753461+001 | 6,296169+001 | +86,037 | 6,44872+006 | +8,415072+005 | 8,439716+005 | +85,620 |
| 15 | 4,926167+001 | +6,491782+001 | 8,149255+001 | +92,808 | 1,174322+005 | +7,983571+005 | 8,069476+005 | +81,632 |
| 16 | 6,334380+001 | +7,698664+001 | 9,513959+001 | +48,256 | 1,694991+005 | +7,518341+005 | 7,707039+005 | +77,295 |
| 17 | 7,210958+001 | +7,398911+001 | 1,047575+002 | +46,501 | 2,195119+005 | +7,012507+005 | 7,348047+005 | +72,618 |
| 18 | 7,722953+001 | +7,999754+001 | 1,111936+002 | +46,009 | 2,658720+005 | +6,476204+005 | 7,000715+005 | +67,680 |
| 19 | 7,981123+001 | +8,207148+001 | 1,151985+002 | +46,147 | 3,066247+005 | +5,942195+005 | 6,686670+005 | +62,706 |
| 20 | 8,077765+001 | +8,228011+001 | 1,174637+002 | +46,553 | 3,396620+005 | +5,462537+005 | 6,432444+005 | +58,127 |
| 21 | 8,091694+001 | +8,669798+001 | 1,185921+002 | +46,975 | 3,630019+005 | +5,097361+005 | 6,257806+005 | +54,544 |
| 22 | 8,082464+001 | +8,738862+001 | 1,190353+002 | +47,235 | 3,750969+005 | +4,899397+005 | 6,170402+005 | +52,562 |

MODAL CONTRIBUTIONS TO AIR IMPEDANCE
 +8,877950+001 +5,923310+000
 +1,580092+002 +1,093669+001
 3,352944+005 1,964649+004
 1,082940+002 6,373750+002

MODAL CONTRIBUTIONS TO WATER IMPEDANCE
 9,159335+001 -2,973473+000
 +5,172952+002 -9,531465+002
 2,044188+004 1,097893+003
 -1,136533+002 3,063604+002

ELECTRICAL POWER
 ACOUSTIC POWER
 REVER CONVERSION EFFICIENCY
 MECHANICAL IMPEDANCE IN AIR
 ELECTRICAL IMPEDANCE IN AIR
 MECHANICAL IMPEDANCE IN WATER
 ELECTRICAL IMPEDANCE IN WATER
 BLOCKED ELECTRICAL IMPEDANCE
 RADIATION IMPEDANCE
 TRANSDUCTION COEFFICIENT
 MAGNETIC FIELD IN COIL
 TRANSMITTING RESPONSE IN PLANE (DB)
 TRANSMITTING RESPONSE AXIAL (DB)
 PERMEABILITY DUE TO HYSTERESIS
 METAL PERMEABILITY
 MEDIUM INERTIAL REACTANCE AIR
 SHELL STIFFNESS REACTANCE AIR
 MEDIUM INERTIAL REACTANCE
 SHELL STIFFNESS REACTANCE

PIN = 1,566289+003 1,318070+002
 PA = 3,061641+004 2,798334+004
 EFF = 1,954710+001
 ZM0TA = 8,927330+001 -5,968743+000
 ZEA = 5,215507+000 5,564922+001
 ZM0TW = 8,530430+001 -3,037054+000
 ZEE = 6,961283+000 5,858091+001
 ZB = 6,108240+000 6,161796+001
 ZL = 6,192478+004 5,623553+004
 HL = 1,866464+004 -1,601161+003
 HR = 5,218987+000 0,000000+000
 TRP = 5,135102+001 +9,02
 TRA = 4,134178+001 -137,90
 UH = 2,261865+005 -1,923649+007
 UHE = 2,242817+005 -1,924019+006
 ZKNA = 0,000000+000 1,803892+005
 ZSTA = 0,000000+000 9,740519+004
 ZKN = 0,000000+000 1,798610+005
 ZST = 0,000000+000 9,809903+004

HANISH, KING, BAIER, AND ROGERS

FARFIELD PATTERN AT INFINITY

0 DEGREES IS BROADSIDE, 90 DEGREES IS IN AXIAL DIRECTION,
 ANGLE PRESSURE IN DB PHASE ANGLE OF PRESSURE

| | | |
|-------|--------|---------|
| 0,00 | 0,00 | -9,02 |
| 2,00 | 0,02 | +9,06 |
| 4,00 | 0,09 | +9,18 |
| 6,00 | 0,21 | +9,37 |
| 8,00 | 0,36 | +9,61 |
| 10,00 | 0,54 | +9,94 |
| 12,00 | 0,75 | +10,30 |
| 14,00 | 0,97 | +10,70 |
| 16,00 | 1,20 | +11,13 |
| 18,00 | 1,43 | +11,59 |
| 20,00 | 1,66 | +12,06 |
| 22,00 | 1,87 | +12,55 |
| 24,00 | 2,06 | +13,04 |
| 26,00 | 2,22 | +13,55 |
| 28,00 | 2,34 | +14,08 |
| 30,00 | 2,43 | +14,62 |
| 32,00 | 2,48 | +15,18 |
| 34,00 | 2,48 | +15,77 |
| 36,00 | 2,43 | +16,38 |
| 38,00 | 2,32 | +17,04 |
| 40,00 | 2,16 | +17,74 |
| 42,00 | 1,93 | +18,51 |
| 44,00 | 1,64 | +19,35 |
| 46,00 | 1,28 | +20,26 |
| 48,00 | 0,85 | +21,33 |
| 50,00 | 0,34 | +22,52 |
| 52,00 | -0,25 | +23,90 |
| 54,00 | -0,93 | +25,50 |
| 56,00 | -1,70 | +27,40 |
| 58,00 | -2,57 | +29,67 |
| 60,00 | -3,53 | +32,45 |
| 62,00 | -4,61 | +35,89 |
| 64,00 | -5,78 | +40,22 |
| 66,00 | -7,04 | +45,73 |
| 68,00 | -8,34 | +52,80 |
| 70,00 | -9,61 | +61,77 |
| 72,00 | -10,72 | +72,76 |
| 74,00 | -11,49 | +85,30 |
| 76,00 | -11,82 | +98,16 |
| 78,00 | -11,74 | +109,84 |
| 80,00 | -11,41 | +119,41 |
| 82,00 | -10,99 | +126,68 |
| 84,00 | -10,59 | +131,87 |
| 86,00 | -10,27 | +135,31 |
| 88,00 | -10,08 | +137,26 |
| 90,00 | -10,01 | +137,90 |

Appendix E

DEFINITION OF MATERIAL PARAMETERS

E1. MAGNETIC PARAMETERS [Ref. Y. Kikuchi "Ultrasonic Transducers," Corona Pub. Co. Tokyo, 1969]

A magnetostrictive rod of length ℓ meters is subjected to an incremental magnetization of ΔJ webers/meter². The incremental strain induced is $\Delta(\delta\ell/\ell)$, which to be completely inhibited requires an *applied stress* $\Delta T = -Y\Delta(\delta\ell/\ell)$, where Y is Young's modulus of elasticity. Equivalently the quantity J can be thought of as inducing an *internal stress* $\Delta T' = -\Delta T$, which for small excitation and linear motion, is proportional to the magnetization: $\Delta T' = h\Delta J$. Here h is the magnetostrictive dynamic constant expressed in units of newton per weber and is the same quantity as λ of Butterworth and Smith. At zero strain the quantity J and the magnetomotive force H are related by the defining relation $\Delta J = \kappa\Delta H$, where κ is the susceptibility (weber-turns per meter-ampere).

If this rod is subjected to an *externally* applied increment of strain $\Delta S = \delta\ell/\ell$, then the magnetomotive force ΔH induced *internally* for small-amplitude strains, and linear motion, is proportional to this strain: $\Delta H' = h^T\Delta S$. Here h^T is a magnetostrictive dynamic constant expressed in units of amperes turns per meter and is the same quantity as γ of Butterworth and Smith.

Instead of individual values of static applied forces one can construct complete curves of changes in length, magnetization, etc. by continuously changing static excitation. Then the defining relations for the material parameters are

$$h = \left(\frac{\partial T'}{\partial J}\right)_S, \frac{1}{Y} = \left(\frac{\partial S}{\partial T}\right)_J, h^T = \left(\frac{\partial H'}{\partial S}\right)_M, \text{ and } \kappa = \left(\frac{\partial J}{\partial H}\right)_S.$$

From this it is seen that the material parameters may be obtained by measuring slopes of $\delta\ell/\ell$, h , and κ versus H or J , where H and J are static (or dc) values. Often it is more convenient to plot equivalent curves in which the condition at constant strain is replaced by that of constant stress or vice versa. Thus one may write the equivalent form

$$h = \left(\frac{\partial S}{\partial H}\right)_T \left(\frac{\partial T}{\partial S}\right)_J / \left(\frac{\partial J}{\partial H}\right)_T$$

or

$$h = \left(\frac{\partial S}{\partial J}\right)_T \left(\frac{\partial T}{\partial S}\right)_J.$$

When the values of h , Y , and κ are obtained, one forms the static (or low-frequency) value of the electromechanical coupling factor k , defined as the ratio of the mechanical energy stored by the magnetostrictive effect in the rod to the electric energy stored electrically. For static conditions this is known to be $k^2 = \kappa h^2 / Y$, since $h = h^T$.

The measurement of h , κ , and k^2 from static curves is made ambiguous by existence of hysteresis. Thus a curve of $\delta\ell/\ell$ or h versus H shows two values of $\delta\ell/\ell$ (or h) for each value of H . Similarly a curve of J versus H for most magnetostrictive materials exhibits hysteresis effects: multiple values of J for each choice of H . It is therefore necessary in the description of material parameters to indicate which branch of the hysteresis curve is being used in making numerical estimates.

In lieu of specifying the susceptibility it is often more useful to specify the magnetic permeability. To do this it is noted that the magnetic induction B and the quantity J are related by the formula $B = \mu_0 H + J$ where μ_0 is the permeability of free space ($4\pi \times 10^{-7}$ volt-second/ampere). Let μ_{rel} be the permeability of a magnetic material relative to that of a vacuum. Then by definition $B = \mu_{\text{rel}} \mu_0 H$. Thus the quantity $J = B - \mu_0 H = (\mu_{\text{rel}} - 1) \mu_0 H = \kappa H$. Thus when κ is measured, one can obtain from it the relative permeability $\mu_{\text{rel}} = (\kappa/\mu_0) + 1$. In magnetostrictive material the quantity J is a function not only of the applied field H but also of the mechanical strain (S). Thus for applied dc fields in a long rod,

$$\Delta J_{\text{dc}} = \kappa_{\text{dc}} (\Delta H_{\text{dc}} + h^T \Delta S_{\text{dc}}).$$

The susceptibility κ_{dc} is measured as the slope of a line from the origin of the static J -versus- H curve to a particular point (the *bias point*) on the curve. In most operating conditions the applied field is the sum of a dc bias at the bias point plus an incremental ac quantity. The incremental quantity J_i is thus

$$J_i = \kappa_i H_i + h^T S_i = (\mu_i - 1) \mu_0 H_i + h^T S_i.$$

Here μ_i is the *reversible permeability* and κ_i is the *reversible susceptibility*, the latter defined as the slope of the J -versus- H curve at the bias point when $H_i \rightarrow 0$. The quantity $\mu_i \mu_0 H_i$ can be regarded as the *reversible magnetic induction*. Occasionally the ac fields are regarded as truly *incremental*. Then κ_i is called the *incremental susceptibility*, or ratio of ΔJ to ΔH at the bias point.

E2. EFFECTIVE YOUNG'S MODULUS

The tangential stress due to (ac) magnetization J of a thin circular ring of radius a and magnetostrictivity h is $T_\theta = Jh$. The accompanying (ac) tangential strain is $S_\theta = v_r / j\omega a$. The equation of motion of an elementary (or differential) segment of the ring (mass m_δ and stiffness K_δ) is

$$F_\delta = j\omega m_\delta v_r + \frac{K_\delta v_r}{j\omega} = J_\delta h A_\theta,$$

in which $K_\delta = A_\theta Y/a$, A_θ is the cross-sectional area of the ring, Y is Young's modulus, and F_δ the net driving force. For a *complete* ring the net force is $2\pi F_\delta$, the total mass is $m = 2\pi m_\delta$, and the total magnetization is $2\pi J_\delta = J$. If the total magnetization is considered to be a *driving force* which is externally applied, the equation of motion for the total ring can be reduced to

$$A_\theta hJ = v_r \left(j\omega m + \frac{2\pi K_\delta}{j\omega} \right).$$

Thus at constant (say zero) magnetization the resonant frequency in the radial mode is given by

$$\Omega_R = \sqrt{\frac{2\pi A_\theta Y_1}{ma}},$$

in which $Y = Y_1 + jY_2$ and $Y_2 \ll Y_1$.

If in contrast the excitation stress is taken to be due to applied magnetic intensity H_δ , then $T_\theta = \kappa h H_\delta$. The equation of motion in this case is

$$F_\delta = \kappa h H_\delta A_\theta = v_r \left[j\omega m_\delta + \frac{K'_\delta}{j\omega} \right].$$

Here the symbol K'_δ is the stiffness of the segment of the ring as modified by the electro-mechanical coupling:

$$K'_\delta = \frac{A_\theta}{a} [Y - \kappa h^2]$$

The force over the entire ring for the case of a driving magnetic intensity $H = 2\pi H_\delta$ is

$$A_\theta \kappa h H = v_r \left(j\omega m + \frac{2\pi}{j\omega} \frac{A_\theta}{a} Y - \frac{A_\theta \kappa h^2}{a} \frac{2\pi}{j\omega} \right).$$

Taking $\kappa = \kappa_1 - j\kappa_2$, $\kappa_2 \ll \kappa$, one can see that at constant (say zero) applied magnetic intensity the resonant frequency is

$$\omega_R = \sqrt{\frac{2\pi A_\theta}{ma} (Y_1 - \kappa h^2)}.$$

Factoring out $j\omega m$ leads to

$$A_\theta h \kappa H = j\omega m v_r \left[1 - \frac{\omega_R^2}{\omega^2} + j \frac{(\Delta\omega)_B}{\omega} \right]$$

Here $(\Delta\omega)_B$ is the effective bandwidth of the resonator. The corresponding temporal damping constant Δ_H (at constant H) is given by

$$\Delta_H = \frac{(\Delta\omega)_B}{2} = \frac{1}{2} \frac{(Y_2 + \kappa_2 h^2)}{\omega a^2 \rho}.$$

Similarly the temporal damping constant (at constant J) is given by

$$\Delta_J = \frac{1}{2} \frac{Y_2}{\omega a^2 \rho}.$$

In summary, to determine the real part of Young's modulus for the magnetostrictive material of a thin circular ring, one drives the ring (without coils) by a purely mechanical force and observes the frequency of maximum radial velocity in the first radial mode. The effective value of Y_1 is then obtained from the formula for the resonant frequency at zero magnetization. To obtain the quantity κh^2 for the same ring, one winds the ring with N turns of coil, applies a dc current, and arranges the ac excitation to be short circuited. Then the ring is mechanically driven, and the frequency of maximum radial velocity is measured.

E3. FORCE FACTOR, EFFICIENCY, AND MATERIAL PROPERTIES

In a piezoactive vibrator consisting of one electrical terminal, where an ac electrical current I can be externally applied, and one mechanical terminal, where an ac mechanical force F can be measured by its effect on an external mechanical system, the ratio of delivered force input current defines the force factor T_{me} (newtons per ampere). An example of such a one dimensional vibrator is a circular magnetostrictive ring, radius a , thickness t , vibrating in the first radial mode. The induced *radial* force on an element of circumferential length is $F_\delta \approx T_{\theta\theta} A_\theta \delta$, where $T_{\theta\theta}$ is the induced tangential stress, A_θ is the cross-sectional area of the ring core, and δ is the angle (radians) subtended by the element. Since $T_{\theta\theta} = T = hJ$, and since the *total* force is obtained when $\delta = 2\pi$, the external force delivered is

$$F_{\text{ext}} = 2\pi A_\theta hJ.$$

The magnetization $J = \kappa H$. For N turns of wire on a circular core the magnetic intensity $H = NI/2\pi a$. Thus the ratio F_{ext}/I , or force factor T_{me} , is

$$T_{me} = \frac{NA_\theta}{a} \kappa h.$$

When the externally applied quantity is at the mechanical, rather than electrical, terminal and induces a velocity v , the ratio of the open-circuit electrical voltage to this applied velocity is also a transduction factor: T_{em} . By conservation of energy it is seen that $T_{me} = T_{em}$. Thus all transduction factors are proportional to κh , making this an important factor in the selection of magnetostrictive materials for applications.

The energy dissipated at the mechanical terminals when velocity v passes through the real mechanical load R_L is $R_L v v^* = R_L |v|^2$. Similarly, at the electrical terminals the energy dissipated in the real electrical load R_{ee} is $R_{ee} I I^* = R_e |I|^2$. Hence the electromechanical efficiency is

$$\eta = \frac{R_L |v|^2}{R_{ee} |I|^2}.$$

At the mechanical terminal the canonical relation of applied force, velocity, current, and mechanical impedance (Z_m) is

$$F = T_{me}I + Z_m v$$

If all external delivered force is removed, the ratio of velocity to current may be found. This is

$$v/I = -\frac{T_{me}}{Z_m}.$$

Thus the efficiency becomes

$$\eta = \frac{R_L |T_{em}|^2}{R_{ee} |Z_m|^2}.$$

Since T_{em}^2 is proportional to $\kappa^2 h^2$ and R_{ee} is proportional to κ , the electromechanical efficiency is proportional to κh^2 . Thus again the important parameter of magnetostrictive materials is κh or κh^2 .

E4. MEASUREMENT OF PERMEABILITY κ

Over a small frequency range ω centered on the frequency of radial resonance the measured electrical impedance Z_c of a circular ring magnetostrictive transducer is

$$Z_c = R_c + j\omega(L_0 + L_i) = R_c + j\omega L_c,$$

in which R_c is the copper loss in the electrical winding, L_0 is the leakage inductance, and L_i is the "iron" core inductance. The theoretical value of L_i is

$$L_i = \frac{N^2 A \mu_t}{2\pi a},$$

where μ_t is the total permeability. The impedance of an air-cored toroidal coil of the same size and shape as the circular ring transducer is measured to be

$$Z_0 = R_0 + j\omega L_0.$$

Subtracting Z_0 from Z_c , one finds that

$$L_i = \frac{Z_c - Z_0}{j\omega}.$$

Writing $\mu_t = \mu_0 + \kappa$, one sees that the (complex) κ is given by

$$\kappa = \frac{2\pi a}{N^2 A_0} \left(\frac{Z_c - Z_0}{j\omega} \right)_{\text{meas}} - \mu_0.$$

E5. CALCULATION OF κh

In Part 1 [1] it was noted that the calculation of the magnetostriction constant $h_{\theta\theta}$ is given by

$$\mu^s |X| h_{\theta\theta} = a \sqrt{(\omega_3 - \omega_2) M^* D_m} / A_0 N,$$

in which $\omega_3 - \omega_2$ is the difference of quadrantal frequencies in the plot of motional impedance, D_m is the diameter of the motional impedance circle, and M is the effective mass of the ring. When the factor $\mu^s |X|$ is regarded as the total permeability of the ring *minus* the permeability of free space, then $h_{\theta\theta}$ is equal to h as defined in Section E1. Hence to determine κh , one can write

$$\kappa h = \frac{a \sqrt{(\omega_3 - \omega_2) m D_n}}{A_0 N},$$

in which the effective mass is taken to be the static mass of the ring. This formula conjoined to the preceding formula for κ allows one to determine h separately.

Appendix F

NUMERICAL INVESTIGATION OF THE AXIAL TRANSMITTING RESPONSE

As noted in Part 1 (p. 44) the Helmholtz integral formula shows that the acoustic field pressure $p(\mathbf{x})$ at any field point can be calculated from a knowledge of the vector velocity $\mathbf{v}(\mathbf{x}_s)$ and the scalar pressure $p(\mathbf{x}_s)$ on the closed surface $\mathbf{S}(\mathbf{x}_s)$:

$$j\omega\phi \oint G(\mathbf{x}|\mathbf{x}_s) \mathbf{v}(\mathbf{x}_s) \cdot d\mathbf{S}(\mathbf{x}_s) + \oint p(\mathbf{x}_s) \nabla_{\mathbf{O}} G(\mathbf{x}|\mathbf{x}_s) \cdot d\mathbf{S}(\mathbf{x}_s) = p(\mathbf{x}).$$

Here time is given by $e^{j\omega t}$, and the normal to \mathbf{S} points into the medium in which $p(\mathbf{x})$ is to be calculated.

The surface \mathbf{S} can be conveniently represented by finite increments. In cylindrical coordinates

$$\Delta\mathbf{S} = \hat{a}_r(\ell\Delta Z_s)2\pi a_{s\ell} + \hat{a}_z 2\pi a_{K_{\text{mean}}} K\Delta a_s; (\hat{a}_r, \hat{a}_z: \text{unit vectors})$$

that is, the radial surface is divided into J annular bands, and the end surface is divided into K radial bands. The symbol $a_{s\ell}$ represents either the inside radius a_i or the outside radius a_o , as required. The symbol $a_{K_{\text{mean}}}$ represents the mean radius of the k th radial band at the end.

In incremental form the field pressure thus may be written

$$p(\mathbf{x}) = \text{I} + \text{II} + \left\{ \begin{array}{l} \text{III} \\ \text{IV} \end{array} \right\} + \text{V}, \quad (\text{F1})$$

where

$$\text{I} = \sum_K j\omega\rho 2\pi a_{K_{\text{mean}}} (q\Delta a_s) \dot{u}_k G(\mathbf{x}|a_{K_{\text{mean}}}, 0, Z=L),$$

$$\text{II} = \sum_{\ell} j\omega\rho 2\pi a_{s\ell} (\ell\Delta Z_s) \dot{w}_{\ell} G(\mathbf{x}|a_{s\ell}, 0, \ell\Delta Z_s),$$

$$\left\{ \begin{array}{l} \text{III} \\ \text{IV} \end{array} \right\} = \sum_K 2\pi a_{K_{\text{mean}}} (k\Delta a_s) p_K \frac{\partial G}{\partial Z}(\mathbf{x}|a_{K_{\text{mean}}}, 0, Z=L),$$

$$\text{V} = \sum_{\ell} 2\pi a_{s\ell} (\ell\Delta Z_s) p_{\ell} \frac{\partial G}{\partial r}(\mathbf{x}|a_{s\ell}, 0, \ell\Delta Z_s).$$

From the integral-equation nature of this formulation the pressures p_K at the ends and p_Q on the radial surface are functions of the axial and radial surface velocities \dot{u} and \dot{w} .

The field point x is now chosen to lie on the z axis, and the individual contributions of terms I through V to the axial pressure are sought. First, the contribution V is easily accounted for. Since $\partial G/\partial r$ is zero on the z axis, the contribution of V to the axial pressure is zero. Second, the contributions of I and II are both due to volume velocity effects and can be handled on the same basis. The Green's function G for them is taken as that of a simple source, and the summations are replaced by integrals. The contribution of I is the axial pressure due to end velocity. The summation on K yields a Bessel function of order zero which is maximum on the z axis. The contribution of II is the axial pressure due to radial velocity. If the volume velocities on the inside radial surface and outside radial surface are exactly equal in magnitude, then II vanishes. This vanishing contribution is called IIa. It describes the "pure dipole effect." If on the other hand the sum of these volume velocities is not zero but yields a net value, then there is an axial pressure whose magnitude is proportional to this net. This pressure contribution is labeled IIb.

The third contribution to the axial pressure is that due to the surface pressure p_K on the annulus area of the end of the shell. As noted earlier, this surface pressure is due to the end velocity $p_K(\dot{u})$ or radial velocity $p_K(\dot{w})$. The axial field pressure due to the surface pressure $p_K(\dot{u})$ is labeled III. The axial field pressure due to surface pressure $p_K(\dot{w})$ is labeled IV. If the volume velocities due to radial motion of the shell exactly cancel, as in condition IIa, the surface pressure p_K generates an axial field pressure, labeled IVa. If the radial volume velocities do not cancel but leave a net velocity, then p_K generates an additional axial field pressure, labeled IVb.

The principal contributions I through IV have been accounted for. To numerically evaluate these contributions at specific frequencies, EIGSHIP was applied with specific special inputs. The resultant calculations appear in Table F1. This table was obtained by running computer program EIGSHIP under different conditions corresponding to the headings of the table columns; for example, the volume velocity of the sides was adjusted by changing the thickness correction factors used by EIGSHIP to obtain inside and outside velocities (Section 7.1.3).

At the frequency $f = 4000$ Hz, EIGSHIP predictions and experiment disagree. From Table F1 the major contribution to the axial pressure at $f = 4000$ Hz is seen to be that due to the surface pressure p_K at the annulus area of the end of the shell, generated by the radial motion of the shell under conditions of zero volume velocity (IVa).

To check the conclusion drawn from these calculations that IVa is the major contributor, EIGSHIP was used again and those influence coefficients in the matrix G [Part 1, p. 44] which relate pressure on endbands to velocity on sidebands were arbitrarily reduced. With each such reduction the corresponding axial (far-field) pressure reported by the EIGSHIP model was also reduced, without however affecting the radial transmitting response, thus verifying the conclusion. In a physical sense these arbitrary reductions of p_K are considered to correspond to the deterioration of the pressure build-up on the annulus area due to the presence of the winding coil and the interior mechanical support of the vibrating shell.

Table F1
 Contribution to the For-Field Pressure in the Axial Direction as calculated
 by EIGSHIP for Ring C in Accordance with Eq. F9.

| Frequency (Hz) | Magnitude and Angle of Complex Pressure, Normalized to the current (0.15 A), and the Equivalent Value in dB | | | |
|-------------------|--|---|---|--|
| | I + II _b + III + IV | I + III + IV _a | IV _a | I + III |
| 1000 | 0.405 N/m ² -0.9° -7.850 dB | 0.465 N/m ² 178.9° -6.650 dB | 0.027 N/m ² -2.7° -31.475 dB | 0.492 N/m ² 178.8° -6.166 dB |
| 2000 | 2.378 N/m ² -3.6° 7.525 dB | 1.450 N/m ² -176.5° 3.226 dB | 0.627 N/m ² -11.6° -4.050 dB | 2.062 N/m ² 179.0° 6.285 dB |
| 4000 | 89.593 N/m ² -119.5° 39.045 dB | 69.269 N/m ² -152.1° 36.811 dB | 73.803 N/m ² -137.7° 37.362 dB | 18.481 N/m ² 111.0° 25.334 dB |
| 6000 | 32.762 N/m ² 113.2° 30.307 dB | 53.613 N/m ² 119.0° 34.585 dB | 48.661 N/m ² 117.7° 33.743 dB | 5.075 N/m ² 131.0° 14.109 dB |

Appendix G

SPECIFIC ACOUSTIC IMPEDANCE OF THE SHELL AND SHELL MOTION

In the theory of progressive acoustic waves in a cylindrical waveguide the acoustic pressure and radial particle velocity are known to have the following dependence on radial coordinate r and axial coordinate z :

$$p \propto J_0(k_r r) e^{ik_z z},$$

$$u_r \propto J_1(k_r r) e^{ik_z z},$$

in which the component wavenumbers k_r and k_z are related to the total wavenumber ω/c by the relation

$$\left(\frac{\omega}{c}\right)^2 = k_r^2 + k_z^2.$$

Here ω is the harmonic frequency of wave motion and c is the local speed of sound. We consider the special case in which $k_z = 0$; that is, we allow only standing waves in the r direction and no propagation in the z direction. Then at the cylinder walls ($r = a$) the specific acoustic impedance of the medium is given by the ratio

$$\frac{p}{u_r} \approx \frac{J_0(\omega a/c)}{J_1(\omega a/c)}.$$

Thus at particular frequencies ω_n where $J_1(\omega_n a/c) = 0$ it is seen that the specific acoustic impedance is infinite, which means the fluid allows no radial motion at the cylinder wall. Now $J_1(x) = 0$ for values $x = x_n$. Thus at frequencies $f_n = \omega_n/2\pi$ one has

$$f_n = \frac{x_n c}{2\pi a}.$$

Choosing $c = 1485$ m/s, letting $n = 1$ for illustrative purposes and noting that from standard theory $x_1 = 3.83$, one sees that

$$f_1 = \frac{3.83}{2\pi} \cdot \frac{1485}{a} = \frac{905.2}{a},$$

where the cylinder radius a has the dimensions of meters. For ring C the radius $a = 0.06587$. Hence the frequency of infinite radial specific acoustic impedance is $f_1 = 13,742$ Hz. In general f_n is independent of the length of the waveguide.